NUMO
原子力発電環境整備機構

NUMO-TR-09-02

Development of Methodologies for the Identification of Volcanic and Tectonic Hazards to Potential HLW Repository Sites in Japan

- The Kyushu Case Study -

Neil Chapman[1], Mick Apted[2], John Beavan[3], Kelvin Berryman[3], Mark Cloos[4], Charles Connor[5], Laura Connor[5], Toshiaki Hasenaka[8], Olivier Jaquet[6], Koji Kiyosugi[5], Nicola Litchfield[3], Sue Mahony[7], Masaya Miyoshi[8], Warwick Smith[3], Steve Sparks[7], Mark Stirling[3], Pilar Villamor[3], Laura Wallace[3], Junichi Goto[9], Tadashi Miwa[9], Hiroyuki Tsuchi[9], Kazumi Kitayama[9]

[1] MCM Consulting, Switzerland
[2] Monitor Scientific LLC, USA
[3] GNS Sciences, New Zealand
[4] University of Texas, USA
[5] University of South Florida, USA
[6] In2Earth Modelling Ltd, Switzerland
[7] University of Bristol, UK
[8] Kumamoto University, Japan
[9] NUMO, Japan

November 2009

Nuclear Waste Management Organization of Japan (NUMO)

Contents

1 Introduction

NUMO is responsible for the siting, development and operation of one or more deep geological repositories for the disposal of high level waste (HLW) and transuranic wastes (TRU) in Japan. The process is expected to take at least 15 years to reach the point of repository construction. During the period before this, NUMO will need to evaluate sites that emerge from the 'volunteer process' (whereby local communities have been invited to volunteer to be considered as potential hosts for the repository) and select a preferred site. This evaluation will involve initially surface based and then underground site characterisation work. Underground characterisation work will only take place at the preferred site. Prior to the surface based investigations, volunteer sites will have first had to pass a test of general suitability and NUMO will then have carried out a detailed, literature-based preliminary evaluation of suitability, prior to accepting them as 'Preliminary Investigation Areas' (PIAs). Because Japan lies in such a tectonically active region of the world on the Pacific rim (the so called 'ring of fire'), a key aspect of all these steps is consideration of the susceptibility of a site to future tectonic activity and tectonically driven processes and events.

In particular, the potential for volcanic and rock deformation impacts on a repository site needs to be considered at each stage of NUMO's siting programme. Whilst the nationwide evaluation factors for qualification (EFQs) for PIA acceptance are designed to remove clearly unsuitable sites from consideration, they cannot guarantee that, over the next tens of thousands of years, the risks of tectonic hazard for a chosen PIA will be acceptable. This is because large parts of Japan that are potentially suitable for siting are directly affected to varying extents by rock deformation, the peripheral impacts of volcanic activity or the possibility of new magma intrusion or volcanic activity. The EFQs were only intended as preliminary screening guidelines to prevent obviously poor candidates entering the siting process.

Consequently, an integration of additional and more refined techniques is required to evaluate sites that pass the EFQ test, so that NUMO can have a clear idea of the likelihood and potential impacts of tectonic events and processes at each PIA. The ITM project was designed to provide NUMO with such a methodology, based upon state-of-the-art approaches used internationally, developed and extended for the specific purposes of NUMO and the specific conditions of Japan: hereafter, we refer to it as the **'ITM Methodology'**.

1.1 Probability: the likelihood of future tectonic impacts on a repository

During the course of the ITM project, both NUMO and the Japanese regulatory agencies were considering how best to handle the evaluation of low probability, disruptive events (e.g. volcanic intrusion, fault rupture) and deformation processes that are discontinuous in time and magnitude in response to continuous regional strain, when carrying out safety assessments of geological repositories for radioactive wastes. Essentially, two approaches have been adopted internationally to address this situation:

- To calculate the health risk[1] to people in the future by combining the probability of a disruptive event occurring with its radiological consequences in terms of releases from a repository: simply, risk = probability x consequence. With this approach, regulatory standards or targets can be defined in terms of risk to an individual.

- To consider the impacts of a disruptive event and calculate the radiological doses[2] to people in the future and then, separately, to discuss the likelihood that this might happen (the so-called 'disaggregated' approach). With this approach, separate regulatory targets for radiation doses might be set for events (or scenarios) with

[1] Health risk is normally defined as the risk of death or serious genetic effects.

[2] Of course, a radiological dose can also be expressed in terms of health risk, by applying accepted dose-to-risk conversion factors.

different degrees of likelihood (often expressed qualitatively; e.g. ‘likely’, ‘less likely’, ‘highly unlikely’).

In either approach, an appreciation of probability is essential: in the first ‘risk approach’ a sound quantitative estimate will provide more confident estimation of risk; in the second, some form of quantification of ‘likelihood’ is needed to decide which category to place an event or scenario into.

The ITM methodology that has been developed in this Project is centred on a probabilistic approach. A probabilistic approach is seen by the ITM group as the only realistic means of quantitatively addressing the uncertainties in assessing possible hazards when there is marked variability in the spatial distribution, the timing, the intensity and the style of the volcanic and deformational events and processes being evaluated (for convenience, in this report, we frequently group these together within the general term ‘tectonic events and processes’). The probabilistic approach being developed is based upon and strongly supported by deterministic models of the underlying tectonic processes that lead to magma intrusion, volcanism and rock deformation.

NUMO is developing both the probabilistic ITM methodology and other, independent, deterministic approaches, in parallel projects that will eventually be deployed at volunteer sites when they arise. The weight that will be given to deterministic and probabilistic evaluation results will depend, to some extent, on the nature and the geographical location of these sites. It will also be influenced by the direction in which regulatory development move over the next few years. As noted above, however, some quantification or estimation of probabilities is required in any reasonable approach to safety evaluation and regulation. For the specific tectonic circumstances of Japan, this is especially relevant and important.

1.2 Using the ITM Methodology

The probabilistic ITM methodology will be used at three important stages of NUMO’s siting programme:

- SITING STAGE 1: during the literature survey (LS) stage when potential PIAs are being assessed. The ITM methodology will use currently available information to allow comparison of sites in terms of confidence that they are likely to prove acceptable with respect to tectonic impacts.

- SITING STAGE 2: during the planning of the PIA site investigations, to identify geoscientific information requirements that will be needed to refine the Stage 1 analysis.

- SITING STAGE 3: at the point where PIAs are being evaluated and compared in order to select a preferred site (or sites) for detailed investigation (as DIAs).

The ITM project is mainly concerned with Stages 1 and 2. As will be seen from this report, the methodology is currently focussed on evaluating comparative hazards of small (25 km^2) areas within a regional or sub-regional context of 100,000 to 10,000 km^2 (see Figure 1.1). This is partly because the project originally developed to compare several possible alternative volunteer sites that might arise within a region. However, it is clear that regional to sub-regional scale assessment of tectonic hazard will also be required even for single sites.

Application of the methodology in Siting Stage 3 is several years into the future and it is expected that it will be most efficient to carry out any necessary updates/refinements on a region-specific basis during the PIA investigations when NUMO has narrowed down to a group of sites. The ITM project has involved methodology development and testing only and does not include actual deployment for volunteer sites/regions.

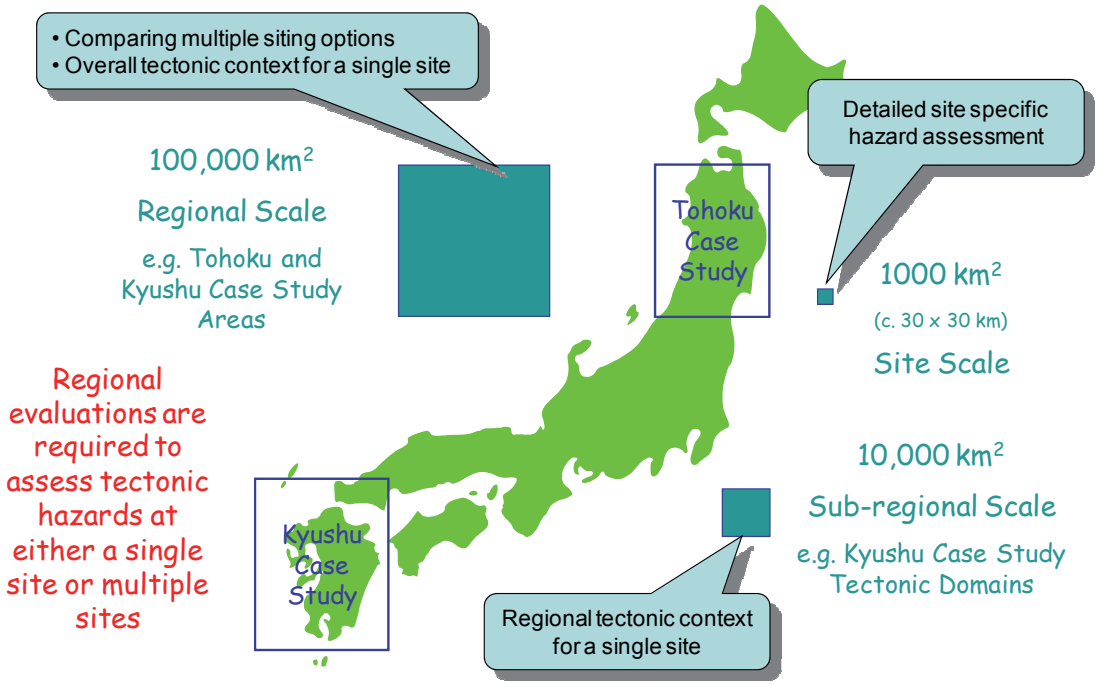

Figure 1.1: The ITM Methodology is applied at the regional to sub-regional scale, whether comparing alternative sites or assessing the tectonic hazard for a single site.

The overall structure of the ITM methodology is described in Section 2 of this report and consists of:

- assembling nationally available data and alternative models of the nature, causes and locations of tectonic processes and events;
- using probabilistic techniques to evaluate the likelihood and scale of future tectonic processes and events, shown as a function of their type and geographical distribution;
- feeding information on these potential likelihoods and impacts to NUMO's performance assessment team so that feedback can be provided on repository performance under tectonic stress;
- providing clearly justified and traceable input to decision-making on consequent site suitability.

For convenience, the methodology for rock deformation and volcanic hazards assessment has been applied as two parallel tasks. This recognises the fact that, although the concept of each approach as shown above is similar, in some parts of the methodology they differ significantly in detail. Consequently, it was found that two teams with different specialities (structural, geophysics and tectonics specialists; volcanologists) worked efficiently in parallel. However, it is most important that, if carried out in this manner in future, the two 'discipline' teams integrate their work frequently, as there are clear overlaps in the processes being evaluated (e.g. magma intrusion has an impact on rock stress regimes and vice versa). NUMO will need to ensure that such integration is carried out effectively when the methodology is applied to 'real' sites.

The methodology was first tested during its development by means of a Case Study of the Tohoku region of northern Honshu (Chapman et al., 2009). The first Case Study looked into the varied strain response of the crustal plate to subduction of the Pacific Ocean plate (the key current tectonic driver for much of Japan) and the mechanisms that underlie the apparent clustering of Quaternary volcanoes in much of Honshu.

The present report covers the final results of a second Case Study designed to further the development and testing of the methodology and look at a tectonically quite different setting in Japan. This Kyushu Case Study was developed specifically to look at the more complex (than Tohoku) interrelationship of rock deformation and volcanism in a region characterised by three or four domains responding to identifiably different tectonic mechanisms. In contrast to Tohoku, it is also an area with significant monogenetic volcanism. During the transition from the Tohoku to the Kyushu Case Studies, the ITM Methodology had also been updated and improved.

This report is a compilation of material provided by research groups from Japan, New Zealand, Switzerland, the United Kingdom and the United States.

1.3 References for Section 1

Chapman, N., M. Apted, J. Beavan, K. Berryman, M. Cloos, C. Connor, L. Connor, O. Jaquet, N. Litchfield, S. Mahony, W. Smith, S. Sparks, M. Stirling, P. Villamor and L. Wallace (2009). Development of Methodologies for the Identification of Volcanic and Tectonic Hazards to Potential HLW Repository Sites in Japan: The Tohoku Case Study. Nuclear Waste Management Organisation of Japan, Tokyo. Technical Report: NUMO-TR-08-03. 135 pps.

2 The ITM Methodology Road Map

This Section provides an outline of the overall concept and methodology that has been developed by ITM in the form of a 'road map'. The methodology development is essentially complete and this road map represents a description and checklist for application to volunteer sites by NUMO staff and contractors in Siting Stages 1 and 2.

As discussed in Section 1, the methodology should be regarded as a living entity, as it must respond to new scientific knowledge and techniques that will arise over the next few years. Consequently, it will have to be revisited from time to time. This is especially true with respect to application in Siting Stage 3 (at the point where PIAs are being evaluated and compared in order to select a preferred site, or sites, for detailed investigation as DIAs), as this may be five or more years into the future.

2.1 Outline of the ITM Methodology

The overall structure of the ITM methodology consists of:

- assembling nationally available data and alternative models of the nature, causes and locations of tectonic processes and events;
- using probabilistic techniques to evaluate the likelihood and scale of future tectonic processes and events, shown as a function of their type and geographical distribution;
- feeding information on these potential likelihoods and impacts to NUMO's performance assessment team so that feedback can be provided on repository performance under tectonic stress;
- providing clearly justified and traceable input to decision-making on consequent site suitability.

A **probabilistic** approach has been selected for the ITM methodology as it is seen as the only realistic means of addressing the uncertainties in predicting possible hazards when there is such variability in the spatial distribution, the timing, the intensity and the style of the volcanic and deformational events and processes being evaluated.

Naturally, the probabilistic approach being developed is based upon and strongly supported by **deterministic** models of the underlying tectonic processes that lead to magma intrusion, volcanism and rock deformation.

For convenience, the methodology for rock deformation and volcanic hazards assessment has been applied as two parallel tasks. This recognises the fact that, although the concept of each approach as shown above is similar, in some parts of the methodology they differ significantly in detail. Consequently, it was found that two teams with different specialities (structural, geophysics and tectonics specialists; volcanologists) worked efficiently in parallel. However, it is **most important** that, if carried out in this way in the future, the two teams integrate their work frequently, as there are clear overlaps in the processes being evaluated (e.g. magma intrusion impacts on rock stress regimes and vice versa). NUMO will need to ensure that such integration is carried out effectively when the methodology is applied to 'real' sites.

The broad structure presented above is shown in more detail in the top-level 'road-map' in Figure 2.1. It comprises a series of eight **Steps**, which are described in Section 2, distinguishing between the 'rock deformation' approach and the 'volcanic' approach, where they involve significantly different activities.

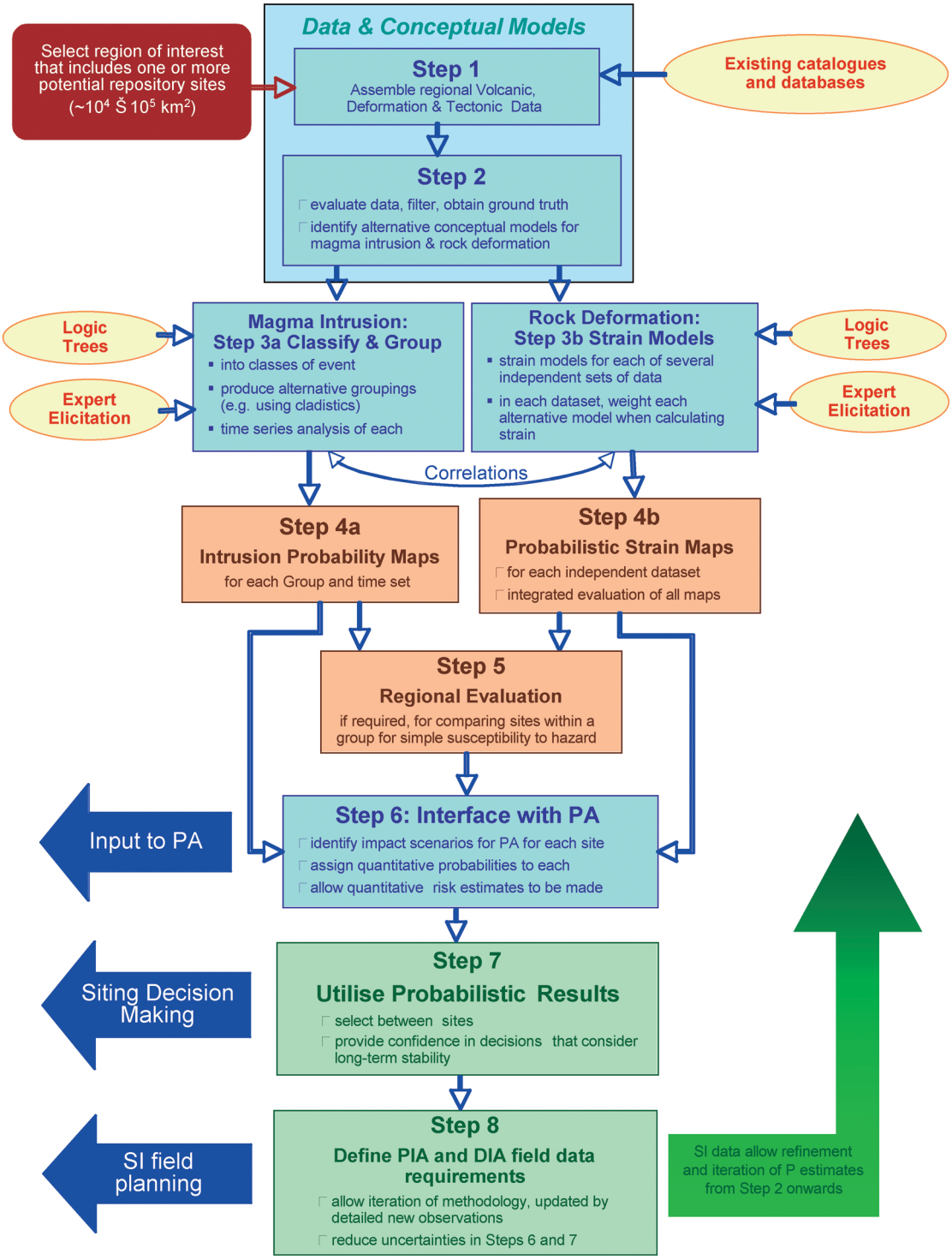

Figure 2.1: The Steps in the ITM methodology, shown as a top-level road-map.

There is considerable depth and detail to the application of the ITM methodology in each of the Steps. This road-map description is intended to provide a simplified overview. The complete detail of what is involved in each analysis is described in the two project Case Study reports.

2.2 The Steps in the ITM Methodology

STEP 1: Assembling the Data

Step 1.1: Define the region of interest: The region of interest should be defined. For deployment of the ITM methodology in **Siting Stage 1** (the LS stage), we expect that the region of interest identified around a site, or group of nearby sites, will be ~10^4 - 10^5 km^2. The larger area is more appropriate when comparing the situation of several siting options. This is based upon our experience in the Case Study areas. Regions need to be large enough both to contain a statistically large enough number of features that are manifestations of the processes being evaluated (e.g. volcanic edifices) and to contain a good spread of data-points for modelling these processes (e.g. GPS stations). They should also be internally consistent, at a rough approximation, with respect to tectonic regime. For example, in the Kyushu Case Study, it was found that the large overall region considered (approximately 100,000 km^2) had to be broken down into several intermediate blocks representing tectonically 'coherent domains', ranging in size from c. 20,000 to c. 50,000 km^2. A region of 10^4 km^2 is at the lowest end of the size range that is likely to be useable and the aim should be to have a region of at least some tens of thousands of square kilometres to ensure that the statistical approach adopted is meaningful.

For deployment at a single site scale (Stage 3: not considered in depth in the ITM project), the methodology is likely to require downscaling to 10^4 km^2 or perhaps 10^3 km^2, the scale depending upon the complexity of the tectonic setting. This has not been done in the Case Studies and would require further test application and probably some modification of the methodology. The regional scale deployment of the methodology described below is based upon estimating probabilities within 5 x 5 km areas. For site scale deployment, a finer grid will be required.

Step 1.2: Data gathering: Following definition of the region of interest, relevant data are obtained from the literature to constrain possible models of magma intrusion and rock deformation. The principal source data at Siting Stage 1 are likely to comprise a limited number of national databases, including the following:

- geological maps;
- uplift and subsidence data;
- topographic maps (onshore and offshore);
- gravity and magnetic maps;
- volcanic edifices/features location, nature and age (Catalogue of Quaternary Volcanoes);
- national onshore and offshore active fault map;
- recorded distribution of seismic events (locations, magnitudes, depths);
- velocity field measurements derived from GPS for all monitoring stations.

Additional geological and geophysical information, such as geological maps, heat flow data and interpretations of the geological, structural and tectonic histories of the region, are needed to support the development of conceptual models of the processes of interest (in **Step 3**). There may also be relevant scientific publications on specific volcanoes or tectonic features, and more generic research publications on relevant processes. This additional information should be augmented by discussions with academic and other research organisations in Japan. Such discussions will be an extremely important part of ensuring both the currency of the models used and the involvement of the national (and international) geosciences community.

When the methodology is applied later in the siting programme, for example, to evaluate tectonic hazard in more detail at a site already identified as a PIA, the integration of LS data from existing catalogues and databases with site investigation data gathered both in the PIA

area and in the area of interest around it, will be an important activity. This will need to be done carefully and consistently, because the probabilistic evaluations may be being used at this stage to support quantitative estimates of radiological impacts.

STEP 2: Sorting the Data and Identifying Alternative Conceptual Models

Step 2.1: Data Sifting and Ground-truth: The data need to be evaluated and sifted. The databases used have not been gathered for the specific purposes of the ITM methodology, so they are not necessarily organised in an appropriate fashion and they may not contain data in the form in which they will be used in **Steps 3 and 4**. The data also need to be evaluated for reliability and consistency. In cases where inconsistent or anomalous data are identified, this needs to be taken into account in the assessment of uncertainty. Such issues have been found to be the case for the Catalogue of Quaternary Volcanoes, where mapped volcanic features include a wide range of different structures with differing significance in terms of processes of magma generation and intrusion. Consequently, this Step requires a close evaluation of what the data actually represent and whether datasets are internally consistent and of uniform quality. It may be necessary to develop derivative datasets that reduce or remove anomalies and inconsistencies, but it is important that such changes are transparent and carefully documented.

It will be essential to obtain 'ground truth' on observations included in some of the databases (but not all: e.g. GPS strain data). For the highest level of confidence in the statistical methods used in **Step 4**, 'ground truthing' is likely to involve a significant effort in a minimal resurveying of the region of interest (e.g. visits to all volcanic structures to ensure that their correct classification is known). NUMO needs to take this into account in its planning: even though field visits to prospective PIAs may be excluded at Siting Stage 1 (LS), regional observations by specialists (even 'drive-by' observations) would likely be most valuable.

An equivalent example for the rock deformation datasets is the requirement to remove the large-scale, elastic subduction-related interseismic overprint from the GPS velocity field. Only the residual strain is considered to be the 'signal' of interest, as it is related to faulting in the crustal rocks of the Japanese islands. It is therefore of use in developing maps that show differential strain for 'cells' across the region of interest that can be linked to localised rock deformation processes. The ITM methodology uses 5 x 5 km cells, as these 25 km^2 blocks represent a representative area to contain a repository that is likely to have an approximate footprint of 10 km^2, plus space around its margins, where there may be additional access works, for example. Clearly, other sizes of cell could be used in an analysis.

Step 2.2: Underlying Conceptual Models: Underlying conceptual geological models need to be identified (or developed) to explain the distribution of features (volcanic edifices) and different styles of rock deformation. These conceptual models have been developed during the ITM work to date. In simple terms, the models are as follows:

- **Distribution of polygenetic volcanoes:** during the Quaternary, and for the next tens of thousands of years (up to ~100 ka) this is controlled by variable magma generation potential in the mantle and crust overlying the subducting oceanic plates. The origin of this variability is not fully understood but is manifest in some structure to the distribution of these volcanoes; for example, 'clusters' of volcanoes with intervening 'gaps' in some areas. The distribution of clusters and gaps is correlated to varying extents to gravity, basement topography and the seismic tomographic structure of the crust and mantle wedge beneath the Japanese archipelago. There is also evidence for temporal variations in volcanism that need to be taken into account in the assessment of future volcanism, which is also not fully understood.

- **Distribution of monogenetic volcanoes:** this aspect of the ITM methodology will not be fully developed until the Western Japan – Kyushu Case Study is completed. One possibility is that locations of monogenetic volcanoes are influenced by local stress variations related to structure. Section 3 of this report discusses progress to date: to date, a volume-predictable model appears to work best, and we have developed a model to suggest that in compressional tectonic settings with constant

magma supply, monogenetic volcanism should be generally volume-predictable. In other words, the exact timing of future eruptions is uncertain, but in a given time interval a given volume of magma should erupt.

- **Regional and Local Strain Budgets:** the upper crustal rocks of the Japanese archipelago are undergoing progressive deformation as a result of horizontal and vertical strain responses to dynamic plate tectonic forces. The amount and style of deformation varies from region to region depending on the geological formations present and the location with respect to the major plate boundaries and other large-scale deformation zone features, such as major (>100 km long) strike-slip fault zones (including the distance from such boundaries/features). The deformation can vary from compression to extension and subsidence to uplift. The resultant strain is manifest as faulting (episodic movement along Quaternary active faults), folding and distributed deformation. The overall strain 'budget' for an area is accessible using a range of indicators, each of which characterises different strain manifestations: GPS data on relative surface movements; coseismic movements, accessible through the seismological database and surface uplift/subsidence rate (which can be combined with other indicators to give an estimate of surface deformation, or 'tilt').

There are also more local controls on strain and stress related to geological and structural heterogeneities. There may be local feedbacks between faulting, deeper ductile deformation and magmatism that results in local departures from regional variations related to plate scale processes.

Following Step 2, the volcanic and rock deformation analyses take separate paths, defined here as **Steps 3a to 4a** for the magma intrusion analysis and **Steps 3b to 4b** for the rock deformation analysis.

It is expected that there would be some feedback to Step 2 from Step 3b. There will be a requirement to update the conceptual models after strain rates are estimated. Feedback between modelling and data are an important aspect of ensuring that alternative models are not overlooked.

STEP 3a: Classifying and Grouping Magma Intrusion Features

For the evaluation of possible future magma intrusion in areas that have not been affected by intrusion in the last ~2 Ma, it is first essential to classify the indicators of past intrusion (starting with the mapped volcanic features in the Quaternary catalogue).

Depending on the area being considered, different means of classification may be reasonable and the first step is to carry out a **'classification analysis of events'** to determine how best to group the intrusion indicators. No internationally accepted scheme of volcano classification exists, so the ITM methodology developed a cladistic approach for the Tohoku Case Study (Chapman et al., 2009) as well as exploring alternative ways of defining volcanic events. In the Kyushu Case Study, where the tectonic environment and styles of intrusion were more complex, classification needed to consider groupings of intrusions based on geochemical affinities of magmas and correlations with tectonic structures that control the spatial occurrence of some groups of intrusion. In this case, there is an even stronger need to ensure that volcanic assessment is integrated with the rock deformation and tectonic structural assessment.

Step 3a.1: Classification Analysis:

Several approaches are possible to assign intrusion events to genetically related groups that can be treated in a consistent manner statistically (i.e. 'event definition'). The use of expert elicitation will greatly improve confidence in the classification schemes developed and, although the method was not trialled during the ITM project, logic trees represent a well-established approach to depicting the results of expert elicitation.

A cladistic approach has been developed to facilitate this classification, which is based on standard taxonomic approaches used for species classification in the biological sciences and for which analysis software is readily available. The methodology is described more fully in an ITM project publication (Hone et al., 2007). In simple terms, it involves defining characteristic properties (such as size, morphology, age, chemical composition, intrusive or eruption style) to each mapped feature and then using a software analysis package (PAUP) to assess all possible ways of grouping the features using these characteristics. The simplest possible groupings that explain the most characteristics are selected (the parsimony principle, or Ockham's razor). The different groups are called clades, although we use the term 'Alternative Groups' for simplicity and because techniques other than cladistic analysis can be used to form alternative groups. In the Tohoku Case Study, the cladistic method was found to work well for the polygenetic volcanoes and to provide a deeper understanding of the strengths and limitations of the volcano database.

Step 3a.2. Database analysis. The database of volcanic features is then analysed to identify alternative data bases, which can be used in the probabilistic analysis. This step involves using the clade groups and field data to verify alternative groupings of volcanoes and volcanic features.

Step 3a.3: Time-series analysis: It is then necessary to carry out a time series analysis of each alternative database to assess whether they display different periodicity (dormancy and activity) and whether this periodicity is structured (i.e. related to eruption history, rather than being random), which is used in **Step 4a**.

Step 3a.4: Sensitivity analysis: It is also important to test the sensitivity of the groupings to the size of the region considered (by extending or reducing the area the number of edifices included is increased or reduced and the statistical groupings may change) and by adding new 'synthetic' volcanoes: a large change in group characteristics could indicate instability in any model invoked to explain the distribution of volcanoes.

The sub-steps in Step 3a can thus be represented as shown in Figure 2.2**.**

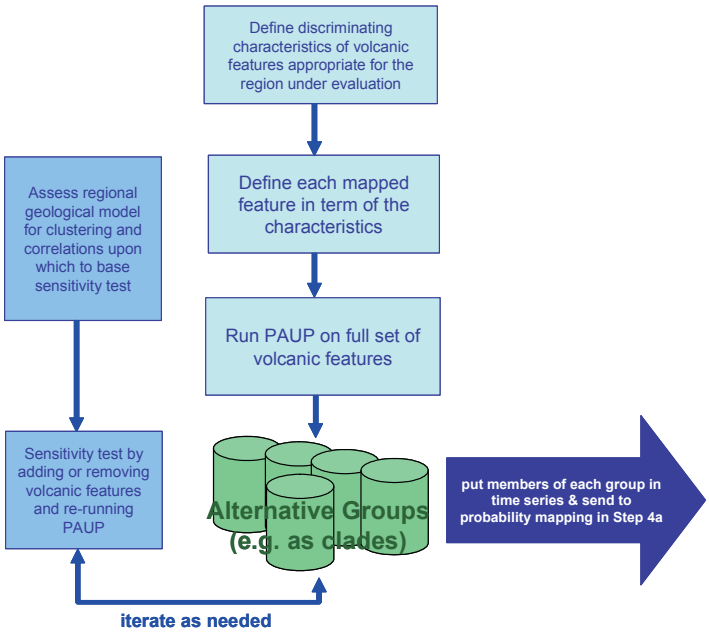

Figure 2.2: Flowchart showing sub-steps used in Step 3a.

STEP 3b: Developing Strain Models and Estimating Strain Rates for Each

For rock deformation, the objective is to calculate strain rates across the region of interest using independent data sources that reflect widely different time averaging: GPS derived

strain (years), surface deformation (tens of thousands of years) and seismic strains from the seismic moment of earthquakes (centuries). These can then be compared. In **Step 4b** these are presented as strain maps.

Each data source may indicate strains that are the result of one or more processes, for each of which there may be alternative tectonic models and interpretations (e.g. boundaries of regions that can be defined as discrete tectonic blocks, dips of major fault zones, amount, degree and depth of subduction coupling). The way that strain is calculated from the raw data will need to account for the relative contributions of these different processes, factoring in the inherent uncertainty introduced by having alternative conceptual models. The contribution from different processes will thus have to be estimated by expert judgement, depending on the degree of belief in the importance of different processes/mechanisms (essentially, reflecting the alternative conceptualisations of what is driving rock deformation in the region).

Step 3b.1: Defining tectonic blocks: A first sub-step in Step 3b is to consider whether the region of interest (or an even larger area if appropriate) can conveniently be divided into stable rock blocks that behave internally in a relatively homogeneous way or respond in a similar way to external, large scale tectonic driving processes. This assessment forms the basis for the subsequent development of strain models, and there may be alternative ways of defining such blocks, which affects the number of models developed.

Step 3b.2: Assembling alternative conceptual models in a Logic Tree: The approach adopted in the ITM methodology is to use Logic Trees to bring together all alternative conceptual models identified; an example of which is shown in Figure 2.3.

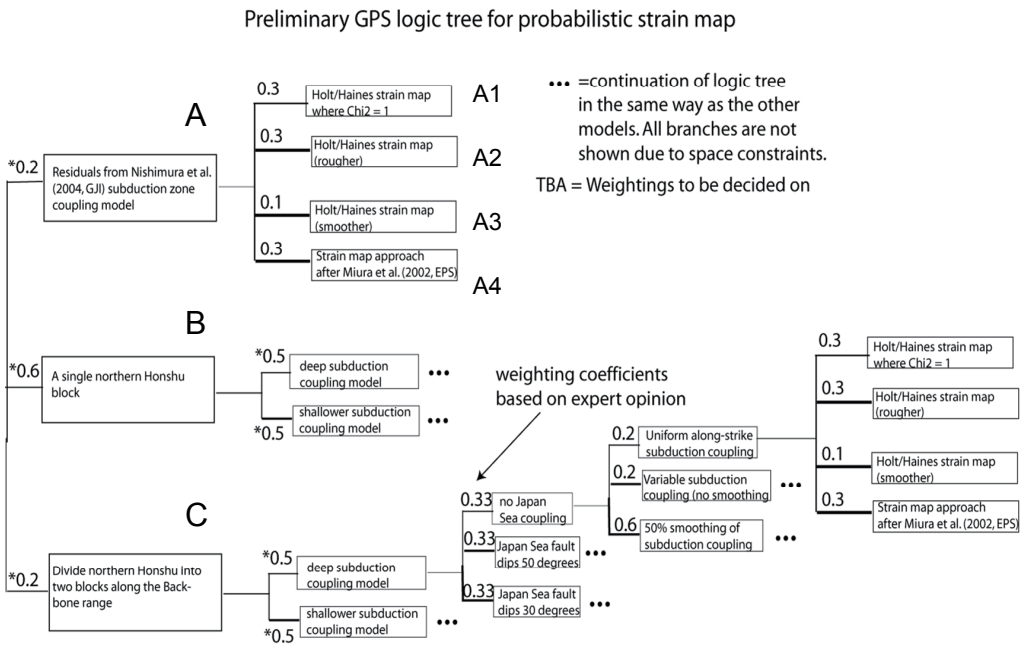

Figure 2.3: Example of part of a Logic Tree used in Step 3b to calculate strains from GPS data for the Tohoku Case Study area (Chapman et al., 2009).

As can be seen in Figure 2.3, the Logic Tree is constructed by asking questions of the form:

- How many alternative explanations (models) could describe strain in this block?': the answer requires a certain number of starting nodes to be established in the tree (A, B, and C in Figure 2.3).

- If Model A is correct, what are the alternative ways of describing its impact on deformation?': the answer produces branches from the node for Model A (A1, A2, A3 and A4 in Figure 2.3).

Continuing in this fashion a tree is generated that incorporates as many alternative conceptualisations of deformation mechanisms and associated uncertainties as are deemed feasible. Following down any one branch to the end defines how strain will need to be calculated for that particular set of model assumptions.

Use of expert judgement: Expert judgement, elicited from a group of experts in Japanese tectonics at a workshop, is factored into the construction of the tree to ensure that it is sufficiently comprehensive of alternative models. The experts then contribute by agreeing weightings for each branch (expressing their degree of belief in the validity of each alternative conceptualisation).

Each strain indicator requires its own logic tree, in order to calculate strain rates. In summary, the three indicators used to date to estimate strain as follows:

- Surface deformation and active faults = mm/km/a strain. The period over which this indicator has 'recorded' strain is ~10,000s years.
- Gradients in GPS velocity = mm/km/a strain. The period over which this indicator has 'recorded' strain is ~10s years.
- Recorded earthquakes = seismic moment + Kostrov equation[3] = strain. The period over which this indicator has 'recorded' strain is ~100s years.

Despite the fact that these indicators record strain over many orders of magnitude of time, the processes that they are recording are widely considered to have been stable in magnitude and direction for about 100,000 years.

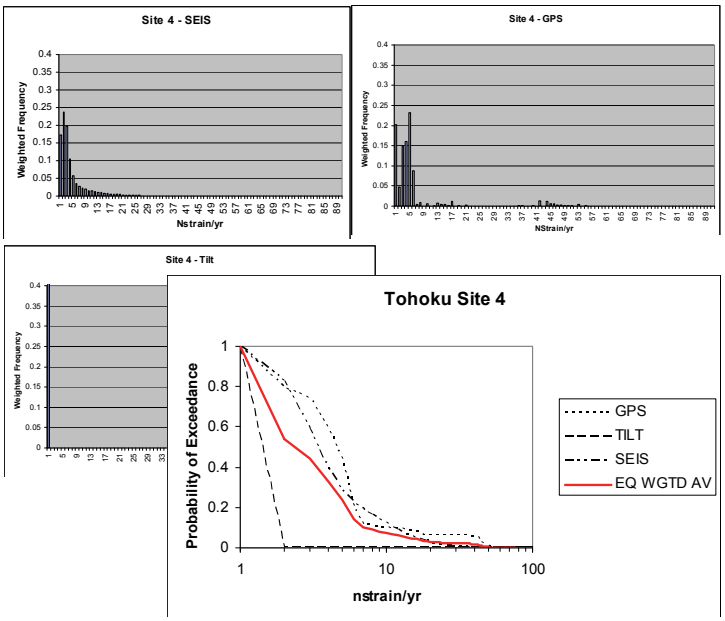

Figure 2.4: Strain rate (nanostrains/a) histograms for multiple model realisations for one of the 'example locations' in the Tohoku Case Study area, calculated (clockwise, from top left) from seismic data, GPS residuals and tilt data. The larger diagram shows the results compiled on a cumulative probability plot, showing the probability of exceeding any given value of strain. The red line is the equally weighted average.

[3] The Kostrov equation relates the seismic strain rate to the sum of the seismic moment tensors of all the earthquakes occurring in a given volume of the crust during a given time-interval.

Step 3b.3: Calculating Strain Rates: For the GPS logic tree example shown in Figure 2.3, there were 148 different strain models (branches) for the Tohoku Case Study. The strain rates for each of these models are calculated separately and as a weighted average. A histogram can be produced of the frequency of calculated strains of a given magnitude at a given location, using all the model results for a particular indicator, which can then combined with the same results from the other indicators (see Figure 2.4). The Step 3b sub-steps in setting up and using the logic trees are outlined in Figure 2.5.

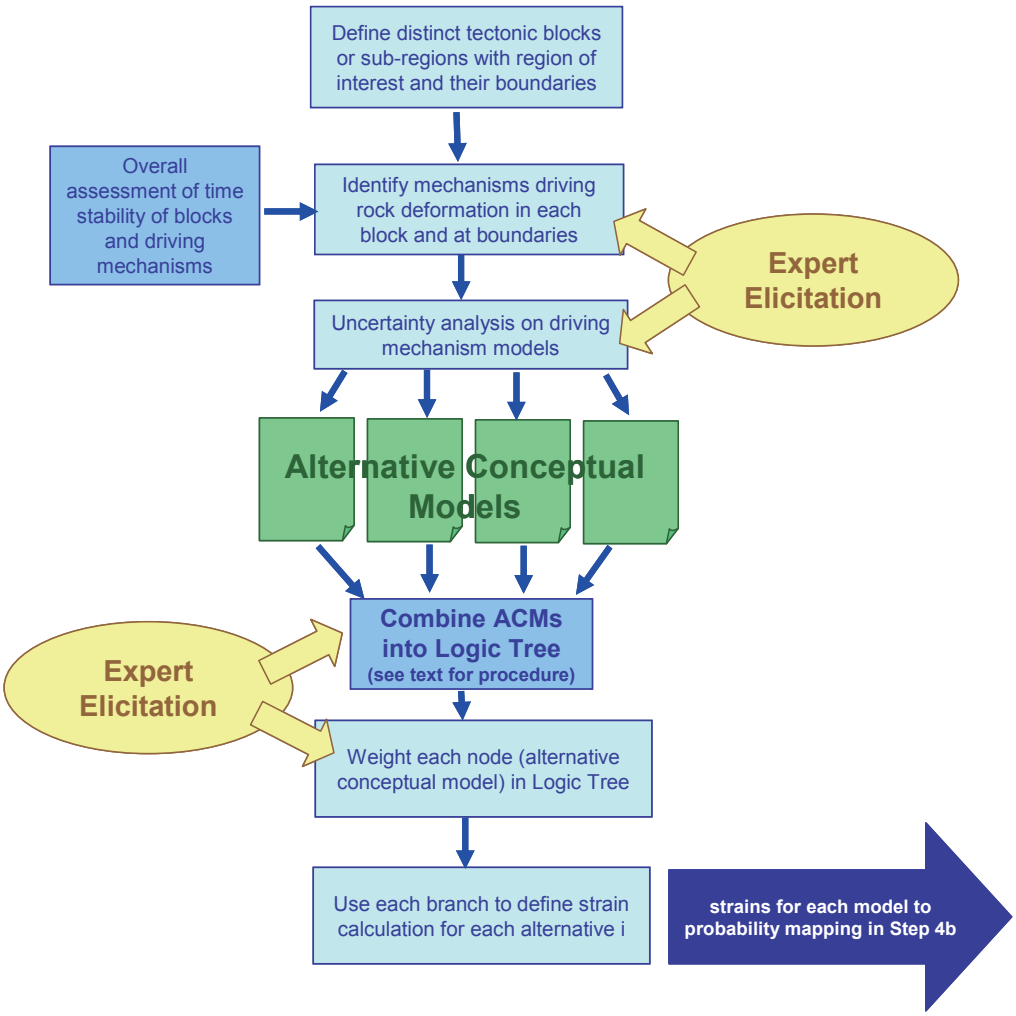

Figure 2.5: Flowchart showing sub-steps used in Step 3b.

STEP 4a: Magma Intrusion Probability Maps

Step 4a.1: Assessing Correlations: The first step in producing probability maps is to see how far the spatial distribution of volcanoes can be correlated with topographical and geophysical indicators of crustal processes. This provides evidence that distribution is not simply random. The check can be made both for all volcanoes in the region of interest and for the groupings derived from **Step 3a**. The probabilities and related uncertainties can then be suitably weighted to reflect these correlations. This sub-step may need to utilise expert elicitation.

As an example, in the Tohoku Case Study, the broad distribution of volcanoes is correlated (although by no means perfectly) to the isostatic gravity anomaly map of the region. The isostatic gravity anomaly map is produced by combining the Bouguer gravity anomaly map with the topographic map, making various assumptions. In the Tohoku study it was calculated assuming a thin elastic crustal plate 10 km thick. The isostatic anomalies reflect magma

generation potential, with the rate of magma accumulation at the intra-crustal Conrad discontinuity and, possibly, the rate of magma flux at the surface (hence the likelihood of future volcanism) being indicated by isostatic anomalies. This can be tested by plotting the historic magma production rate against the isostatic anomaly per unit area, but this has not so far been tested in the ITM methodology development.

In Kyushu, the distribution of volcanism is closely tied to tectonic strain, manifest in the distribution of active faults, GPS-derived strain and the distribution of historical seismicity. On local scales, some volcanoes are closely associated with fault zones (Figure 2.6). Regionally, volcanism in Kyushu closely follows regional tectonic structure. For example volcanoes of the Northern Extensional arc are closely associated with the Shimabara-Beppu Graben. ITM methodology calls for development and implementation of probabilistic models that reflect these geological patterns.

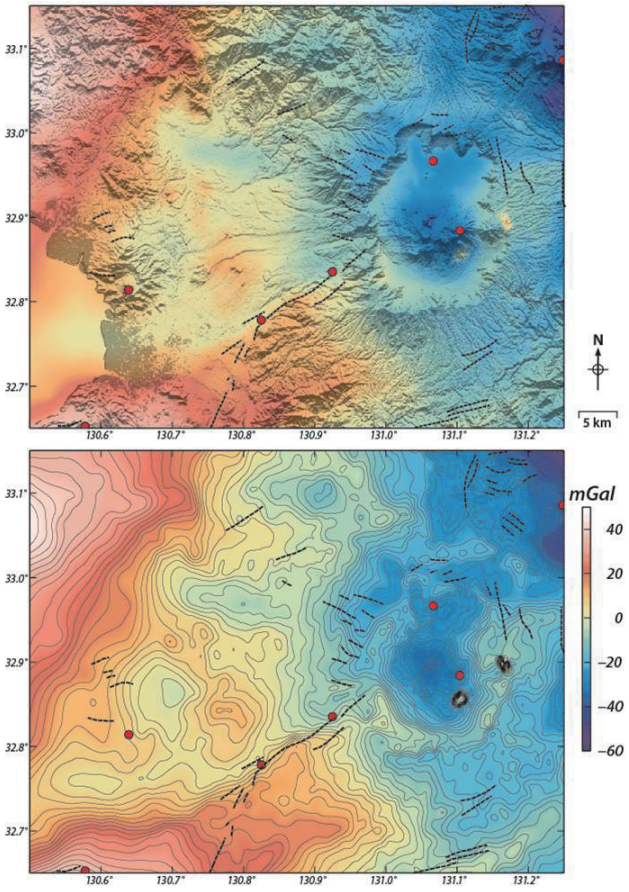

Figure 2.6: Regional gravity about Aso caldera and the SW Simabara-Beppu graben. Two small-volume Quaternary volcanoes (Akai and Omine) are found SW of Aso along graben-bounding fault. Active fault traces (dashed lines) differ in some areas from distribution of crustal-scale gravity anomalies. Volcanism in this area provides a clear example of volcano-tectonic interaction that is common in Kyushu.

Step 4a.2: Calculating Probabilities of Magma Intrusion: For the probabilistic mapping, three types of probability can be estimated:

- P1 – the probability of a volcano edifice forming in the region of interest during the period of interest (e.g. a probability of 2 x 10^{-4} for a period of one year)
- P2 – the probability that a volcano will form in a specific area within the region of interest, such as a 5 x 5 km block, or a region extending to 15 km beyond the boundaries of a PIA (e.g. a probability of 1 x 10^{-4} for an area of 25 km^2)
- P3 – given that a volcanic event occurs in this specific area, the probability that it will impact the repository site itself.

Then, the probabilistic volcanic hazard is given by P1 x P2 x P3. A variety of well-developed statistical methods is available for estimating such probabilities, and the estimations can be done either for all magma intrusion modes or for the various alternative groupings defined in **Step 3a**. For subsequent assessment of impact scenarios in **Step 6** it is important to assess the probability of different types of event occurring, so looking at each alternative group is a primary strategy of the ITM methodology.

The ITM methodology produces (principally) estimates of P2, in the form of regional probability maps, as these are of most use for assessing specific locations or sites. The same 5 x 5 km squares are used as for the rock deformation evaluation. Estimation of P3 will be a site-specific issue for Step 6, which will need to look at both the structural and geological properties of the location, the type of intrusion being considered and the repository concept that would match the site.

Geostatistical and Bayesian methodologies provide a way to assess conceptual, spatial and parametric uncertainty. The methods used in the ITM methodology are:

- **Kernel Method:** Generation of a non-homogeneous distribution map, using a Gaussian or Epanechnikov kernel method, with an applied smoothing function (with the effect of a range of bandwidths tested). The method is subject to uncertainties in calculated probabilities at any given point on the regional map, principally caused by local variability of data density (or overall sparsity in terms of the number of volcanic events over the last 2 Ma). These uncertainties vary from point to point. Figure 2.7 shows an example probability map for a small sub-region of the Tohoku Case Study area (Chapman et al., 2009), with the two green locations selected to show how uncertainty can vary depending on proximity to an existing cluster. Figure 2.8 shows example results for different alternative groupings of volcanoes. It can be seen that the optimum bandwidth for the kernel function is different for the two groups.

  As discussed under **Step 3a**, the introduction of additional 'synthetic' volcanoes can help quantify this uncertainty and the ITM methodology is also testing a Monte Carlo sampling approach for estimating uncertainty in probability at a given site for a given data set and a given smoothing bandwidth. An alternative method under test is to use adaptive kernel functions, where the value of the kernel depends on the local data density. The Monte Carlo approach is shown in the flow chart in Figure 2.9.

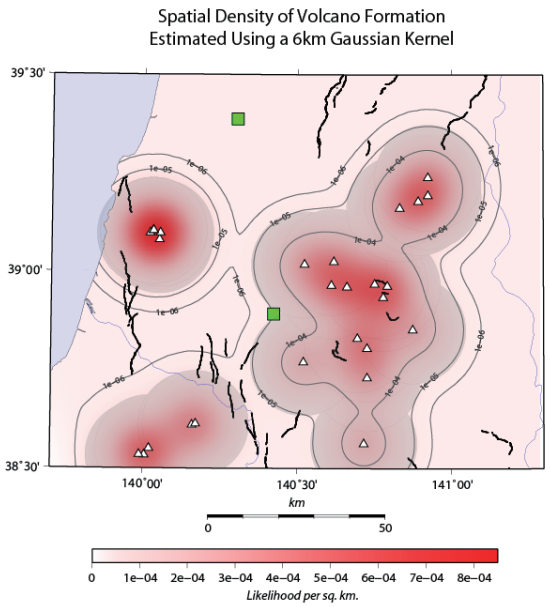

Figure 2.7: Spatial density of likelihood of new volcano formation in a sub-region of the area used in the Tohoku Case Study (Chapman et al., 2009). This realisation uses a 6 km Gaussian kernel and the probability refers to a period equivalent to that over which the mapped volcanic features were formed – about 2 Ma.

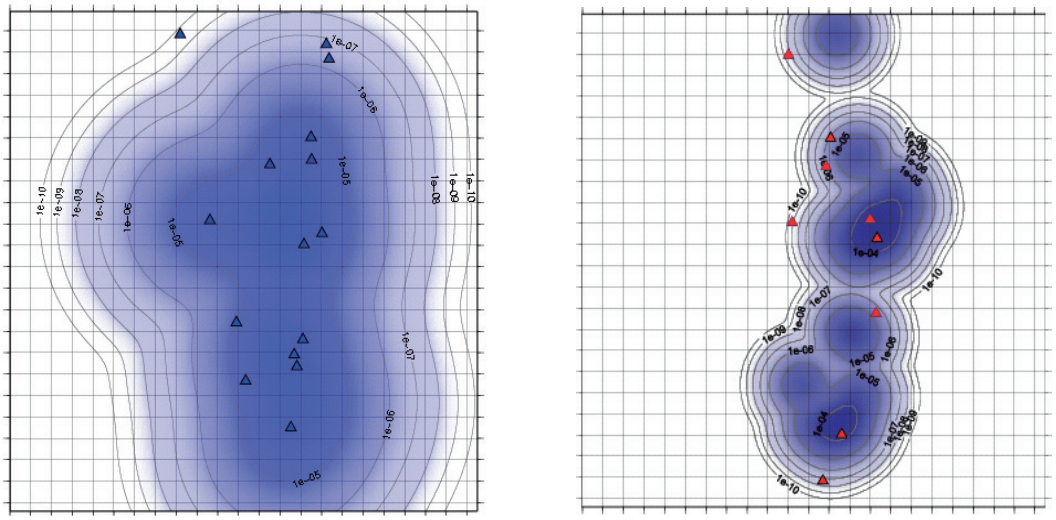

Figure 2.8: Probability contours (per year) for new volcanoes in part of the Tohoku Case Study area, showing the different kernel bandwidths that are required to provide an acceptable model for two different groups of volcano: left, explosive volcanoes, with a 33 km bandwidth; right, extrusive volcanoes, with a 12 km bandwidth.

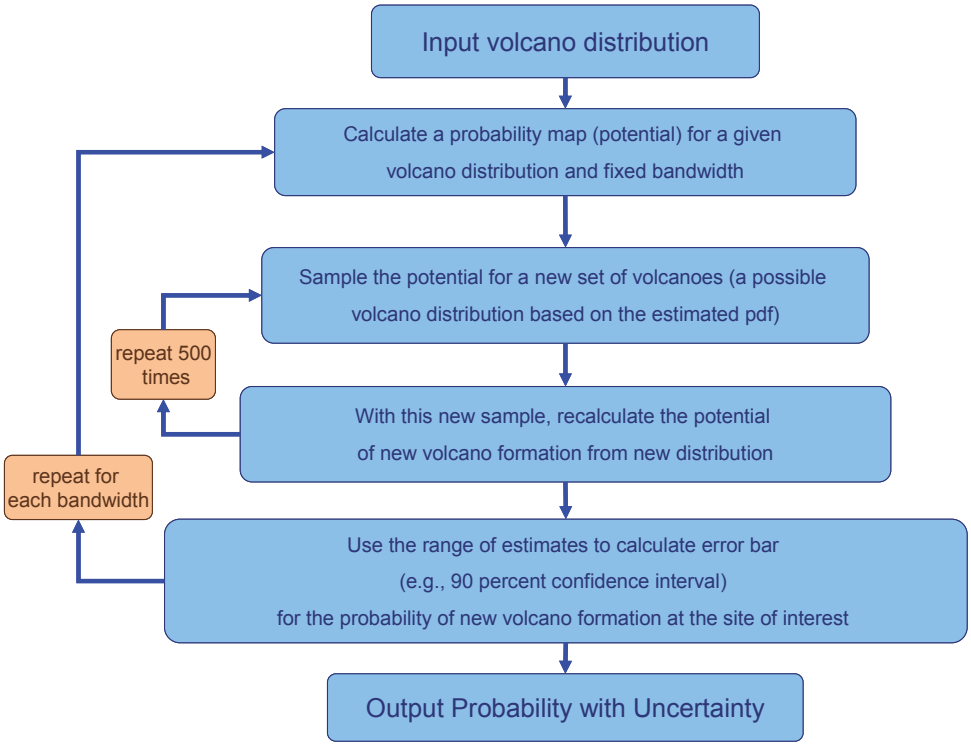

Figure 2.9: Flowchart showing the Monte Carlo sampling approach that is being developed to assess uncertainties in non-homogeneous probability mapping.

- **Cox Process Method:** This multivariate approach is able to use a range of different set of geoscientific data – for example, 3-D seismic velocity tomography of the crust and upper mantle, using a conceptual model where the tomographic features are related to magma generation potential. This is supported by the correlation of these structures with specific volcanoes or with Quaternary volcano clusters.

  The basis of the approach is to consider the potential for volcanism in an area to be randomly structured: even though our geological knowledge suggests there to be correlations with geological and geophysical data, randomness is brought on by our inherent uncertainty. Unlike Poisson distributions, which assume a constant potential with time for new volcanoes, and the non-homogeneous approach (see above: the other method used by the ITM methodology) which assumes a deterministic potential conditioned by selection of a kernel value, the Cox process approach assumes the potential to be entirely stochastic. The detailed methodology used is described by Jaquet et al. (2008a; 2008b; 2009).

  The Cox process approach allows the estimation of a volcanic potential map, which is then statistically correlated to the seismic tomography map, in order to produce a probability map by Monte Carlo simulations. The overall approach is shown in Figure 2.10, while Figure 2.11 shows one of the results from the Tohoku Case Study.

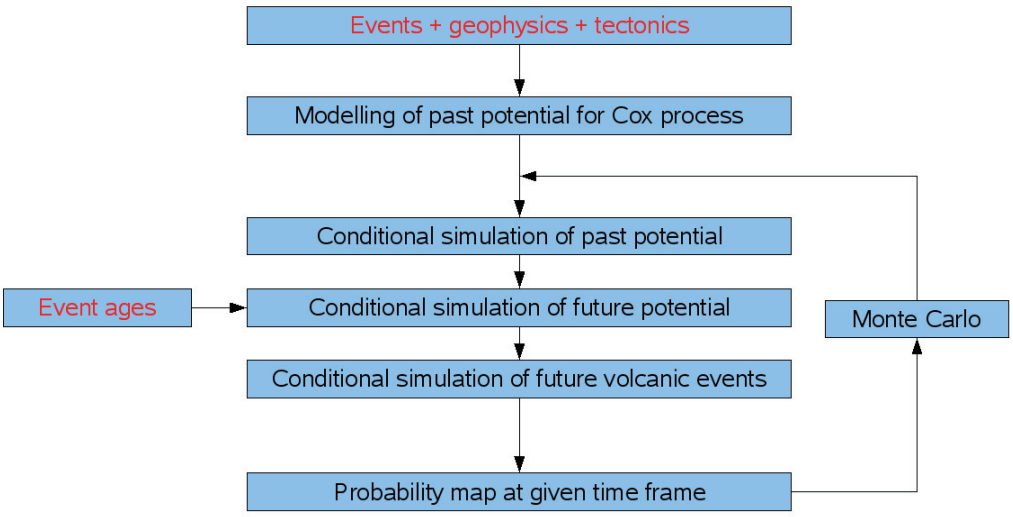

Figure 2.10: Flowchart showing the Cox process approach used to derive volcanic probability maps.

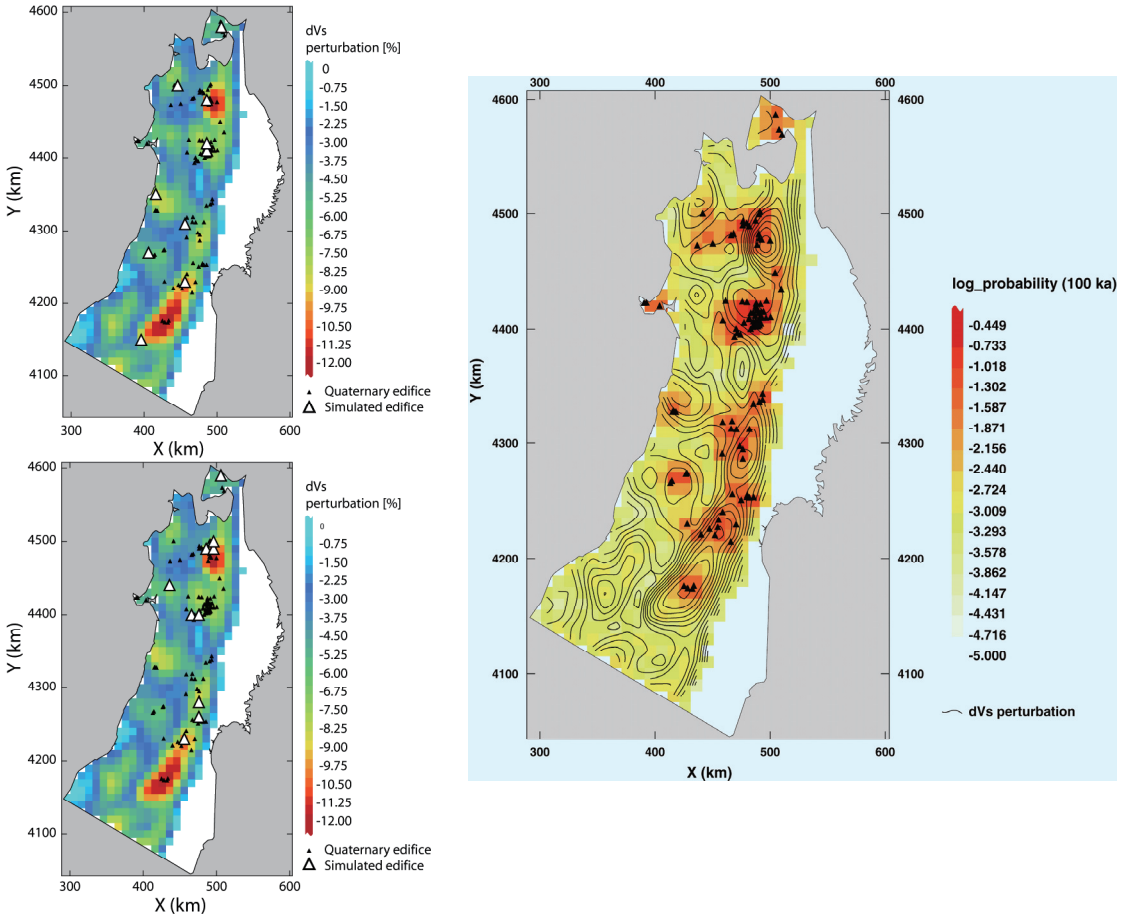

Figure 2.11: (a1) and (a2): left, top and bottom: Two Cox simulations with a multivariate potential of volcanism. The simulated events are likely to be located in zones with past activity as well as in zones with seismic anomalies. (b): right: Probability of formation of a new volcano in the next 100,000 years using the Cox process approach, correlated with the seismic tomography data for Tohoku region.

STEP 4b: Probabilistic Strain Maps

Step 4b.1: Constructing Different Strain Maps: For each indicator, the calculated strain rates from **Step 3b** are converted to strain maps for each conceptual model branch of the Logic Tree. The maps show calculated strains within the 5 km x 5 km areas. As noted above, this is a reasonable resolution for the datasets being used and is also a useful size with respect to expected repository footprint (~10 km^2), but site-scale rather than regional scale application of the methodology would require use of a finer grid. The strain rates are also presented together on a single map, combining them using the weightings assigned to each branch of the logic tree. The weighted map is thus a probabilistic representation of strain, representing the most likely strain averaged over the time period for which the particular indicator has been 'recording'. For application in later Steps, only the maps of the most highly weighted conceptual model alternatives (branches) and the combined, fully weighted probabilistic version are likely to be useful.

Step 4b.2: Comparison and Differencing: The weighted, probabilistic maps for each separate indicator (i.e. GPS, seismic and tilt) are then compared. Because the different strain indicators have variable coverage of a region, their use is complementary. The probabilistic weighted maps for each indicator can, for instance, be differenced to assess the overall correlation between strain indicators. This picks out areas where the datasets are inconsistent in their strain estimates. Combined with the variability shown in the strain rate histograms for

any selected area, such inconsistencies will identify locations where there is significant uncertainty regarding deformation process, which may also be reflected in a wider range of strain rate potential (as can be seen in Figure 2.3, for example). If a potential repository site lies within such a region, this would require special attention in Step 8, to ensure that adequate data were gathered during the PIA investigation programme to try to reduce the uncertainty. An example of one of the strain maps generated in the Tohoku Case Study is shown in Figure 2.12, where the weighted average GPS strain data are shown together with the location of volcanoes.

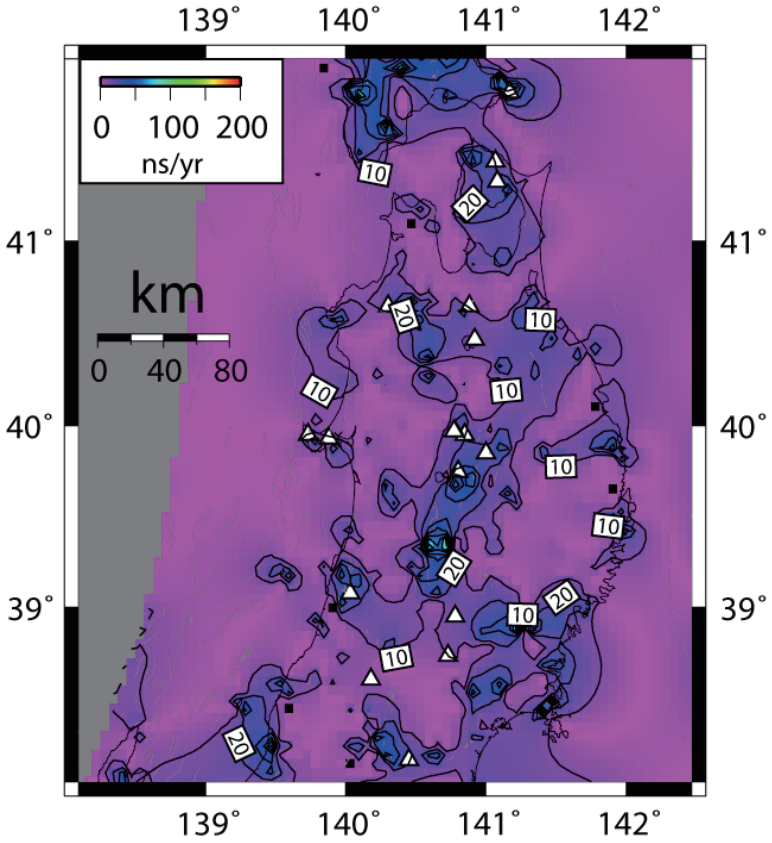

Figure 2.12: Weighted average strain map (contoured in nanostrains/a) for the Tohoku region, based on all 148 strain maps from the GPS-based logic tree (Figure 2.3). Here, the location of volcanoes is also shown (white triangles) as the integration of Steps 4a and 4b is a key exercise carried out in Step 5. A weak positive correlation can be seen between the location of the volcanic front and the location of elevated contractional strain, which is being investigated in the methodology development programme.

STEP 5: Integrated Evaluation of Each Potential Repository Site

The information from **Steps 4a and 4b** can be used directly in Step 6 – for example, to carry out a detailed assessment of a single site or a few alternatives. However, it is possible to combine the data from Steps 4a and 4b to carry out an evaluation of a larger group of sites so that they can be compared at a relatively simple level in terms of their overall susceptibility to tectonic hazard. This was the objective of the two Case Studies. The text below assumes that a large set of sites (say 5 – 10) is being compared.

Depending on the interpretations arising from the separate strain maps for each indicator, it may be considered useful to produce a combined, higher level logic tree that weights belief in relevance of the three strain measures and factors volcanic strain into the logic tree and the weighting process. Conversely, the likelihood of magma intrusion, as indicated on the probability maps, needs to be interpreted in the light of deformation history and the mapped strain rate variations around the site.

Figure 2.13 shows an example of the estimated uncertainties (1σ) in strain values for the different strain indicators at four different example locations from the Tohoku Case Study.

Step 5 combines the data from Steps 4a and 4b to carry out an evaluation of a large group of sites so that they can be compared at a relatively simple level in terms of their overall susceptibility to tectonic hazard. This was the objective of the two Case Studies. The text below assumes that a large set of sites (say 5 – 10) is being compared.

For multiple site comparisons, Step 5 produces individual site assessments that provide the following information in an identical format:

- description of the geological and tectonic setting of the site;
- evaluation of the likelihood of each different type of magma intrusion considered possible, in both the region around the site and at the site itself, over a period of up to 100,000 years[4];
- evaluation of the uncertainties in the likelihoods;
- evaluation of the best estimate rock deformation potential (expressed as strain probability histograms) and mechanisms over the same period of time – and the related uncertainties.

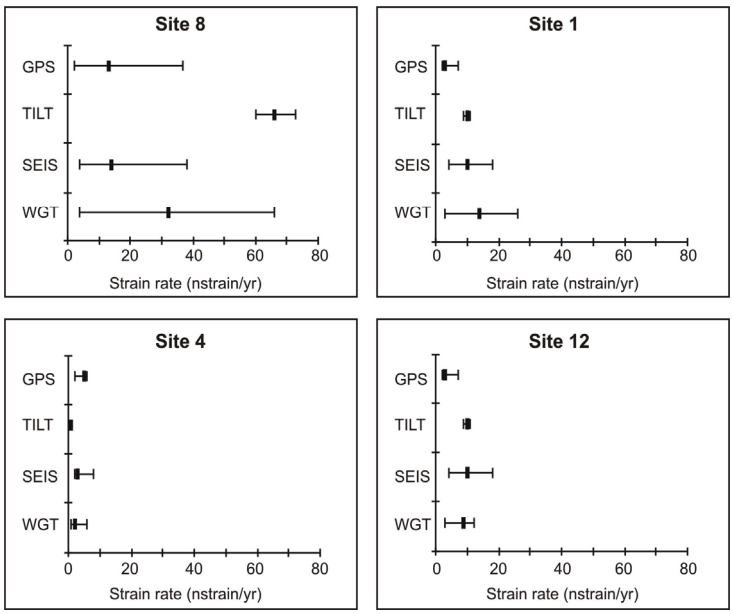

Figure 2.13: estimated uncertainties (1σ) in strain values for the different indicators (GPS, tilt and seismic, plus weighted average) at four different example locations from the Tohoku Case Study.

Depending on the interpretations arising from the separate strain maps for each indicator, it may be useful to produce a combined, higher level logic tree that weights the three strain measures, and factors volcanic strain into the logic tree and the weighting process. Conversely, the likelihood of magma intrusion, as indicated on the probability maps, needs to be interpreted in the light of deformation history and the mapped strain rate variations around the site.

Figure 2.14 shows the equally weighted average strains using all indicators for all the 14 example locations in the Tohoku Case Study (Chapman et al., 2009). These might be regarded as 'best estimate' values for the purposes of this methodology demonstration but, in a real site inter-comparison exercise, expert judgement would be required to assign weights to the different indicators, which would depend on confidence in both the data and the regional models. Clearly, these will vary from one area and one site to another.

[4] The methodology could be developed further to provide estimates for 1 Ma, but this would require the use of much larger (longer duration, ~10 Ma) datasets and would involve greater uncertainties (especially concerning the time stability of the underlying tectonic processes). Knowledge of future volcanic hazard is, in any case, of diminishing interest for safety assessment at times even after only 10,000 years, as the hazard of the waste has decreased to levels equivalent to natural uranium ores by this stage.

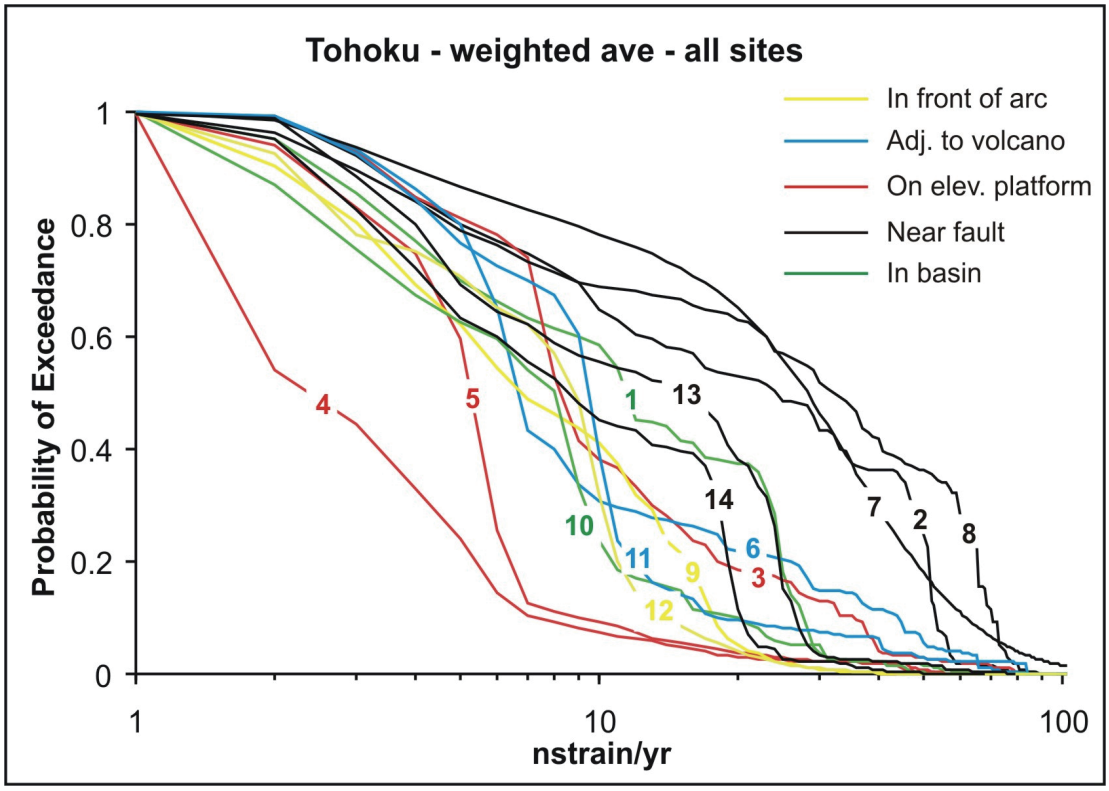

Figure 2.14: Graph showing the probability or likelihood of exceeding strains of given magnitude, based on the equally weighted average strains (using all three strain indicators) for all the 14 example locations in the Tohoku Case Study (Chapman et al., 2009).

STEP 6: Interfacing with the NUMO Performance Assessment work

The methodology up to this stage is designed to deliver a set of probability maps that have taken account of uncertainty in both conceptual models and data and which contain integrated interpretations of the sites being investigated by NUMO.

Knowledge of the likelihood of various tectonic hazards affecting a site is of limited value to NUMO unless it can evaluate whether the impacts would be acceptable or not (in terms of regulatory standards for radiological exposures to the public). This is a task for the NUMO safety assessment team, who will be carrying out detailed performance assessment studies of the long-term behaviour of the repository and its engineered barriers. However, information on both **likelihood** and **impacts** is essential for safety assessment and both **likelihood** and **consequences** are together directly linked through a specific 'event definition'.

The role of the ITM methodology at this stage is thus to provide the PA team with information on the nature of the tectonic hazards, so that it can construct **scenarios** upon which to base these analyses, and to provide quantitative probability estimates of the likelihood of occurrence of these scenarios. As discussed in Section 1 of this report, two approaches have been adopted internationally to utilise this information in safety assessment:

- To calculate the health risk[5] to people in the future by combining the probability of a disruptive event occurring with its radiological consequences in terms of releases

[5] Health risk is normally defined as the risk of death or serious genetic effects.

from a repository: simply, risk = probability x consequence. With this approach, regulatory standards or targets can be defined in terms of risk to an individual.

- To consider the impacts of a disruptive event and calculate the radiological doses[6] to people in the future and then, separately, to discuss the likelihood that this might happen (the so-called 'disaggregated' approach). With this approach, separate regulatory targets for radiation doses might be set for events (or scenarios) with different degrees of likelihood (often expressed qualitatively; e.g. 'likely', 'less likely', 'highly unlikely').

In either approach, an appreciation of probability is essential: in the first 'risk approach' a sound quantitative estimate will provide more confident estimation of risk; in the second, some form of quantification of 'likelihood' is needed to decide which category to place an event or scenario into.

The information required for either of these approaches is generated in **Step 6** and comprises the following:

1. A description of the nature of each magma intrusion event and rock deformation process that could feasibly affect the repository (the basis for the scenario).

2. The likelihood of each magma intrusion event impacting both the repository directly and the surrounding rock mass.

3. The variation of this probability with time over the next 100,000 years.

4. The best estimate of the magnitude and duration of rock deformation that could affect the repository.

5. A description of how the events and processes would initiate, develop and progressively impact the repository and the barriers.

Using this information, the PA team will be able to develop scenarios for tectonic impacts and assign probabilities to them.

The ITM methodology involves the production of a matrix that will compile the information in items (1) and (5) above. This matrix can be used to inform the scenario development work, which could be carried out jointly by the PA team and the ITM group. Figure 2.15 shows a generic example of part of a matrix for indirect (hydrothermal) impacts on the repository structures (excluding the engineered barrier system – which is in a separate matrix) and the surrounding rock. This type of matrix could be developed to be considerably more detailed, depending on the requirements of the scenario analysis.

The matrix will need to take account of the types of repository design and engineered barriers that would be appropriate to the sites being studied, so input from NUMO repository design work will be required. Simple factors, such as repository depth and horizontal and vertical dimensions could have a significant bearing on the level of impact of each type of rock deformation or magma intrusion.

For the methodology development work, only one selected magmatic intrusion scenario and one rock deformation scenario have been evaluated and presented as illustrations. For eventual area and site-specific use of the ITM methodology, this exercise will have to be comprehensive.

[6] Of course, a radiological dose can also be expressed in terms of health risk, by applying accepted dose-to-risk conversion factors.

Barrier Safety Function	*Temperature Impacts*	*Hydrological Impacts*	*Mechanical Impacts*	*Chemical Impacts*
Plugs: Short-circuit EDZ in tunnels	**Thermal alteration: Cracking and disaggregation**			**Inflowof magmatic brine: Change in pH?**
Seals: Prevent fast transport in shafts	**Thermal alteration: Cracking and disaggregation**			**Inflowof magmatic brine: Change in pH?**
Depth: Anti-intrusion and radiation protection				
Hydrology: Long, slow advective transport	**Increased temperature: Bouyancy effects**	**Modified hydraulic head: Changed flow rate and direction**		
Rock: Retard radionuclides (sorption, matrix diffusion)				**Inflowof magmatic brine: Changes in complexation?**

No Impacts	*Limited Impacts*	*Moderate Impacts*	*Extreme Impacts*

Figure 2.15: Impact Matrix of the repository and surrounding rock for an illustrative indirect-volcanism impact scenario assuming imposition of a hydrothermal convection system 10 km from a polygenetic volcanic centre. Impacts can be categorised mainly as 'global, slow, 'permanent', and 'barrier degradation'.

STEP 7: Utilising the Probabilistic Results

Step 7 is where the probabilistic results and any safety assessment results based upon them are used by NUMO to assist in making siting decisions. Various decision points can be considered:

1. At the point where a single volunteer site comes forward in a non-excluded area. NUMO may wish to consider the overall susceptibility of the site to tectonic impacts before it accepts the site as a PIA, so that it can gain an initial impression of the extent to which tectonic issues might be critical to a future safety case. This will enable them to gauge 'programme risk' – whether they would be taking on a site with a low or high likelihood of proving unsuitable from the tectonic viewpoint. This would use the data from the LS up to the point of Step 4, possibly without carrying out any PA work in Step 6. The output would inform NUMO decision makers so that can be fully aware of any tectonic contribution to overall project risk and be able to answer questions about tectonic hazard with confidence.

2. Where there are several possible volunteer sites in the same region, so that the relative susceptibility of the sites can be assessed – essentially at Step 5, as illustrated in the two Case Studies and described further below. This comparative assessment could help NUMO to focus or prioritise the site investigations and decide the order in which sites are evaluated.

3. When one or two sites are being considered for the final DIA. At this point, PIA information would be available and the ITM methodology would have been iterated with progressively improving data. In addition, feedback would be available from quantitative

safety assessments in Step 6, using Step 4 information. By this stage, there should be a full understanding of the actual tectonic hazard for any sites being considered for the DIA and the ITM information should be at a sufficient level to feed directly into license application level documentation.

However, each of these possible decision points is a potentially far-reaching stage of NUMO's work and siting decisions will always involve many other factors (both technical and non-technical). At present, it is not clear how NUMO might wish to manage this Step for any of these three stages of their programme. Further development is consequently anticipated here, as the PIA siting programme begins to find potential sites, as the NUMO safety assessment work evolves and as the national regulatory standards become more developed and the use of likelihood and risk become clearer.

No impact analyses have been carried out so far as part of NUMO's parallel PA development work, so it is not possible at the moment to assess radiological impacts associated with any particular scenario. For the purposes of illustrating the methodology, Figure 2.16 shows an example of how probability values for volcanism, derived from Step 4a might contribute to understanding siting confidence, as might be required at the second decision point described above (comparing multiple sites). It shows, for the 14 Tohoku Case Study example locations, one example of how 'low, medium and high' levels of confidence might be allocated to each site with respect to susceptibility to a scenario of direct magmatic intrusion within the next 10,000 years. The quantitative boundaries between the levels of confidence are arbitrarily selected here, simply to illustrate the approach.

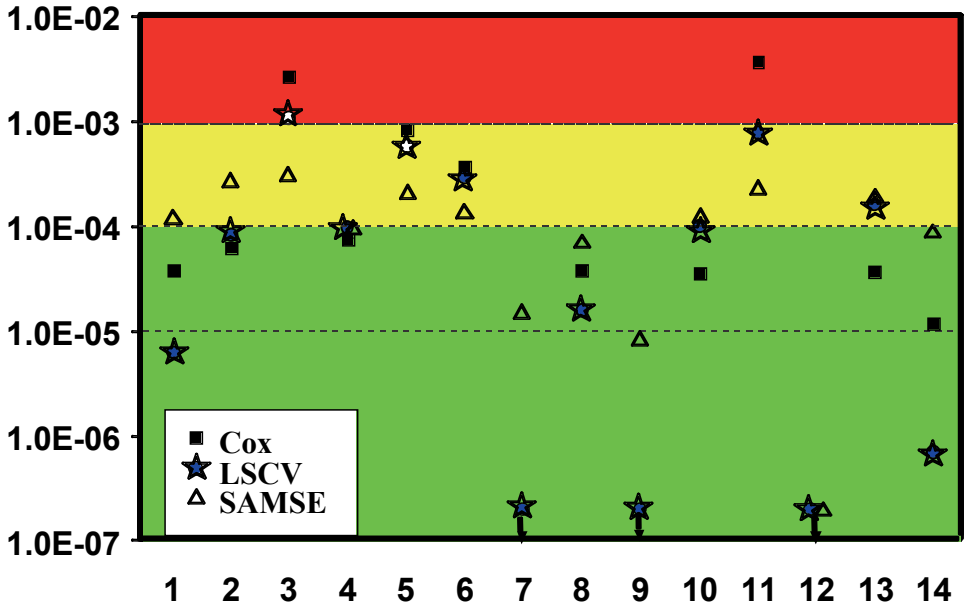

Figure 2.16: An example of 'low' (red), 'medium' (yellow) and 'high' (green) confidence levels allocated to each of the 14 Tohoku Case Study example locations, based on the probability of a direct magmatic intrusion scenario occurring within the next 10,000 years (for different statistical methods in Step 4a.2). The quantitative boundaries chosen for the levels are arbitrary examples, simply to illustrate the approach.

STEP 8: Defining PIA and DIA field tectonic data requirements

The aim of **Step 8** is to identify which additional data will be required from PIA site investigations to reduce the uncertainties in the evaluations in each previous Step. In particular, after Steps 4, 6 and 7 during the LS stage, the ITM methodology will need to be reiterated to produce more refined evaluations of probabilities and better definition of the nature of impacts for input to the decision to move from PIA to DIA (and to the progressive development of SAs, as work on the PIAs proceeds). The following classes of information feed into the ITM Methodology:

1. **Regional (data coverage):** filling gaps in the large regional databases that were used in **Step 3**. It is clear that some classes of information will be of patchy quality and coverage (e.g. age data for volcanic features; active fault parameters; seismic data), which contributes to the overall uncertainty in the **Step 4** probability mapping. Whilst it cannot hope to fill all such gaps, NUMO should be prepared to gather this type of information, so the development of an efficient programme that identifies the most important and 'fillable' gaps that would have maximum impact on reducing uncertainty is important. Definition of these critical data gaps is region-specific, but the two Case Studies have identified obvious improvements.
2. **Regional (ground truth):** ensuring that the key data used in **Step 3** are fully understood and being used correctly for classification and for setting up strain models. A certain amount of this work will already have been undertaken in **Step 2**, but it may be found that a more thorough evaluation is needed by the time **Step 7** has been reached. As was found for the Tohoku volcanics work (**Step 3a**), the results are highly dependent on what a catalogue entry is assumed to mean and field investigation has shown that all the data need to be checked. This is not necessarily a large operation, but it would involve field reconnaissance visits to features (volcanic, faults, etc) by experts across the whole of the region of interest, preferably during the LS stage, but repeated if needed during the PIA investigations.
3. **Local and Site-Scale:** many topics of relevance to the ITM methodology will be studied in any case during PIA investigations. For example, even *without* the need to develop the tectonic probability models and evaluations of ITM, NUMO will already be seeking evidence of hidden active faults, characterising local active faults in detail, measuring uplift rates and looking at geothermal heat flux as part of its 'normal' site investigation programme. However, the ITM methodology will provide better results if it has access to *additional* information. The scope of this information will be site-specific, but the following data needs will need to be considered (for the reasons given):
    - age and eruptive style/volumes of local volcanics to constrain the intrusion probability estimates and impact definition;
    - more detailed, local-scale gravity and magnetic surveys to identify hidden volcanic structures or deformation zones that would affect the probabilistic statistical evaluation;
    - strain mechanism and history of faults and other large deformation features in the neighbourhood of the site to constrain site context with respect to 'rock blocks' used in regional strain budget modelling;
    - establishment of local fixed and temporary GPS stations to localise GPS strain within the regional picture, seeking small differences that could reflect an overlay of site-scale deformation.

2.3 References for Section 2

Chapman, N., M. Apted, J. Beavan, K. Berryman, M. Cloos, C. Connor, L. Connor, O. Jaquet, N. Litchfield, S. Mahony, W. Smith, S. Sparks, M. Stirling, P. Villamor and L. Wallace (2009). Development of Methodologies for the Identification of Volcanic and Tectonic Hazards to Potential HLW Repository Sites in Japan: The Tohoku Case Study. Nuclear Waste Management Organisation of Japan, Tokyo. Technical Report: NUMO-TR-08-03. 135 pps.

Hone, D.W.E, Mahony, S.H., Sparks, R.S.J. & Martin, K.T. (2007). Cladistics analysis applied to the classification of volcanoes. *Bulletin of Volcanology*, **70**, 203−220.

Jaquet O., Lantuéjoul C. and Goto, J. (2009 in press). Cox process models for the estimation of long-term volcanic hazard. In Volcanism, Tectonism, and the Siting of Nuclear Facilities, edited by C.B. Connor, N.A. Chapman and L.J. Connor.Connor L. (2008a) Probabilistic methodology for long term assessment of volcanic hazards, Nuclear Technology, 163, pp. 180-189.

Jaquet O., Lantuéjoul C. and Goto J. (2008b) Estimation of long-term volcanic hazard using a Cox process with a multivariate potential, VIII International Geostatistics Congress, GEOSTATS 2008, Santiago Chile, pp.167-176.

Jaquet O., Lantuéjoul C. and Goto, J. (2009 in press). Cox process models for the estimation of long-term volcanic hazard. In Volcanism, Tectonism, and the Siting of Nuclear Facilities, edited by C.B. Connor, N.A. Chapman and L.J. Connor.

3 The Geology and Tectonics of Kyushu. Part 1: Tectonic Setting and Evolution from 150 Ma to 15 Ma

Japan is part of the "Ring of Fire," the belt of earthquakes and volcanic activity that distinguishes the active margins of the Pacific ocean from the passive margins of the Atlantic ocean (Figure 3.1). In the 1920s, the great seismologist K. Wadati, discovered that earthquakes beneath northern Japan form an inclined zone extending from locations very near the Japan Trench to depths of about 500 km beneath the Japan Sea. This trench is a north-south trending bathymetric depression about 150 km east of the mainland that is as deep as 9000 m. The towering volcanoes of northern Japan are centred about 75 km from one another and form a curving line that is about 100 km above the inclined seismic zone. In the 1930s, Japanese seismologists discovered that many of the earthquakes near the Japan trench are the result of large thrust fault movements indicating the floor of the Pacific basin is moving beneath Honshu. A similar pattern of volcanism and earthquake activity is found along the Ryukyu trench that is as deep as 5200 m and extends 2200 km from Kyushu to Taiwan.

The cause of the active tectonic movements affecting the Earth was not well explained until the late 1960s when the realisation was made that the outer part of the Earth is divided into pieces, known as plates, about 100 km thick (Takeuchi et al., 1970). The plates consist of both the crust and cool uppermost mantle that has sufficient long-term strength that earthquake-generating ruptures can occur. Plate boundaries come in three forms that are recognised by the common type of fault movement: divergent with normal faulting, convergent with thrust faulting, and transform with strike-slip faulting. Plates separate from one another creating new ocean crust in the process of seafloor spreading at ocean ridges and come together consuming ocean crust in the process of subduction at locations demarked by ocean trenches, inclined seismic zones, and lines of explosive volcanoes. Plates slide past one another at transform boundaries.

Most of the geology of Japan is the result of subduction-related processes since the Mesozoic (Sugimura and Uyeda, 1973). The patterns of active faulting and seismicity along with direct GPS measurements delineate where tectonic motions are underway (Sagiya et al., 2000). To a first order, the current tectonics of the Japanese islands can be explained by the interaction of four plates: Pacific, Philippine Sea, Eurasian and North American (Figure 3.1). The eastern part of the Eurasian plate is broken with a large fragment, the Amur subplate moving at a slightly different speed and direction than the parent plate (Wei and Seno, 1998; Heki et al., 1999). With the development of GPS geodesy in the 1990s, small differential subplate movements can be directly measured. The North American plate continues across the Bering Sea into eastern Asia and down past the Kamchatka-Kurile trench segments to Japan. An elongate southern prong of the North American plate extends southwards to Japan. This prong has broken off and is moving as the Okhotsk subplate.

The active tectonics of Northeast Japan (northern Honshu and Hokkaido) are the manifestation of the interactions between the Amur and Okhotsk subplates with the Pacific plate. Subduction along the Japan Trench at a speed of about 9 cm/a (90 km/Ma) is concurrent with convergence near the eastern edge of the Sea of Japan at a speed of 1 to 1.5 cm/a (10 to 15 km/Ma) (Okamura et al., 1995). The active tectonics of Kyushu at the northern end of the Ryukyu arc-trench system are the focus of this Case Study. The active tectonics of Southwest Japan (Kyushu, Shikoku, and southwest Honshu) are the manifestation of the interactions of the Philippine Sea plate and Amur subplate (Seno, 1977; Taira, 2001). Plate convergence beneath Kyushu is at a speed of about 7 cm/a (70 km/Ma) (Seno et al., 1993; Zang et al., 2002). East-central Honshu, just south of Tokyo, near 34°N, is the convergent junction of three plates: a triple junction between the Philippine Sea, Pacific, and North American (Okhotsk) plates.

Prior to middle Cenozoic time, the entire length of the Japanese islands was underthrust by the Pacific plate (Taira, 2001). At about 45 Ma, tectonic movements changed in the western Pacific region and the Philippine Sea plate was created to the south. This plate is unique amongst the large plates in that it is nearly entirely surrounded by subduction zones. Because

of the lack of a spreading ridge connection to a surrounding plate, the movement history of the Philippine Sea plate is not well determined (Hall et al., 1995; Lee and Lawver, 1995).

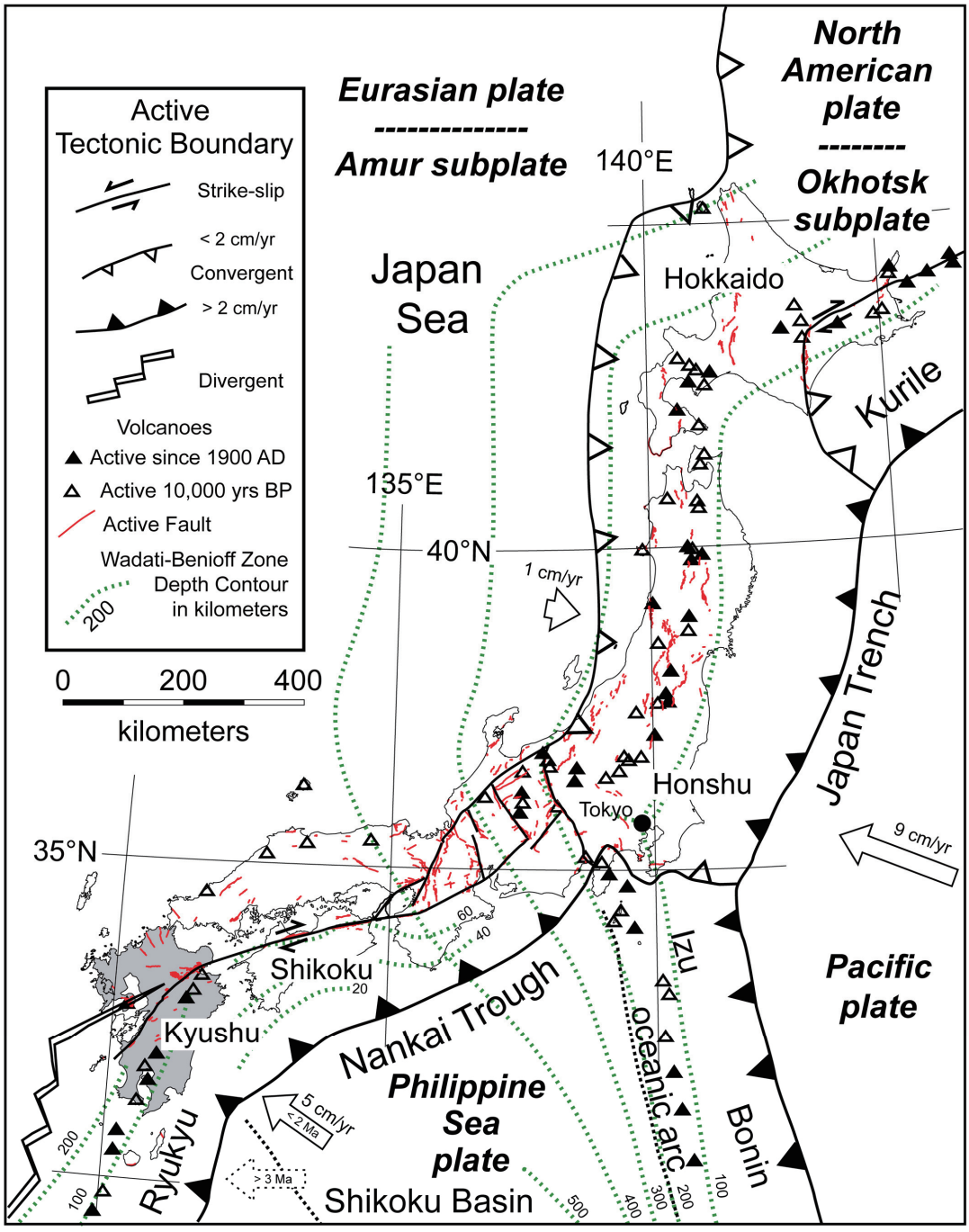

Figure 3.1: Tectonic setting of Kyushu within the Japanese island arc. The locations of active faults and volcanoes that have been active in the last 10,000 years are also shown.

The eastern edge of the Philippine Sea plate is underthrust by the Pacific plate forming the Izu-Bonin-Mariana arc-trench system. The western edge of the Philippine plate subducts beneath Asia creating the Ryukyu arc-trench system. The Izu arc and triple junction interSection has migrated northwards along the Ryukyu trench passing southern Japan to its present position. In so doing, subduction beneath Shikoku, and southwest Honshu changed from the underthrusting of the Pacific plate to the underthrusting of the Philippine plate along the Nankai Trough.

3.1 Kyushu Basement Terranes

Kyushu is the third largest Japanese island with an area of nearly 36,000 square kilometers. Most of the basement of Kyushu is composed of four geologic terranes, from north to south: Sangun, Ryoke, Chichibu, and Shimanto belts. The brief descriptions of these terranes that follows are mostly summaries from Kimura et al. (1991) and Taira (2001).

The basement of the northern part of the island is primarily composed of the Sangun Metamorphic Belt, a terrane largely composed of Permian to Triassic sedimentary rocks that were variably metamorphosed under high-pressure/low-temperature conditions (Nishimura, 1998). This terrane was intruded and widely metamorphosed by voluminous Jurassic to Cretaceous arc plutons. The southern boundary of the Sangun belt is the Oita-Kumamoto Tectonic Line.

The Ryoke Belt includes sedimentary rocks of late Paleozoic to Middle Mesozoic that was metamorphosed by voluminous Cretaceous (~100 to 80 Ma) arc plutons. The Higo subterrane, located only in west-central Kyushu, consists of greenschist to granulite facies rocks that were metamorphosed in the Triassic (Hamamoto et al., 1999). The extent of high temperature/low-pressure metamorphism varies greatly in intensity depending upon proximity to the Cretaceous plutons. The Ryoke belt is separated from the southern basement terranes by the Usuki-Yatsushiro Tectonic Line, an extension of the Median Tectonic Line that continues as a well-defined right-lateral strike-slip fault zone into Shikoku and the Kii peninsula. No Mesozoic magmatic rocks occur south of the Usuki-Yatsushiro/Median Tectonic Line.

In east-central Kyushu and south of the Usuki-Yatsushiro/Median Tectonic Line is a 10 km wide peninsula underlain by a wedge-shaped exposure of the Sanbagawa Belt. This outcrop area is the southwestern limit of the 700 km long belt that is well exposed in northern Shikoku and central Kii (Banno and Nakajima, 1992). The Sanbagawa Belt is composed of high-pressure/low-temperature blueschist facies metabasalts with lesser sediments recrystallised in the middle Cretaceous, between 90 to 70 Ma (Wallis, 1998). The Ryoke and Sanbagawa belts were recognised as the classic example of paired metamorphic belts (Miyashiro, 1961) that were later juxtaposed along a major strike-slip fault zone.

The Sanbagawa Belt is in fault contact with the Chichibu Belt, a 10 to 20 km wide terrane that trends northeast across the middle of Kyushu. This terrane is composed of weakly metamorphosed Carboniferous to Jurassic strata with local chaotic melange zones containing blocks of greenstone, chert, and limestones. The southern boundary of the Chichibu Belt is the Butsuzo Tectonic Line.

The southern third of the island is composed of the Shimanto Belt, the late Cretaceous to Paleogene accretionary prism that is the western end of the 1800 km long terrane that forms the southern half of Shikoku and the Kii peninsula of Honshu (Taira et al., 1982; Mackenzie et al., 1987). The Shimanto Belt is composed of two main units: relatively coherent sequences of interbedded sandstone and shale and chaotically mixed units of shale-matrix melange containing slabs and blocks of basaltic lavas that are commonly pillowed, limestones and radiolarian cherts.

3.2 Tectonic History of Kyushu Region

Most of the bedrock of the Japanese islands was assembled as a result of westward subduction along the eastern margin of Asia. Large accretionary prisms were constructed in the late Paleozoic to early Jurassic that are mostly composed of deep ocean sediments (shales, cherts, and pelagic limestones) and trench deposits (sand-rich) that were deformed by folding, faulting, and flowage during offscraping and underplating and then locally blanketed by slope deposits. In the Mid-Jurassic, between about 175 to 135 Ma, a major period of strike-slip faulting occurred along the margin of Asia that created the Oita-Kumamoto Tectonic Line and other high-angle fault contacts between displaced pieces of the late Paleozoic to early Jurassic accretionary prism.

In the very latest Jurassic or earliest Cretaceous, a major phase of fast subduction began that continues to this day off northeast Japan. This generated the enormous volume of arc magmas that invaded the Ryoke and Higo terranes and caused widespread high-temperature/low-pressure metamorphism. At the same time, the Sanbagawa and Chichubu terranes were accreted. The Sanbagawa terrane is largely composed of ocean crust and overlying sediments that was imbricated and underplated beneath the leading edge of the new subduction zone and thoroughly metamorphosed and intensely deformed under high-pressure/low-temperature conditions. The Chichubu Belt and the older part of the Shimanto Belt are mostly trench sediments that were offscraped or slope deposits that accumulated at the same time. All of this accretion and metamorphism was caused by the subduction of the Pacific plate beneath the eastern edge of Asia.

Between 50 to 40 Ma, a profound tectonic event occurred. The Pacific plate changed direction from northwest to a more westerly trend. This change is recorded as the major kink (dated at 43 Ma) in the Hawaii-Emperor seamount chain as well as several other seamount chains in the Pacific plate farther to the south. The change in plate motion was coeval with the initiation of subduction along a major northwest-trending transform zone extending from New Zealand to a location north of the Equator. This formed the Izu-Bonin-Mariana and Tonga-Kermadec arc-trench systems (Hall et al., 1995; Lee and Lawver, 1995). Whether the initiation of subduction caused the change in Pacific plate motion or the change in Pacific plate motion caused the initiation of subduction is debated. Either way, the northern part of the Philippine Sea plate was bounded by a pair of westward-dipping subduction zones. The Eastern boundary of the Philippine plate north is the Izu-Bonin-Mariana arc-trench system. The western boundary north of Taiwan is a west-dipping subduction zone that generated the Ryukyu arc-trench system. South of Taiwan, the western boundary is east-dipping subduction zone that generated the Manila trench and Luzon arc as the edge of Eurasia descends beneath the Philippine plate. The trench-trench-trench (TTT) triple junction now located off the Izu peninsula that was established somewhere between Taiwan and Kyushu has migrated northwards ever since (Figure 1).

The TTT triple junction appears to have reached the southern tip of Kyushu at about 25 Ma (Kimura et al., 2005). From about 32 to 23 Ma, Japan began to rift from Asia (Jolivet et al., 1994). Seafloor spreading in the Sea of Japan created new ocean crust in the backarc region between 23 to 12 Ma as Southwest Japan (southern Honshu and Shikoku) rotated clockwise about 45 degrees and Northeast Japan shifted eastward with a small counterclockwise rotation (Ishikawa, 1997). As this occurred, the TTT triple junction migrated more eastward than northward resulting in highly oblique and very slow convergence beneath southwest Japan. This movement caused significant left-lateral strike-slip offset along the Median Tectonic Line. As the TTT triple junction migrated northwards, the plate interactions along southern Japan abruptly switched from the subduction of the Pacific plate to the Philippine Sea plate.

The tectonic changes along southern Japan were concurrent with a major event in the eastern edge of the Philippine Sea plate that may somehow be related. The Izu-Bonin-Mariana arc split with backarc spreading creating the Shikoku Basin between 25 to 15 Ma (Karig, 1974; Sdrolias et al., 2004). The Kyushu-Palau Ridge is the remnant arc, nearly 400 km behind the Izu-Bonin-Mariana arc. The opening of the Shikoku Basin created new ocean crust that was still hot as it was underthrust beneath Kyushu and Shikoku islands and the Kii peninsula. The combination of spreading and underthrusting accounts for the minor but very anomalous forearc magmatism from 17 to 12 Ma (Hibbard and Karig, 1990; Kimura et al., 2005) and the widespread, low-temperature metamorphism of the Shimanto Belt on Kyushu and Shikoku. The remnant of the split arc is the Kyushu-Palau submarine ridge, a segment of ocean crust greatly thickened by subduction-generated magmatism.

3.3 Summary

The overall geologic history that created the basement terranes of Kyushu is well understood as a result of the long-term westward subduction of the Pacific ocean seafloor. Subduction in the late Paleozoic to mid-Mesozoic created the Sangun accretionary prism, which makes up the northern part of the island. This accretionary event was followed by a period of major

strike-slip transform faulting between about 175 to 135 Ma that shuffled the accretionary prism and made some of the high angle fault zones that are mapped as tectonic lines. The reinitiation of westward subduction in the very latest Jurassic or earliest Cretaceous generated voluminous magmatism that invaded the northern half of the island and the large accretionary prism that makes up most of the southern half of Kyushu. The major plate motion change at about 43 Ma that isolated the Philippine Sea plate led to the northwards migration of the trench-trench-trench triple junction that is now located at the Isu peninsula. As the triple junction passed south Japan, backarc spreading occurred to form the Sea of Japan. Slow convergence with left-lateral strike-slip movement along the Median Tectonic line caused the Ryoke belt with abundant Mesozoic plutons to become juxtaposed directly against the Sanbagawa-Chichibu-Shimanto accretionary terranes. Westward subduction of the Philippine plate generated the Ryukyu trench and arc.

3.4 References for Section 3

Aoki, Y., Tamano, T., and Kato, S., 1982, Detailed structure of the Nankai Trough from migrated seismic Sections: American Association of Petroleum Geologists Memoir 34, p. 309-322.

Banno, S., and Nakajima, T., 1992, Metamorphic belts of the Japanese islands: Annual Reviews of Earth and Planetary Sciences, v. 20, p. 159-179.

Chai, B. H. T., 1972, Structure and tectonic evolution of Taiwan: American Journal of Science, v. 272, p. 389-422.

Cloos, M., Sapiie, B., Quarles van Ufford, A., Weiland, R. J., Warren, P. Q, and McMahon, T. P., 2005, Collisional delamination in New Guinea: The geotectonics of subducting slab breakoff: Geological Society of America Special Paper 400, 51 pp.

Cox, A., and Engebretson, D., 1985, Change in motion of Pacific plate at 5 Ma BP: Nature, v. 313, p. 472-474.

Hall, R., Ali, J. R., Anderson C. D., and Baker, S. J., 1995, Origin and motion history of the Philippine Sea plate: Tectonophysics, v. 251, p. 229-250.

Hamamoto, T., Osanai, Y., Kagami, H., 1999, Sm-Nd, Rb-Sr, and K-Ar geochronology of the Higo metamorphic terrane, west-central Kyushu, Japan: The Island Arc, v. 8, p. 323-334.

Heki, K., Miyazaki, S., Takahashi, H., Kasahara, M., Kimata, F., Miura, S., Vasilenko, N., F., Ivashchenko, and Ki-Dok, A., 1999, The Amurian plate motion and current plate kinematics in eastern Asia: Journal of Geophysical Research, v. 104, p. 29,147-29,155.

Hibbard, J. P., and Karig, D. E., 1990, Structural and magmatic responses to spreading ridge subduction: An example from southwest Japan: Tectonics, v. 9, p. 207-230.

Ishikawa, N., 1997, Differential rotations of north Kyushu Island related to middle Miocene clockwise rotation of SW Japan: Journal of Geophysical Research, v. 102, p. 17,729-17,745.

Jolivet, L, K., Tamaki, K., and Fournier, M., 1994, Japan Sea, opening history and mechanism: A synthesis: Journal of Geophysical Research, v. 99, p. 22,237-22,259.

Kamata, H., 1989, Volcanic and structural history of the Hohi volcanic zone, central Kyushu, Japan: Bulletin of Volcanology, v. 51, p. 315-332.

Kamata, H., and Kodama, K., 1994, Tectonics of an arc-arc junction: An example from Kyushu Island at the junction of the Southwest Japan Arc and the Ryukyu Arc: Tectonophysics, v. 233, p. 69-81.

Karig, D. E., 1974, Evolution of arc systems in the western Pacific: Annual Reviews of Earth and Planetary Sciences, v. 2, p. 51-75.

Kimura, J.-I., Stern, R. J., and Yoshida, T., 2005, Reinitiation of subduction and magmatic responses in SW Japan during Neogene time: Geological Society of America Bulletin, v. 117, p. 969-986.

Kimura, M., 1985, Back-arc rifting in the Okinawa Trough: Marine and Petroleum Geology, v. 2, p. 222-240.

Kimura, T., Hayami, I, and Yoshida, S., 1991, Geology of Japan, University of Tokyo Press, 287 pp.

Kodaira, S., Takahashi, N., Park, J.-O., Mochizuki, K., Shinohara, M., and Kimura, S., 2000, Western Nankai Trough seismogenic zone: Results from a wide-angle ocean bottom seismic survey: Journal of Geophysical Research, v. 105, p. 5,887-5,905.

Kodama, K., and Nakayama, K.-I., 1993, Paleomagnetic evidence for post-late Miocene intra-arc rotation of south Kyushu: Tectonics, v. 12, p. 35-47.

Lee, T.-Y., and Lawver, L. A., 1995, Cenozoic plate reconstruction of Southeast Asia: Tectonophysics, v. 251, p. 85-138.

Mackenzie, J. S., Needham, D. T., and Agar, S. M., 1987, Progressive deformation in an accretionary complex: An example from the Shimanto belt of eastern Kyushu, southwest Japan: Geology, v. 15, p. 353-356.

Malavieille, J., Lallemand, S. E., Dominguez, S., Deschamps, A., Lu, C.-Y., Liu, C.-S., Schurle, P., and the ACT Scientific Crew, Arc-continent collision in Taiwan: New marine observations and tectonic evolution: Geological Society of America Special Paper 358, p. 187-211.

Miki, M., Matsuda, T., and Otofuji. Y., 1990, Opening mode of the Okinawa Trough - paleomagnetic evidence from the south Ryukyu Arc: Tectonophysics, v. 175, p. 335-347.

Miyashiro, A., 1961, Evolution of metamorphic belts: Journal of Petrology, v. 2, p. 277-311.

Nishimura, Y., 1998, Geotectonic subdivision and areal extent of the Sangun belt, inner zone of Southwest Japan: Journal of Metamorphic Geology, v. 16, p. 129-140.

Okamura, Y., Watanabe, M., Morijiri, R., Satoh, M., 1995, Rifting and basin inversion in the eastern margin of the Japan Sea: Island Arc, v. 4, p. 166-181.

Pollitz, F. F., 1986, Pliocene change in Pacific-plate motion: Nature, v. 320, p. 738-741.

Sagiya, T., and Thatcher, W., 1999, Coseismic slip resolution along a plate boundary megathrust: The Nankai Trough, southwest Japan: Journal of Geophysical Research, v. 104, p. 1,111-1,129.

Sagiya, T., Miyazaki, S., Tada, T., 2000, Continuous GPS array and present-day crustal deformation of Japan: Pure and Applied Geophysics, v. 157, p. 2303-2322.

Sdrolias, M., Roest, W. R., and Muller, R. D., 2004, An expression of Philippine Sea plate rotation: The Parece Vela and Shikoku basins: Tectonophysics, v. 394, p. 69-86.

Seno, T., 1977, The instantaneous rotation vector of the Philippine Sea plate relative to the Eurasian plate: Tectonophysics, v. 42, p. 209-226.

Seno, T., Stein, S., and Gripp, A. E., 1993, A model for the motion of the Philippine Sea plate consistent with NUVEL-1 and geological data: Journal of Geophysical Research, v. 98, p. 17,941-17,948.

Sibuet, J.-C., Deffontaines, B., Hsu, S.-K., Thareau, N., Le Formal, J.-P., Liu, C.-S., and the ACT party, 1998, Okinawa trough backarc basin: Early tectonic and magmatic evolution: Journal of Geophysical Research, v. 103, p. 30,245-30,267.

Sugimura, A., and Uyeda, S., 1973, Island Arc -- Japan and its Environs: Elsevier, Amsterdam, 247 pp.

Taira, A., 2001, Tectonic evolution of the Japanese island arc system: Annual Reviews of Earth and Planetary Sciences, v. 29, p. 109-134.

Taira, A., Okada, H., Whitaker, J. H., McD., and Smith, A. J., 1982, The Shimanto Belt of Japan: Cretaceous - lower Miocene active-margin sedimentation: Geological Society of London Special Publication 10, p. 5-26.

Takeuchi, H., Uyeda, S., and Kanamori, H., 1970, Debate about the Earth: Approach to Geophysics through Analysis of Continental Drift: Freeman, Cooper and Company, San Francisco, 281 pp.

Utu, K., Hoang, N., and Matsui, K., 2004, Cenozoic lithospheric extension induced magmatism in Southwest Japan: Tectonophysics, v. 393, p. 281-299.

Wallis, S., 1998, Exhuming the Sanbagawa metamorphic belt: The importance of tectonic discontinuities: Journal of Metamorphic Geology, v. 16, p. 83-95.

Wei, D., and Seno, T., 1998, Determination of the Amurian plate motion: American Geophysical Union, Geodynamics series, v. 27, p. 337-346.

Yanagi, T., Nakada, S., and Watanabe, K., 1992, Active volcanoes and geothermal systems in the fault zone of middle Kyushu: 29th International Geological Congress (IGC) Field Trip A23, p. 1-31.

Yamaji, A., 2003, Slab rollback suggested by latest Miocene to Pliocene forearc stress and migration of volcanic front in southern Kyushu, northern Ryukyu Arc: Tectonophysics, v., 634, p. 9-24.

Zang, S. X., Chen, Q. Y., Ning, J. Y., Shen, Z. K., and Liu, Y. G., 2002, Motion of the Philippine Sea plate consistent with the NUVEL-1A model: Geophysical Journal International, v. 150, p. 809-819.

Zhao, D., Ochi, F., Hasegawa, A., Yamanto, A., 2000, Evidence for the location and cause of large crustal earthquakes in Japan: Journal of Geophysical Research, v. 105, p. 13,579-13,594.

4 The Geology and Tectonics of Kyushu. Part 2: Tectonic Evolution of southwest Japan since 15 Ma

The tectonics of southwest Japan has undergone complex and marked changes over the last 15 Ma, but throughout this period it has been dominated by the interaction between the Philippine Sea Plate (PSP) and the Amur, or Amurian Plate (which is considered a “sub-plate” of the Eurasian plate) (Figure 3.1). The major driver of tectonics in southwest Japan over the last 15 Ma is the ever-evolving subduction history of PSP. This contrasts with northern Japan which has been experiencing relatively straightforward, long-lived subduction of the Pacific Plate in a northwest direction beneath northern Japan. The subducting PSP can be spatially split into two parts of significantly different ages separated by the Kyushu Palau Ridge (KPR), with Eocene-Cretaceous PSP crust of the West Philippine Basin subducting at the Ryukyu trench and beneath southern Kyushu, and younger (27-15 Ma) Shikoku basin crust subducting at the Nankai Trough. The age difference of the subducted segments of the PSP has a crucial influence over the angle of subduction achieved by each slab segment, which in turn has an important spatial control on the complexity of the tectonic and volcanic evolution of this region. This will be discussed fully in this Section, and later Sections.

For convenience of discussion, the tectonic development in southwest Japan since 15 Ma can be broken down into periods from 15-10 Ma, from 10-6 Ma, from 6-2 Ma and from 2 Ma - present.

4.1 15 Ma to 10 Ma

A summary of the tectonic configuration during the 15-10 Ma period is shown in Figure 4.1. By 15 Ma, back-arc rifting in the Sea of Japan and spreading in the Shikoku Basin had ceased.

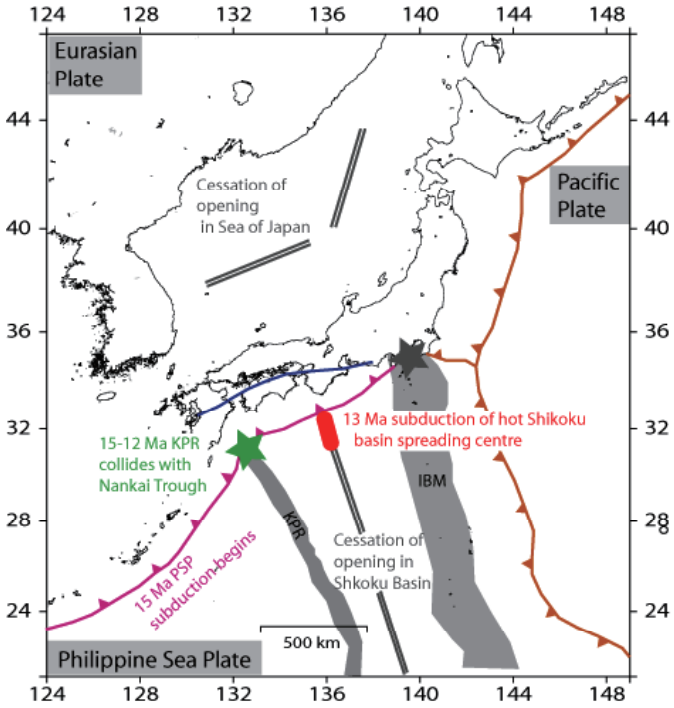

Figure 4.1. Major tectonic events occurring in the time period 15-10 Ma. At 15 Ma the Sea of Japan and Shikoku Basin ceased spreading. Between 15-12 Ma the Kyushu Palau Ridge collides with the Nankai trough (green star shows subduction point). At 13 Ma the hot spreading centre of the Shikoku basin begins to subduct (thick red line shows subduction point). The Median Tectonic Line (blue line) shows normal faulting during the mid Miocene. KPR = Kyushu-Palau ridge; IBM = Izu Bonin Marianas arc; PSP = Philippine Sea Plate

The northern margin of the Shikoku basin reached southwest Japan at roughly 15 Ma, and PSP/Eurasian relative plate motions were such that the PSP began to subduct northwards beneath the Eurasian Plate (Watanabe, 2005). The basement of this central zone is intruded by a line of mid Miocene (15-10 Ma) I-type felsic granite plutons, providing good evidence for subduction related volcanism occurring at approximately 15-10 Ma in this area (Kimura et al., 2005). The continued northward subduction of the PSP also led to the collision of the Kyushu Palau ridge with the Nankai Trough, at around 15-12 Ma (Kimura et al., 1996). The Shikoku basin crust was still very young when it began subducting beneath Eurasia, with volcanic activity in the Shikoku basin continuing until around 12 Ma, as recorded on the Kinan seamounts (Kobayashi et al., 1995). As such, at around 13 Ma the most recently active spreading centre of the Shikoku basin began subducting beneath southwest Japan. The response to this was distinctive adakitic fore-arc volcanism (Takahashi et al., 1999).

4.2 10 Ma to 6 Ma

Some workers propose that northward subduction of the PSP beneath the Eurasian Plate ceased from 10-6 Ma (Uto, 1989; Kamata, 1992) (Figure 4.2). Conflicting views are held by other authors who either suggest there was no late Miocene halt in subduction of the PSP (e.g. Kimura et al, 2003), or suggest an alternative time period for a 'stagnant' phase in subduction (e.g. Taira, 2001 suggests 14-8 Ma).

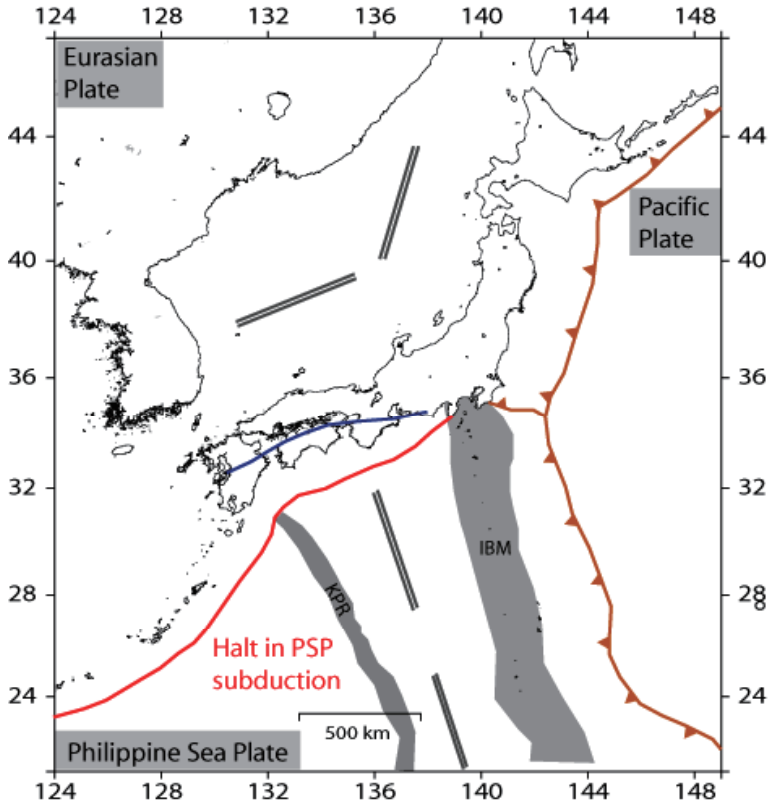

Figure 4.2: Major tectonic changes occurring in the time period 10-6 Ma.

The proposed halt in subduction is summarised by Kamata and Kodama (1994) and mainly supported by volcanic evidence (i.e. lack of a subducted plate signature in erupted lavas during this time). Whether or not there was an actual halt in PSP subduction from 10-6 Ma is inherently difficult to resolve, as it is very challenging to find direct evidence for an actual halt in subduction of the PSP slab, while it is much more straightforward to recognize initiation of subduction-related processes (e.g. arc volcanism, back arc spreading etc).

4.3 6 Ma to 2 Ma

In Kyushu, characteristics of the modern-day subduction regime began around 6 Ma, as shown in Figure 4.3. Re-initiation of subduction was accompanied by a change in subduction direction, with the PSP subducting in a NNW direction (Seno, 1989). The NNW direction of PSP subduction meant that the intersection point of the Kyushu Palau ridge with the trench migrated north east along the Nankai Trough. Subduction of the PSP beneath the Ryukyu arc at this time was coincident with the commencement of back arc rifting in the Okinawa Trough (e.g., Sibuet et al., 1987). NNW subduction of the PSP at the Nankai trough during this time period was nearly perpendicular to the plate boundary (e.g., Kamata and Kodama 1994) (compared with the present day, where there is currently dextral obliquity).

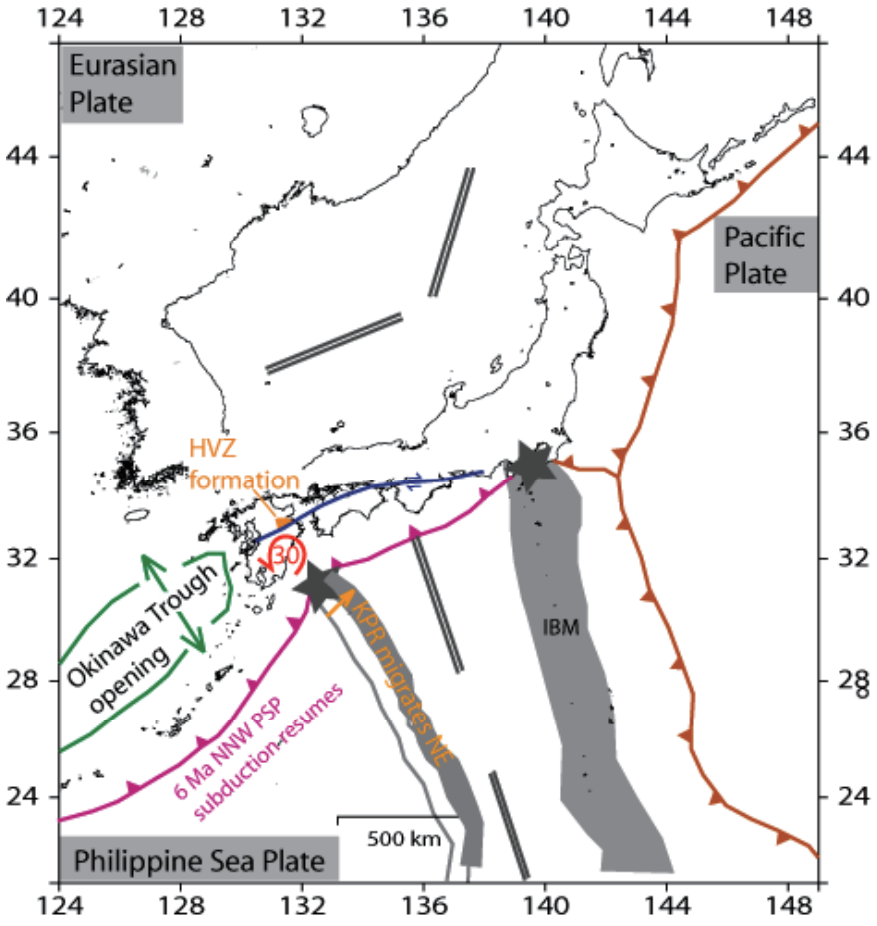

Figure 4.3: Major tectonic changes occurring in the time period 6-2 Ma. The Philippine Sea Plate (PSP) began subducting once again, in a NNW direction. The Kyushu Palau ridge (KPR) subduction point began migrating NE up along the Nankai Trough due to relative plate motions. The Okinawa Trough began opening. The MTL began dextral motion, and there was clockwise rotation of the forearc sliver in south Kyushu. The Hohi volcanic zone (HVZ) formed on the edge of the Median Tectonic Line (MTL). IBM = Izu Bonin Mariana arc.

Palaeomagnetic data led Kodama and Nakayama (1993) to conclude that southern Kyushu underwent about 30 degrees of anticlockwise rotation after the latest Miocene. Anticlockwise rotation of southern Kyushu also facilitated rifting in the Beppu-Shimabara Graben (BSG) region. Evidence for extensional deformation in southern Kyushu for the past 5 Ma (Tada, 1985; Yamaji, 2003), and slab rollback of the PSP after 5 Ma (Yamaji, 2003), is also consistent with the anticlockwise rotation of southern Kyushu since ~6 Ma. Wallace et al. (2009) suggest that anti-clockwise rotation of southern Kyushu occurs in response to the along-strike change in buoyancy properties of the subducting PSP (e.g., along-strike change from young Shikoku Basin subduction to subduction of the Eocene-Cretaceous crust of the West Philippine Basin).

North of the MTL in northeastern Kyushu, a rectangular volcano-tectonic depression 70 km long and 40 km wide (the Hohi volcanic zone and associated Beppu Graben), began forming at ~6 Ma (Kamata & Kodama, 1994). Temporal evolution of volcanism in the Hohi Volcanic Zone suggests that volcanism subsequently migrated inwards towards the central part of the current Beppu graben (Kamata, 1989; Kamata & Kodama, 1994; Figure 4.4).

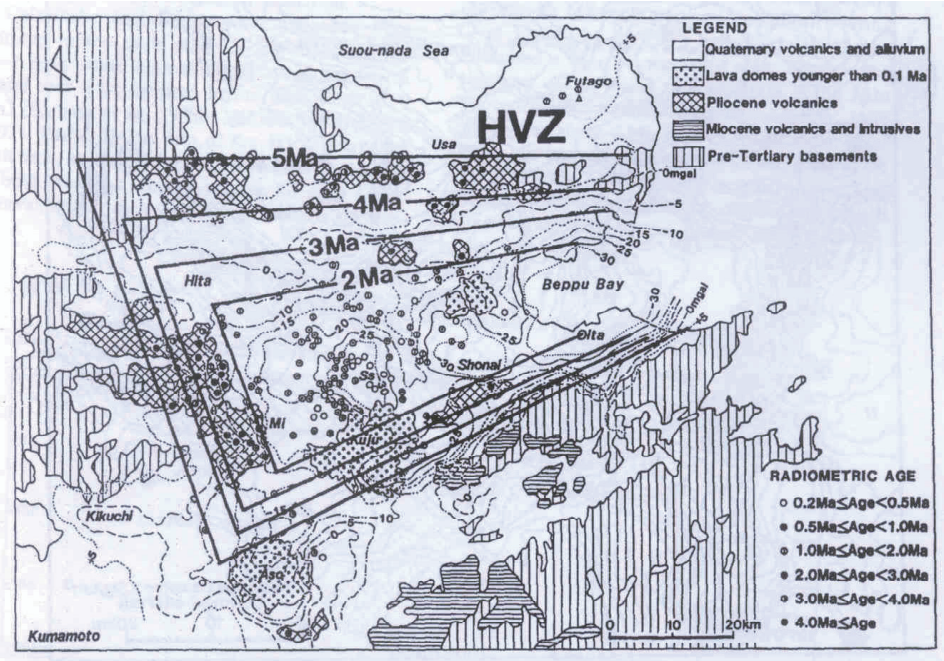

Figure 4.4: Evolution of volcanism in the Hohi Volcanic Zone after Kamata and Kodama (1994). Radiometric ages of volcanic rocks are shown. This map demonstrates that older volcanics occur on the outer boundaries of the graben, while younger deposits concentrate in the centre of the Graben.

Extensional faulting also migrated in the same fashion, from a 45-km-wide zone in 5-6 Ma to a 11 km-wide zone around 1 Ma (Katama, 1989). Presence of lineations (old faults?; see Figure 6.1) parallel to and outside (north and south) the current graben boundaries from analysis of gravity and magnetism maps support the inward migration of faulting. This inward migration of faulting is common in rifts worldwide, as the crust gets thinner along the rift axis, the boundary faults become inactive and activity shifts to the axial faults (Ethiopian Rift: Hayward and Ebinger, 1996; Taupo Rift, New Zealand: Villamor & Berryman, 2006). This also agrees with the presence of thinner seismogenic crust in the Beppu graben area than that outside the graben (Figure 4.5).

4.4 2 Ma to Present

Since the beginning of the Quaternary, Kyushu has entered its latest tectonic phase (see Figure 4.6). At this time the PSP shifted its subduction direction from NNW to NW (Matsuda, 1980; Nakamura et al., 1984; Okamura, 1988). This resulted in an increased dextral component of subduction, leading to intensified dextral motion along the Median Tectonic Line (MTL) (Kamata and Kodama, 1994; Kamata, 1998; Itoh et al., 1998a). Okada (1980), Ichikawa (1980) and Sangawa (1986) suggest that the MTL was a thrust/reverse fault in the early Quaternary and then became a dextral strike-slip fault during the second half of the Quaternary.

The change in PSP subduction direction also heralded a change in migration direction of KPR along the PSP-Eurasian margin. Since 2 Ma the position of the KPR subduction has been migrating southwestward, opposite to the previous direction (Figure 4.7). There may have also been a decreasing rate of extensional deformation in the Hohi area (Beppu Graben) with time (Kamata and Kodama, 1999), which could be related to encroachment of the KPR and subduction of the buoyant Shikoku Basin beneath northeast Kyushu (thus lessening the extensional stress in the region with time). Between 1-0.7 Ma, a north-south extensional stress

field was present in the Hohi volcanic zone (Kamata et al., 1988). By 0.7 Ma, a compressional stress regime was active within the Hohi volcanic zone, in particular in the area of the Shishimuta caldera (Kamata et al., 1988).

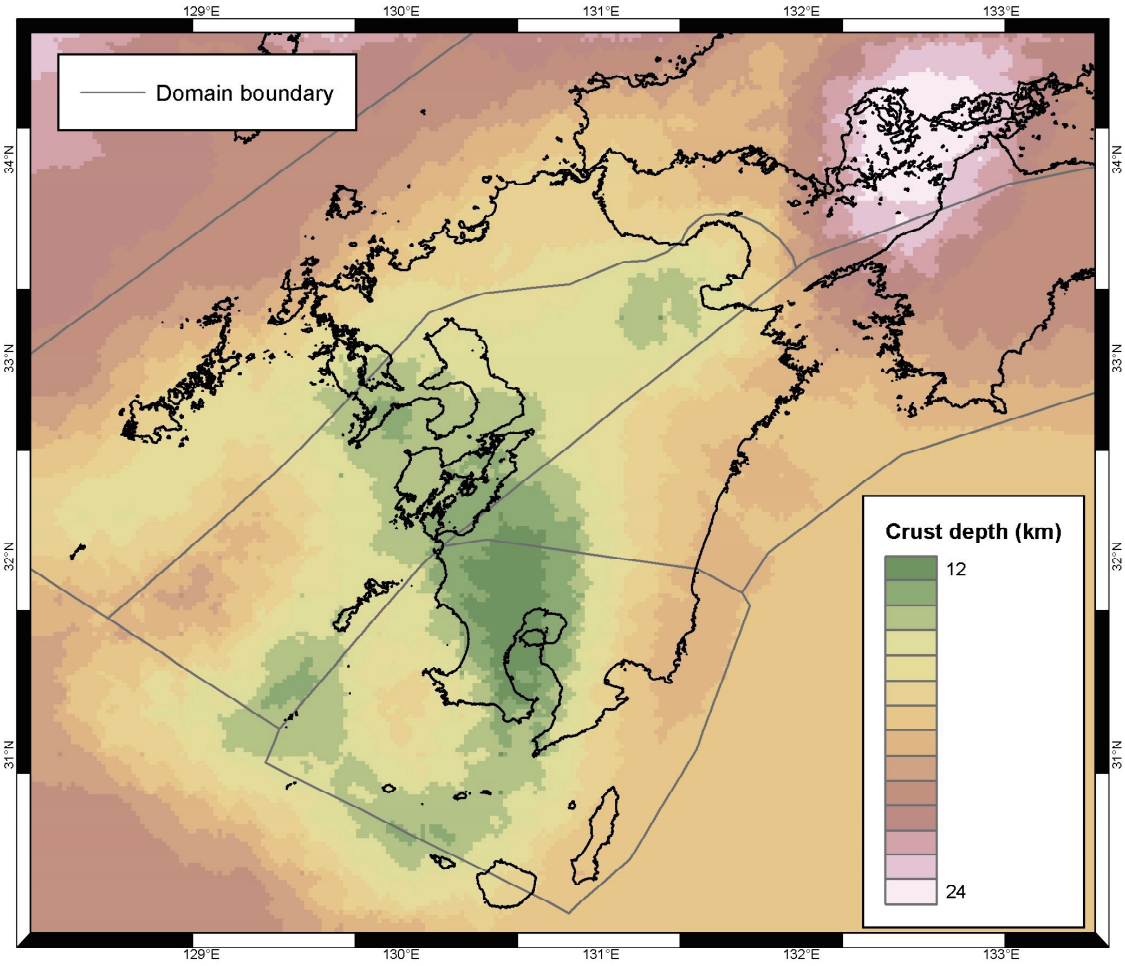

Figure 4.5: Map of the depth of the seismogenic crust from earthquake depth distribution data

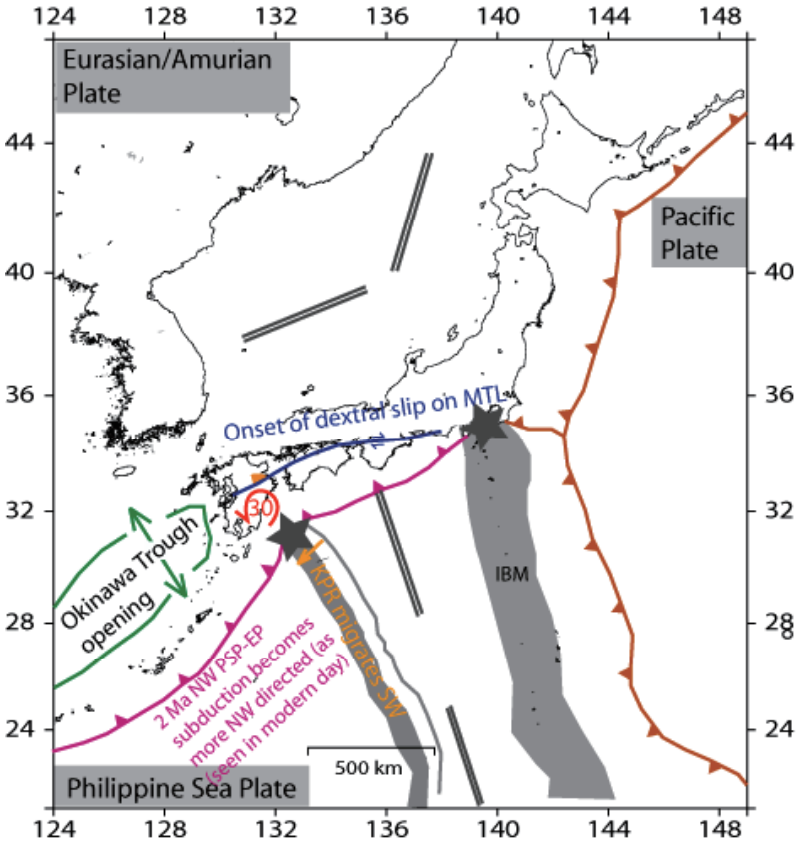

Figure 4.6: Major tectonic changes occurring in the time period 2-0 Ma. The Philippine Sea Plate (PSP) changed subduction direction to NW, which caused an onset of dextral motion on the Median Tectonic Line (MTL). The KPR began migrating SW along the Nankai Trough due to the change in plate motion direction. This may have caused a change form extensional to compressional regime in the HVZ leading to a slow down in magma production.

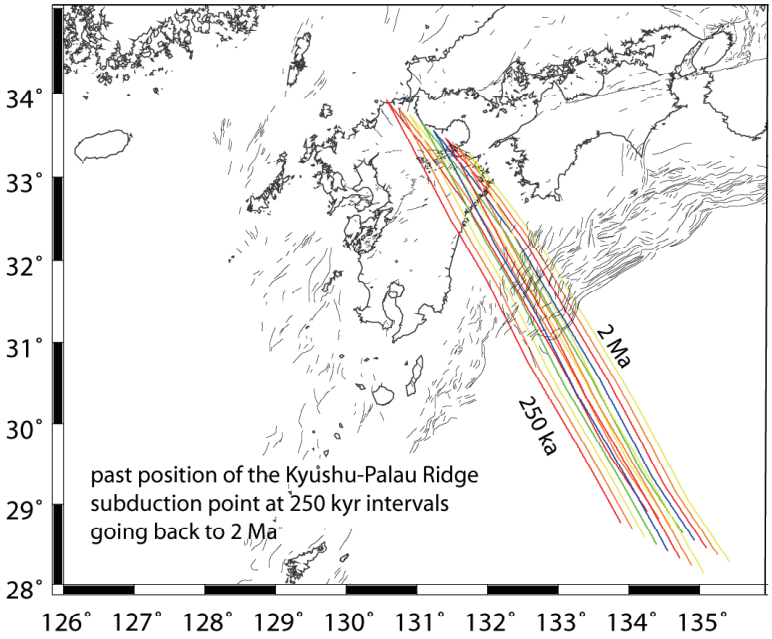

Figure 4.7: Reconstruction of the position of the Kyushu-Palau ridge from 250 ka to 2 Ma, shown at 250 ka intervals. Ridge position reconstructed based on present-day relative motin between the Philippine Sea Plate and the Amurian Plate. This shows that the ridge was subducting adjacent to the NE end of Kyushu at 2 Ma, and has since migrated southwest to its current position.

4.5 Present Day Tectonic Situation

Current tectonics in Kyushu is dominated by ~72-79 mm/a convergence of the PSP and the Amurian Plate at a slightly oblique (right-lateral sense) angle. Strike-slip and extensional faulting is ongoing in the BSG in central Kyushu (e.g., Kamata, 1992; Kamata and Kodama, 1999) (Fig. 4.8). Southwest, along-strike of the BSG, active back-arc rifting continues to occur in the Okinawa Trough (e.g., Lee et al., 1980; Sibuet, et al., 1987). Active extension also occurs in the Kagoshima graben in southern Kyushu (e.g., Aramaki, 1984; Kodama et al., 1995) at rates (from GPS) of <7-8 mm/a (Wallace et al., 2009) and there is some geological evidence for active normal faulting (e.g., Japan's Active Fault Research Centre's Active Faults Database: http://www.aist.go.jp/RIODB/activefault/cgi-bin/index.cgi). North-south extension in the Shimabara Graben, right lateral shear along the Oita-Kumamoto line, and strong left-lateral shear across southern Kyushu is evident from modern-day GPS velocities (see discussion in Section on Strain Rates from GPS). GPS velocities also suggest that anti-clockwise rotation of southern Kyushu may be ongoing today. Wallace et al. (2009) suggest that the left-lateral shear in southern Kyushu revealed by GPS measurements is a result of Kyushu-Palau Ridge collision (see Section on Strain Rates from GPS).

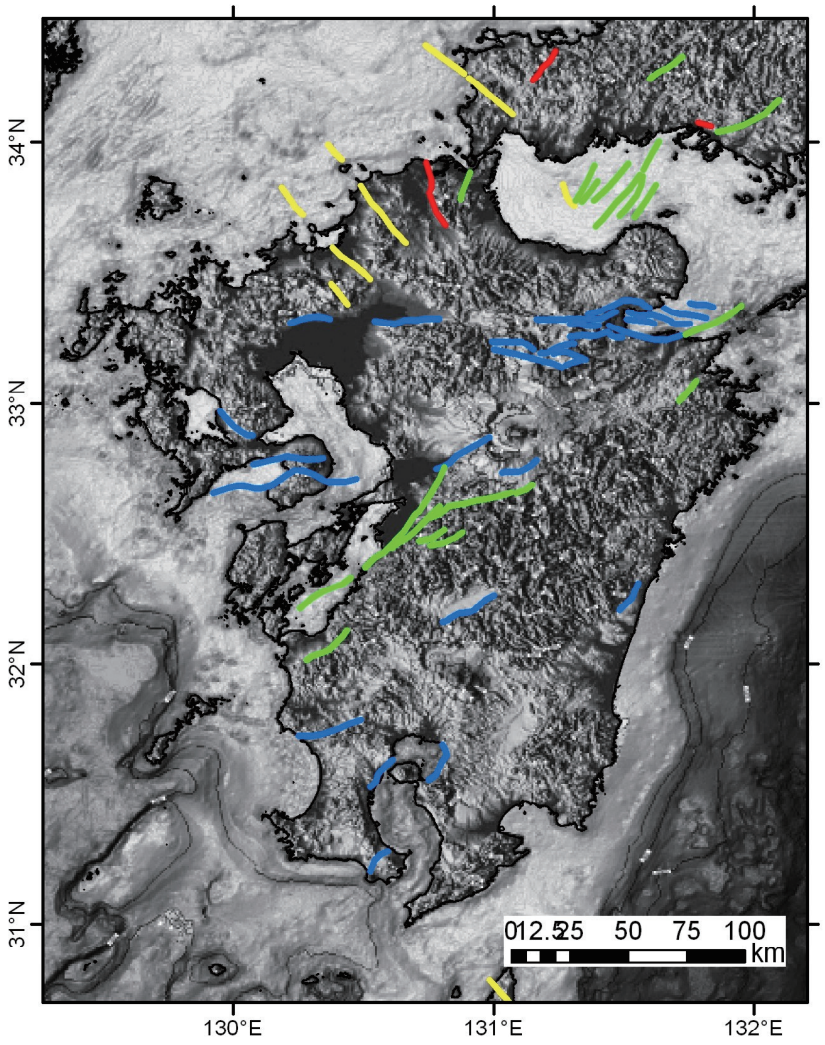

Figure 4.8: Active faults in southwest Japan from the Active Fault Research Centre's active fault database (http://www.aist.go.jp/RIODB/activefault/cgi-bin/index.cgi). The faults are color-coded by sense of movement (green = dextral; blue = normal, red = reverse, yellow = sinistral).

In general, historical seismicity in Kyushu consists of numerous offshore thrust earthquakes related to subduction at the Nankai/Ryukyu Troughs, and normal and strike-slip events within central Kyushu related to deformation in the BSG (Figure 4.9). Most normal faulting earthquakes in central Kyushu indicate approximately north-south directed extension,

consistent with geological studies. There is also a zone of east-west trending left-lateral strike-slip earthquakes northwest and northeast of the Kagoshima Graben, which corresponds with the zone of high left-lateral shear strain from GPS. Similarly, in northern Kyushu, there are several significant left-lateral strike-slip earthquakes with focal planes that strike transverse to the margin that correspond to some known, active left-lateral faults (Figure 4.9, and see Figure 4.8 for location of left-lateral faults near these earthquakes in northwest Kyushu). The March 2005 M_w 7.0 earthquake offshore Fukuoka City is related to this zone of faulting in northern Kyushu. Previous workers have suggested that these left-lateral events occur due to "bookshelf" style faulting within a region of overall right-lateral transpression (Kanaori and Kawakami, 1996). A large variety of earthquakes representing virtually every sense of faulting occur in Kyushu, reflecting the complex and dynamic active tectonic setting there.

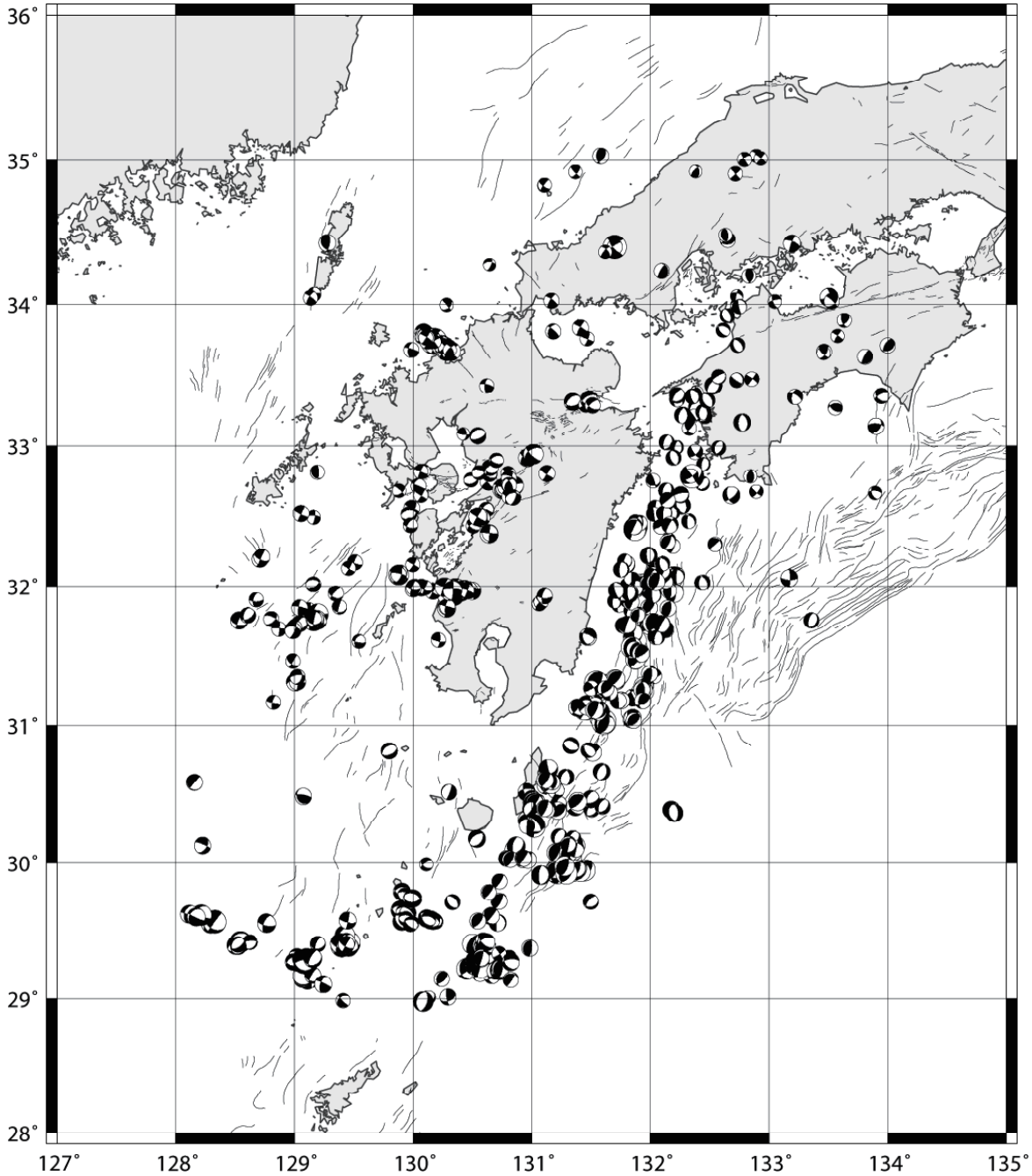

Figure 4.9: Focal mechanism plots for earthquakes in southwest Japan from 1997-2006. Based on CMT solutions from the JMA catalogue (data from http://www.fnet.bosai.go.jp).

4.6 References for Section 4

Aramaki, S., 1984, Formation of the Aira Caldera, southern Kyushu, 22,000 years ago, J. Geophys. Res., 89(B10), 8485-8501.

Hayward, N., and Ebinger, C., 1996, Variations in the along-axis segmentation of the Afar rift system: Tectonics, v. 15, p. 244–257.

Ichikawa, K. 1980. Geohistory of the Median Tectonic Line of southwest Japan. *Mem. Geol. Soc. Jpn.* **18**, 187–212.

Itoh, Y., K. Takemura, H. Kamata. 1998. History of basin formation and tectonic evolution at the termination of a large transcurrent fault system: deformation mode of central Kyushu, Japan. *Tectonophysics.* **284**, pp135–150.

Kamata, H., Uto, K., Uchiumi, S., 1988. Geochronology and evolution of the post-Shishimuta caldera activity around the Waitasan area in the Hohi volcanic zone, Kyushu, Japan. Bull. Volcanol. Soc. Jpn. 33, 305-320.

Kamata, H., 1989, Volcanic and structural history of the Hohi volcanic zone, central Kyushu, Japan: Bulletin of Volcanology, v. 51, p. 315–332.

Kamata, H. 1992. Right-lateral movement of the Oita-Kumamoto Tectonic Line as a western extension of the Median Tectonic Line, originated from rightward, oblique subduction of the Philippine Sea plate. *Mem. Geol. Sot. Jpn*., **40**, pp53-63.

Kamata, H. 1998. Quaternary volcanic front at the junction of the South-west Japan Arc and the Ryukyu Arc. *Journal of Asian Earth Sciences.* **16**, pp67-75.

Kamata, H. & K. Kodama. 1994. Tectonics of an arc-arc junction: an example from Kyushu Island at the junction of the Southwest Japan Arc and the Ryukyu Arc. *Tectonophysics.* **233**, 69-81.

Kamata, H. & K. Kodama. 1999. Volcanic history and tectonics of the Southwest Japan Arc. *The Island Arc.* **8**, 393-403.

Kanaori Y, Kawakami S. 1996. Microplate model and large inland earthquakes of southwest Japan: implications for generation of the 1995 M7.2 Hyogo-ken-nanbu earthquake. *Zishin* 49:125–39 (In Japanese)

Kimura, G., 1996, Collision orogeny at arc-arc junctions in the Japanese islands: The Island Arc. **5**, pp 262–275.

Kimura, J. I., T. Kunikiyo, I. Osaka, T. Nagao, S. Yamauchi, S. Kakubuchi, S. Okada, N. Fujibayashi, R. Okada, H. Murakami, T. Kusano, K. Umeda, S. Hayashi, T. Ishimaru, A.

Kimura, J-I., R. J. Stern, T. Yoshida. 2005. Reinitiation of subduction and magmatic responses in SW Japan during Neogene time. *GSA Bulletin.* **117**, pp. 969–986, doi: 10.1130/B25565.1

Kobayashi, K., S. Kasuga, K. Okino. 1995. Shikoku Basin and Its Margins. In “Backarc Basins: Tectonics and Magmatism”. By Brian Taylor. Published by Springer, 1995. ISBN 0306449374, 9780306449376. p398

Kodama, K., H. Tashiro, T. Takeuchi. 1995. Quaternary counterclockwise rotation of south Kyushu, southwest Japan. *Geology*. **23**, pp 823–826.

Kodama, K., K. Nakayama. 1993. Paleomagnetic evidence for post-late Miocene intra-arc rotation of south Kyushu, Japan. *Tectonics.* **12**, pp35–47.

Lee, C.S., G.G. Shor, D.D. Bibee, R.S. Lu and T.W.C Hilde, 1980, Okinawa Trough: Origin of a back-arc basin, *Mar. Geol., 35,* 219-241.

Matsuda, T., 1980, Traces of Izu Peninsula—its direction of movement during the recent several million years, *Earth Monthly, 2*, 164-8.

Nakamura, K., K. Shimazaki, N. Yonekura. 1984. Subduction, bending and eduction. Present and Quaternary tectonics of the northern border of the Philippine Sea plate. *Bull. Soc. Geol. Fr.* **26**, pp221–243.

Ninomiya, A. Tanase. 2003. Late Cenozoic volcanic activity in the Chugoku area, southwest Japan arc during back-arc basin opening and reinitiation of subduction. *The Island Arc*. **12**, pp22–45

Okada, A., 1980. Quaternary faulting along the Median Tectonic Line of southwest Japan. *Mem. Geol. Soc. Jpn*. **18**, pp79–108.

Okamura, Y., 1988, subduction of seamount and paleo subduction direction of the Philippine Sea Plate, *Earth Monthly, 10*, 603-7.

Sangawa, A. 1986. The history of fault movement since Late Pliocene in the central part of southwest Japan. *Bull. R. Soc. N.Z*. **24**, pp75–85.

Seno, T., 1989. Philippine Sea plate kinematics. *Modern Geol*. **14**, 87–97.

Sibuet, J.-C. and ten co-authors, 1987, Back arc extension in the Okinawa Trough, *J. Geophys. Res., 92*, 14041-14063.

Tada, T., 1985. Spreading of the Okinawa Trough and its relation to the crustal deformation in Kyushu (2) (in Japanese with English abstr.) *Zisin, J. Seismol. Soc. Jpn*. **38**, pp1–12.

Taira, A. 2001. Tectonic Evolution of the Japanese Island Arc System. Annu. Rev. Earth. Planet. Sci. **29.** 109-134

Takahashi, M. 1999. Large felsic magmatism of the Miocene outerzone of southwest Japan. *Earth Monthly,* Special Volume 23, 160—168. (in Japanese)

Uto, K. 1989. Neogene volcanism of Southwest Japan: Its time and space based on K-Ar dating. *Ph.D. Thesis, Univ. Tokyo*, 184 pp.

Villamor, P., and Berryman, K.R., 2006, Evolution of the southern termination of the Taupo volcanic zone, New Zealand: New Zealand Journal of Geology and Geophysics, v. 49, p. 23–37.

Wallace, L.M., S. Ellis, K. Miyao, S. Miura, J. Beavan, J. Goto. 2009. Enigmatic, highly active left-lateral shear zone in southwest Japan explained by aseismic ridge collision. *Geology*. (In Press)

Watanabe, Y. 2005. Late Cenozoic evolution of epithermal gold metallogenic provinces in Kyushu, Japan. *Mineralium Deposita*. **40**. 307-323. doi: 10.1007/s00126-005-0025-7

Yamaji, A. 2003. Slab rollback suggested by latest Miocene to Pliocene forearc stress and migration of volcanic front in southern Kyushu, northern Ryukyu Arc. *Tectonophysics.* **364**, pp9–24.

5 Volcanic History of Kyushu

Section 4 gave an insight into the complexity of the tectonics (and, thus, the volcanism) encountered in Kyushu. This Section details the volcanic episodes that have occurred in Kyushu throughout the last 15 Ma. The volcanism is discussed in similar time intervals to the tectonics in the Section 4, to allow the reader to draw comparisons with the two histories. Unlike tectonic events, which are relatively standardised and well defined (e.g. strike slip vs. dip slip faulting), volcanoes have much less well-established standards. This volcanic history Section begins by introducing the broad classification of the volcanoes described in this account, and the areas in which they occur.

5.1 Dating and Classifying Volcanoes

Tough challenges are faced in trying to establish when a volcano actually formed. It is far easier to date the youngest activity (usually an eruption) of a volcano, than it is to pinpoint the time when the first activity of that volcano occurred. The oldest rocks are often buried by later eruptions or removed by erosion. In creating a detailed volcanic history of Kyushu, this dating issue becomes an important factor in the confidence we can have in our reconstructions, as we later attempt to link the origins of volcanic episodes with other physical processes occurring at that time. This lack of knowledge of exactly when volcanoes formed adds some ambiguity to our assessments, specifically when working towards forecasting where future volcanoes will form. Many volcanoes have age data regarding a range of eruptions or eruptive episodes. This can help suggest how long-lived that particular volcanic centre has been and this knowledge can then be used to suggest future volcano occurrences. In this study, the oldest available eruption date of the volcano is taken to be the time at which it formed.

Another difficulty faced is classifying different ‘types’ of volcano. A thorough approach would be to treat each volcano like an entry into a field notebook. If information on the volcano is recorded as a detailed description of all the features of the volcano, then volcanoes would not get pigeon-holed as a certain ‘type’ of volcano, e.g. caldera, stratovolcano etc. The danger with classifying a volcano as one type is that volcanoes do not tend to be ‘type A’ or ‘type B’. They tend to be a mixture of types, forming a wide spectrum. Distinguishing clear definitions of volcanoes is also difficult, due to their evolutionary nature. However volcanoes must be assigned certain working classifications (e.g. caldera, lava dome), otherwise volcano studies would be impossible. In the case of the Japanese volcanoes there are many workers collecting excellent data; however there are classification issues. In the first edition of the Japanese ‘Database of Quaternary Volcanoes, 1999’ (Committee, 1999) there were cataloguing issues of ‘what is a volcano’ and ‘what is an edifice’, amongst others. In the Tohoku Case Study, one method of classification was attempted on a set of these data, using cladistic methods to classify the volcanoes broadly into groups (see Chapman et al., 2009).

5.2 The Kyushu Volcano Dataset

In this study, a dataset of the Kyushu volcanoes has been created by collating data from many different sources, such as the excellent AIST online Quaternary volcano database (AIST, 2008), as well as information gathered from various field trips, individual papers and Japanese websites. In this dataset, volcano ages mostly ranged up to 6 Ma; however information regarding mid to late Miocene volcanism has also been included in this account. The information regarding older volcanism generally has less accurate details regarding volcano locations, due to poor preservation potential in older volcanic systems. This dataset was created with the aim of characterising volcanism in Kyushu at different times and in different areas. An overall aim was to elucidate the volcanological history of Kyushu and to relate it to the complex tectonic history occurring concurrently.

The location of volcanism in Kyushu appears to be strongly linked to the local and regional tectonics. There have been studies of the tectonic influence on volcanism (e.g. Nakajima & Hasegawa, 2007; Kamata and Kodama, 1999), using the composition and timing of volcanism in Kyushu to explain the tectonic history and to establish the current tectonic setting

underpinning Kyushu. The interpretation of the volcano-tectonic interaction in Kyushu developed in the ITM project is dealt with in the following Section.

5.3 Introduction to the Three Volcanic Regions

Kyushu can be divided into four main tectonic 'domains' as described in the following Section (Section 6). However it was considered prudent to use slightly different divisions and names for the areas of interest when describing the volcanic history. Partly, this reasoning is that the tectonic domains are based on tectonic events, so using these domains would assume that the tectonic and volcanic events are related. Also, the names of the tectonic domains relate to the Quaternary tectonic situation, so could be confusing when looking at the Miocene to present volcanic history. For the purpose of describing the volcanic history, Kyushu is divided into 3 Sections: the north western, central and southern volcanic regions, demonstrated by Figure 5.1.

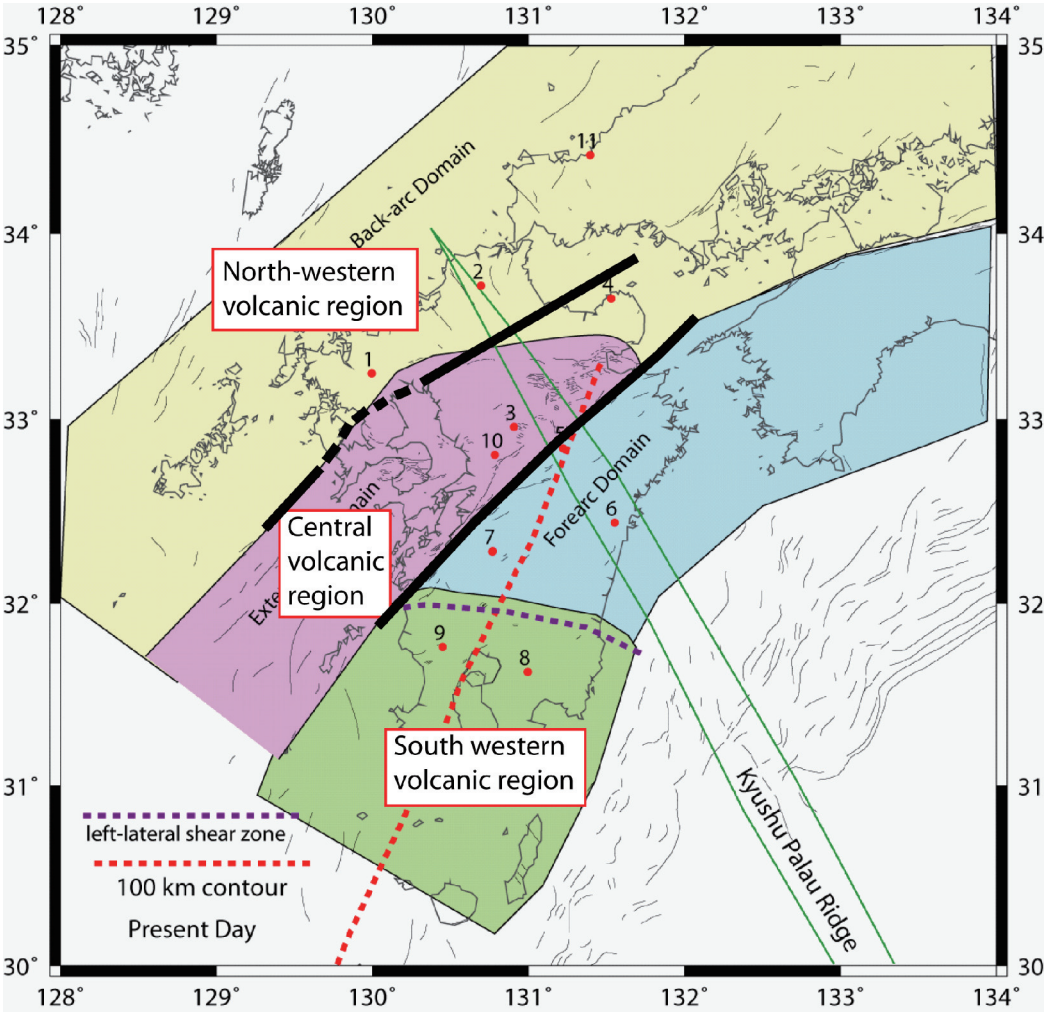

Figure 5.1: The differences between the tectonic domains and the volcanic regions are subtle, but clear. The thick black line marks how Kyushu is divided into the three volcanic regions for the purposes of this study. The tectonic domains (see Section 6) evolve with time (not shown here) whereas the volcanic regions are kept the same, to allow easy understanding of the accompanying descriptive account of the volcanism. The north western/central volcanic region boundary is slightly different to that of the tectonic domains. In the east the volcanic boundary is located further north, due to volcanism further east along the BSG (e.g. Futago volcano). In the west the north western/central boundary is dashed, as this area is slightly ambiguous. Evolved rhyolite volcanoes (Arita rhyolites) occur alongside flood basalts (Higashimatsuura basalts), thus the boundary between different types of volcanism is unclear.

The northwest region has seen a range of volcanic activity over the past 15 Ma, from widespread flood basalts to mature rhyolitic volcanoes. Typical volcanism of this area is episodic back-arc volcanism, with a proliferation of monogenetic volcanoes. The central region is a long-lived area of volcanism, with activity changing in style through time. Styles of activity range from voluminous lava plateaus and monogenetic volcanoes to lava domes, cinder cones, ignimbrite plateaus and huge calderas. The southeastern region has had periods of major widespread lava eruptions as well as recent massive caldera formation along the arc front since 0.3 Ma.

5.3.1 Types of volcanism and occurrence throughout Kyushu

Volcanism in Kyushu is driven by the subduction of the Philippines Sea Plate (PSP) beneath the Eurasian Plate at the Ryukyu trench and the Nankai trough (see Figure 3.1). Kyushu displays a clear volcanic arc, as well as sporadic back-arc volcanism. However there are anomalies, such as Unzen volcano, which appears to be influenced by arc and back-arc processes. Back arc volcanism in Kyushu is largely found in the northwestern region; however, influences of non-arc type magmas are found in other areas at different times, due to the migration of the volcanic front. Current back arc volcanism is typified by monogenetic volcanism. However, back arc volcanism in Kyushu has previous been characterised by widespread flood basalts, and even some more evolved polygenetic systems (e.g. Arita rhyolites). This mixture of types of behaviour in the back arc exemplifies the changing nature of volcanism in Kyushu.

The back arc region of Kyushu has been suggested by some workers (e.g. Shinjo et al., 2000) to also be influenced by a heat source off the coast of NW Kyushu, related to the Sea of Japan/Shikoku basin. The Okinawa trough is actively spreading into the adjacent central region of Kyushu, adding an extra dimension to the magmas generated in this region. Forearc volcanism is currently non-existent in Kyushu. However, in the mid Miocene, SW Honshu experienced fore-arc volcanism, so it should not be automatically assumed that volcanism cannot occur in the fore arc region. The forearc region of Kyushu is the southeastern corner of the island, coinciding with the forward domain (Figure 5.1).

Typical arc volcanism has been prevalent in Kyushu for the last 2 Ma, but the activity has been notably more explosive since 0.3 Ma. Since 2 Ma, the volcanic arc has formed on a clearly defined NE-SW trend. The volcanic arc is defined by a variety of volcanic manifestations, from huge calderas (e.g. Aso, 18 x 25 km diameter), small calderas (e.g. Ikeda-ko), lava dome complexes (e.g. Kuju) and polygenetic stratocones (e.g. Sakurajima). The volcanic front continues down through the Ryukyu arc towards Taiwan, tracing the surface location of the 100 km depth contour of the subducting PSP. The large calderas in the Kyushu volcanic arc often appear to have precursory voluminous andesitic lava flows.

5.3.2 Geochemistry of the volcanic rocks in Kyushu

This short Section summarises data on the geochemistry of the central volcanic region. Geochemistry provides essential indicators to help infer the source conditions of magma genesis beneath volcanic regions. There are key signatures that help to trace the stages of magma evolution and fingerprint the tectonic setting through well-established global correlations between tectonic processes and magma chemistry. Figure 5.2 shows the six geochemical discrimination diagrams used in this study with examples of data from Kyushu.

Back-arc basaltic alkaline volcanism typically shows elevated alkalis and trace and minor element characteristics of Ocean Island Basalts (OIB) on a Ti-P-Mn plot and Intraplate volcanics on a Nb-Zr-Y diagram. Such volcanic geochemistry characterises the back arc region. Subduction zone volcanism is usually characterised by a subduction fluid component and for example low Nb and Ti, defining distinctive geochemical fields. Arc related rocks can also be divided in tholeiitic and calcalkaline varieties and both varieties occur in the young volcanic arc (< 2 Ma). A special class of arc volcanic rocks are known as adakites and are characterised by high Sr/Y ratios. Adakites are commonly associated with subduction of young hot lithosphere. This high ratio is seen in the arc volcanoes from Aso trending north eastwards along the arc, including Aso, Kuju, Yufu and Oninomi (Figure 5.2). Adakites are

thought to be caused by the initiation of volcanism, the subduction of a still hot plate, or direct melting of the slab. Subducting beneath these volcanoes is the young, hot Shikoku basin, the likely cause of these adakites.

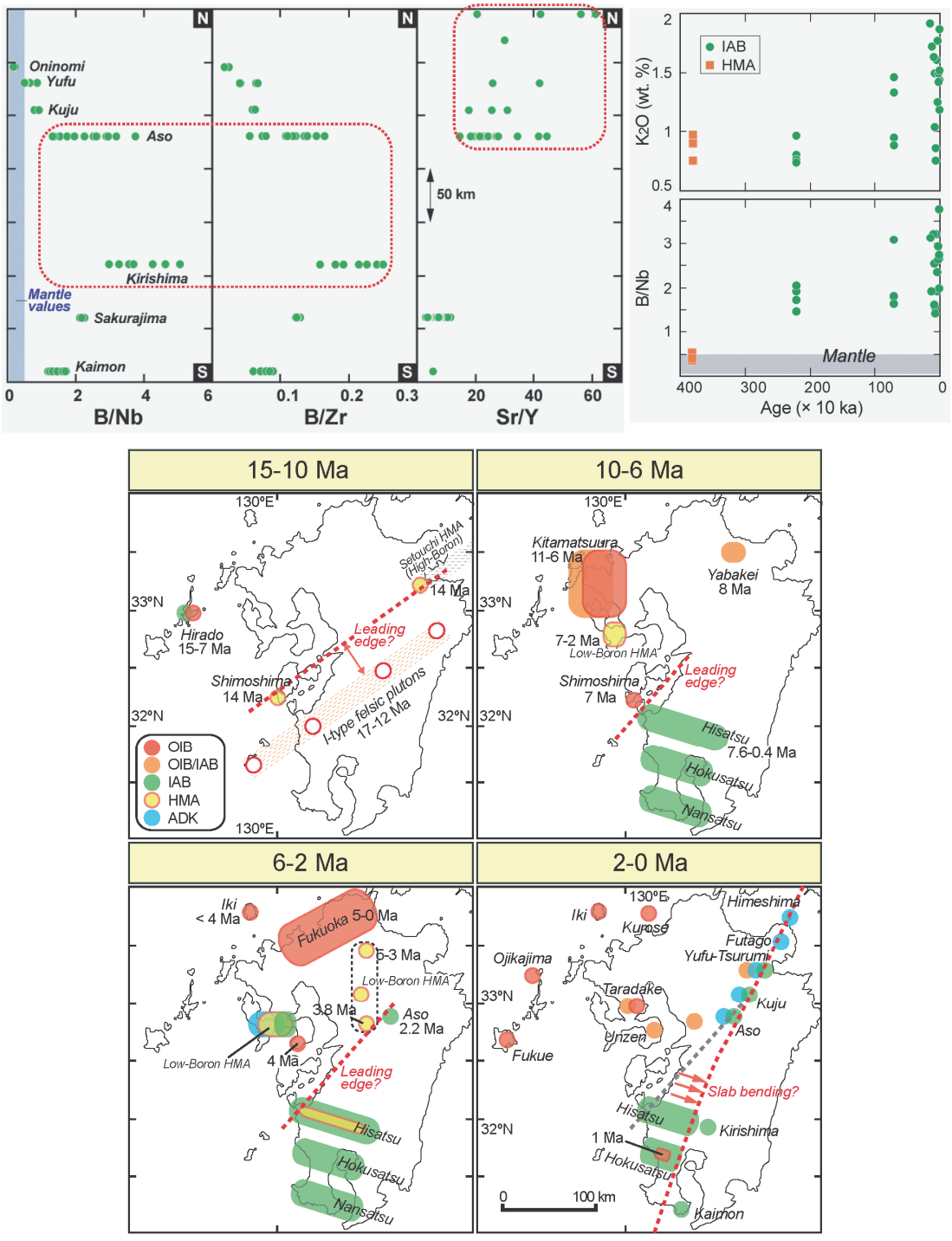

Figure 5.2: This concise summary of the geochemistry of volcanoes in Kyushu supports tectonic and volcanic evidence for the evolution of Kyushu. The upper left plot demonstrates elevated B/Nb and B/Zr ratios at Aso and Kirishima volcanoes. This can be interpreted as the source magma of Kirishima and Aso volcanoes being influenced by the water-rich Kyushu Palau ridge as it subducts. The high Sr/Y ratios seen in Oninomi, Yufu and Kuju volcanoes represent adakitic lavas, a product of subducting the still hot Shikoku Basin. The upper right plot demonstrates the changing composition of lavas produced at Aso volcano with time. There is an apparent increase in the fluid-mobile elements of B/Nb and K_20, showing a trend from initial high magnesium andesites towards more typical island arc basalts. The maps provide a geochemical interpretation of the tectonic and volcanic regimes affecting Kyushu through the last 15 Ma.

In Kyushu rocks with exceedingly high ratios of fluid mobile elements such as potassium and boron (K_2O and B/Nb or B/Zr) are observed as a distinctive class (Miyoshi et al., 2008). Such compositions suggest that the magma genesis region was very water rich. Aso and Kirishima volcanoes show elevated B/Nb and B/Zr ratios compared to the normal arc values (Figure 5.2). This suggests that material subducted at the Nankai trough was particularly rich in water bearing minerals or water rich sediments. K_2O, B/Nb and other fluid-mobile elements of Aso basaltic rocks are also seen to have increased with time. The chemical composition of the mantle beneath Aso volcano seems to have changed between 3.8 and 2.2 Ma to have a much higher K_2O and B/Nb content (Figure 5.2). This could be inferred to be a result of fluid addition from the subducted PSP to the mantle beneath the Aso area.

Figure 5.2 shows a possible evolution of the tectonics in Kyushu based on the geochemical tracers identified. High magnesium andesites (HMA) identify the volcanism above the leading edge of the subducting plate, adakites (ADK) likely represent very hot areas of melt generation, ocean island basalt (OIB) represent volcanism unrelated to subduction and island arc basalts (IAB) are arc volcanoes. This reconstruction suggests how, with time, the leading edge of the plate has retreated south eastwards, and rotated anticlockwise, or perhaps even bent.

5.4 Volcanic history of Kyushu since 15 Ma

The main time divisions discussed here are similar to the divisions used in the tectonic history in the previous Section 4. However, here the account begins at around 15 Ma, dealing with volcanism from 15-10 Ma, 10-6 Ma, 6-2 Ma, then providing a more detailed account of the Quaternary volcanism from 2-1 Ma, 1-0.3 Ma, 0.3-0.01 Ma and 0.01-0 Ma (Holocene). Each of the major time divisions shows major changes in the volcanism that divide it from adjacent Sections. Changes in volcanism are due to new volcanism, shut down of volcanism, erupted volume, style, activity, etc. It should be noted that unless otherwise stated, all age information comes from the online AIST database (AIST, 2008).

5.4.1 15-10 Ma

Japan is the product of repeated episodes of accretion via subduction processes, plus associated arc volcanism. Beneath Kyushu, the most recent ‘episode’ of subduction (albeit intermittent), involved the subduction of the PSP beneath the Eurasian Plate (EP), from around 15 Ma. Figure 5.3 presents a summary of volcanism in this period.

Evidence of volcanism associated with this mid Miocene subduction is only recognisable today in the form of a band of I-type felsic plutonic rocks. These are assumed to represent the igneous activity associated with the arc volcanism occurring further northwest of this band at the time. The NE-SW trend of this band of plutons across the central volcanic region implies a northwestward subduction direction, similar to what is seen today. These plutons form part of much more widespread igneous activity which took place within the SW Japan forearc between 17-13 Ma (Kano et al., 1991). Tatsumi and Maruyama (1989) demonstrated that this subduction of the young, hot PSP between 17 to 10 Ma (Takahashi, 1981; Tatsumi, 1983), led to the formation of high magnesium andesites (Setouchi HMAs) in SW Japan.

Meanwhile, offshore, at 15 Ma the final stages of Sea of Japan opening led to rifting of the western margin of NE Honshu (Yamaji, 1990). This rifting was accompanied by eruption of a large volume of submarine volcanic rocks, commonly called “Green Tuff” (Taira, 2001), as well as some dykes in NW Kyushu.

Initial volcanic activity occurred at 15 Ma at the most northerly volcanic centres associated with Kyushu: Iki, Hirado and Oki Islands. The volcanism at Iki is very long lived, with the initial stage reported to occur from 15-4.3 Ma, and most recent stages occurring in the late Quaternary. In the northern Goto Islands, volcanic activity occurred on Hirado Island at 15 Ma, then again from 9-6 Ma (Uto et al., 2004). It has been suggested that this is associated with the Sea of Japan magmatism. However from around 11 Ma an asthenospheric heat source off NW Kyushu (Shinjo et al., 2000) appeared to be feeding volcanism in that area, so perhaps there are mixed magma sources. Back arc monogenetic volcanism in the

northwestern region also began in this period, with monogenetic volcano clusters up to 15-40 km in diameter.

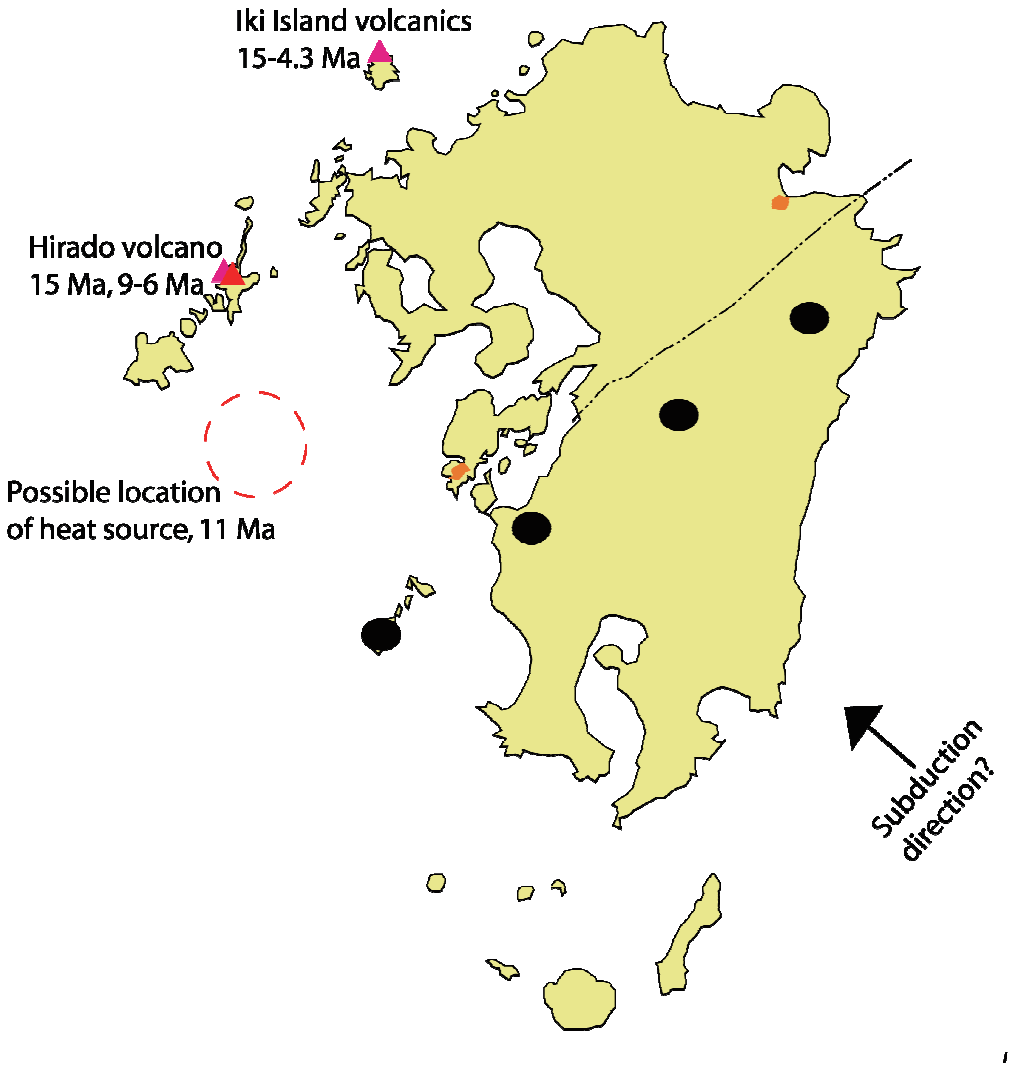

Figure 5.3: From 15-10 Ma the position of the volcanic front is unknown, however can be inferred from the location of a band of I-type felsic plutons trending NE-SW across central Kyushu. There is some minor volcanism in the northwestern volcanic region.

Notes to this and Figures 5.4 to 5.9: The location of the HVZ is taken from Kamata & Kodama 1994, the location of the Beppu Shimabara Graben is after Hoshizumi, 2006, the location of the Median Tectonic Line, Hisatsu, Hokusatstu, Nanasatsu volcanic rocks are taken from Shinjo et al., 2000, the location of the I-type felsic plutons are after Kimura et al., 2005. Figures 4-10 are a series of maps illustrating the changes in volcanism in the past 15 Ma.

5.4.2 10-6 Ma

At the same time as the proposed halt in PSP subduction beneath the EP, volcanism largely ceased, but did continue in certain areas of Kyushu (see Figure 5.4). The nature of the volcanism from 10-6 Ma was different to that which occurred pre-10 Ma: there were no large-scale igneous systems as represented by the plutons which formed in the previous time period); all volcanism was now predominantly effusive in nature.

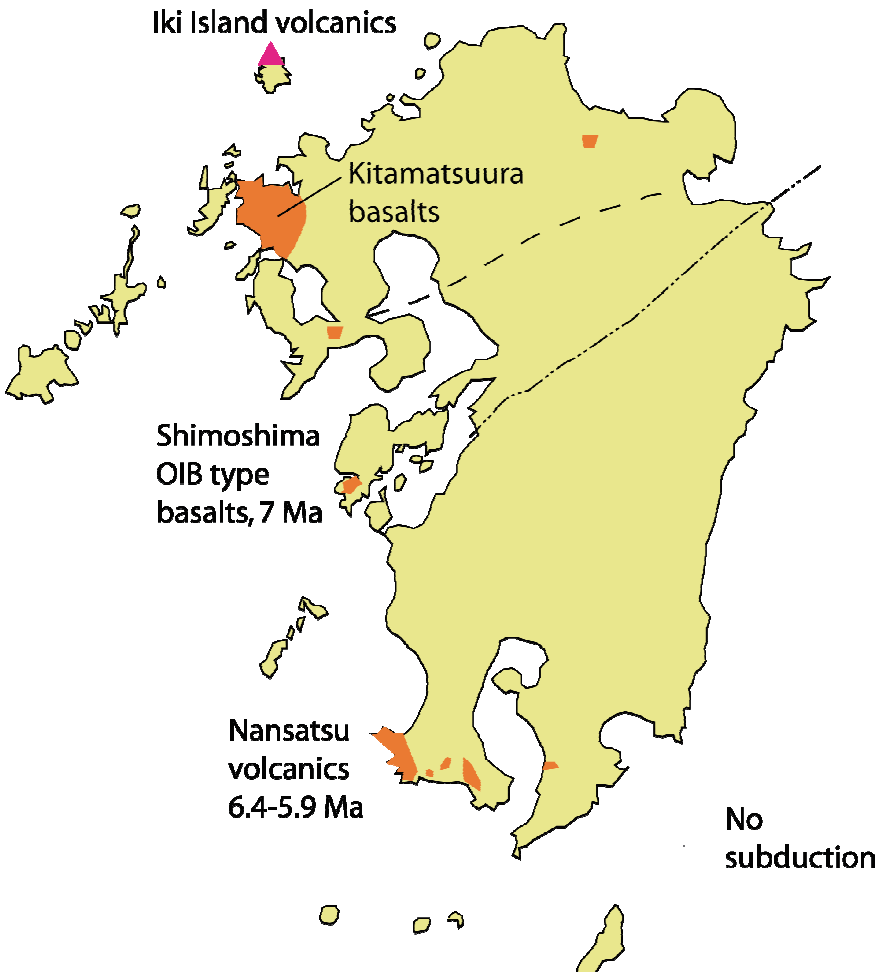

Figure 5.4: 10 – 6 Ma. During the halt in Philippine Sea Plate subduction, voluminous lava outpourings occur sporadically through time; however, they are only located along the very western edge of Kyushu.

The volcanism that occurred in Kyushu at this time was mostly localised in the northwestern region, with a smaller amount in the southern region (see Figure 5.4). Iki island was still volcanically active, and new volcanic episodes occurred in the Kitamatsuura region. These formed eight, highly voluminous and episodic alkali basalt lava flows, all sloping gently to the northwest and each approximately 100 m thick. The geochemistry of the magmas erupted in this time period showed a low plate component; for example, the Shimoshima area erupted OIB type basalts at 7 Ma (Nagao et al., 1992). Calc-alkaline volcanism was absent during this time. Howeve,r Kamata and Kodama (1994) describe how mantle xenolith-bearing basanites erupted between 9.5-6.5 Ma, supporting the idea that the oceanic plate did not subduct during this period (Uto, 1989).

In general, the late Miocene and Pliocene volcanic activity in the southwestern volcanic region forms three zones from north to south, the Hisatsu, Hokusatsu and Nansatsu zones. The most southerly of these zones, the Nansatsu zone, was the site of calc-alkaline volcanism at the end of this period (Hedenquist et al., 1994), indicating the inception of subduction at around 6.4 Ma.

5.4.3 6-2 Ma

Six million years ago significant changes took place in the subduction regime of the PSP, when the PSP re-initiated subduction beneath the EP. The nature of much of the volcanism throughout Kyushu also changed at this time (see Figure 5.5).

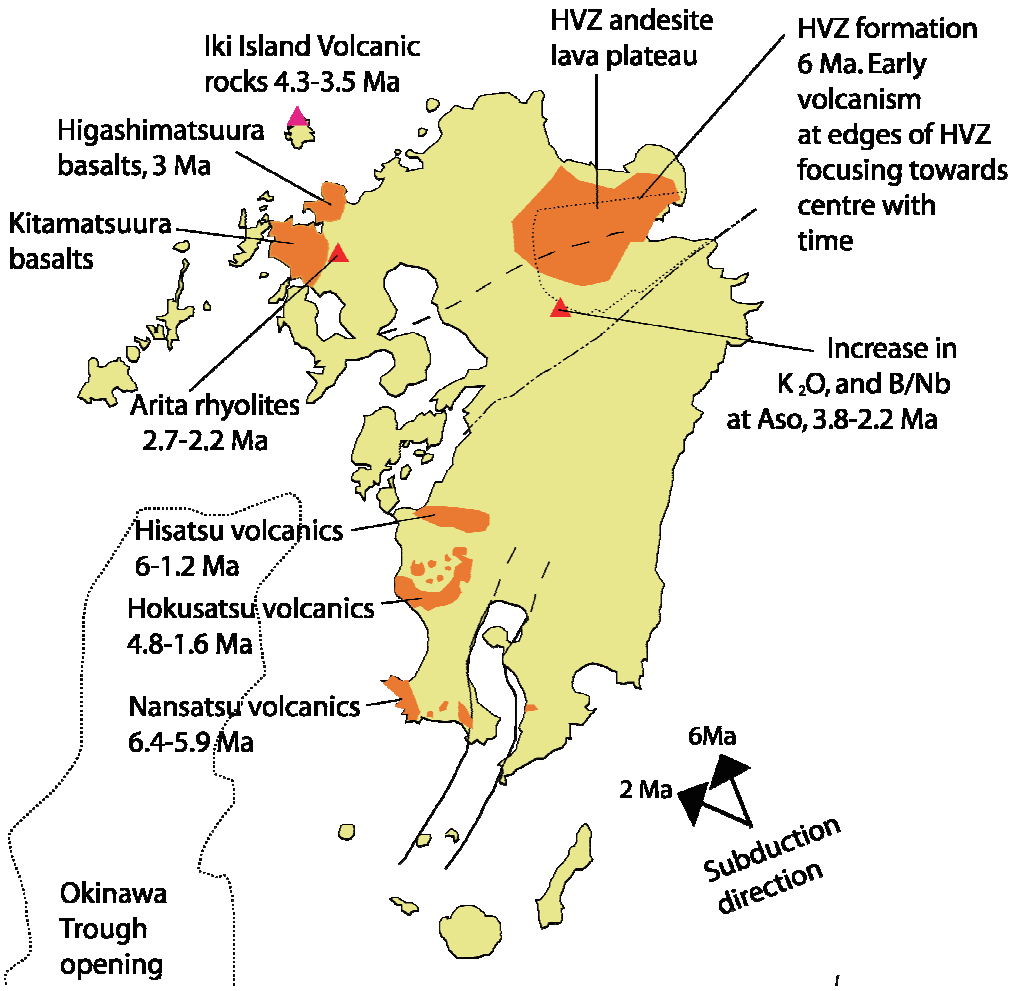

Figure 5.5: 6 – 2 Ma. Re-initiation of subduction at approximately 6 Ma is closely followed by the formation of the Hohi Volcanic Zone (HVZ). Volcanism in the HVZ initially formed at the edges of the zone and focused into the centre with time. Widespread andesite lava plateaus also formed from the HVZ at this time. An increase in B/Nb and K_20 are noted at Aso, likely due to the re-initiation of subduction and so increase in the slab fluid content of magmas generated in this region. Widespread lavas continue in the north western and southern regions. A series of rhyolite stratovolcanoes form at and near Arita suggesting a more long lived volcanic centre rather than the episodic behaviour of the lava plateau forming eruptions.

However the northwest volcanic region showed little change and still exhibited voluminous effusive volcanism. The Kitamatsuura basalts continued, as well as strong alkali volcanism at Oki Island from 7-4 Ma and Iki Island from 4.3-3.5 Ma. These were joined by the development of another flood basalt area the Higashimatsuura basalts, located to the east of the Kitamatsuura area. The Higashimatsuura basalts erupted at about 3 Ma, forming five main, 50 m thick lava flow units, each episode occurring over one hundred thousand years or less. Both the Kitamatsuura and Higashimatsuura basalt areas demonstrate short-lived outpourings, showing how this northwestern region is typified by 'episodic' volcanism.

However, anomalous to the regional stereotype of episodic basalt outpourings, the eruption of much more evolved rhyolite magmas occurred at about 2.7-2.2 Ma, at Arita and surrounding areas. The Arita rhyolites lie to the east of the Kitamatsuura basalts and are accompanied by related andesites and basalts. The Arita rhyolites are very unusual for this region as they imply a longer-lived volcanic centre, rather than short episodes of activity. Iki Island showed an increase in the intensity of activity since the initial phase, with 'Stage 1' activity from 4.3-

3.5 Ma, swiftly followed by 'Stage 2' at 3.5-2.8 Ma. These stages were much more intensive than the initial (Stage 0) basaltic activity, with Stage 1 producing andesites, basalts and trachyandesites, and Stage 2 producing rhyolites and basalts (Sano 1995). The Stage 1 volcanism on Iki Island is rather unusual for Kyushu, as between 4-3 Ma there is very little volcanism anywhere else in Kyushu.

The central volcanic zone also saw a discernable increase in volcanism at this time. The formation of the Hohi Volcanic Zone (HVZ) in the central region marked the start of highly explosive volcanism, last seen in Kyushu at about 12-10 Ma. Early HVZ volcanism occurred at the edge of the tectonic boundaries of the HVZ seen today. With time, the volcanism focused towards the centre of the HVZ (Kamata & Kodama, 1994). Activity within the HVZ produced voluminous eruptions of andesite as lava flow plateaus, which were intruded by east-west trending feeder dykes.

The central volcanic regions of Kyushu have been studied in relation to their eruptive volumes through time, with the HVZ recording its maximum eruption rate at 5 Ma, then decreasing throughout the Pliocene to the present (Kamata and Kodama., 1994). At the same time, eruptive volumes have increased in the Shimabara peninsular area (Yokose et al., 1999). However the total volume of erupted material was much higher in the HVZ than in the Shimabara area. These facts indicate the differing volcanic and tectonic histories within the eastern and western parts of the central volcanic region.

Further west than the HVZ, the K_2O, B/Nb and other fluid-mobile elements in the Aso basaltic rocks (still in the central volcanic zone) increased from 3.8 to 2.2 Ma. This suggests an increasing fluid content in the mantle beneath the Aso area.

During this time period, the southern volcanic region underwent some repeated (but not continuous) activity in the Hokusatsu zone. This activity occurred from 4.8 to 1.6 Ma and comprised widespread andesitic/dacitic lava flows and pyroclastic cones (Uto and Uchiumi, 1997). The more southerly, Nansatsu zone also produced plateau lavas from 6.4-5.9 Ma. However, the exact vent locations of these are unknown.

5.4.4 2-1 Ma

The start of the Quaternary is fairly well established as the start of recent arc volcanism in Kyushu (e.g. Watanabe, 2005). Also occurring at this time were some fairly major tectonic events, such as the collision of the Kashima-Daiichi and Japan Group sea mount chains at the Kanto triple junction (near Tokyo), the opening of the Okinawa Trough near Kyushu, and the change in subduction direction of the PSP from NNW to NW, beneath the EP. This slight change in subduction direction had significant effects on the related plate tectonic and volcanic regimes. The MTL exhibited strongly intensified dextral motion, which still continues today. Significant changes in the mode of eruption and whole-rock chemistry also occurred throughout Kyushu (Kamata and Kodama, 1994) (see Figure 5.6 for a summary).

The northwestern volcanic region was the site of a considerable amount of volcanism from 2 - 1 Ma. Continuing on from the previous time period (6-2 Ma), there was more volcanism in the Iki monogenetic volcano group and the final stage of the Arita rhyolites at Ureshino volcano.

The Iki volcanics changed compositionally to form mainly basalt scoria cones during Stages 3-5 (2.5-2.2 Ma, 1.7-1.4 Ma, 1-0.6 Ma) (Sano, 1995). Further west, off the mainland of Kyushu, the Goto Islands had considerable activity; at Kishuku from 1.07-0.66 Ma, Ojikajima monogenetic volcano group from 1.1-0.3 Ma, and at Ukujima polygenetic stratovolcano from 1.3-1.1 Ma. In terms of eruptive volumes, Ojikajima peaked at 1 Ma and 0.6 Ma with intense volcanism, lasting for 0.1 Ma in the centre of the volcanic field. Ukujima is unusual amongst the volcanoes in the Goto Islands in that it was not basaltic or monogenetic. Ukujima produced rhyolites, basalts and andesites similar to the Taradake basalts (Sudo et al., 1998). Taradake is located on the mainland, in the Nagasaki prefecture, to the north of Unzen volcano. It has been active in two main stages, the older stage being from 1.3-1.0 Ma, which produced stratovolcanoes and lava domes of andesite, basalt and dacite. Further to the east

(but still in the NW zone), Kurose volcano, a small islet north of Genkai-jima, had basaltic activity at 1.1 Ma.

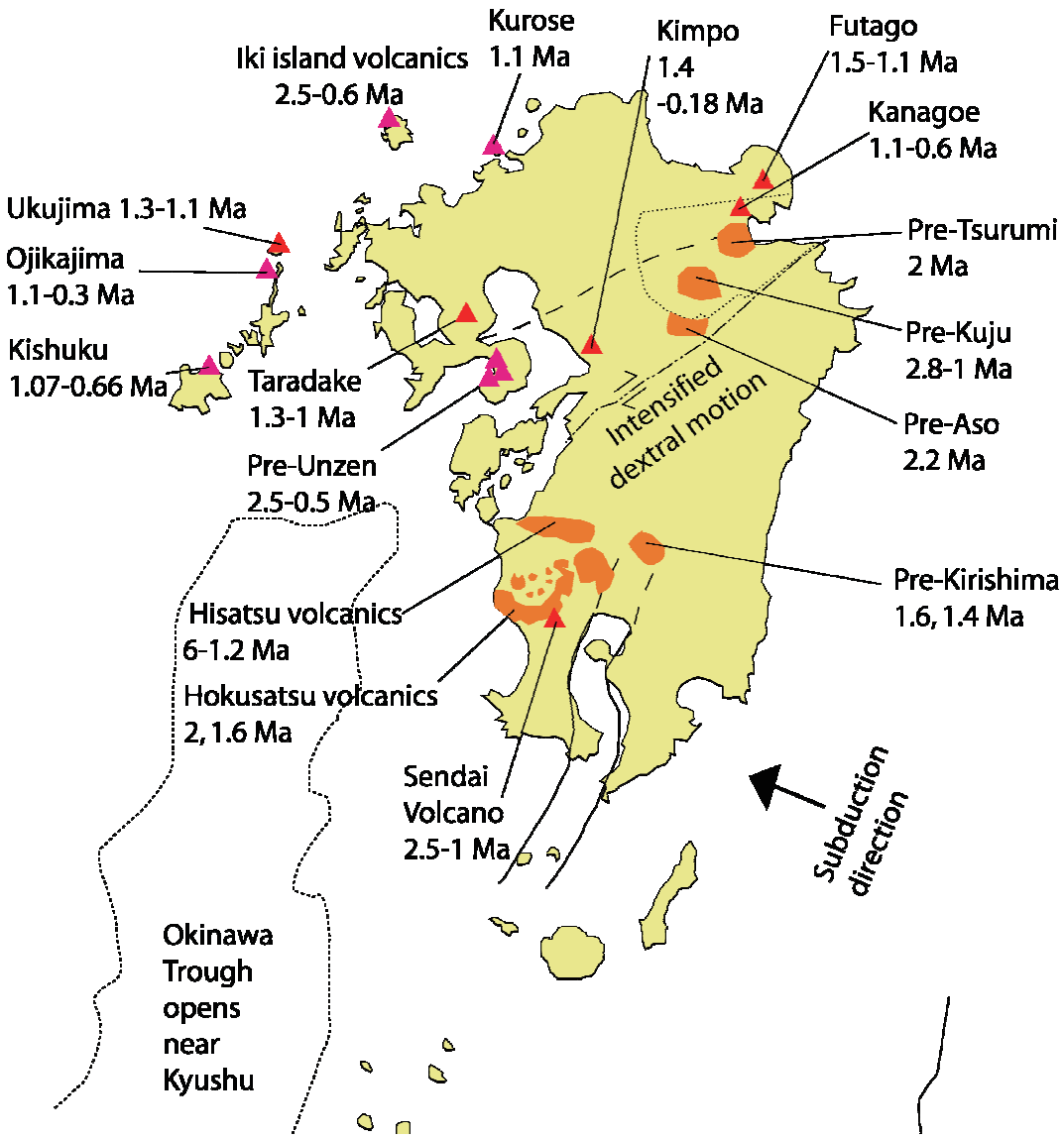

Figure 5.6. At 2 Ma the subduction direction altered to north-west, which in turn intensified the dextral motion on the Median Tectonic Line (MTL), and opening in the Okinawa Trough reached western Kyushu. Volcanism in the western part of the Beppu Shimabara Graben was dominated by stratovolcanoes. There were many lava shield volcanoes/lava plateaus formed at around 2 Ma, commonly associated with locations of future more explosive volcanism. N.B. The size and shape of the lava plateaus of Pre-Kirishima, Pre-Aso, Pre-Kuju and Pre-Tsurumi are estimates.

Volcanism in the central volcanic region during 2-1 Ma largely took the form of voluminous andesite shield lavas, laying the foundations for later stages of volcanism in the extensional regime of the Beppu-Shimabara graben region. In the eastern part of the central zone, Futago volcano produced andesitic and dacitic lava domes and lava flows, which formed from about 1.5/1.46-1.1 Ma. This activity was followed nearby at 1.1-0.6 Ma by Kanagoe andesitic stratovolcano.

At this time, volcanism in the HVZ had passed its peak activity phase (6-5 Ma), but was still evolving in nature, with the formation of andesite/dacite lava domes at 2 Ma and a marked increase in K_20 component at 1.6 Ma. Yufu/Tsurumi, Kuju and Aso are three of the largest volcanic centres in the central volcanic zone today. However, the precursory activity of these volcanic centres began around 2-1 Ma. From east to west, 'Pre-Tsurumi' formed andesite lava plateaus at approximately 2 Ma. 'Pre-Kuju' was initially andesitic, with the Yoshinomoto andesite from 2.8-2.4 Ma, the Matsubara andesite at 2.4-2.1 Ma, the Kusu group at 1.7-1.3 Ma, followed later by the Yamacogawa rhyolite at 1.3-1.0 Ma (Mashiro, 2006). Early activity at Aso began at 2.2 Ma with basaltic eruptions (Takahashi & Kobayashi, 1999). However, this was just the beginning at Aso, as there was more precursory activity before the caldera forming eruptions.

Further to the west but still in the central volcanic region, Kimpo volcano (near present day Kumamoto City) was active from 1.4 Ma until around 0.18 Ma, as an andesitic and dacitic stratovolcano with lava domes. 'Pre-Unzen' volcanics on the Shimabara peninsula initiated around 2.5 Ma, with episodic monogenetic volcanism of olivine basalt and pyroxene andesites, until 0.5 Ma, when present-day Unzen began to form.

Volcanic activity in the southern volcanic region during 2-1 Ma follows a similar pattern to the central volcanic zone, with 'pre-caldera' andesitic lavas occurring where major volcanic activity occurs today. 'Pre-Aira caldera' activity described by Masafumi et al., (2000), is apparent from 3-1 Ma with eruptions of andesitic lava flows (Hokusatsu volcanic rocks). Younger Hokusatsu lava flows and pyroclastic cones are also obvious at 2 and 1.6 Ma (Uto and Uchiumi, 1997). 'Pre-Kirishima' formed shield volcanoes from andesite lava flows at 1.6 Ma forming the Kurino Group and at 1.4 Ma with the Siratori Group. On a smaller scale than the Aira and Kirishima activity, Sendai volcano (west of the present day volcanic front), formed a pyroclastic cone and erupted basaltic and andesitic lava flows from 2.5-1 Ma.

5.4.5 1-0.3 Ma

During the period 1-0.3 Ma there were no dramatic changes in the tectonic regime of Kyushu. The MTL still experienced an intensified dextral motion, and localised areas of the HVZ experienced changes between compressive and extensional stress regimes. Figure 5.7 presents a summary of the volcanism at this time.

In the northwestern volcanic region, volcanism continued in the Fukue monogenetic volcano group with development of Kyonotake, a small shield volcano at 0.34-0.26 Ma. At the northern end of the Goto Islands, the Ojikajima basaltic monogenetic volcano group had four intense volcanic episodes from 1.08-0.3 Ma. By the third intense episode at 0.7-0.56 Ma, the eruptive locations spread out to the east and west.

The final episode of volcanism from 0.56-0.3 Ma displayed reduced intensity, and the vent locations focused into the centre of the volcanic field. The final activity at Ojikajima stopped at 0.3 Ma, with higher MgO levels than the previous stages of volcanism.

The central volcanic region showed continued activity in all the major areas, with large increases in the number of volcanic centres identified through this 1-0.3 Ma period. Working from west to east, activity at the younger stage of Taradake from 0.8-0.4 Ma formed andesite, basalt and dacite lava domes as part of the stratovolcano. Further south from Taradake on the Shimabara peninsula, Unzen volcano grew rapidly from 0.5-0.3 Ma, producing multiple pyroclastic flows. In this first two hundred thousand years, the rate of growth of Unzen was faster than the rate of subsidence in the Shimabara graben.

Further east, activity preceding the Aso caldera forming events continued intermittently, with 'Pre-Aso' andesite pyroclastic flow plateaus and pyroclastic cones at 0.84 Ma, lava flows from Neko-dake (part of 'Pre-Aso') from 0.7-0.4 Ma, then biotite rhyolites at 0.45 Ma (Takahashi and Kobayashi, 1999). Further east again, many new volcanic centres formed between 1-0.3 Ma within the HVZ. There are two loosely clustered groups of volcanoes, one group near present day Kuju, and one group further east near present day Yufu/Tsurumi. Between 1-0.3 Ma the first activity in the group near Kuju occurred in the Shishimuta caldera. The

Shishimuta caldera is a breccia-filled, funnel-shaped depression, 8 km wide and greater than 3 km deep (Kamata, 1988), which violently erupted the 110-km^3 Yabeki pyroclastic flow between 1-0.9 Ma. This older, more productive, Shishimuta phase lasted from 1-0.7 Ma. A modification in the local stress regime of the HVZ led to a change from a north-south extensional regime to a dominantly compressional regime at 0.7 Ma. This change in local stress conditions was coincident with a change in the style of volcanic activity at Shishimuta caldera. The younger Shishimuta caldera activity began at 0.7 Ma, so that from 0.7-0.3 Ma, small volume lavas and lava domes were produced.

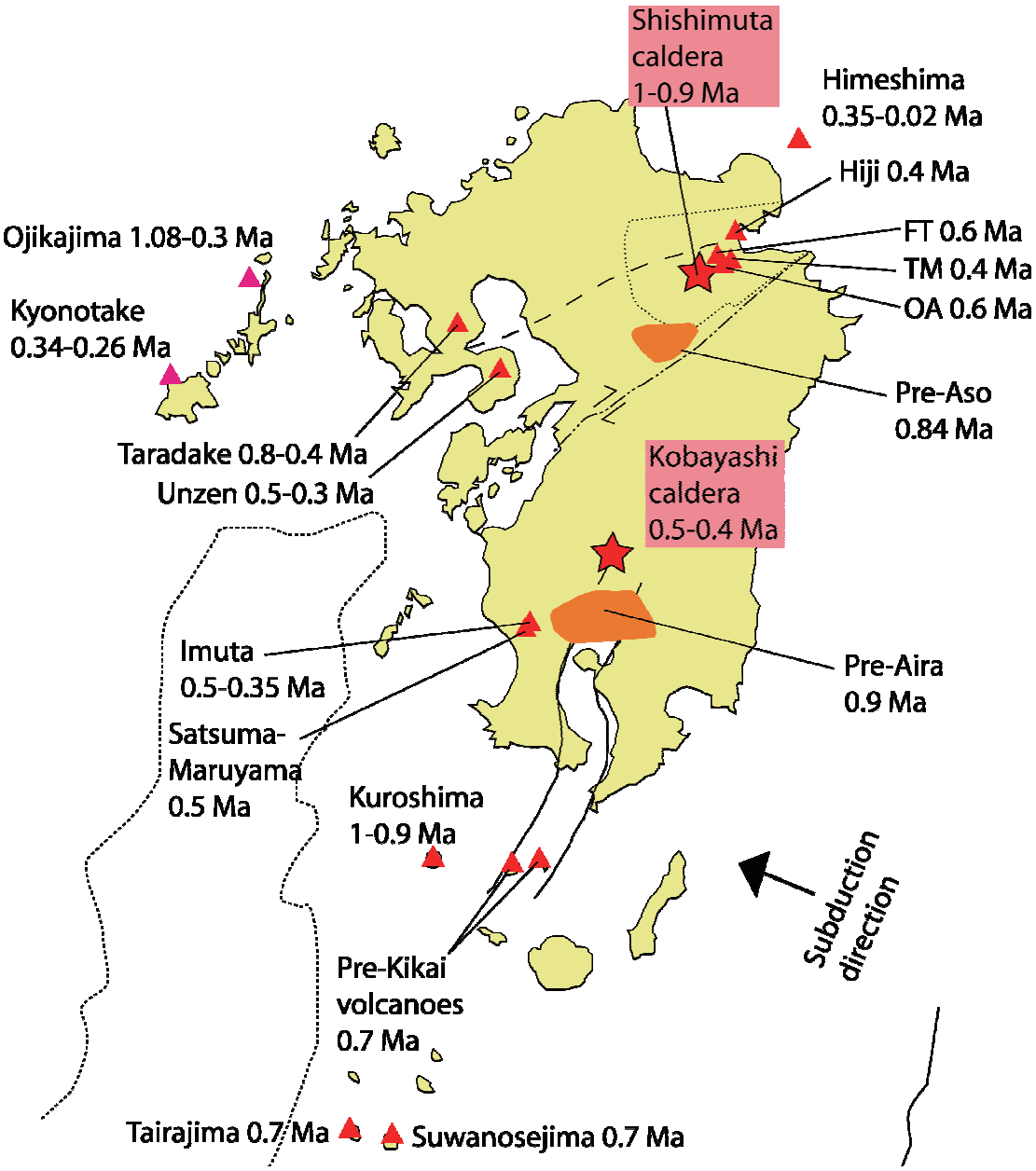

Figure 5.7: 1 to 0.3 Ma. There are no major tectonic changes at 1 Ma, however the volcanism does change in nature. The major change is the start of caldera formation in Kyushu, at Shishimuta and Kobayashi. The HVZ gains an influx of stratovolcanoes slightly north west of Shishimuta caldera.

Post Shishimuta caldera activity has been dominated by monogenetic volcanism (Kamata, 1988). Near the Shishimuta caldera, three other centres in the Kuju area became active at 0.6

Ma. Haneyama volcano produced rhyolitic and dacitic lava flows for one hundred thousand years, Waita yama produced lava domes and stratovolcanoes until 0.4 Ma (Kamata, 1988), and Noinedake-Hanamureyama formed andesite and dacite lava flows and domes until 0.3 Ma.

In the far east of the central region, activity also began around 0.6 Ma, with Ojikayama-Amagoidake and Fukumanyama-Tateishiyama erupting andesite and dacite lava domes and flows for one hundred to two hundred thousand years. From 0.4 Ma, Takahirayama-Mizuguchiyama had a short one hundred thousand year burst of andesite and dacite lava dome forming activity. In the same time period, Hiji volcano, located slightly further east, also produced andesite and dacite lava flows. Offshore and slightly east of Futago volcano, Himeshima volcano showed recent (0.35-0.02 Ma) dacite and rhyolite lava dome and pyroclastic flow forming activity.

Southern Kyushu volcanism in the time period 1-0.3 Ma started at 0.9 Ma with 'Pre-Aira caldera' lava plateaus formed by eruptions of andesitic lava flows in northern Aira (Yuwandake andesite), and basaltic to rhyolitic lava and pyroclastic flows in western Aira. Slightly to the northwest of the 'Pre-Aira' volcanism, a small volcanic depression called the Imuta caldera formed in the centre of a ring of lava domes between 0.5-0.35 Ma. Nearby, the two Satsuma Maru-yama lava domes formed, also at 0.5 Ma. Further north from Aira, slightly to the northwest of where present day Kirishima volcano resides, two calderas formed after 0.5 Ma. The first caldera to form was the Kobayashi caldera from 0.5-0.4 Ma. Kakuto caldera formed one hundred thousand years later at 0.3 Ma, slightly east of Kobayashi caldera. Both calderas produced voluminous dacitic and rhyolitic pyroclastic flow plateaus.

Between 1-0.3 Ma the Ryukyu arc, south of Kyushu, started to become established. The large (ca. 20 x 17 km diameter) Kikai caldera is one of the most northerly volcanoes of the Ryukyu arc and has been active with pre-caldera volcanism since 0.7 Ma. The pre-caldera volcanoes (Yahazu-dake and Takeshima) are located on the caldera rim. However, Kikai caldera-forming eruptions occurred later and are described in the next Section. Moving south through the Ryukyu arc, Kuroshima andesite stratovolcano was active prior to Kikai, from 1-0.9 Ma. Further south and at the same time as the initial volcanism at Kikai (0.7 Ma), Taria jima and Suwanosejima formed andesitic stratovolcanoes with Strombolian and Vulcanian activity.

5.4.6 0.3-0.01 Ma

There were no large-scale tectonic changes that occurred at 0.3 Ma; the only notable tectonic change was the change from extensional to compressional stress regime in the HVZ. However, the nature of volcanism did change quite drastically at this time (see Figure 5.8). The southern volcanic zone became a highly productive area: volcanism focused in the central zone, and activity in the northwestern zone declined steadily. This could be related to recent onset of extension and progressive rollback of the slab. The gigantic calderas of Kyushu formed during this time period, with caldera forming eruptions of Aso, Aira, Kakuto, Ata and Kikai.

The northwestern volcanic region at this time was concentrated into the Fukue monogenetic volcano group, with activity from 0.25-0.13 Ma at Akadaki and cinder cones and lava flows at 0.018 Ma at Oni-dake.

The major events of the central volcanic zone were the four caldera forming eruptions of Aso volcano, at 0.3 Ma (Aso 1), 0.14 Ma (Aso 2), 0.12 Ma (Aso 3), and 0.09 Ma (Aso 4). All of these massive eruptions formed widespread pyroclastic flow plateaus. Post-caldera volcanoes of Aso such as Naka-dake and Take-dake began to form from 0.022 Ma (Miyabuchi et al., 2004). Aso has two flank volcanoes that have formed along a fault running west from Aso towards Kumamoto City. The first of these flank volcanoes to form was Akai volcano at 0.3 Ma, which had continued sporadic activity until 0.18 Ma. Akai volcano erupted immediately prior to the Aso 1 eruption, and produced dacitic lava flows and a pyroclastic cone. Today, Akai stands only 33 m high and is located approximately 30 km west of Aso. The other flank volcano of Aso is Omine monogenetic volcano, which formed between the

major eruptions of Aso 3 and Aso 4 (i.e. between 120-90 Ka), and is located approximately 15 km west of the centre of Aso caldera.

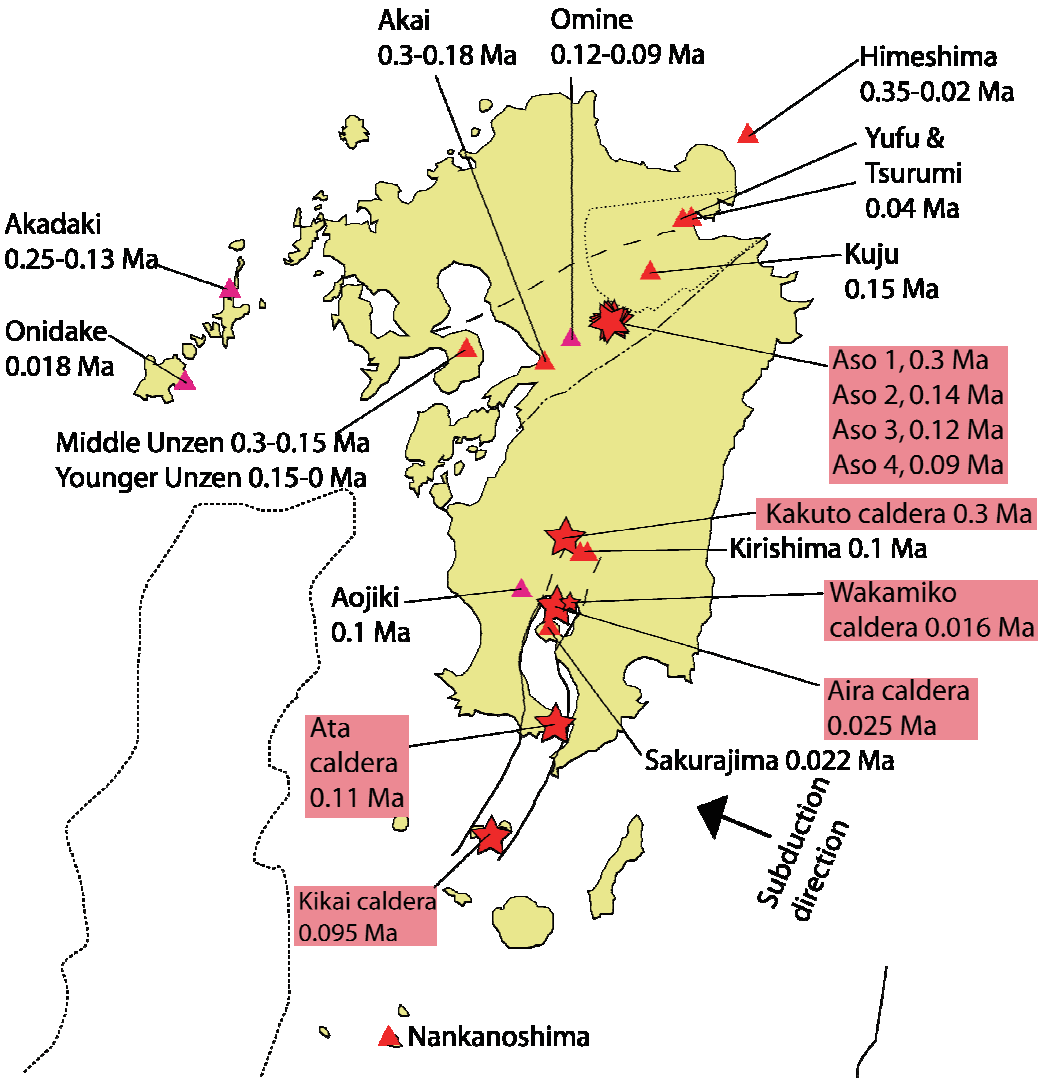

Figure 5.8: 0.3 to 0.01 Ma. From 0.3 Ma volcanism in Kyushu is dominated by gigantic calderas, namely Aso, Kakuto, Aira, Ata and Kikai. These calderas all form within grabens, the Beppu-Shimabara graben in the north and the Kagoshima graben in the south.

Other volcanism occurring in the central volcanic region between 0.3-0.01 Ma includes the Himeshima volcano group, off the eastern coastline of Kyushu (0.35-0.02 Ma), activity in the HVZ at Tsurumi, Yufu and Kuju volcanoes, and at Unzen volcano in the west. Tsurumi and Yufu volcanoes both formed andesitic and dacitic lava dome stratovolcanoes from about 0.04 Ma. The activity at Yufu ceased just over one thousand years ago, whereas Tsurumi was last active in 1974. The first activity of present day Kuju volcano began at 0.15 Ma, with the volcano group now covering an area measuring 20 km E-W and 15 km N-S, lying on the wide Hane-yama lava plateau of Plio-Pleistocene age (International Volcanological Association,

1962). The early stages of Kuju formed multiple craters measuring up to 1 km x 0.5 km and 200 m deep, followed in later stages by massive lava domes which protruded through the flank of the main cone.

In the western part of the central volcanic region at this time, Unzen volcano transitioned between the Middle and Younger stages. The Middle stage occurred at 0.3-0.15 Ma producing lava flows, the Younger stage began at 0.15 Ma continuing to the present day producing both lava flows, domes and pyroclastic flows.

The southern volcanic region shows evidence of massive changes throughout the time period 0.3-0.01 Ma, with the formation of several enormous calderas. The most northerly volcanic centre in the southern volcanic region is that of Kirishima volcano. Kirishima has two overlapping calderas associated with it, Kakuto and Kobayashi. Kakuto caldera is 15 x 10 km in diameter and formed at 0.3 Ma, located slightly north west of present day Kirishima volcano. The older stage of Kirishima volcano occurred from 0.3-0.15 Ma with andesitic shield volcanism. The younger stage of Kirishima volcano has formed stratovolcanoes since 0.1 Ma, with many eruptions in historical time. Further south is the massive Aira caldera (approximately 20 x 18 km), which is now the home of Sakurajima volcano. Following on from the previously mentioned 'Pre-Aira caldera' activity at 0.9 Ma, there were two more episodes of pre-caldera volcanism. The first of these was from 0.5-0.1 Ma with eruptions of basaltic and rhyolitic lava flows in the southern caldera area (Masafumi et al., 2000). The final pre-caldera activity was from 0.1-0.025 Ma with eruptions of andesitic lava and pyroclastic flows in the northern part of the caldera and rhyolitic lava flows in both the northern and southern areas of the caldera (Masafumi et al., 2000). An interesting feature noted by Masafumi et al., (2000) is the presence of Osumilite, 15 km apart on opposite sides of the caldera rim during 0.04-0.03 Ma, perhaps suggesting that a large magma chamber has been present under Aira caldera since about 0.04 Ma.

The Aira caldera forming eruption occurred at 0.025 Ma and was the source of the massively voluminous Ito pyroclastic flow and widespread co-ignimbrite ash "AT". The Ito pyroclastic flow led to the formation of a huge ignimbrite plateau, which deposited thickly all over southern Kyushu and can be traced far beyond Kyushu. Sakurajima is a post caldera volcano, which formed at 0.022 Ma and is located on the southern rim of Aira caldera. In the north eastern corner of the Aira caldera is the submarine Wakamiko caldera. The Wakamiko caldera is younger (0.016 Ma) and smaller (approximately 6 x 3 km) than the Aira caldera. On a smaller scale, Aojiki scoria cone (part of the Kamo monogenetic volcano group) is a small basaltic maar, which erupted at 0.1 Ma and is located approximately 20 km NW of Sakurajima volcano. Further south in the Kagoshima graben, lying at the mouth of Kagoshima bay, Ata caldera formed at 0.11 Ma. Ata caldera is a 25 km (E-W) x 12 km submarine caldera, which has two possible locations. The northerly location was the source of the Ata pyroclastic flow, which formed a rhyolitic and dacitic pyroclastic flow plateau. The more southerly possible location of Ata caldera has post caldera cones located on the rim of the caldera, such as Kaimondake volcano.

The formation of huge calderas continued down into the Ryukyu arc, with the enormous 20 x 17 km diameter Kikai caldera. Kikai is located approximately 40 km south west of the southern tip of Kyushu. After the pre-caldera activity (described in the previous Section) there were two episodes of caldera formation, one at 95 ka and then again at 6.3 ka. The 6.3 ka caldera forming eruption produced a widespread co-ignimbrite ash fall tephra known as the K-Ah (Kikai-Akahoya). This eruption has been classed as VEI 7 (Newhall & Self, 1982) and the largest eruption in the Holocene in Japan (Torrence and Grattan, 2002). There are several post-caldera cones located within the submarine caldera. Further south in the Ryukyu arc is Nakanoshima, an andesitic and dacitic stratovolcano that is still active today.

5.4.7 Active Volcanism (Holocene)

In the last ten thousand years there have been no major tectonic changes throughout Kyushu. Using relative sea level change as an indicator of tectonic change (possibly associated with volcanic unrest), the start of the Holocene did see a rapid sea level rise of 25 m, recorded in Hiroshima Bay (Yasuhara & Seto, 2006), followed later in the Holocene by a sea level fall of 5

m to present levels. The sea-level curve for Hiroshima Bay is similar to curves for tectonically stable areas of Japan (e.g. Osaka Bay), thus we can extrapolate that Kyushu experienced similar sea level changes (Yasuhara & Seto, 2006). Large-scale caldera volcanism in Kyushu during the Holocene is represented by the 6.3 ka eruption of Kikai caldera, mentioned above. However, Kikai caldera is located in the Ryukyu arc, south of Kyushu, and there have been no large caldera eruptions on mainland Kyushu in this period (see Figure 5.9). It is worth noting that the Japanese Meteorological Agency (JMA) has defined active volcanoes in Japan as "Volcanoes which have erupted within the past 10,000 years or volcanoes with vigorous fumarolic activity."

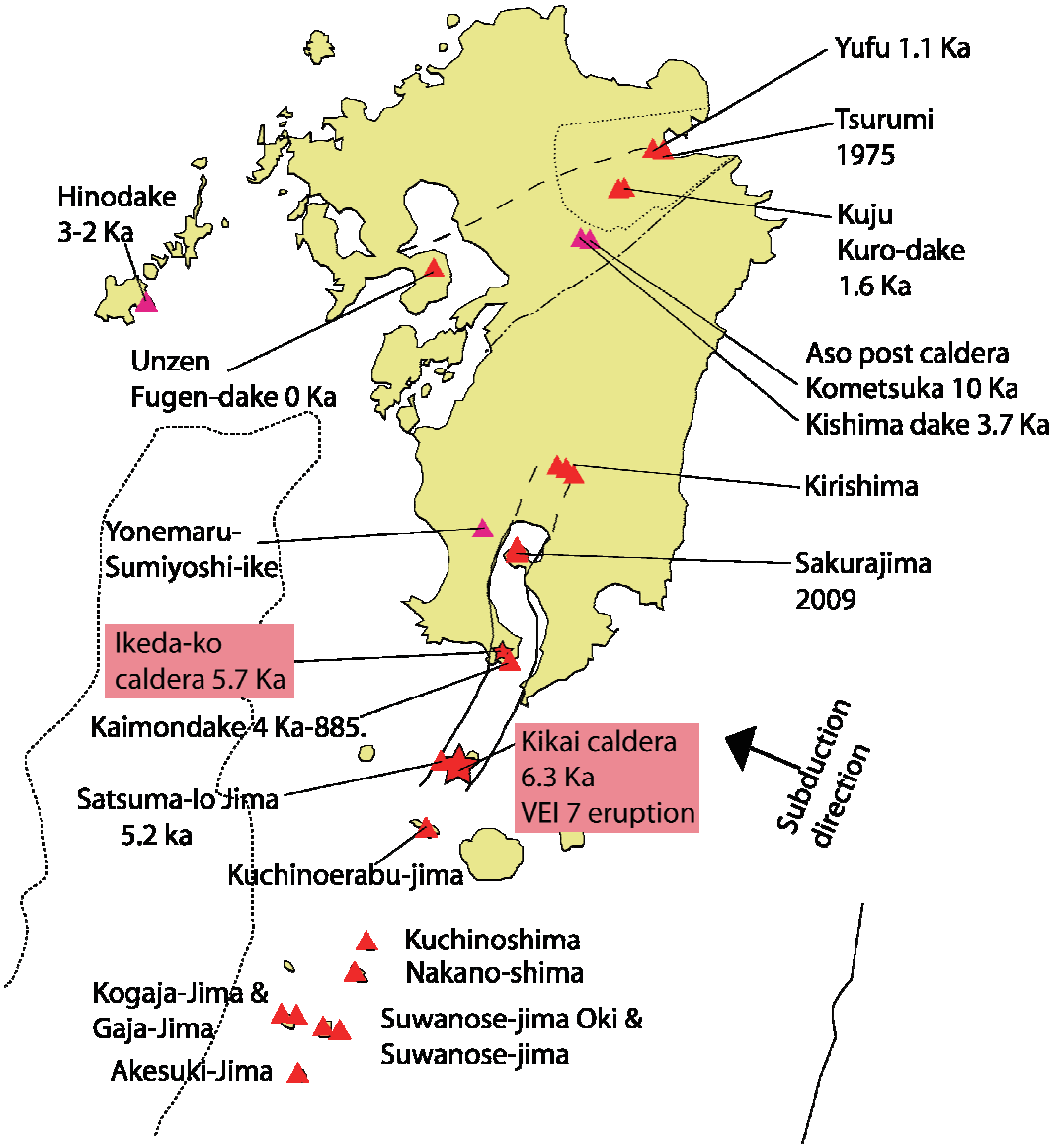

Figure 5.9: Holocene volcanism has seen the volcanic front firmly extend down in the Ryukyu arc, with the largest Holocene eruption occurring at Kikai volcano. The long-lived centres of Fukue, Unzen, Aso, Kuju, Yufu/Tsurumi, Kirishima, Sakurajima continue to have active stratovolcanoes. The Holocene has had no widespread lava plateau eruptions.

Much of the volcanism in the previously discussed period (0.3-0.01 Ma) has continued to the present. In the northwestern volcanic region, a large proportion of the volcanism is monogenetic, so Holocene activity is understandably located at new centres. Hino-dake is part of the Fukue monogenetic volcano group in the southern Goto Islands and the youngest active centre, forming basaltic lava flows at 3-2 ka.

The central volcanic region is still physically dominated by the enormous Aso caldera. Active volcanism in Aso caldera today continues in the post-caldera phase of the volcano. There are two centres within Aso caldera that are classed as active. The younger of these is Kometsuka basaltic scoria cone, which formed at 10 ka and still shows perfect scoria cone morphology. Kishima dake is the youngest new centre, which formed a basaltic scoria cone at 3.7 ka. However, since Kishima dake formed, several of the ten or so stratocones and cinder cones clustered in the middle of the caldera have erupted again, as recently as 2005. Whether this activity marks the end of caldera forming events at Aso caldera, or whether there are more to come, is unclear. Previously, a progression in magma compositions from rhyolite to basalt has been noted to occur in each caldera forming stage, suggesting an enormous caldera must have been located beneath the volcano. Seismic tomography data suggests that beneath Aso today is an enormous 'hot zone' of primed mantle; whether this is part of a vast magma chamber is unknown.

Further to the northeast, Holocene activity at Kuju volcano took the form of the growth of lava domes, which produced six major andesitic to dacitic tephra deposits (Siebert & Simkin, 2002). Eruptive activity at Kuju volcano has migrated eastward during the last 5000 years, with the most recent activity at Kuro-dake lava dome at 1.6 ka (Siebert & Simkin, 2002). Further to the east, lava dome forming stratovolcanoes Tsurumi and Yufu are both classed as active. Tsurumi produced lava flows within the last one thousand years and possibly magmatic-related ash clouds in the mid 1970s. Yufu is classed as active but has had no activity since 1.1 ka. In the west, on the Shimabara peninsula, the currently active Unzen volcano resides in the Shimbara graben. In the last ten thousand years, Unzen has shown repeated lava dome formation, leading to devastating pyroclastic flows. The 1991 pyroclastic flows from the then newly formed Heisei-shinzan lava dome were particularly destructive, due to the inhabited nature of the flanks of the volcano. There were nearly ten thousand pyroclastic flows counted in a five-year period after the formation of the Heisei-shinzan dome.

The southern volcanic region underwent continued volcanism in two of the major volcanic centres, as well as several new volcanic centres. The most northerly of these is Kirishima volcano, which lies on the southern edge of Kakuto caldera. Kirishima volcano comprises a series (International Volcanological Association, 1962) of older, gently sloping volcanoes and about 20 younger steep cones (International Volcanological Association, 1962). These centres have formed an elliptical volcano zone (approximately 30 km x 20 km) trending NW-SE, with volcanism younging towards the southeast. Further south, Sakurajima volcano began erupting 22,000 years ago at the southern rim of the Aira caldera and is still one of the most active volcanoes in the world today. Sakurajima is the compound cone of three stratovolcanoes, namely Kita-dake, Naka-dake and Minami-dake, with the southern cone, Minami-dake being active today. There have been several large eruptions; most notable in recent times is the 1914 eruption, prior to which there was a large earthquake, followed a few days later by a highly explosive phase of eruption. Another large earthquake occurred, then, shortly afterwards, the eruption became effusive and lava flows continued for several months. After this eruption, the centre of the Aira caldera (north of Sakurajima) was observed to subside, implying Sakurajima volano did not source its magma from directly beneath, but instead drew the magma from the same magma source as the Aira caldera.

New volcanic centres in the southern volcanic region included two maars (Yonemaru and Sumiyoshi-ike maar) that erupted at 7 Ka, northeast of Sakurajima, and three centres at the southern tip of Kyushu. The very southerly volcanism of Ikeda-ko and Kaimondake volcanoes lies directly west of Ata caldera. Ikeda-ko is a small caldera lake, 4 km in diameter, which formed at 5.7 ka with eruptive compositions of rhyolite, dacite and andesite lavas. Nabeshima-dake lava dome formed within Ikeda-ko caldera at 4.3 ka. Ikeda-ko is part of the Ibuski volcanic group, which comprises many maars, lava domes and strato volcanoes, some pre-dating Ata caldera and many post-dating Ata caldera. Slightly younger than Ikeda-ko at 4 Ka, and located 5 km southwest, is Kaimondake volcano. Kaimondake is a perfectly formed cone, comprising a stratovolcano with a lava dome on top, on the western rim of Ata caldera. Eruptions have occurred as recently as the year 885, with sub-plinian eruptions of mainly basaltic and andesitic lava, as well as producing copious scoria.

The Ryukyu arc has shown a vastly increased rate of volcanism in the Holocene. The 6.3 ka K-Ah eruption of Kikai caldera proved to be the largest in the Holocene, but other areas in the Ryukyus also showed intensified volcanism with the formation of around 16 new volcanic centres in the last 10 ka. The new volcanic centres mainly consist of andesitic lava domes, stratovolcanoes and lava domes, although there is some rhyolitic volcanism and several small (e.g. 7 x 10 km) calderas. Several post-caldera cones formed on the Kikai caldera rim, such as Satsuma Io-jima, which has been active since 5.2 ka with andesitic, rhyolitic and basaltic stratovolcanoes, lava domes and pyroclastic cones.

5.5 Future volcanism in Kyushu

The highly dynamic and changeable nature of volcanism in Kyushu in the past 15 Ma suggests that it is highly likely to continue to change in style and location into the future. Insights into possible future locations of volcanism require use of more than just the volcanic history. Tectonic and geochemical insights allow development of a complete evolutionary story of Kyushu. Establishing a complete story is essential to understand the processes that underpin these changes in location and styles of volcanism, and the timescales on which these changes operate. Section 7 integrates the volcanic, tectonic and geochemical histories to formulate several alternative hypotheses of the evolution of Kyushu and the issue of the likelihood of future volcanism is discussed in depth in Sections 12 and 13.

5.6 References for Section 5

AIST (2008). Active fault database of Japan. National Institute of Advanced Industrial Science and Technology, http://riodb02.ibase.aist.go.jp/activefault/index_e.html.

Chapman, N., M. Apted, J. Beavan, K. Berryman, M. Cloos, C. Connor, L. Connor, O. Jaquet, N. Litchfield, S. Mahony, W. Smith, S. Sparks, M. Stirling, P. Villamor and L. Wallace (2009). Development of Methodologies for the Identification of Volcanic and Tectonic Hazards to Potential HLW Repository Sites in Japan: The Tohoku Case Study. Nuclear Waste Management Organisation of Japan, Tokyo. Technical Report: NUMO-TR-08-03. 135 pps.

Committee for Catalog of Quaternary Volcanoes in Japan Ver.1.0 (1999): Catalog of Quaternary Volcanoes in Japan, published by The Volcanology Society of Japan.

Hedenquist, J. W., Matsuhisa, Y., Izawa, E., White, N. C., Giggenbach, W. F., Aoki, M. 1994. Geology, geochemistry, and origin of high sulfidation Cu-Au mineralisation in the Nansatsu District, Japan. *Economic Geology*. **89**. 1-30.

Hoshizumi, H. 2006. What type of volcano is in Kyushu? *13th Extension Lecture, Volcanol. Soc. Japan.* 9-10.

International Volcanological Association (1962). Catalogue of the active volcanoes of the world including solfatara fields. Pts 10-14, 1960-62. Part XI: Japan, Taiwan and Marianas, by Hisashi Kuno.

Kamata, H. 1989. Shishimuta caldera, the buried source of the Yabakei pyroclastic flow in the Hohi volcanic zone, Japan. *Bulletin of Volcanology*. **51**, pp 41-50. Doi:10.1007/BF01086760

Kamata, H. & K. Kodama. 1994. Tectonics of an arc-arc junction: an example from Kyushu Island at the junction of the Southwest Japan Arc and the Ryukyu Arc. *Tectonophysics.* **233**, pp69-81.

Kamata, H. & K. Kodama. 1999. Volcanic history and tectonics of the Southwest Japan Arc. *The Island Arc.* **8**, pp393-403.

Kano, K., Kato, H., Yanagisawa, Y., Yoshida, F., 1991. Stratigraphy and geologic history of the Cenozoic of Japan. *Rep. Geol. Surv. Jpn*. **274**, pp114.

Kimura, J-I., R. J. Stern, Y. Takeyoshi. 2005. Reinitiation of subduction and magmatic responses in SW Japan in Neogene time. *GSA Bulletin*. **117**, pp969-986.

Masafumi, S., Ishihara, K., Tatsumi, Y. 2000. Pre-caldera Volcanic History in Aira Caldera area. K-Ar Dating of Lavas from Kajiki and Kokubu Areas in Northern Part and Ushine Area in Southern Part of Caldera. *Bulletin of the Volcanological Society of Japan.* **45**. 1-12.

Masahiro, D. and I. Michinori. 2006. Volcanic Stratigraphy in Western Oita, Kyushu, Japan-Part 1: The Tsuetate Area. *J Geosci Osaka City Univ.* **49**, pp119-135.

Miyabuchi, Y., H. Hoshizumi, K. Watanabe. 2004. Late Pleistocene tephrostratigraphy of Aso volcano, southwestern Japan, after deposition of AT ash. *Bull. Volcanol. Soc. Japan*. **49**, pp51-64.

Miyoshi, M., Fukushima, T., Sano, T. and Hasenaku, T. (2008). Subduction influence of Philippine Sea plate on the mantle beneath northern Kyushu, S.W. Japan: an examination of boron contents in basaltic rocks. *J. Volc. Geotherm. Res.*, **171**, 73-87.

Nagao, T., S. Kakubuchi, Y. Matsumoto. 1992. Trace element compositions of the Cenozoic basalts in northern Kyushu, SW Japan. *Exploration of volcanoes and rocks in Japan, China and Antarctica, Commemorative papers for ProfessorYukio Matsumoto*. Yamaguchi, Semura Froppy Printing, pp265-271.

Nakajima, J. and A. Hasegawa. 2007. Subduction of the Philippine Sea plate beneath southwestern Japan: Slab geometry and its relationship to arc magmatism. *Journal of Geophysical Research.* **112**, pp B08306- B08306, doi:10.1029/2006JB004770.

Newhall, C. G. and S.Self. 1982. The volcanic explosivity index /VEI/ - An estimate of explosive magnitude for historical volcanism. *Journal of Geophysical Research*, **87**, p. 1231-1238. Doi: 10.1029/JC087iC02p01231

Sano, T. 1995. Geology of Iki Volcano Group: Lava flow stratigraphy mainly based on K-Ar dating. *Bulletin of Volcanological Society of Japan.* **40b,** pp329-347.

Shinjo, R., J. D. Woodhead, J. M. Hergt. 2000. Geochemical variation within the northern Ryukyu Arc: magma source compositions and geodynamic implications. *Contrib Mineral Petrol.* **140**, pp263-282.

Siebert L, Simkin T (2002-). Volcanoes of the World: an Illustrated Catalog of Holocene Volcanoes and their Eruptions. Smithsonian Institution, Global Volcanism Program Digital Information Series, GVP-3, (http://www.volcano.si.edu/world/). Accessed 12th January 2009.

Sudo, M., K. Uto, Y. Tatsumi and K. Matsui. 1998. K–Ar geochronology of a Quaternary monogenetic volcano group in Ojika Jima District, Southwest Japan. *Bulletin of Volcanology.* **60**, pp171-186.

Taira, A. 2001. Tectonic Evolution of the Japanese Island Arc System. *Annu. Rev. Earth. Planet. Sci*. **29.** 109-134

Takahashi, M. 1981. Abnormal magmatism in island arcs. *Chikyu.* **30**, pp382-388.

Takahashi, M. and T. Kobayashi. 1999. Volcanoes in Kyushu, Field Guide, Volcanoes in Japan, **5**, Tsukiji Shokan Co. Ltd.

Tatsumi, Y. 1983. High magnesian andesites in the Setouchi volcanic belt, southwest Japan and their possible relation to the evolutionary history of the Shikoku inter-arc basin, *in* Hilde, T.W.C., and Uyeda, S., eds., Geodynamics of the western Pacific-Indonesian region: *American Geophysical Union Geodynamics Series*, **11**, p. 331–341.

Tatsumi, Y., and S. Maruyama. 1989. Boninites and high-Mg andesites: Tectonics and petrogenesis, *in* Crawford, A.J., ed., Boninites and related rocks: London, Unwin-Hyman, p. 50–71.

Torrence, R., and J. Grattan. 2002. Natural Disasters and Cultural Change. Published by Routledge. ISBN 0415216966, 9780415216968, pp313.

Uto, K. 1989. Neogene volcanism of Southwest Japan: Its time and space based on K-Ar dating. *Ph.D. Thesis, Univ. Tokyo*, 184 pp.

Uto, K., N. Hoang, K. Matsui. 2004. Cenozoic lithospheric extension induced magmatism in Southwest Japan. *Tectonophysics.* **393**, pp281-299.

Uto, K. and S. Uchiumi. 1997. K–Ar ages for Maruyama lava domes in Hiwaki Town, Kagoshima Prefecture, Southwest Japan: a Quaternary volcano constituting a second volcanic row of Ryukyu arc. *Bulletin of the Volcanological Society of Japan* **42** pp. 299–302.

Watanabe, Y. 2005. Late Cenozoic evolution of epithermal gold metallogenic provinces in Kyushu, Japan. *Mineralium Deposita*. **40**. 307-323. doi: 10.1007/s00126-005-0025-7

Yamaji, A. 1990. Rapid intra-arc rifting in Miocene Northeast Japan. *Tectonics*, **9**, pp365-378.

Yasuhara, M., and K. Seto. 2006. Holocene relative sea-level change in Hiroshima Bay, Japan: a semi-quantitative reconstruction based on ostracodes. *Paleontological Research* **10(2)**, pp99-116. Doi: 10.2517/prpsj.10.99

Yokose, H., T. Yanashima, W. Kikuchi, N. Sugiyama, A. Shinohara, T. Takeuchi, K. Nagao, K. Kodama. 1999. Episodic magmatism since 5 Ma in the western part of Beppu-Shimabara graben, Kyushu, Japan. *J. Miner. Petrol. Econ. Geol*. **94**, pp338–348.

6 Discrimination of Tectonic Domains and Selection of Example Locations

One of the major outcomes of the Kyushu Case Study is recognition of the fact that each region of Kyushu has quite distinctive volcanic and tectonic processes occurring, when compared to other parts of Japan. Moreover, due to the rapidly evolving tectonic setting, we expect these processes to evolve both temporally and spatially. Thus, we anticipate that it will become necessary to use approaches to volcanic and rock deformation hazard estimates that are tailored specially for each tectonic region of Kyushu. This will particularly be the case if the method progresses forward to a time-varying hazard model (e.g. allowing the future tectonic hazard estimates to vary with time). To facilitate this, we have divided Kyushu into domains that have distinct tectonic and volcanic characteristics.

Additionally, for the purposes of the present study, a group of eleven locations ('example locations') was selected across the Kyushu region so that the results of the probabilistic rock deformation and volcanic evaluations could be discussed in terms of different tectonic settings within the region.

6.1 Definition of tectonic domains

We have divided the Kyushu region into 4 tectonic domains: the Back-arc, Extensional Arc, Southern Arc and Forearc (Figure 6.1). Within each of these domains, there are common tectonic and volcanic characteristics, but the intensity of these processes can vary within a domain (e.g., depending of the proximity of a location to an active fault and/or volcano).

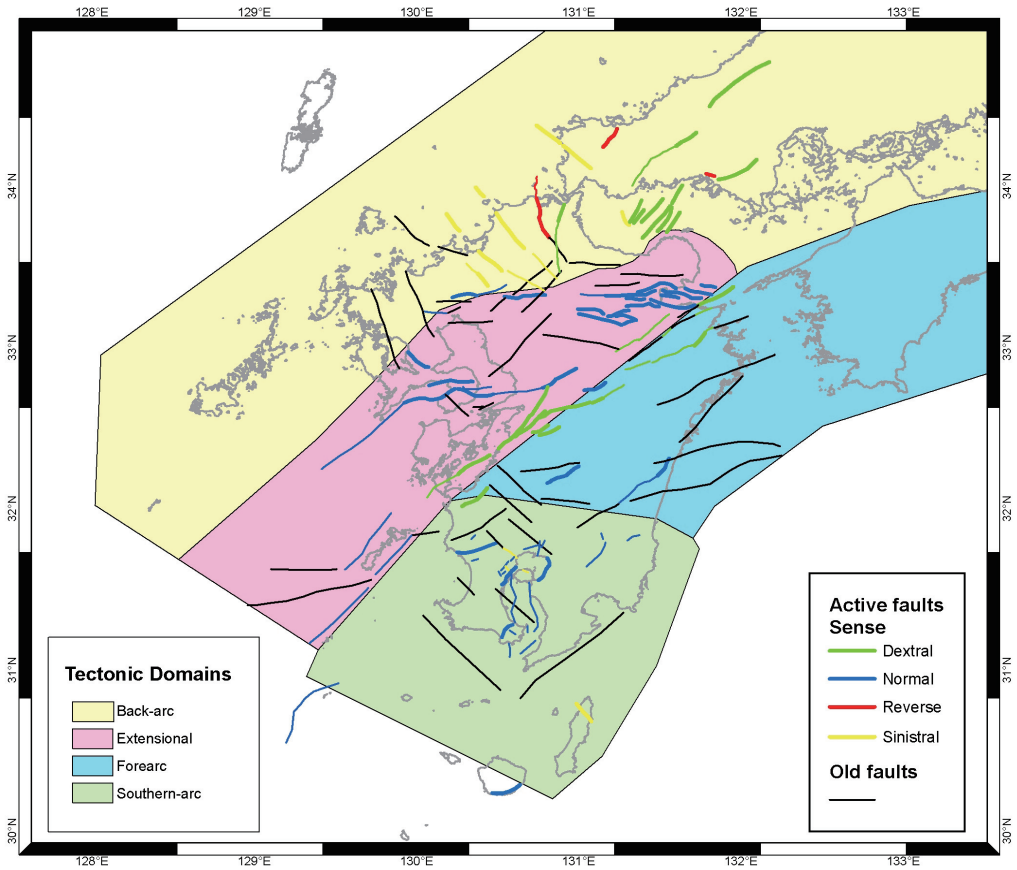

Figure 6.1: Tectonic domains in the Kyushu region and active faults classified by the sense of movement (see Section 8 for more information on active faults). We also include some "old" (inactive—black lines) faults on this map, for reference.

The configuration of the tectonic domains in Kyushu is strongly influenced by the current subduction processes. For example, the location of a domain with respect to the subducting slab often determines whether or not the domain will be influenced by volcanic processes. The buoyancy characteristics of the subducting plate will also influence the type and intensity of stresses that the upper crust will experience in response to the convergent plate motions. The crust in Kyushu has an inherited geometry and rheology as a consequence of previous deformation phases (see Section 3). The interaction between current subduction processes and inherited crustal properties will also influence the characteristics of the domain.

6.1.1 The Back-arc domain

The Back-arc domain comprises the NW part of Kyushu and extends to the southwest of Honshu (Figure 6.1). In most cases, this domain is located beyond the edge of the current subducting slab (see Figure 3.1 for location of subducting slab). Current tectonic activity is defined by the presence of NW trending, active left-lateral strike slip faults (Figure 6.1), strike-slip earthquake focal mechanisms and E-W maximum compressive stress tensor axis (Figure 6.2). The tectonic activity is low in this area with sparse shallow (<30 km) seismicity (Figure 6.3), and low fault slip rates <0.5 mm/a (see Section on strain rates from surface deformation). Quaternary volcanism (mainly monogenetic) in this area has been present for a long time, and occurs in short bursts of volcanic activity. Chemical and petrological evidence show that volcanism in this area is consistent with a back-arc environment (see Section 5).

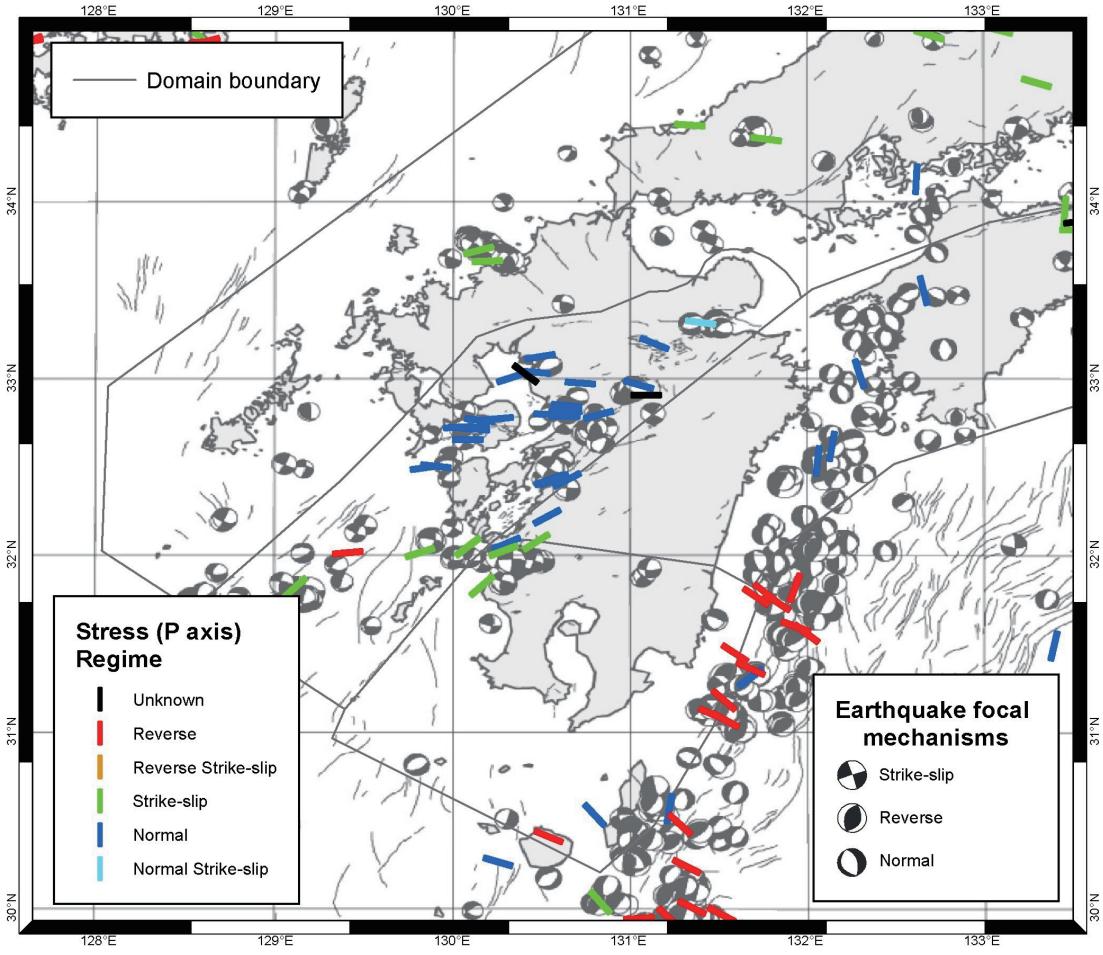

Figure 6.2: Earthquake focal mechanisms (based on CMT solutions from the JMA catalogue, from http://www.fnet.bosai.go.jp) and maximum horizontal compressional stress axes for the Kyushu region. Stress data from World Stress maps Programme.

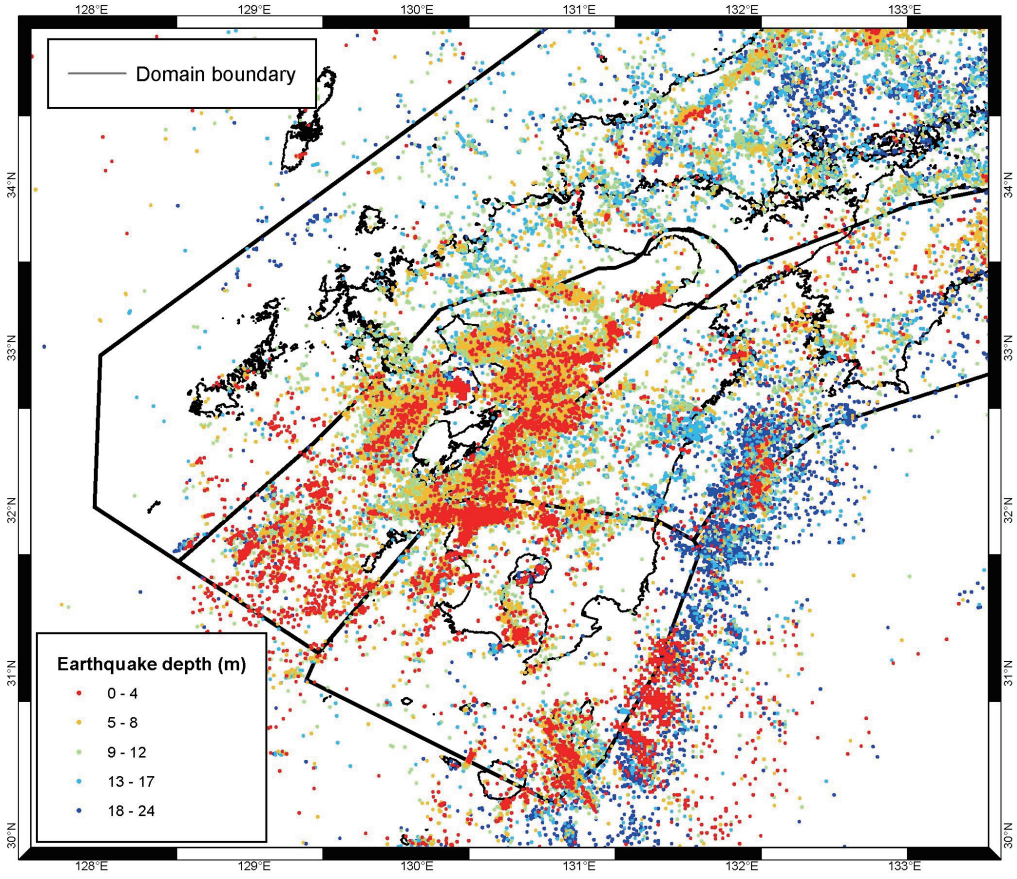

Figure 6.3: Seismicity in the upper plate (earthquakes of all magnitudes, above 20 km of depth and from 1983 to 1995).

The tectonic history of the back-arc domain has not changed much in the last 6 Ma, so we may reasonably not expect it to change much in the next 1 Ma. The area has been always relatively distant from the subducting slab (a back-arc environment) and it is becoming more distant from the subduction margin at its southern end due to the rollback of the subducting slab and subsequent anticlockwise rotation of southern Kyushu (see Section 4). This implies that the tectonic rates and style here might not be expected to change significantly over the next 1-2 Ma. However, given the E-W oriented maximum compressive stress regime in this domain, it is possible that any pre-existing NW-trending faults that are currently inactive, could reactivate in the future in response to the overriding tectonic stress field. Monogenetic volcanism may also occur in a somewhat random fashion that will be difficult to predict.

6.1.2 The Extensional Arc domain

The Extensional Arc domain comprises the central part of Kyushu and the northern part of the Okinawa Trough. The northwestern boundary of the Extensional Arc domain roughly delimits the northwestern extent of normal faulting and arc-type volcanism. The southeastern boundary of the Extensional Arc domain roughly coincides with the Oita-Kumamoto Line (which could be considered the southeast boundary of the Beppu-Shimabara Graben) (Figure 1). The current tectonic regime, as expressed by focal mechanism and stress tensor analysis (Figure 6.2) is mainly dominated by N-S extension (with the maximum horizontal stress axis in an E-W direction) within the onshore part (eastern half) of the domain. In the offshore (western) part of the domain, the maximum horizontal stress axis takes on a more NE trend and most of the recent seismicity is largely strike-slip. Active faults onshore (Figure 6.1), are mainly E-W striking normal faults that form several E-W grabens known as the Beppu–Shimabara graben system. Northeast-striking strike-slip faults occur along the southeast boundary of the Beppu-Shimabara Graben, and may be a continuation of the Median Tectonic Line in Shikoku. GPS data indicate high shear strain rates along the Oita-Kumamoto

line (see Section 9) suggesting up to several mm/a of right lateral strike slip here. Documented rates of active faulting are relatively high in this area compared to the Back-arc and Forearc domains. Active fault slip rates range from 0.1 to 2.6 mm/a for the E-W trending normal faults and from 0.5 to 1.5 mm/a for the strike-slip faults (see Section 8). Seismicity is high in the area with a larger percentage of earthquakes with Magnitudes < 2, typical of volcanic areas (Figure 6.3; see also Section 10). Volcanism is extensive in this domain, with numerous caldera-type eruptive centres (see Section 5.4). Most of the active volcanism in this domain is located above or near the 100 km slab contour line (with the marked exception of Unzen; see Section on Evolution of volcanism from 15 Ma), consistent with models for arc magmatism being generated where the slab is at ~100 km depth (see Figure 3.1 for location of 100 km depth slab contour). In general, current volcanism in this domain has an intra-arc and a back-arc character, sometimes within the same volcano.

One important aspect of the temporal evolution of the Extensional Arc domain (on timescales of 1-2 Ma) is the expected change in subducted plate geometry with time. For example, as the shallowly subducting Shikoku Basin migrates south along the margin (due to oblique relative plate motions), extension and volcanism in the NE part of this domain may decrease with time (see discussion in Section 7).

6.1.3 The Southern Arc domain

The Southern Arc domain comprises the southernmost part of Kyushu (Figure 6.1). The domain is located above the current subducting slab and ongoing arc volcanism is present above the 100 km depth contour of the subducting slab (Figure 3.1). Based on sparse focal mechanism and stress tensor data (Figure 6.2), there is a dominance of strike-slip earthquakes, and a NE trending maximum horizontal stress axis is present in the NW part of the domain (close to the main strike-slip faults on the Southern Arc domain's boundary with the Extensional Arc domain). Active faults (Figure 6.1 and Section 8) are mainly normal, except for a few strike-slip faults in the northwestern corner of the domain. Active faulting in the Kagoshima Graben, is associated with the N-S trending volcanic arc but mapped faults seem to have a NE trend. Deformation rates from active faults in this domain are low (0.1 to 1.5 mm/a on ~ 5 faults; see Section "Strain rates from surface deformation"). However seismicity rates are high, especially in the Kagoshima area (with a large number of earthquakes with M<2; Figure 6.3 and Section 10) and on the northern boundary of the domain (possibly associated with a 1997 earthquake sequence (Fujiwara et al., 1998).

GPS data suggest large extensional strain occurs throughout the southern arc domain (possibly up to 8 mm/a across the whole domain) and may be particularly focused on the Kagoshima graben area. Given that this rapid extension is not reflected by the active faults mapped there, it is possible that there are a number of undiscovered or uncharacterised active normal faults; alternatively, much of this extensional strain budget may be accommodated via volcanic processes such as dike intrusion. GPS data also reveal large shear strains (left-lateral sense) cutting across southern Kyushu, in the northern portion of the southern arc domain (see Section on Strain rates from GPS). Wallace et al. (2009) suggest that this left lateral shear occurs due to the collision of the Kyushu Palau Ridge (KPR) with the subduction margin (see Section 9 for further discussion of this). We propose that the location of this shear will migrate to the south with time, within the southern arc domain, as the collision point of the KPR migrates south along the margin. This is an important aspect of the temporal evolution of the margin that must be considered when estimating rock deformation hazards out to time periods >500 ka.

Current volcanism in the Southern Arc domain is largely consistent with arc-type volcanism (see Section on evolution of volcanism from 15 Ma). Over the last few million years, the active volcanic front in this area has migrated from west to east (to its current position today), probably as a consequence of rollback of the subducting Philippine Sea plate. This is a crucial aspect of the plate boundary evolution that must be accounted for in any future volcanic hazard models that are extrapolated out to 1-2 Ma from present.

6.1.4 The Forearc domain

The Forearc domain (Figure 6.1) corresponds to an area located mainly above the shallow part of the subducting plate slab (<100 km depth; Figure 3.1). Only the southwestern-most part of the domain is located above the 100 km contour but volcanism is absent along this Section of the subduction zone (see Section 5). The reason for the absence of volcanism in this area has not yet been explained. The current tectonic regime is not well defined in the area. Focal mechanism and stress tensor data are almost absent in the onshore part of the domain (Figure 6.2). Offshore focal mechanism and stress tensor data are associated with processes occurring at the subduction plate boundary. The few known active faults in the area have a NE strikes and normal senses of slip in the southern area but show strike slip near the boundary with the Extensional Arc domain (Figure 6.1). Tectonic rates seem to be low in the area. Active faults have slip rates of <0.5 mm/a (Section 8). The shallow seismicity rate is low (Figure 6.3 and Section 10) compared to the Extensional Arc and Southern Arc domains. Deformation inferred from GPS is patchy, and can be high in places. This may be related to uncertainties and problems with the subduction interface coupling model used to remove the elastic component of GPS strain, rather than being due to actual ongoing tectonic strain that will be accommodated on structures in the upper crust.

Given the proximity of this domain to the subduction margin, it is possible that the tectonic and volcanic regime could evolve from its present state within the Forearc domain on 1-2 Ma timescales. However, we are currently unable to predict how this might occur, and it is equally likely that the general tectonic and volcanic characteristics of this domain may be static over the next few millions of years.

6.2 Selection of example locations in Kyushu for more detailed evaluation

The locations selected for this study are spread across the tectonic domains defined above to sample an array of tectonic and volcanic situations (Figure 6.4). The locations and the criteria for selection are (Figure 6.4):

- Within the **Back-arc domain**:
    - **Location 1** is a representative location in the back-arc region, in an area of low seismic, geologic, and GPS-derived strain rates. It is however, situated on a low slip-rate (0.1 mm/a) active fault.
    - **Location 2** is a representative location in the back-arc region between two left-lateral cross faults (with low slip rates, <0.1-0.3 mm/a).
    - **Location 11** is a representative location in the back-arc region located in the southern part of the Abu volcanic field. This location is useful for exploring the influence of monogenetic volcanism on the volcanic hazard estimates.
- Within the **Extensional Arc domain**:
    - **Location 3** is located near Aso Volcano. This will probably be one of the higher hazard locations.
    - **Location 10** is located SW of Aso. This was chosen in order to assess the influence of our assumption that the Kyushu Palau Ridge subduction point intersection with the BSG might influence the probability of Aso-type volcanism (e.g., highly active and voluminous increasing with time towards the southwest time). It is also situated on an active fault with a moderate slip rate (0.9 mm/a).
    - **Location 4** is near the northern-most volcanoes on the arc trend. This location was chosen to test the influence on the hazard maps of our assumption that the

arc volcanism will eventually shut-down in northern Kyushu, as the flat slab beneath Shikoku and southwest Honshu migrates southwest with time.

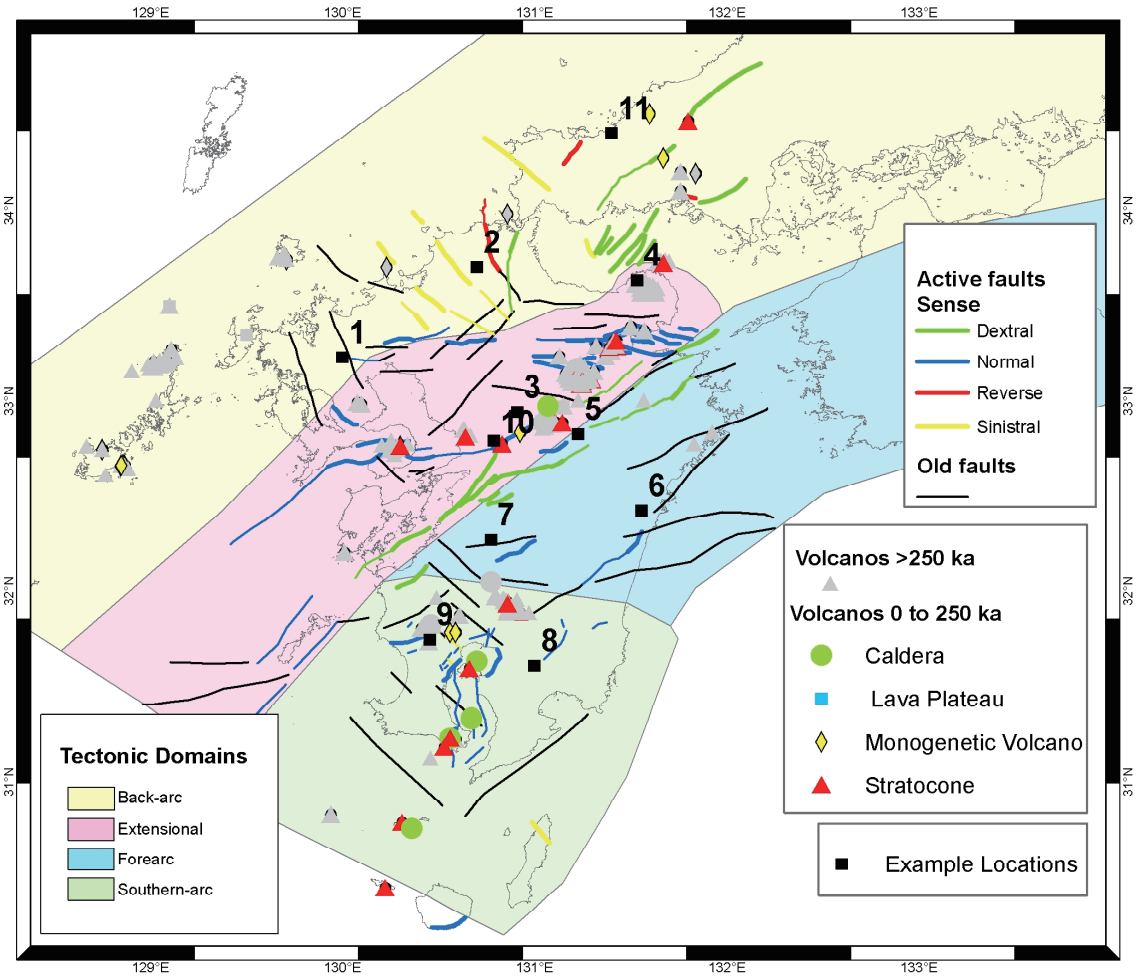

Figure 6.4: Map of example locations with faults and volcanoes overlain. Note: black lineations are inactive faults and are only shown for informative purposes.

- Within the **Southern Arc domain**:

  - **Location 8** is located in the forearc just east of the Kagoshima Graben. This location was chosen to look at the influence on the hazard probability estimates of including the possibility of trenchward arc migration (as a function of possible slab rollback). It is also situated on a low slip-rate (0.1 mm/a) active fault.
  - **Location 9** is just west of the Kagoshima Graben. This location occupies the former volcanic arc (before it migrated eastward to the Kagoshima Graben area) (according to Yamaji et al., 2003). This location was also chosen to look at the influence of the model that includes eastward arc migration. Presumably the hazard at location 8 might be higher than at location 9?

- Within the **Forearc domain**:

  - **Location 5:** while in the stable area of the forearc, this location is just east of the southwestern boundary of the BSG and east of Aso volcano. This location was

chosen to assess the probability of volcanism just outside the boundary of the BSG, close to Aso, and in the forearc terrane that appears unaffected by recent volcanism.

- **Location 6** is located in a stable area at a moderate distance to an active fault and far away form volcanoes, but with possibly high uplift rates.
- **Location 7** is located in an area at a moderate distance to an active fault although slightly closer to the BSG, and above the 100 km slab contour.

6.3 References for Section 6

Fujiwara, S., H. Yarai, S. Ozawa, M. Tobita, M. Murakami, H. Nakagawa, and K. Nitta, 1998, Surface displacement of the March 26, 1997, Kagoshima-ken-hokuseibu earthquake in Japan from synthetic aperture radar interferometry, *Geophys. Res. Lett., 25(24)*, 4541-4544.

Yamaji, A. 2003. Slab rollback suggested by latest Miocene to Pliocene forearc stress and migration of volcanic front in southern Kyushu, northern Ryukyu Arc. *Tectonophysics.* **364**, pp9–24.

7 Volcano-tectonic Interactions in Kyushu and Implications for Future Tectonic and Volcanic Evolution

In this Section we discuss the nature of volcano-tectonic interactions within the Kyushu region. We use this information to anticipate how patterns of volcanism and faulting will evolve over the next 2 Ma. We anticipate that some major plate boundary features such as the location of the subducting slab, and changes in physical characteristics of the subducting plate, among others will greatly influence future patterns of faulting and volcanism. This is supported by our understanding of past spatial relations between volcanism and plate boundary configuration.

7.1 Interplay Between Volcanism and Faulting

There is a clear coincidence between extensional (normal) faulting in Kyushu and the location of active volcanism (Figure 7.1).

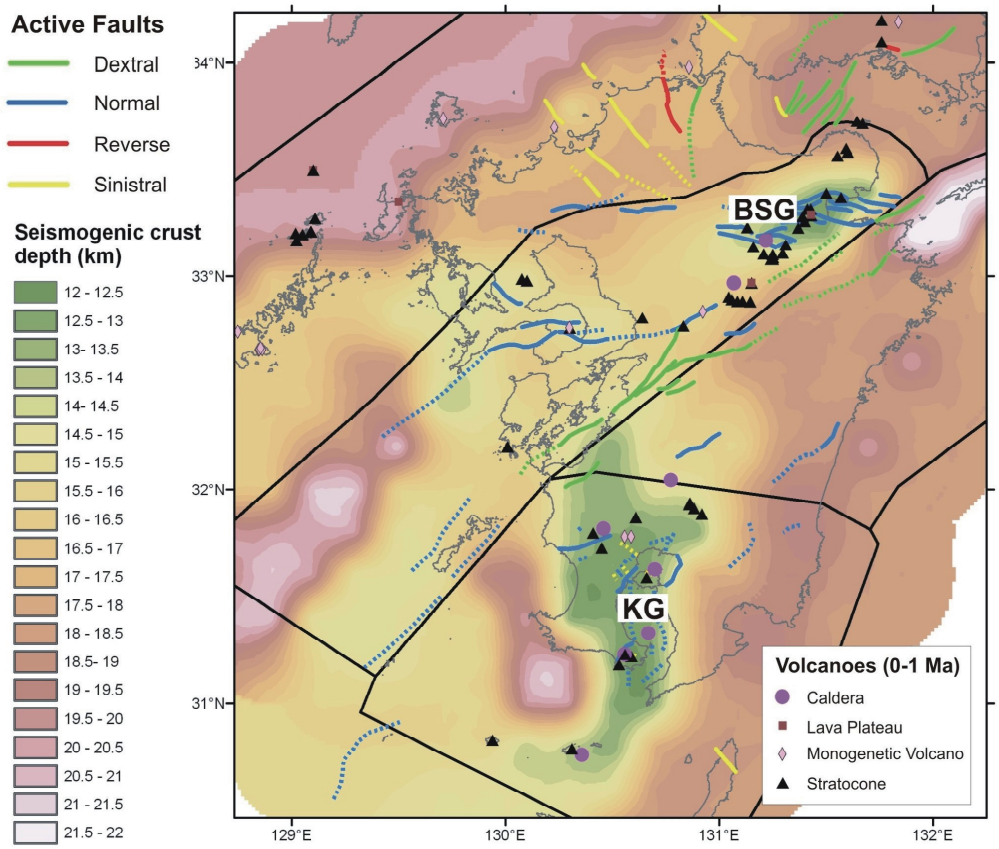

Figure 7.1: Maximum seismogenic depth of crustal earthquakes overlain by active faults (coloured lines – solid lines from Active Fault Research Centre database, http://www.aist.go.jp/RIODB/activefault/index_eng.html, dashed lines added in this study, see Strain Rates from Surface Deformation Section)and active volcanoes (coloured symbols). Note the marked correlation between active faulting and the location of active volcanism, particularly in the Beppu-Shimabara Graben (BSG) and the Kagoshima Graben (KG) region.

It is likely that volcanism and extensional faulting tend to be co-located in Kyushu. There are numerous reasons that this could be the case. For example, tectonic thinning/extension of the crust can create space for magma to migrate towards, and can influence the geometric development of a volcanic front. Crustal thinning can also induce decompression melting in

the mantle. Conversely, magmatism can thermally weaken the crust creating a favourable situation for the development of faulting and the localisation of tectonic strain. Such processes will also create positive feedback loops, enhancing the co-existence of volcanism and extensional strain. Moreover, processes related to volcanism (e.g., dike-intrusion) can accommodate some of the extensional strain budget (reducing the amount of tectonic extension that must occur via faulting). The co-existence of active volcanic systems and extensional tectonics is observed in numerous other locations on Earth (for example, North Island, New Zealand; eastern California; east Africa). Given the rapidly changing nature of the overall tectonic boundary conditions in Kyushu (see this Section and Section on Tectonic evolution in the last 15 Ma), and the likely interdependence between volcanism and rock deformation in the Kyushu region, one might imagine that the temporal and spatial evolution of volcanic and rock deformation activity in Kyushu will be highly variable.

One example of a likely interplay between the location of volcanism and rock deformation is in the Kagoshima Graben. GPS data suggest that significant extension (<7-8 mm/a; Wallace et al., 2009) now occurs in the Kagoshima Graben area, and there is some evidence for active normal faulting there (e.g., Japan's Active Fault Research Centre's Active Faults Database: http://www.aist.go.jp/RIODB/activefault/cgi-bin/index.cgi). Given the lack of well-developed fault zones in that region, it is likely that extension has only recently begun in the Kagoshima Graben area, and it may be related to the recent trenchward migration of the active volcanic arc (see discussion in Section on evolution of volcanism from 15 Ma). For example, thermal weakening of the crust in the Kagoshima area due to recent arc magmatism has provided a weak zone favourable for the initiation of crustal extension there.

Although we have not yet explored this in detail, the relationship between volcanism and the location of bedrock faulting (i.e., inactive, or "old faults") should also be assessed. For example, in the back-arc region of Kyushu the orientations of bedrock structures may influence the spatial occurrence of monogenetic volcanism in that region.

7.2 Large-scale Plate Tectonic Influences

One of the first-order controls on the tectonic and volcanic evolution of Kyushu is the configuration of the subducting slab. Numerous studies have suggested that the location of the modern–day volcanic arc is controlled by the position of the 100 km depth contour of the subduction interface (e.g., Tatsumi, 1986; Yamaji, 2003, among others; Figure 7.2).

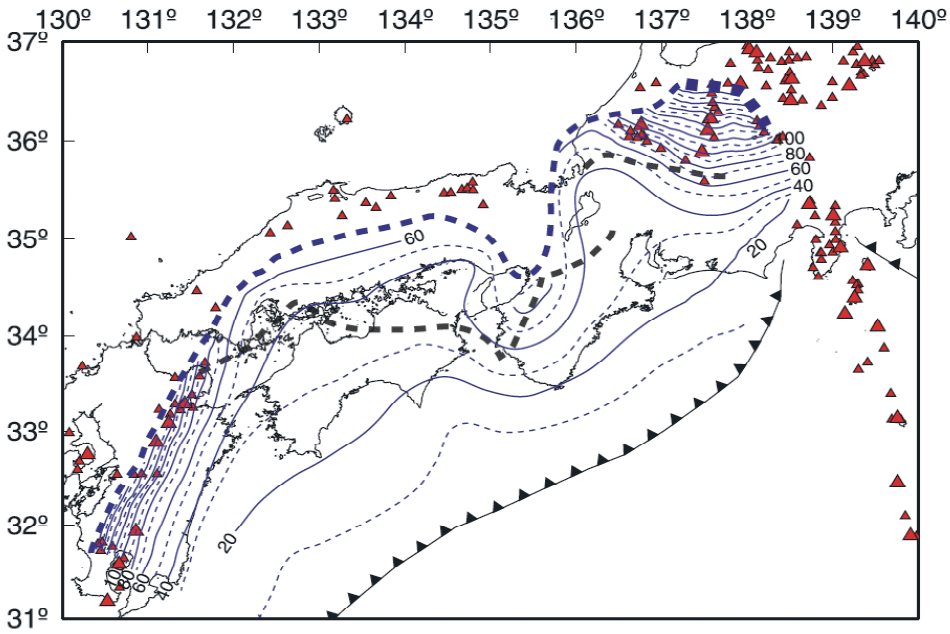

Figure 7.2: Contours of subduction interface (in 10 km intervals) beneath southwest Japan as determined from seismological studies by Nakajima and Hasegawa (2007). Red triangles show locations of active volcanoes.

One of the notable features of the slab configuration beneath southwest Japan is the variation in dip; beneath southwest Honshu the slab is very shallow-dipping, whereas beneath northern Kyushu, the slab is much steeper (Figure 7.2). It is likely that this change in slab geometry is influenced by the major along-strike change in buoyancy of the lithosphere (Shikoku Basin lithosphere is warmer and more buoyant; southwest of the Kyushu-Palau ridge the oceanic lithosphere is colder and denser). Given that this boundary (marked by the Kyushu-Palau Ridge) between Shikoku Basin crust and older oceanic lithosphere is continually migrating southwest, we must take into account the impact on the future configuration of the subducted slab and how this might influence the spatial and temporal occurrence of volcanism and future development of fault systems.

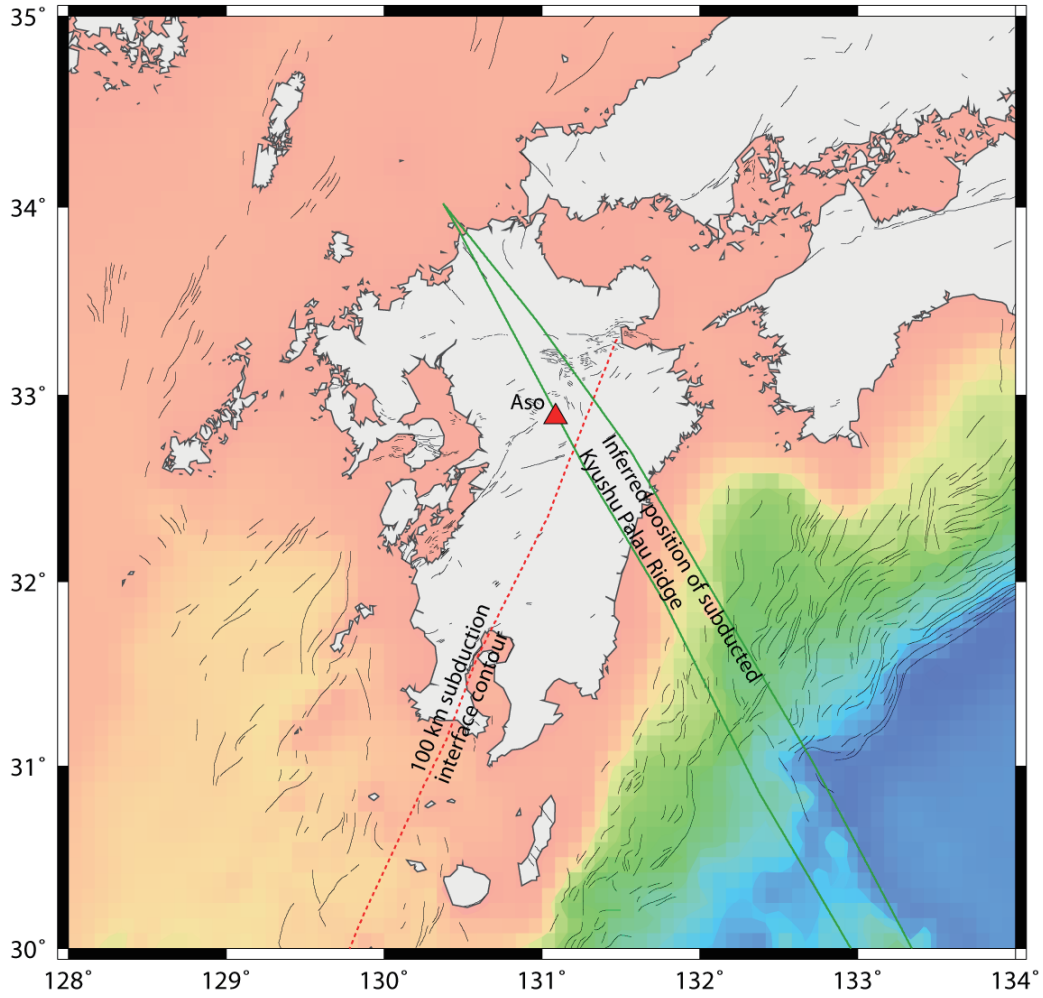

Figure 7.3: Inferred position of the subducted Kyushu Palau Ridge (outlined in green) relative to the position of Aso volcano (red triangle) and the 100 km contour (red dashed line) of the subduction interface.

The subducted Kyushu-Palau Ridge projects to the 100 km subduction interface contour at a point roughly coincident with Aso Volcano (Figure 7.3). The Kyushu-Palau Ridge is a remnant volcanic arc (>26 Ma; see Deschamps and Lallemand, 2002, and references therein), and is likely a rich source of fluids, which could be responsible for the voluminous magmatism at Aso, in the region of Kyushu-Palau Ridge subduction. The extensional nature of this region also lends itself well to caldera-type volcanism, and the thinned nature of the crust there makes it a favourable location for magma migration to the surface. Thus, Aso volcano is (1) located above the 100 km depth contour of the subducting slab, (2) the Kyushu Palau Ridge is subducting beneath Aso, and (3) Aso is located on the edge of the Beppu-Shimabara extensional area. All of these factors together could explain the location and highly voluminous nature of Aso volcano. As the Kyushu-Palau ridge/trench intersection point migrates southwest with time, it is possible that voluminous Aso-type volcanism could similarly occur further southwest of its present position in the future.

The position of the leading edge of the subducted slab may also play some role in magmagenesis and flow patterns in the mantle wedge that lead to basaltic volcanism in the back-arc region. To a first order, the region of back-arc volcanism coincides with the leading edge of the subducted Philippine Sea slab.

7.2.1 Key tectonic elements that influence faulting

In Section 9, we discuss in detail how subduction of the Kyushu-Palau Ridge may drive rapid left-lateral shear of southern Kyushu, as observed by GPS velocities and recent seismicity. In our conceptual model, we suggest that where buoyant lithosphere is being subducted at the Nankai trough (Figure 7.4), the forearc is pushed landward (e.g., northwest) due to the collisional resistance forces transmitted across the plate boundary; conversely, the Cretaceous oceanic slab subducting beneath southwest Kyushu at the Ryukyu Trench may be rolling back (e.g., Yamaji, 2003), pulling the southern part of the Kyushu forearc seaward relative to the northern half of the forearc. We suggest that these competing effects drive rapid left-lateral shear across southern Kyushu (Wallace et al., 2009). Due to the southwest-ward migration of the Kyushu-Palau Ridge subduction point (at a rate of 40 km/Ma), this zone of left-lateral shear is expected to migrate southwest with time, and this migration should be taken into account in the future evolution of rock deformation in Kyushu.

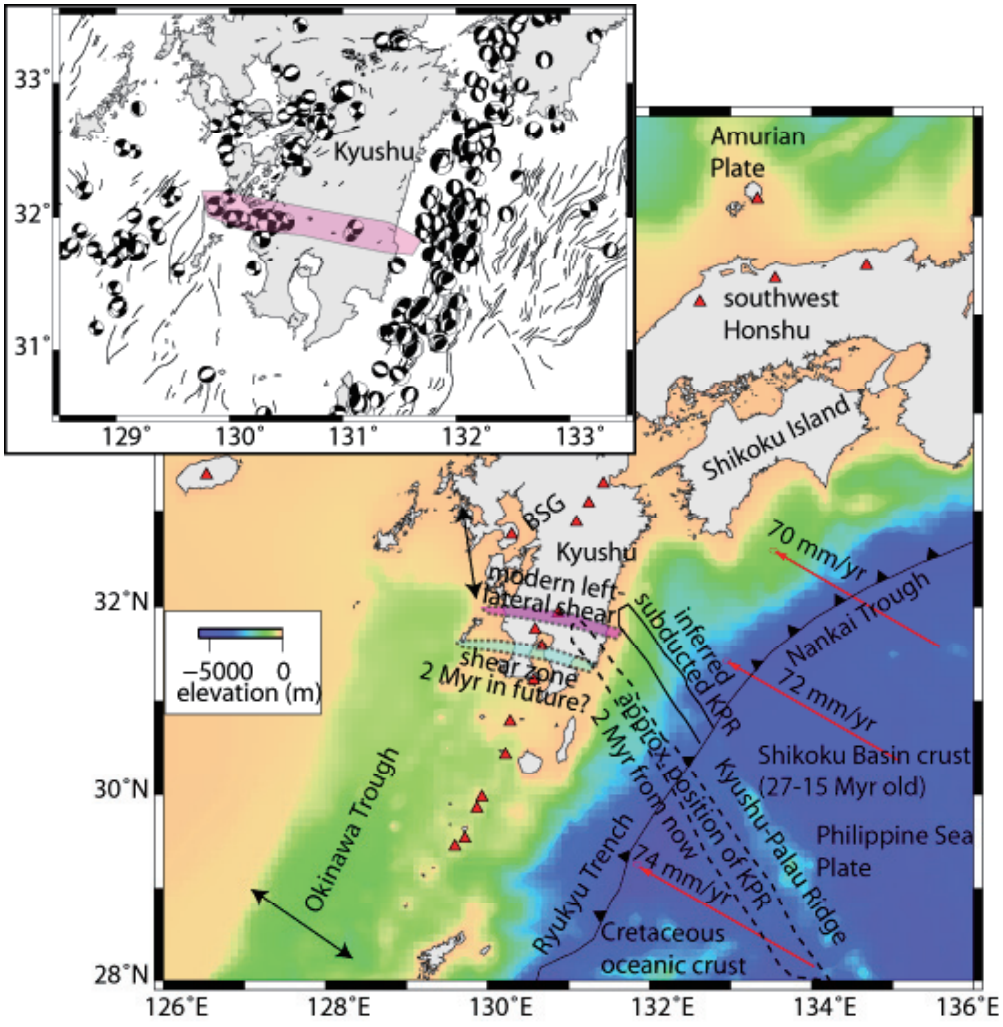

Figure 7.4: Plate tectonic setting of the Kyushu region. Red arrows represent motion of the Philippine Sea Plate (PSP) relative to the Amurian (AMUR) plate. BSG = Beppu-Shimabara Graben. Straight arrows show approximate backarc rifting directions in BSG and Okinawa Trough. Figure also illustrates projected migration of the Kyushu-Palau Ridge 2 million years into the future. Red triangles show approximate locations of some of Kyushu's active volcanoes.

Collision of buoyant features (aseismic ridges, oceanic plateaus, seamount chains) with subduction margins is known to cause rapid tectonic block rotations in many locations throughout the western Pacific (e.g., New Zealand, Papua New Guinea, Tonga, Vanuatu, and the Marianas; Wallace et al., 2005). A similar process may explain the rapid anti-clockwise rotation of southeast Kyushu observed by paleomagnetic techniques (Kodama et al., 1995) since ~2-6 Ma. The transition from collision of the Kyushu-Palau Ridge with the Nankai Trough to subduction of normal, negatively buoyant oceanic crust southwest of the ridge collision point may lead to rapid rotation of southeast Kyushu. Where a buoyant indentor enters a subduction zone, convergence is inhibited due to high collisional resistance forces, and the convergent plate boundary microblock is "pushed" into the upper plate as shortening is transferred from the trench into the backarc region. Where subduction of more negatively buoyant oceanic lithosphere occurs, the subducting slab may either roll-back (e.g, Molnar and Atwater, 1978), or the position of the slab will remain stationary with respect to the surrounding mantle (e.g., Uyeda and Kanamori, 1979). The slab suction effect (caused by flow patterns induced in the mantle by the subduction process) causes the large, upper plate to move toward the subduction zone, and requires the forearc to stay in contact with the subducting plate (e.g., Conrad and Lithgow-Bertelloni, 2004). Wallace et al. (2005) suggest that these two competing effects (i.e., a landward push on the forearc at the collision point, and a trenchward pull where normal subduction occurs) exert a torque on the forearc microplate, causing it to rotate relative to the lower plate about a pole near where the buoyant indentor enters the subduction zone (Figure 7.5). Therefore, in addition to influencing the left-lateral strike-slip faulting in southern Kyushu (see preceding paragraph), we also suspect that the Kyushu-Palau Ridge greatly influences the kinematics of tectonic rotation of southeast Kyushu and extension in the Kagoshima and Beppu-Shimabara Grabens. If our proposed model is correct, it can be used to construct models for projecting deformation patterns into the future arising from possible collision/subduction induced rotation of southeast Kyushu. Due to the rapid along-strike migration of the ridge collision point (Figure 7.4) the kinematics of rotation and deformation of southeast Kyushu may be expected to change rapidly if our conceptual model is correct.

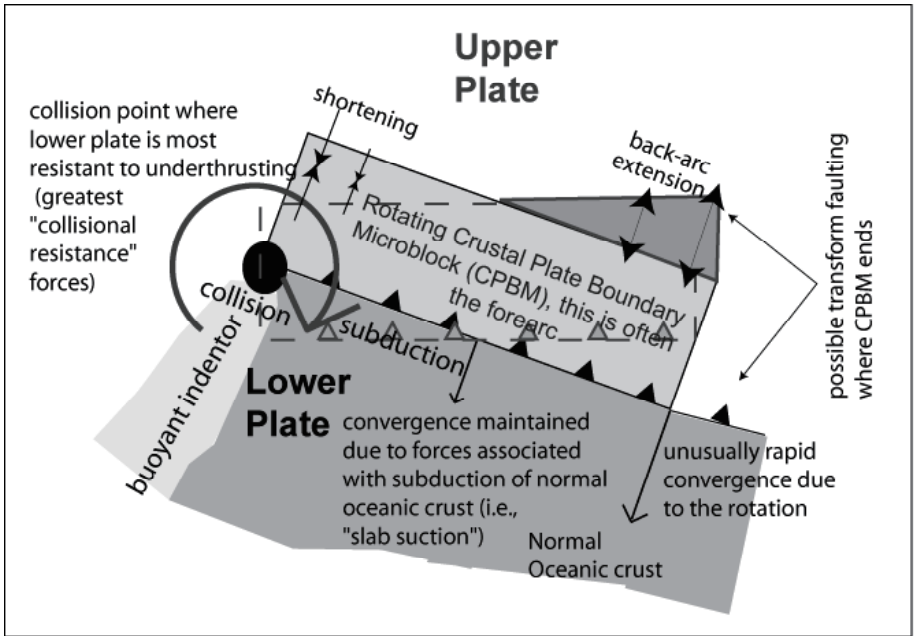

Figure 7.5: Schematic of collision/subduction-induced tectonic block rotation model (after Wallace et al., 2005).

Extensional forces arising from ongoing rollback of the subducting Philippine Sea slab greatly influence, and probably drive the extensional deformation in the upper plate in Kyushu. On the other hand, as subduction of the more buoyant, shallowly-subducting Shikoku basin crust migrates southwest towards Kyushu, extensional deformation may be decreased in some places in the future due to a lack of rollback of the Shikoku basin portion of the Philippine Sea

slab. For example, one might expect rifting in northeast Kyushu to shut-down at some point in the next few million years as the shallowly subducting Shikoku basin moves into that region.

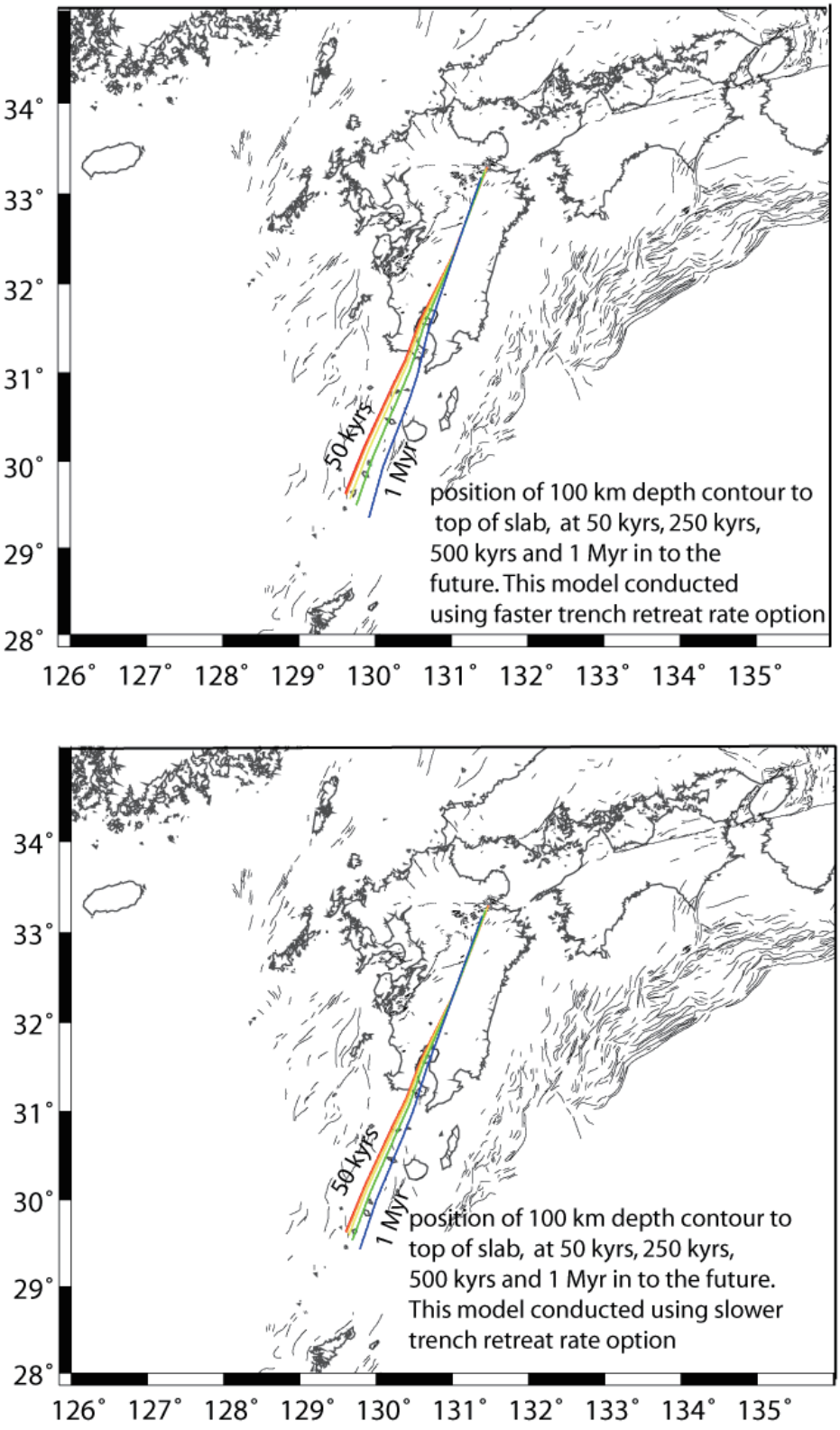

Figure 7.6: Future projections of the 100 km depth contour to the top of the slab using (a) the upper end of possible trench retreat (rollback) rates and (b) the lower end of likely trench retreat (rollback) rates. It is hypothesised that most of the arc volcanism in Kyushu will occur roughly above the 100 km contour.

7.3 Evolution of Volcanism and Tectonism over the Next 1 Ma

The configuration of the subducting slab, as well as the laterally varying buoyancy properties of the subducting plate exert a major influence on the nature of volcanism and tectonic deformation in Kyushu. Given that these properties will tend to evolve spatially with time, we show a series of models predicting the position of the 100 km depth to the subducting plate interface, and the Kyushu-Palau Ridge at intervals up to 1 Ma into the future, and discuss the implications of this for evolution of faulting and volcanism in Kyushu over the next 1 Ma.

To calculate the future configuration of the subducted slab, we take the current trench retreat rates and relative plate convergence directions and project the current subduction interface configuration (Nakajima and Hasegawa, 2007) up to 1 Ma into the future, relative to a fixed upper (Amurian) plate. We assume relative plate motions and trench retreat rates to be constant throughout this period. We use trench retreat rates that reflect the rate of extension in the back-arc during this time, which we assume is a proxy for the rate of trench retreat. Given that the actual trench retreat rates are somewhat uncertain, we use high and low estimates of trench retreat to show the range of possible models (Figure 7.6). The angle of subduction is also kept constant. The “forward” projections of the slab configuration is taken at a variety of times (50 ka, 100 ka, 250 ka, 500 ka and 1 Ma into the future). We also project the position of the Kyushu-Palau ridge at various time intervals 1 Ma into the future. The Kyushu-Palau Ridge migration is constrained using current Philippine Sea-Amurian Plate relative motions. Figure 7.6 shows the position of the 100 km contour for depth to the top of the slab up to 1 Ma into the future. The future positions of the Kyushu Palau Ridge is shown in Figure 7.7. In the following paragraphs, we will discuss the influence of the migration of the 100 km subduction interface contour and the Kyushu Palau Ridge on the future volcanic and tectonic evolution of the margin.

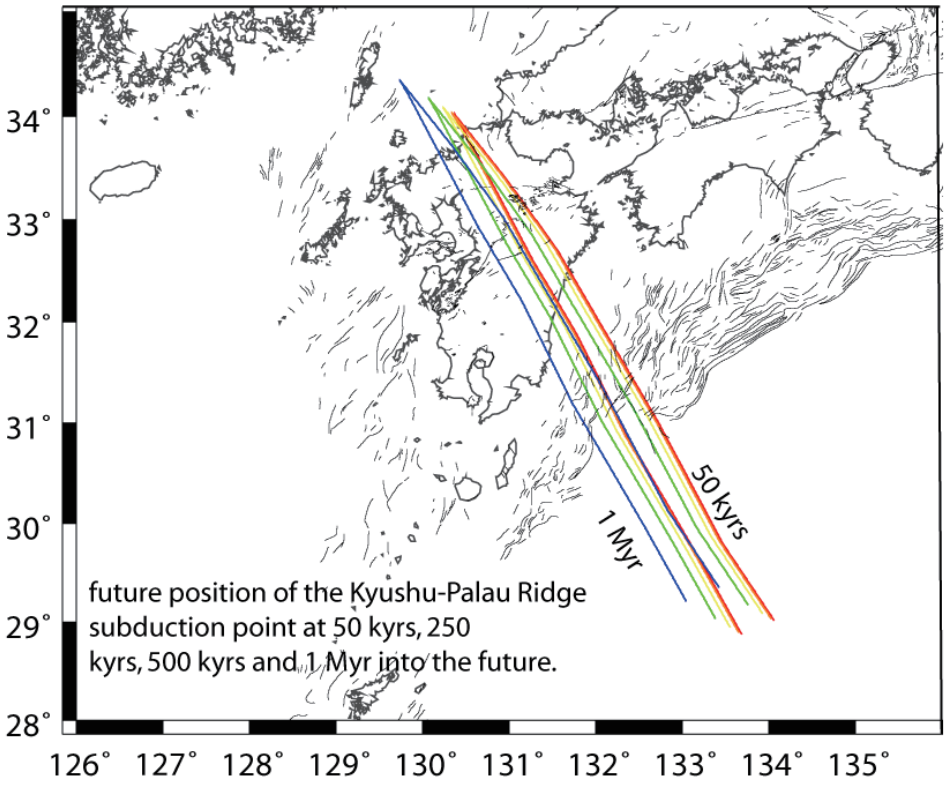

Figure 7.7: Future position of the subducting Kyushu-Palau Ridge. Migration of ridge determined by current ridge position and current Amurian-Philippine Sea Plate relative motions.

Many previous workers have noted that most of the arc volcanoes in Kyushu (with the exception of Unzen) lie in a region generally above the 100 km contour of the subducting slab. Due to a southward increase in back-arc extension rate and southward steepening of the subducting slab, there is a southward increase in slab rollback rate. This causes the 100 km depth contour of the subducted slab to migrate eastward more rapidly in southern Kyushu (e.g., Kagoshima region) compared with regions of Kyushu further north (Figure 7.6). We suggest that the projected future positions of this 100 km contour can be used as a proxy for possible migration of the volcanic arc into the future. Such a model is consistent with a general trenchward migration of the volcanic arc with time (see Section 5). In practice, this would probably result in a "stretching" of elevated volcano hazard probabilities in a trenchward direction. Zones of extensional faulting are likely to follow the arc migration, as zones of deformation continue to exploit areas of the crust weakened by magmatism. Moreover, continued rollback of the Philippine Sea slab and possible tectonic rotation of the Kyushu forearc will change the orientation of the trench, and the orientation of maximum extensional stresses in the upper plate, which may impact the geometry and evolution of rifting in Kyushu.

Conversely, due to the oblique relative plate motions in southwest Japan, the shallowly-dipping portion of the subducting slab beneath southwest Honshu and Shikoku will eventually migrate southwest along the plate boundary, and at some point in the future flat-slab subduction will occur beneath Kyushu. We suggest that the migration of flab slab subduction will eventually terminate arc volcanism in northern Kyushu. Such a model is justified by the lack of arc volcanism above the flat slab subducting beneath southwest Honshu.

The Kyushu-Palau Ridge subduction point is migrating southwest along the Ryukyu Trench/Nankai Trough, due to relative plate motions and the orientation of the ridge (Figure 7.4). Since 2 Ma, the subduction point of the ridge has migrated from the northeastern end of Kyushu southwest to a point roughly coincident with Aso Volcano (Figure 7.3 and also see Section on tectonic evolution in the last 15 Ma). It is assumed that the Kyushu-Palau Ridge subduction point will continue to migrate southwest along the margin. Prior to 2 Ma, the ridge was migrating northwards along the margin, due to a more northerly plate convergence direction prior to 2 Ma (e.g., Yamaji, 2003). We suggest that region above the interSection of the 100 km depth contour of the slab with the subducted Kyushu-Palau Ridge will have an elevated likelihood of voluminous Aso-style volcanism (see previous discussion). Given that the Kyushu-Palau Ridge subduction point will migrate southwest along the margin with time (at ~40 km/Ma), it is possible that regions in the Beppu Shimabara Graben <40 km southwest of Aso may have an elevated likelihood of Aso-style volcanism <1 Ma into the future. Likewise, we suggest that left-lateral shear currently occurring in southern Kyushu will track above the Kyushu-Palau Ridge subduction point; thus, we expect that the rock deformation hazard south of the currently active left lateral shear zone in southern Kyushu will increase with time.

7.4 Implications for Tectonic/Volcanic Hazard Evaluation

In addition to the dramatic temporal evolution of the plate margin that may be caused by the impingement and along-strike migration of the Kyushu-Palau Ridge, it is important to remember that the tectonic setting in Kyushu has undergone significant changes in recent times. There was a change in plate motion direction at ~2 Ma (e.g., Matsuda, 1980; Okamura, 1988), and reinitiation of subduction at the Nankai Trough at ~ 6 Ma (Kamata and Kodama, 1994). Kamata and Kodama (1999) discuss how both of these events have led to major changes in the deformation and volcanism patterns in Kyushu in the last ~2 Ma. We caution that such recent changes in the tectonic setting and crustal deformation in the Kyushu region may make it difficult to assume that the modern-day deformation pattern will be representative of crustal deformation patterns in Kyushu in the near future (i.e., next hundred thousand to million year time frame). In comparison to the Northern Honshu/Tohoku region, the tectonic setting in Kyushu is much less temporally stable and will be far more difficult to assess confidently in terms of future rock deformation hazard. Moreover, consideration of all viable tectonic models (i.e., not just those discussed in this report) for the evolution of the Kyushu

region (using a logic tree approach) is imperative when conducting a probabilistic tectonic and volcanic hazard assessment.

7.5 References for Section 7

Conrad, C.P. and Lithgow-Bertelloni, C., 2004, The temporal evolution of plate driving forces: Importance of “slab suction” versus “slab pull” during the Cenozoic: *J. of Geophy. Res., v. 109,* doi:10.1029/2004JB002991.

Deschamps, A., and Lallemand, S., 2002, The West Philippine Basin: An Eocene to early Oligocene back arc basin opened between two opposed subduction zones, Journal of Geophysical Research, v. 107, p. 2322-2346.

Kamata, H., and K. Kodama, 1994, Tectonics of an arc-arc junction: an example from Kyushu Island at the junction of the Southwest Japan Arc and the Ryukyu Arc.

Kodama, K., H. Tashiro, and T. Takeuchi (1995), Quaternary counterclockwise rotation of south Kyushu, southwest Japan, *Geology, 23,* 823-826, 1995.

Molnar, P., and Atwater, T., 1978, Interarc spreading and Cordilleran tectonics as alternatives related to the age of the subducted oceanic lithosphere: Earth and Planetary Sci. Letters, v. 41, p. 330-340.

Nakajima, J., and A. Hasegawa (2007), Subduction of the Philippine Sea plate beneath southwestern Japan: Slab geometry and its relationship to arc magmatism, J. Geophys. Res., 112, B08306, doi:10.1029/2006JB004770.

Okino, K., Ohara, Y., Kasuga, S., and Kato, Y., 1999, The Philippine Sea: New survey results reveal the structure and the history of the marginal basins, Geophysical Research Letters, v. 26, p. 2287–2290.

Sdrolias, M., Roest, W.R., and Mueller, R.D. (2004a), An expression of the Philippine Sea plate rotation: the Parece Vela and Shikoku Basins, *Tectonophysics.. 394,* 69-86.

Tatsumi, Y., 1986, formation of the volcanic front in subduction zones, Geophys. Res. Lett,. , 13, 717-720.

Uyeda, S., and Kanamori, H. ,1979, Back-arc opening and mode of subduction: *J. of Geophys. Res*., v. 84, p. 1049-1061.

Wallace, L.M., McCaffrey, R., Beavan, J., and Ellis, S., 2005, Rapid microplate rotations and backarc rifting at the transition between collision and subduction, *Geology, 33***:** 857-860.

Wallace, L.M., S. Ellis, K. Miyao, S. Miura, J. Beavan, and J. Goto, 2009, Enigmatic, highly active left-lateral shear zone in southwest Japan explained by aseismic ridge collision, *Geology, 37(2)*, 143-146.

Yamaji, A., 2003, slab rollback suggested by latest Miocene to Pliocene forearc stress and migration of volcanic front in southern Kyushu, northern Ryukyu arc, *Tectonophysics, 365*, 9-24.

8 Strain Rates from Surface Deformation

Surface fault traces, uplifted and subsided former shorelines, and deformed, formerly flat or inclined surfaces such as river terraces, are all manifestations of past rock deformation, often associated with major earthquakes resulting from fault rupture in the brittle shallow crust. Fault slip rates are readily converted to strain rates provided the width over which the deformation occurs (the fault's process zone) can be determined. Uplift or subsidence of marine terraces often, but not always, results from movement on active faults in the coastal area. By assuming fault dip then uplift can be converted to fault slip rate and thus to strain rate. Deformation of marine and fluvial terraces and other areal measures of deformation such as elevations of former erosion surfaces are readily assessed as surface strain rates provided the age of the deformed feature can be ascertained.

In this Case Study, we planned to develop an integrated surface deformation strain model by combining active fault data with folding, uplift and subsidence, as defined by tilted fluvial and marine terraces. However, the terrace data proved insufficient (see Section 8.2), so we have only been able to use active fault data to determine surface deformation strain rates.

8.1 Active fault datasets

The active faults used to calculate strain rates in this study (Figures 8.1 and 8.2) were obtained from two datasets. The faults denoted by solid lines in Figures 8.1 and 8.2 are from the active fault database provided on the website of the Active Fault Research Centre (AFRC) of the National Institute of Advanced Industrial Science and Technology (AIST) (http://www.aist.go.jp/RIODB/activefault/index_eng.html) (hereafter referred to as the AFRC database). This database was used to obtain the general location and parameters for the faults (discussed further below), which were then located more accurately by digitising the centreline of active fault traces (and fault trace zones) from the digital database of Nakata and Imaizumi (2002).

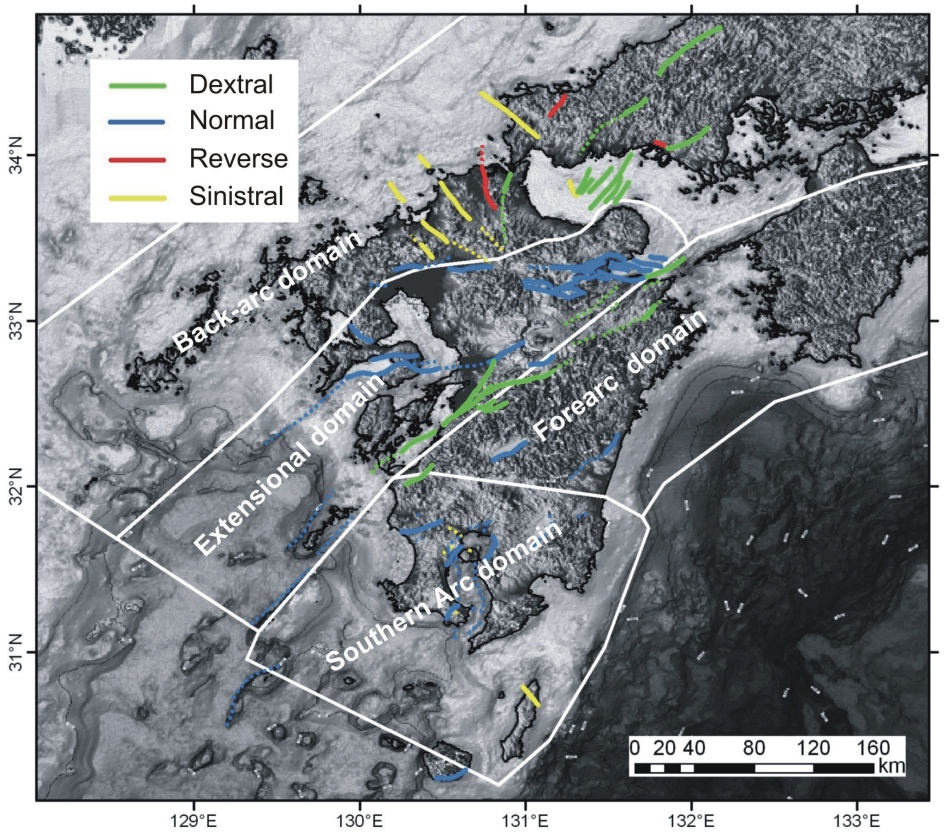

Figure 8.1: Active fault source map for the Kyushu region, colour coded by sense of movement. Solid lines are faults from the ARFC active fault database, dashed lines are faults added in this study.

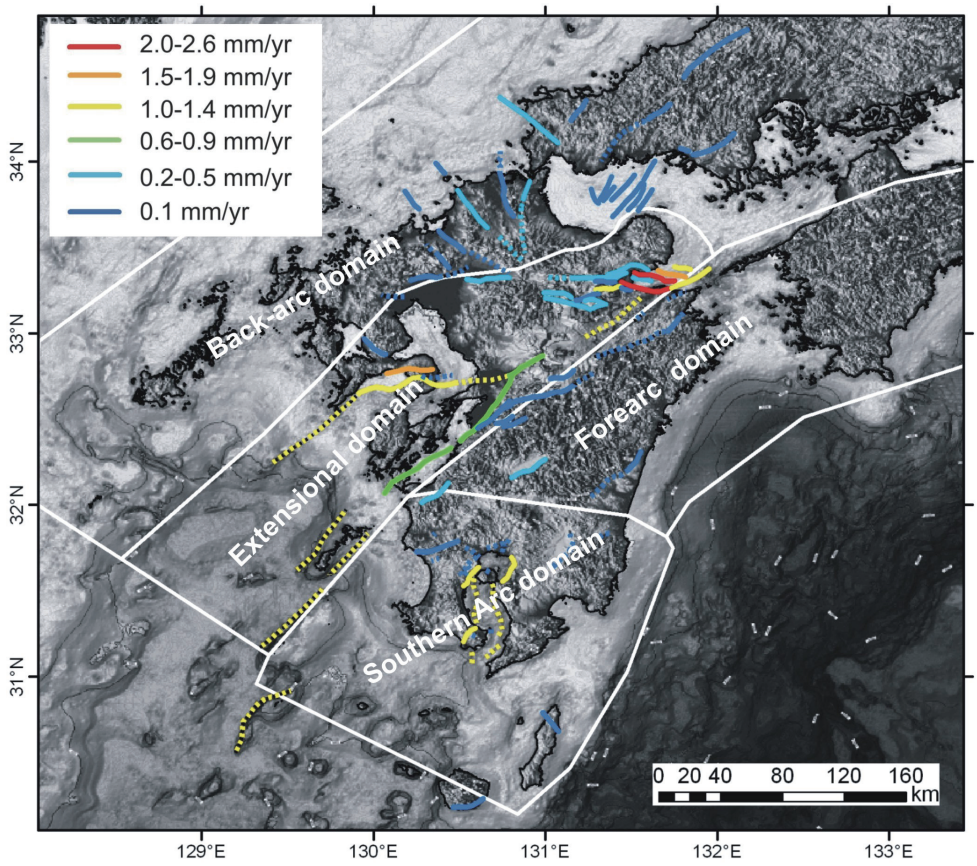

Figure 8.2: Active Fault source map for the Kyushu region, colour coded by slip rate. Solid lines are faults from the ARFC active fault database, dashed lines are faults added in this study.

The AFRC database currently only contains ~300 active faults in Japan, and as such likely under-represent the total number of active faults in Kyushu. This is particularly likely to be the case for slow slip faults (e.g., Class C Faults, which have slip rates of 0.01-0.1 mm/a). We also suspect some fault traces are buried by the thick volcanic ash deposits near the volcanoes. Therefore, active faults were added (dashed lines in Figures 8.1 and 8.2) based on assessment of other available digital datasets. These datasets included topographic maps (from Nakata and Imaizumi, 2002), geological maps (Geological Survey of Japan, AIST, 2002a), a gravity field map (Geological Survey of Japan, AIST, 2002b; Figure 8.3), and a magnetic field map (Geological Survey of Japan, AIST, 2005; Figure 8.4). Using these datasets a number of lineaments were identified, and those that have a sharp geomorphic expression on the topographic maps and correspond to bedrock faults on geologic maps were added to the active fault dataset. Several of the newly added active faults (dashed lines) correspond to active fault traces in other active fault databases such as the Research Group for Active Faults of Japan (1991), and many are extensions of the faults from the AFRC active fault database (Figures 8.1 to 8.4). The remainder are shown as thin solid lines on Figures 8.3 and 8.4 and may constitute major “old faults”, i.e., those that are no longer active. These are useful for consideration of both past and future tectonic evolution of the domains (see Sections 6 and 7).

For most of the faults from the AFRC database, parameters such as *sense of movement* (Figure 8.1) and mean net *slip rate* (Figure 8.2) were obtained directly from the database. Slip rate uncertainties had to be assigned however, which was done using our expertise with assigning uncertainties to other active fault datasets (e.g., the National Seismic Hazard Model of New Zealand). This could certainly be improved by using local (Japanese) expert elicitation. For the added faults that are along-strike of faults with parameters in the AFRC database, the same parameters were assigned. For the remainder, parameters were assigned based on that for the nearby faults, tectonic domain, and/or orientation. For example, all additional faults in the extensional domain were assigned to be normal faults. In the Southern Arc Domain, NE-striking faults were assigned to be normal faults, whereas NW-striking faults

were assigned to be sinistral strike-slip faults (Figure 8.1). Many of the newly added faults or faults with no slip rates in the AFRC database correspond to faults classified as “class B” (slip rate 0.1-1 mm/a) by the Research Group for Active Faults of Japan (1991). Therefore, for these faults, we assigned a mean net slip rate of 0.1 mm/a in areas of generally low slip rate (e.g., the forearc or backarc domains), whereas faults in areas of generally higher slip rate (e.g. extensional domain and southern arc domain), were assigned a mean net slip rate of 1 mm/a (Figure 8.2). Slip rate uncertainties were assigned as described above.

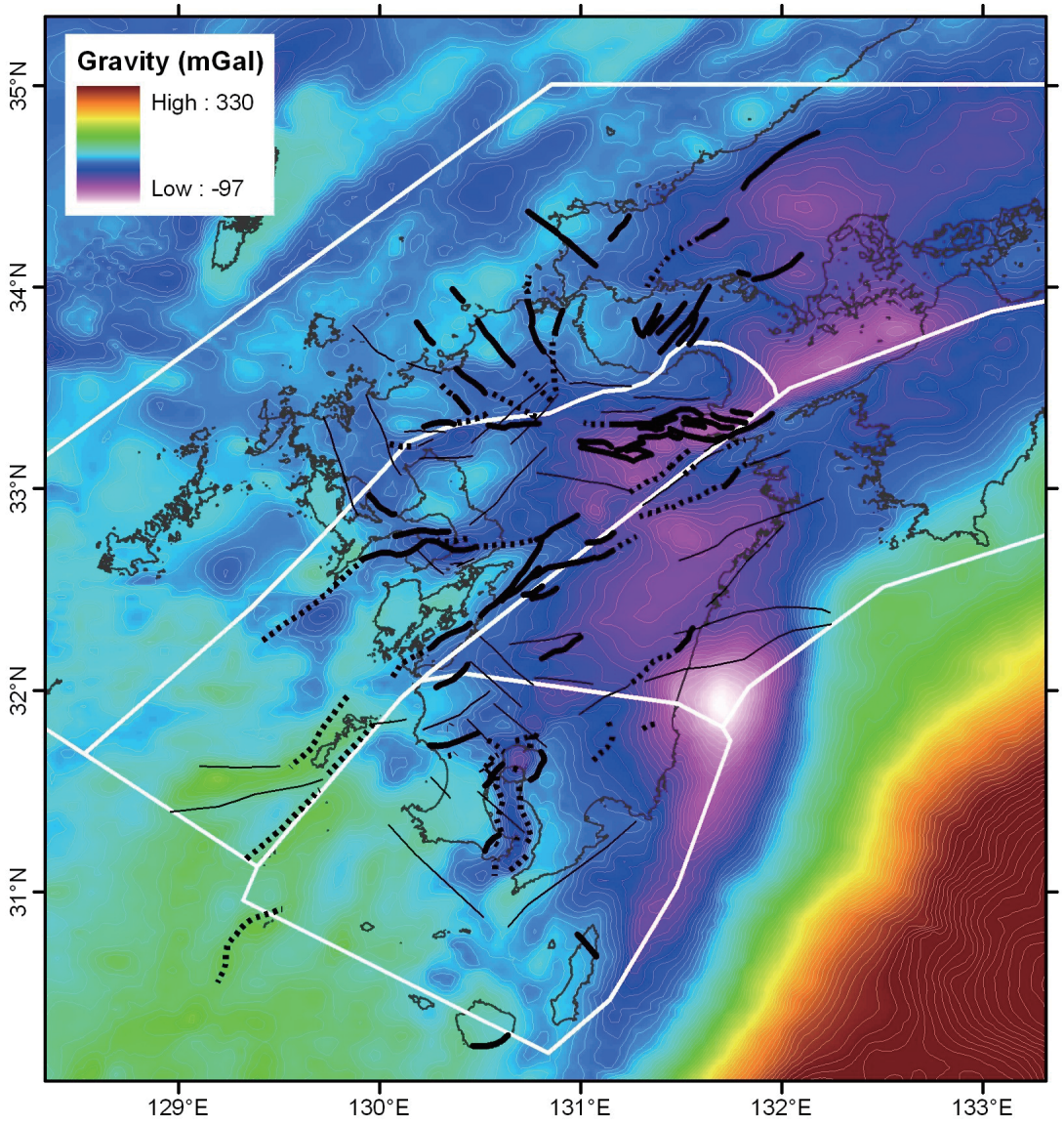

Figure 8.3: Bouguer gravity map of the Kyushu region (Geological Survey of Japan, 2002b). Bold solid lines are active faults from the ARFC active fault database, bold dashed lines are active faults added in this study, thin soild lines are lineaments identified which may constitute “old faults”. White lines are the domain boundaries.

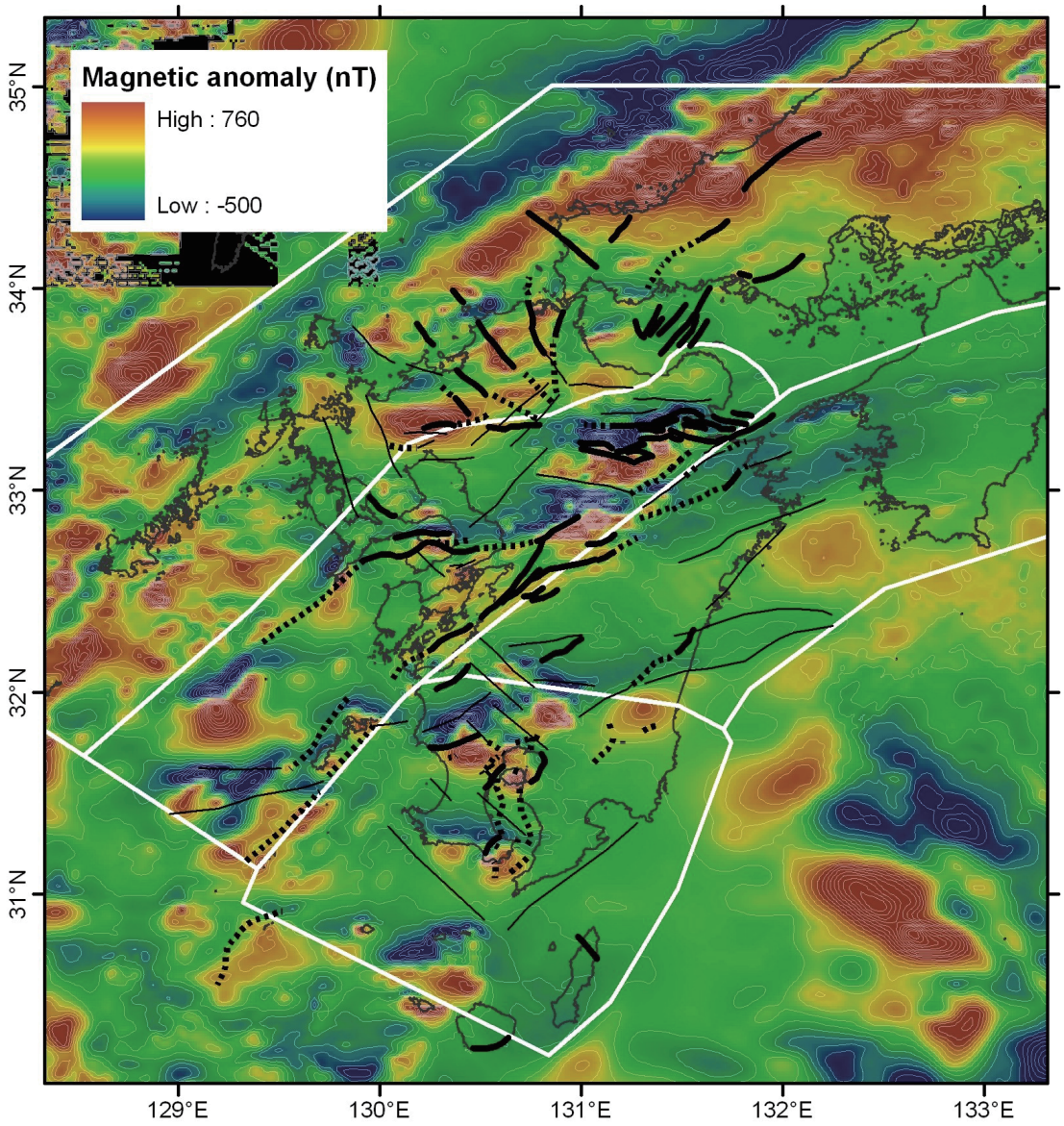

Figure 8.4: Map of the magnetic field of Kyushu area (Geological Survey of Japan, 2005). Bold solid lines are active faults from the ARFC active fault database, bold dashed lines are active faults added in this study, thin soild lines are lineaments that may constitute “old faults”. White lines are the domain boundaries.

8.2 Vertical deformation datasets

Vertical deformation datasets, as compiled by CRIEPI and supplied by NUMO, are limited for Kyushu (Figure 8.5). The most extensive dataset are marine terrace altitudes, particularly the altitude of the peak last interglacial, 125 ka, shoreline (red dots on Figure 8.5). These record relatively low rates of uplift around the coastline (calculated from terrace altitude divided by age), with the highest rates in the Miyazaki Plain area (MP, 0.7-0.9 mm/a).

Buried marine deposits of equivalent age to the marine terraces (125 ka) have been identified in a few boreholes in the north and west, in a few places in sufficient detail to construct contours of burial depth (blue dots and lines on Figure 8.5). These record relatively low rates of subsidence around the coastline, with the highest rate being in the eastern side of the Beppu-Shimabara Graben (BG, -0.7 mm/a).

The most limited dataset is uplift or subsidence data from inland. The available data are altitude differences between river terraces formed during the penultimate glacial period (~140 ka) and the Last Glacial Maximum (~20 ka; orange dots on Figure 8.5). These river terraces can be correlated to the marine terraces and demonstrated to record uplift between terrace forming events (Yoshiyama and Yanagida, 1995), thus uplift rate is the altitude difference divided by the age difference. Data are available for only two locations, the Miyazaki Plain, where the uplift rates match the marine terrace uplift rates, and an inland basin (Figure 8.5).

Because of the lack of inland data, it is not possible to construct a vertical deformation contour map and, therefore, to calculate reliable uplift or tilt strain rates across Kyushu. Therefore, these data are not used in the surface deformation analysis.

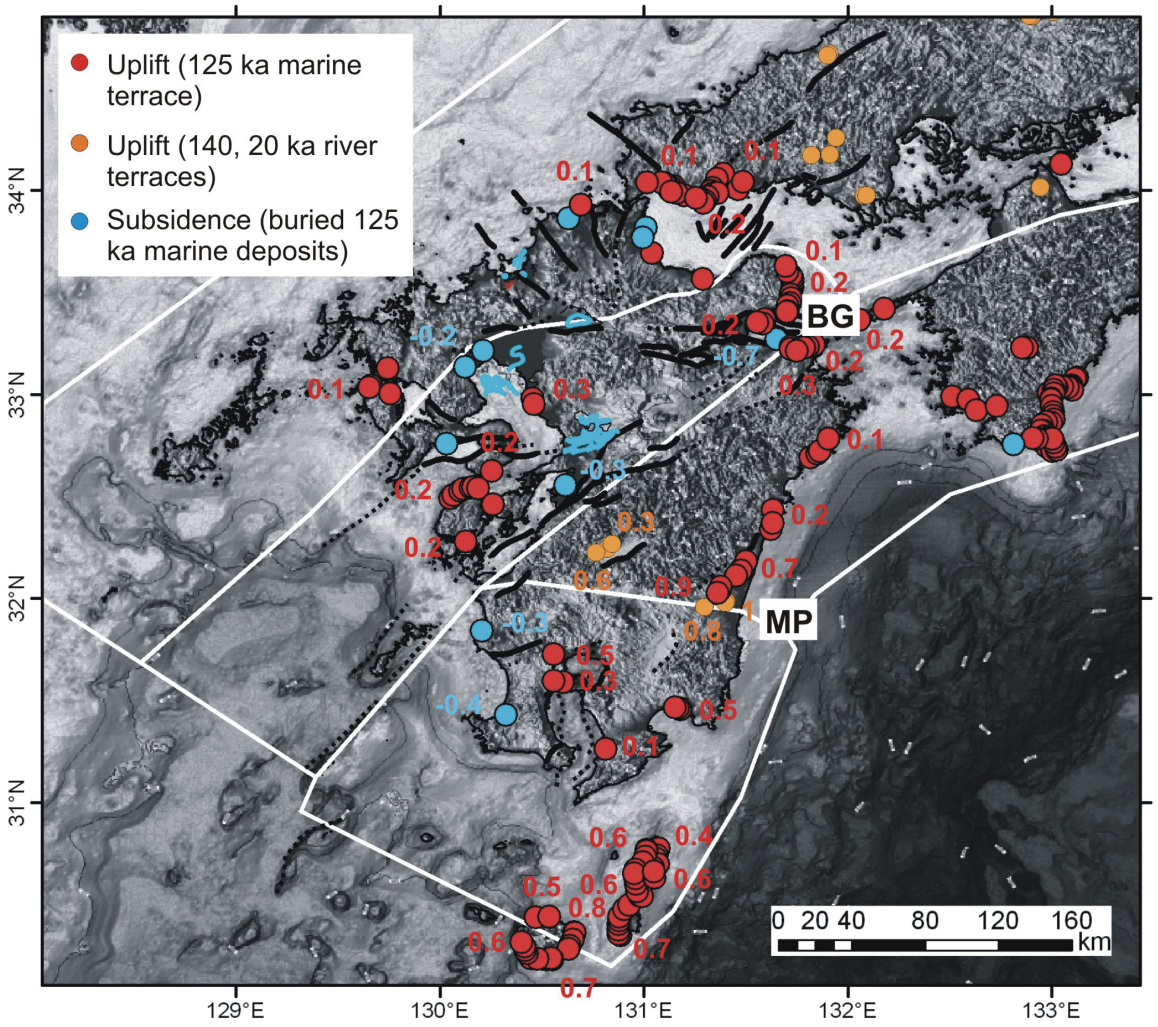

Figure 8.5: Available vertical deformation datasets. The numbers are representative uplift and subsidence rates (mm/a). BG is Beppu-Shimabara Graben, MP is Miyazaki Plain. White lines are the domain boundaries.

8.3 Active Fault Strain Rate Calculations and Logic Tree

Active fault strain rate is calculated from the formula:

Strain rate = horizontal slip rate (mm/a) / width (km) * 10^{-6}

For dip-slip faults, horizontal slip rate has to be converted from net slip rate by:

Horizontal slip rate = net slip rate / cos(dip)

Therefore, the components of the active fault strain rate calculation for which uncertainty needs to be captured in a logic tree are slip rate, dip, and fault width.

The Kyushu active fault logic tree is shown in Figure 8.6. The first branch delineates fault type (or sense of movement, as described in the previous Section) to account for the extra calculation for dip-slip faults, to convert net slip rate to horizontal slip rate. For strike-slip faults, the net slip rate was assumed to be pure strike-slip (i.e., pure dextral or sinistral, with no oblique component). The width options shown in the second branch were assigned taking into account factors such as maximum fault zone width in the Nakata and Imaizumi (2002) active fault database, fault spacing, and considerations of the styles of faulting in Kyushu. Fault dips for the dip-slip faults are based on the values listed in the AFRC database. The final branch is net slip rate, which was described in the previous Section. All the weightings have been assigned by the report authors (i.e., have not undergone local Japanese expert elicitation).

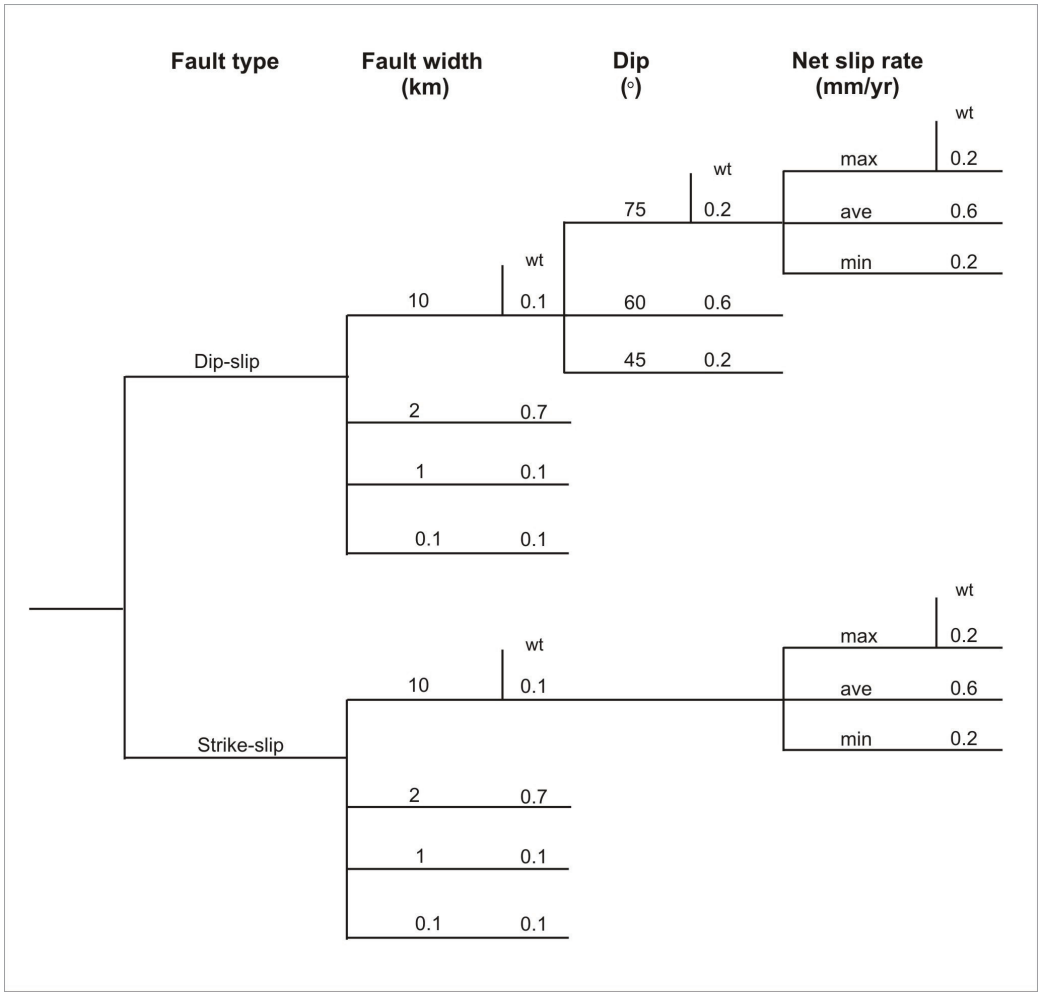

Figure 8.6: Summary logic tree for calculating strain rate from active faults. Note only one set of branches is shown. The logic tree branches and weightings (wt) were assigned by the report authors.

8.4 Active Fault Strain Map and Example Location Calculations

In Figure 8.7 we show an example active fault strain map for the highest weighted realisation of the active fault logic tree shown in Figure 8.6 (fault process zone width 2 km, fault dip of 60º, and average net slip rate). Active fault strains are calculated for only those grid squares that contain active faults, which results in very high strain rates in those squares, no strain outside of them, and a blocky appearance to the strain map. Not surprisingly, the highest strain rates correspond directly to the active faults with the highest slip rates (Figure 8.2), namely those in the Beppu-Shimabara Graben, and along the Oita-Kumamoto Line.

Alternative strain maps derived from differing parameters would vary considerably, particularly with estimation of fault width (encompassing fault complexity and the width of the process zone around an active fault). We also draw attention to the probable incomplete mapping of Class C faults in the study area, and therefore the likely underestimation of active fault strains.

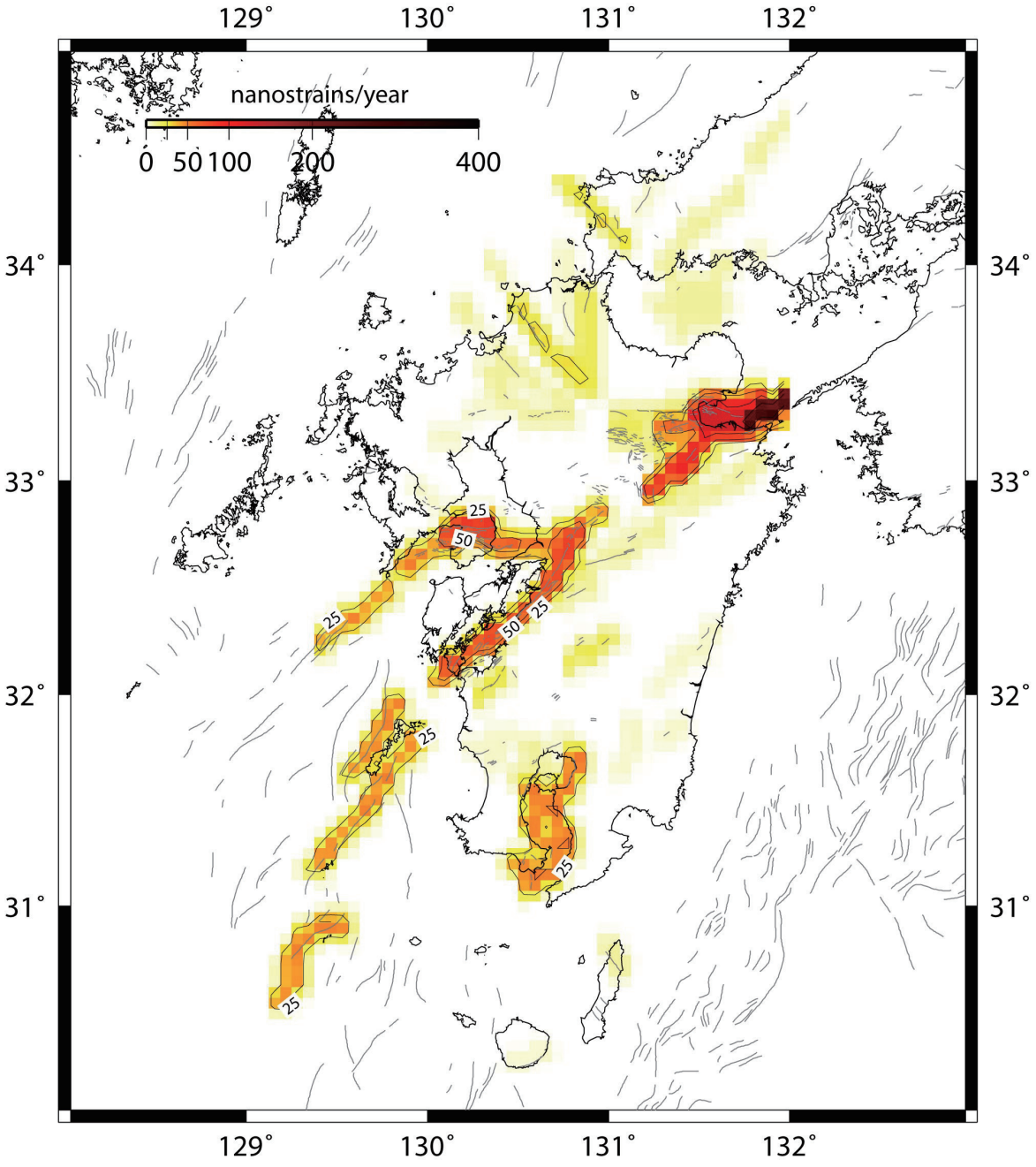

Figure 8.7: Strain map calculated for the active faults shown in Figures 8.1 and 8.2. The map is for the highest weighted realisation of the active fault branch of the logic tree shown in Figure 8.4

In Figure 8.8 we show the relationship between the locations of known active faults and the 11 example locations where we will compare rock deformation strain and hazard. Three example locations (1, 8, 10) fall within the process zones up to 10 km distant from the delineated fault traces.

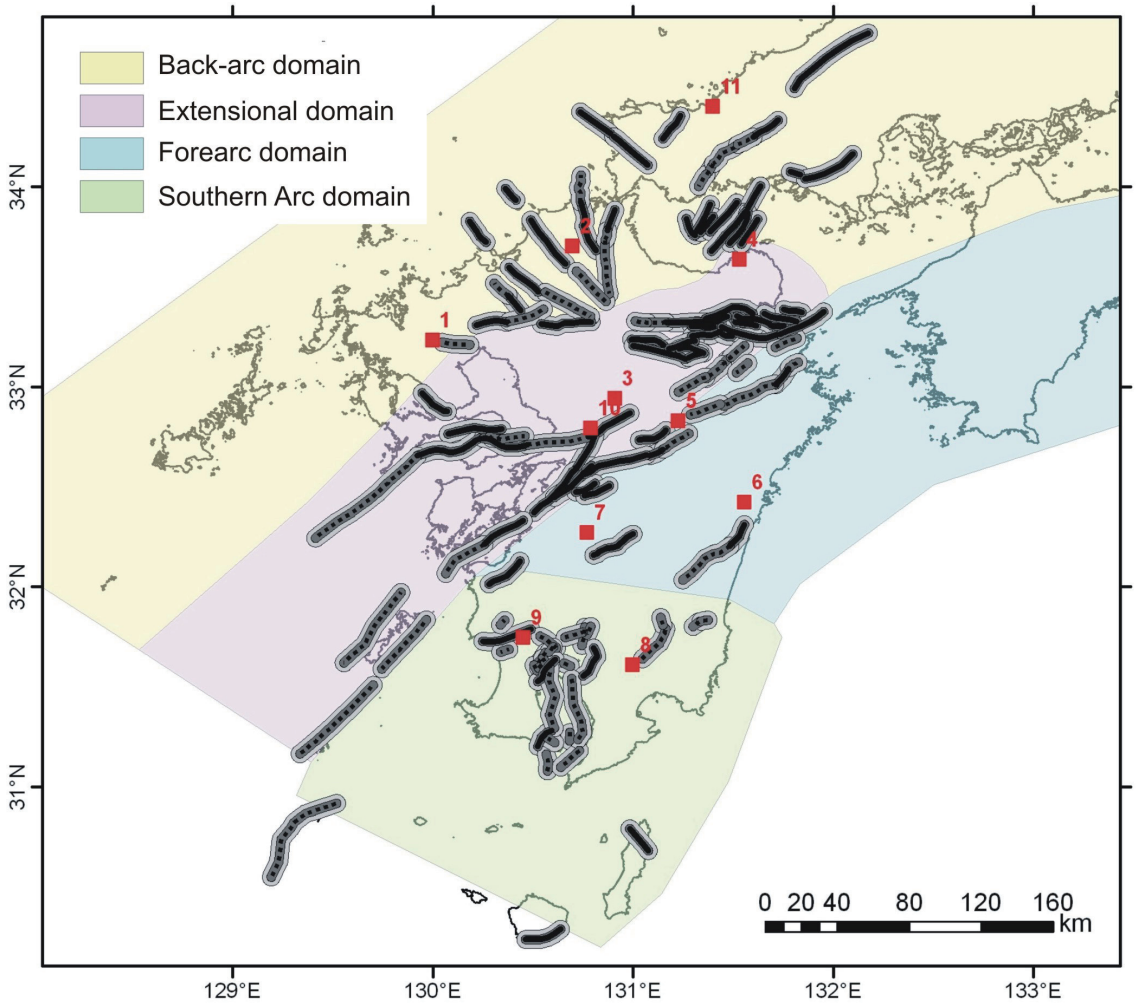

Figure 8.8: Locations of the 11 example locations with respect to active faults. The centreline of each active fault is shown as a black line, and the shaded zones indicates the 5 km and 10 km wide process zones around each fault.

The strain values for all of the branches of the active fault logic tree for the 3 example locations which are situated on active faults are shown as histograms in Figure 8.9. The strain rates for example locations 1 (Back-arc domain) and 8 (Southern Arc Domain) have a wide distribution (note the maximum value is 355 nanostrains/a), but the majority is <30 nanostrains/a. This reflects the low slip rate of the faults on which they are situated (average 0.1 mm/a). The strain rates for example location 8 (Extensional domain) are more tightly distributed (maximum 100 nanostrains), but the peak is 80 nanostrains/a, reflecting the higher slip rate (average 0.9 mm/a) of the fault on which the example location is situated.

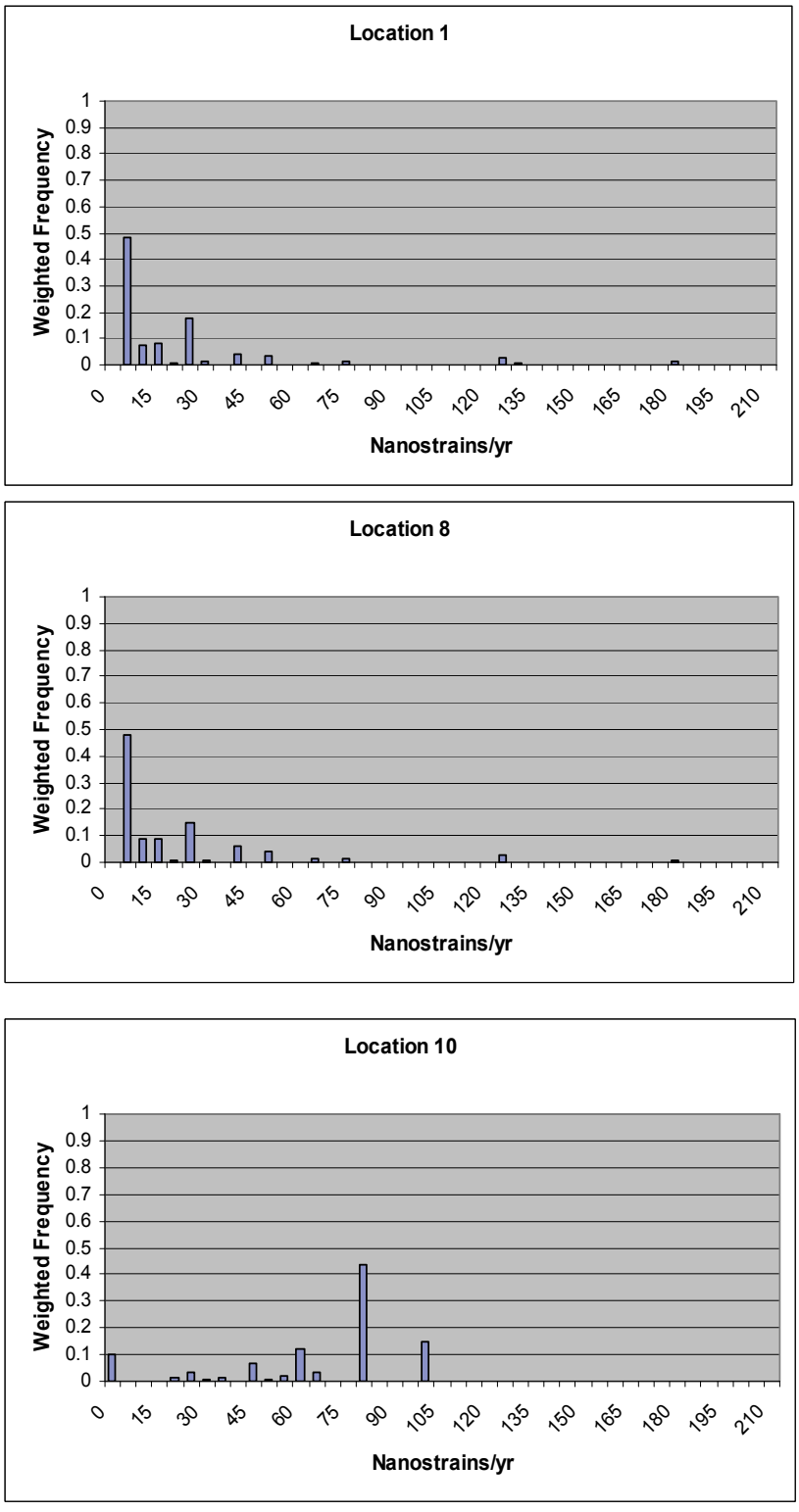

Figure 8.9: Histograms of active fault strain at three example locations located on or close to active faults, as shown in Figure 8.6. The discrete probability histograms show the probability of a strain rate being within a 5 nanostrains/a bin width. The histograms are constructed by sampling all possible combinations of parameter values in the active fault logic tree (Figure 8.6) and calculating a strain rate for each combination. The histogram is produced by sorting the calculated strain rates according to 5 nanostrain bins. The horizontal extent of the curve on the x-axis and shape of the histogram therefore fully quantifies the underlying distribution of strain rate uncertainty. Note that the histogram for locations 1 and 8 are truncated, and the total range is 355 nanostrains/a.

8.5 References for Section 8

Geological Survey of Japan, AIST (2002a). Geological Maps of Japan 1:200,000 (Images) Version 2. Digital Geoscience Map G-3.

Geological Survey of Japan, AIST (2002b). Geoscientific maps of Southern part of Korea, western part of Japan and their adjoining areas. Digital Geoscience Map P-4.

Geological Survey of Japan, AIST (2005). Aeromagnetic Database of Japan. Digital Geoscience Map P-6.

Nakata, T., Imaizumi, T. (2002). Digital active fault map of Japan.

Research Group for Active Faults of Japan (1991). Active Faults in Japan. Revised Edition, University of Tokyo Press, 437 pp.

Yoshiyama, A., Yanagida, M. (1995). Uplift rates estimated from relative heights of fluvial terrace surfaces and valley bottoms. Chigaku Zasshi = Journal of Geography, **104**, 809-826.

9 Strain Rates from GPS

This Section presents our use of GPS data to quantify the rates of tectonic deformation in Kyushu. We overview the GPS data used, review the elastic block model approach to interpret the data and remove elastic strain effects from subduction coupling. We have developed a logic tree for estimation of rock deformation strain in Kyushu from GPS, involving 120 different GPS strain models. For each of these strain models, we have estimated and removed the influence of elastic strain due to subduction zone coupling from the GPS velocity field using a variety of elastic block model configurations, which we also outline here. We show a weighted average of the logic tree results, in terms of areal strain, shear strain, and the 2nd invariant of the strain tensor. We also show the distribution of strain values at several example locations in the region, and discuss these results within the context of the tectonic setting of the region. We also present a hypothesis for the existence of a high shear strain zone in southern Kyushu detected by GPS.

9.1 GPS Data Used

Velocities of GPS sites throughout Japan are derived from combination of SINEX (Solution INdependent EXchange format) files provided to us by the Geographical Survey Institute (GSI; http://mekira.gsi.go.jp/) from their daily processing of the Geonet Continuous GPS (CGPS) network in Japan (~1200 CGPS sites in total). The daily network processing of the Geonet network is conducted by GSI, with Bernese GPS processing software (Rothacher and Mervart, 1996; Beutler et al., 2001) using standard processing methods. The SINEX files we use are from one day every three months for the period 1996-2004. In order to combine the daily SINEX files to estimate velocities for the CGPS sites in Japan relative to a known terrestrial reference frame, we use GLOBK software (e.g., Herring, 2001).

To help place the Japanese dataset in a global context, we also use daily solutions from Scripps Institute of Oceanography processing of the global IGS network of GPS sites (http://sopac.ucsd.edu), as well as SINEX files from processing of a subset of ~10 Japanese sites and several global sites that have been submitted by GSI to the Crustal Dynamics Data Information System (CDDIS; http://cddis.gsfc.nasa.gov/). Using GLOBK we estimate a rotation and translation of each dataset into the ITRF2000 reference frame (Altamimi et al., 2002), for each day. To accomplish this, we tightly constrain the coordinates of a subset of the most reliable IGS GPS stations to their known ITRF2000 values. We do this for each set of daily solutions, obtaining a time series of site positions in the ITRF2000 reference frame. The ITRF2000 velocities at each GPS station are calculated by a linear fit to the daily ITRF2000 coordinates. The uncertainties in the linear fits are derived using a white-noise model, so the uncertainties are seriously underestimated (e.g., Zhang et al., 1997; Williams et al., 2004). We multiply the formal uncertainties by 5 to give “reasonable” values of about 1 mm/a uncertainty in horizontal velocities for long-running stations within Japan (T. Nishimura, pers. comm., 2005). Ideally, the GPS velocity errors should be assessed more rigorously. This will require maximum-likelihood analysis of (probably daily, perhaps weekly) time series of GPS positions, to define the appropriate noise model for the data and to calculate a realistic velocity uncertainty (e.g., Williams et al., 2004; Langbein, 2004).

It is important to avoid the effects on our velocity estimates from large earthquakes and slow slip events. The major events influencing the GPS time series in Kyushu from 1996-2003 are two large thrust earthquakes (M_s 6.7) near Hyuga-nada in 1996 (e.g., Yagi et al., 2001), the 1996-1997 Bungo Channel slow slip event (e.g., Hirose et al., 1999), and the 1997 Kagoshima-ken-hokuseibu earthquake (Fujiwara et al., 1998). To remove the influence of coseismic displacements from the time series, we removed the time series data prior to 1998 in the regions affected by these events. GPS sites in the Kagoshima region were affected by an inflation event at Aira caldera throughout the GPS measurement period (Kriswati and Iguchi, 2003); we used Mogi source parameters for the inflation event estimated by Nishimura et al. (2004) to remove this effect from the dataset. We also conducted a visual inspection of the daily position time series for all the sites in the Kyushu and southwest Honshu region to be sure that there was no non-linear behaviour recorded by the GPS sites that is not representative of steady movement during the interseismic period.

To interpret the GPS site velocities in a tectonically meaningful way, it is important to place the velocities into a “plate-fixed” reference frame (in this case, we choose Eurasia-fixed). We do this at the inversion/tectonic modelling stage of this work (see Section 4) by estimating a rotation of the entire dataset that minimizes the velocities at sites known to be on the stable Eurasian Plate. The GPS velocity field in southwest Japan is shown in a Eurasia-fixed reference frame in Figure 9.1.

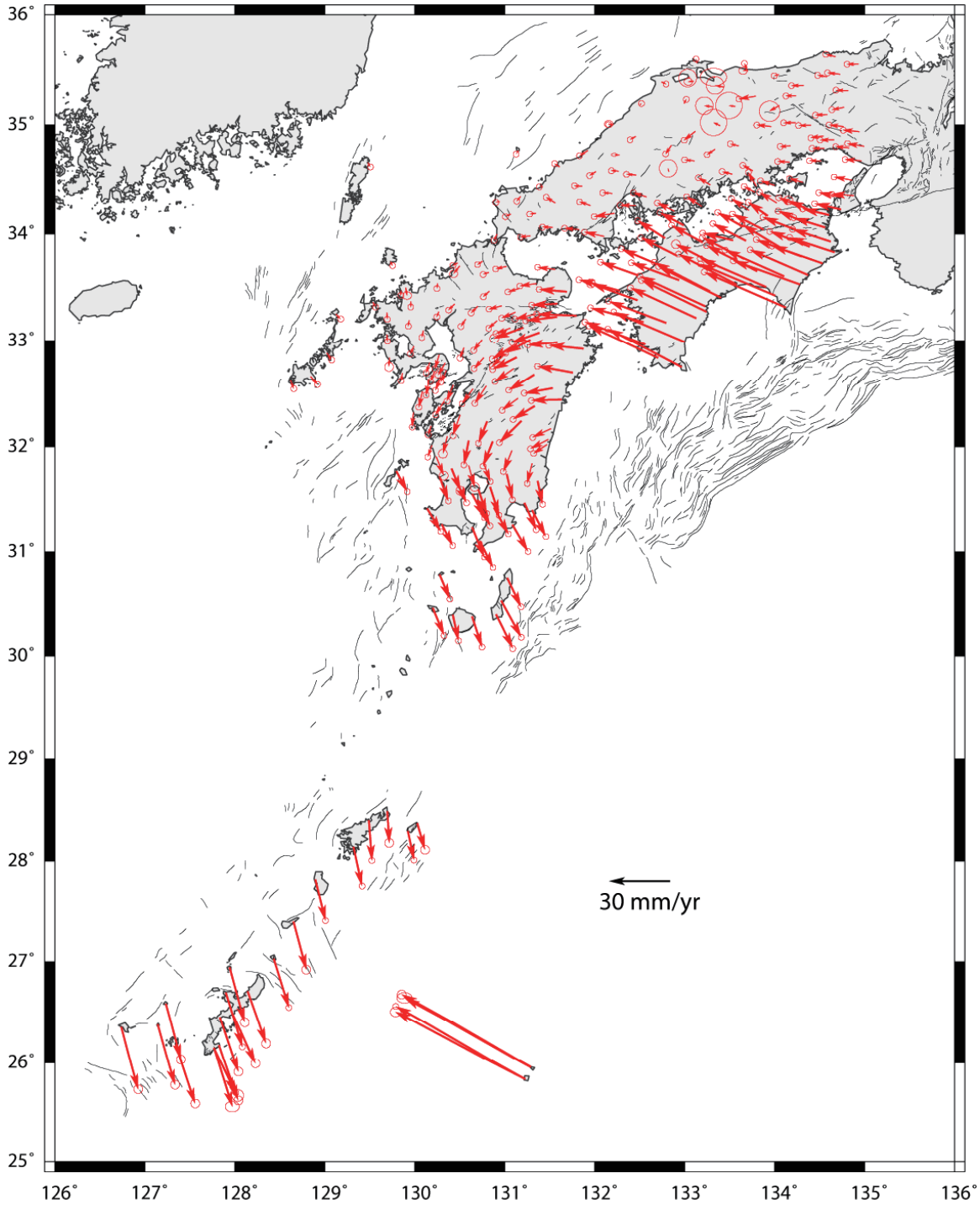

Figure 9.1: The GPS velocity field for southwest Japan (relative to the Eurasian Plate). Thin black lines show active faults.

In addition to the GPS velocities described earlier, we use published GPS velocities in the inversion from Heki et al. (1999), Calais et al. (2003), Sella et al. (2002), Beavan et al. (2002), and Prawirodirdjo et al. (2004). These datasets help us to further place the southwest Japan GPS dataset into a regional plate kinematic context. This is critical as we must be sure to account for all of the possible relative motion between the various tectonic plates in the system that could be influencing the GPS measurements in Japan.

In addition to the GPS velocities we also include earthquake slip vectors from events on the Nankai Trough and Ryukyu Trench (from Harvard CMT, http://www.globalcmt.org/CMTsearch.html) as these data give us information about the relative motion between the Kyushu forearc relative to the underthrusting Philippine Sea Plate. We also include slip vector data for the Median Tectonic Line (MTL) in Shikoku that is consistent with the geological observations of nearly pure right-lateral slip on that fault.

9.2 Approach Used to Model GPS Data in Kyushu

Large, complex strain patterns are apparent in the GPS strain map in southwest Japan (Figure 9.2). However, much of this strain is related to interseismic coupling on the offshore subduction zone boundary. To isolate the strains that may reflect permanent deformation of the upper plate, we must remove this effect.

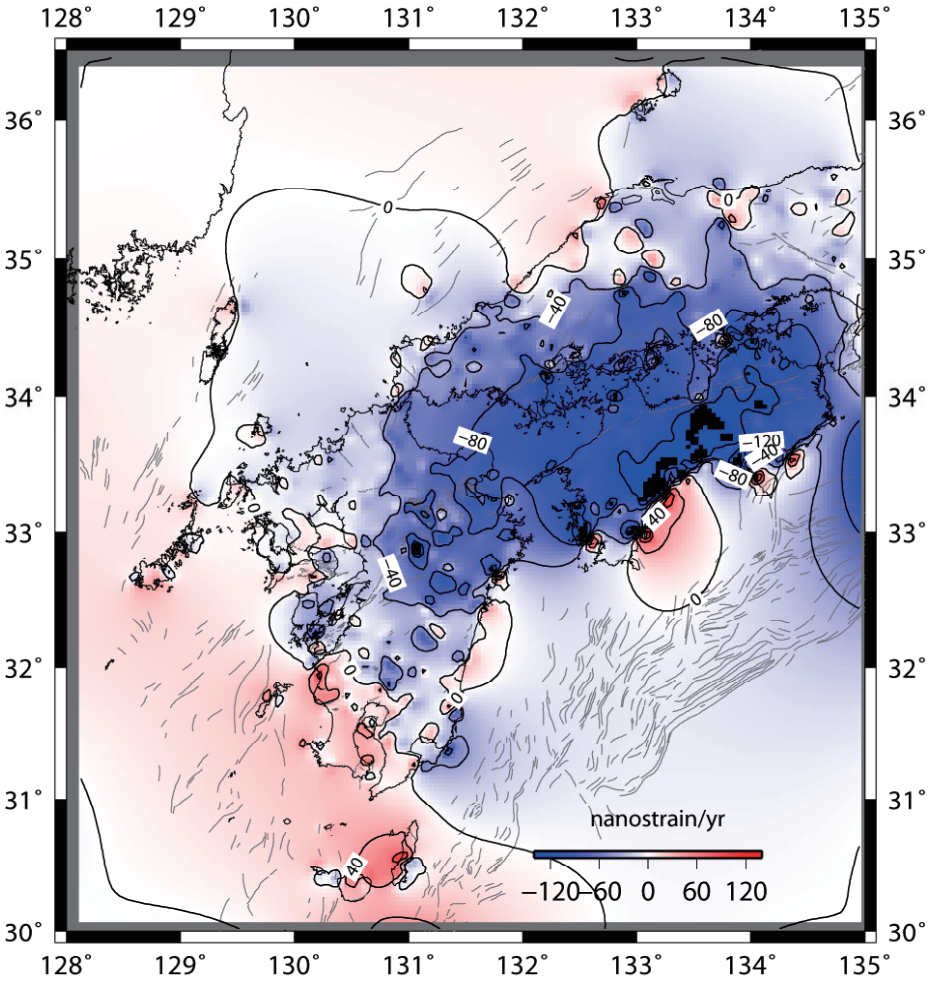

Figure 9.2(a): Areal strain rates (in nanostrains/a) from the raw GPS velocity field (Figure 9.1; no elastic strains removed) estimated using the Haines and Holt method.

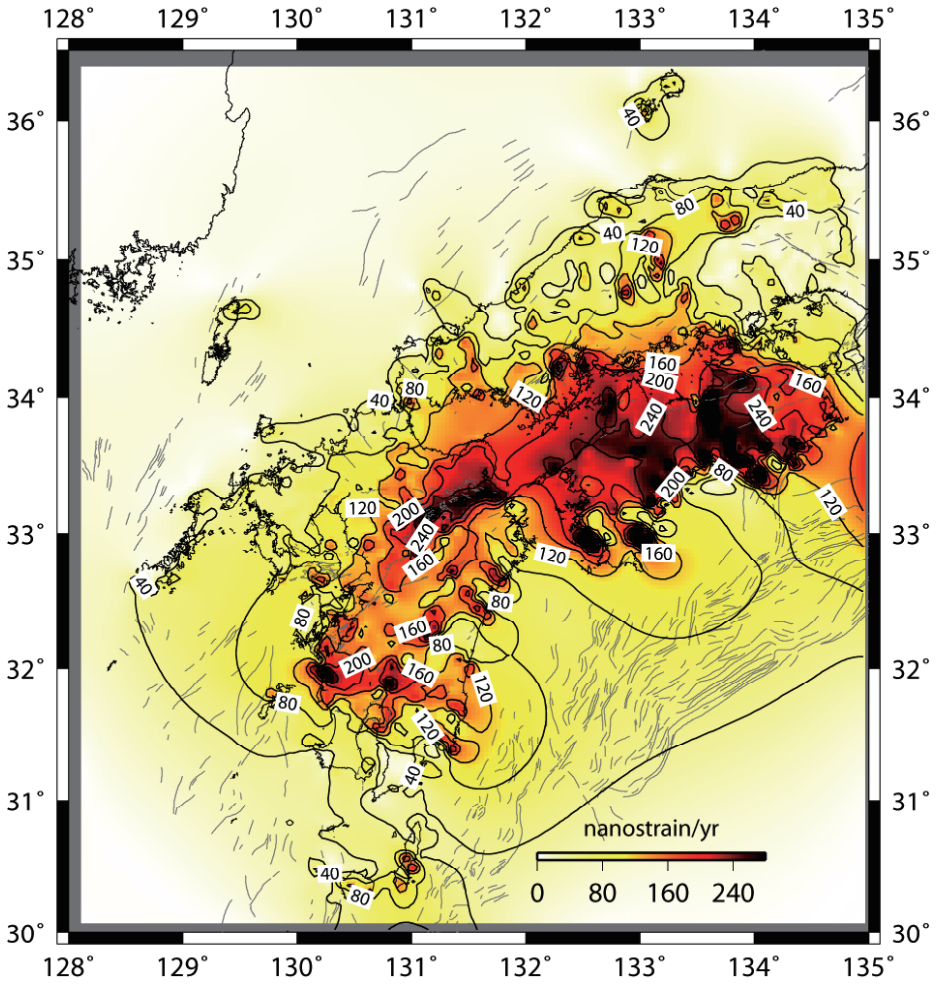

Figure 9.2(b): Shear strain rates (in nanostrains/a) from the raw GPS velocity field (Figure 9.1; no elastic strains removed) estimated using the Haines and Holt method.

Recently, many studies have shown that GPS velocities measured in zones of active faulting during the interseismic period are explained by interseismic elastic strains, as well as long-term rotation of crustal blocks in the deforming zone (e.g., McCaffrey et al., 2000; McCaffrey, 2002, 2005; McClusky et al., 2001; Meade and Hager, 2005; Wallace et al., 2004, 2007). Methods have been devised by McCaffrey (1995, 2002) and Meade and Hager (2005) to invert GPS velocities for long-term rotations of tectonic blocks, and elastic strain due to coupling on block-bounding faults. Recently, Nishimura and Hashimoto (2006) have used a similar method to the elastic block approach for interpreting GPS velocities in Kyushu. For the purposes of rock deformation/tectonic hazards assessment, if the elastic deformation estimated from the inversion for the fault coupling parameters is subtracted from the original GPS velocities, the resulting velocity field will be approximately free of the elastic effects of interseismic coupling on known, major active faults in the region. These residual velocity and strain-rate fields may be interpreted in terms of deformation due to other minor faults or perhaps zones of distributed deformation.

McCaffrey's (1995, 2002) method performs a non-linear inversion to simultaneously estimate the angular velocities of elastic blocks and coupling coefficients on block-bounding faults, to give the best fit to the GPS velocities, and optionally, earthquake slip vectors, and geological fault slip rates and azimuths. The data misfit, defined by the reduced chi-squared statistic (χ_n^2), is minimised. The method also allows us to optimally rotate multiple GPS velocity solutions into a common reference frame. McCaffrey's approach also has the benefit of including all of the bounding plates so that we can establish the plate motion budget that needs to be accounted for in the plate boundary zone. Once the elastic deformation effects due to interseismic coupling on the Ryukyu Trench and Nankai Trough (estimated using the elastic block method) have been removed from the GPS velocity field, the residual strain (largely due

to possible upper-plate deformation) can be mapped using a variety of methods (e.g., Haines and Holt, 1993; Beavan and Haines, 2001; Sagiya et al., 2000; Miura et al., 2004). Given the uncertainties inherent in GPS measurements, GPS techniques are unable to reliably detect strain rates below a certain threshold (this threshold will be dependent on the quality of the GPS network and data and distribution of GPS sites); thus, GPS should not be used on its own to determine if a site is tectonically stable (i.e., additional geological and seismological investigations will be needed to confirm tectonic stability.)

9.3 Elastic Block Model Set-up for Kyushu

We have investigated six different elastic block model configurations for the southwest Japan region. In all of the models, we define a Eurasian Plate, Amurian Plate, Philippine Sea Plate, Southwest Japan Block, and Okinawa Block (Figure 9.3).

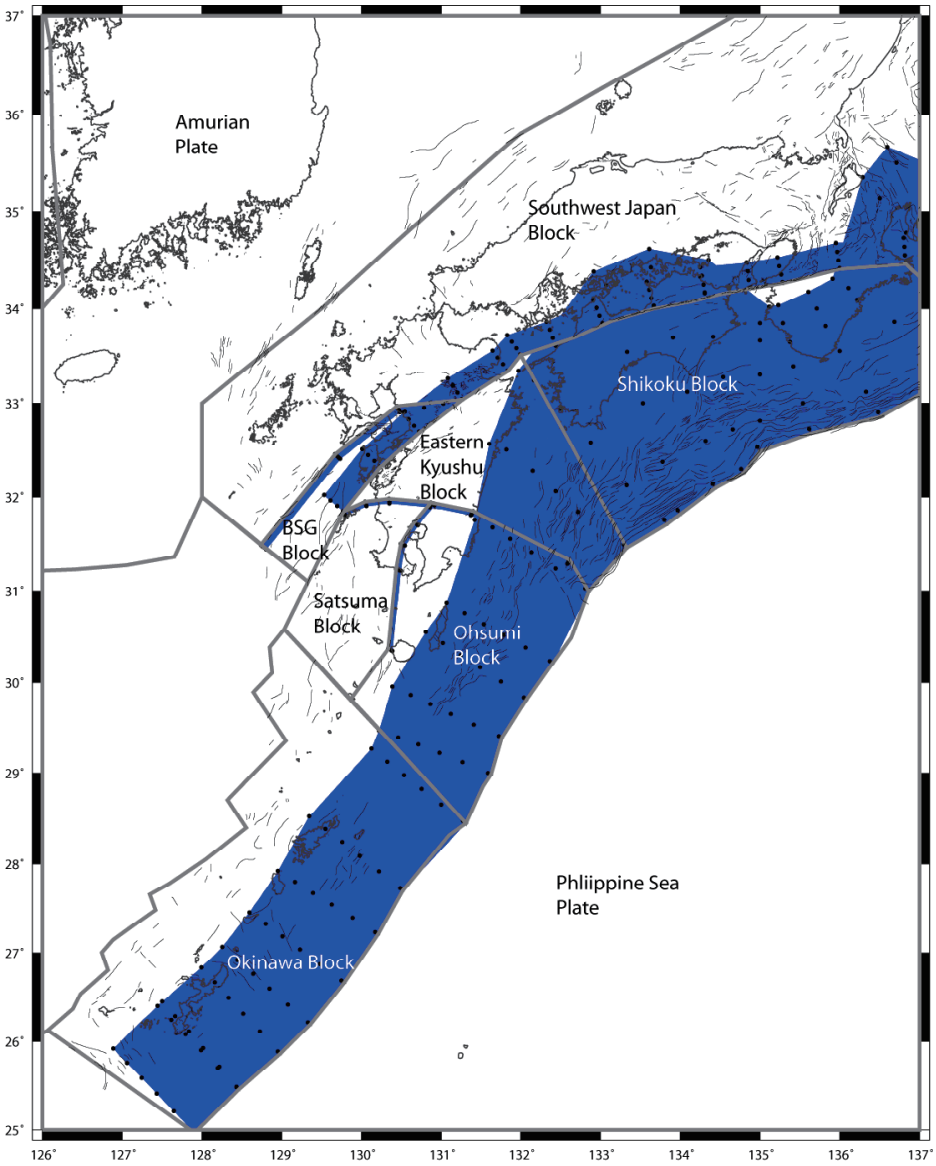

Figure 9.3: Block model set-up for southwest Japan, where the southwest Japan forearc is divided into four separate blocks. Note, we have conducted six different models where various combinations of these blocks are connected together, forming composite blocks (see discussion in text). Dark grey lines are block boundaries, blue planes are a plan-view of faults used in the model (black dots represent nodes defining the fault planes).

We define most of the boundaries of the large plates (Amurian, Philippine Sea and Eurasian Plates) based on a digital compilation of tectonic plate boundaries by Bird (2003). The

inclusion of these larger plates also helps us in establishing the overall plate motion budget that must occur across the plate boundary zone in southwest Japan. The Southwest Japan/Amurian Block boundary is defined by a zone of distributed faulting near the west coast of Japan (Gutscher and Lallemand, 1999), which is also associated with strike-slip events (probably right-lateral, striking parallel to the margin; Figure 9.4).

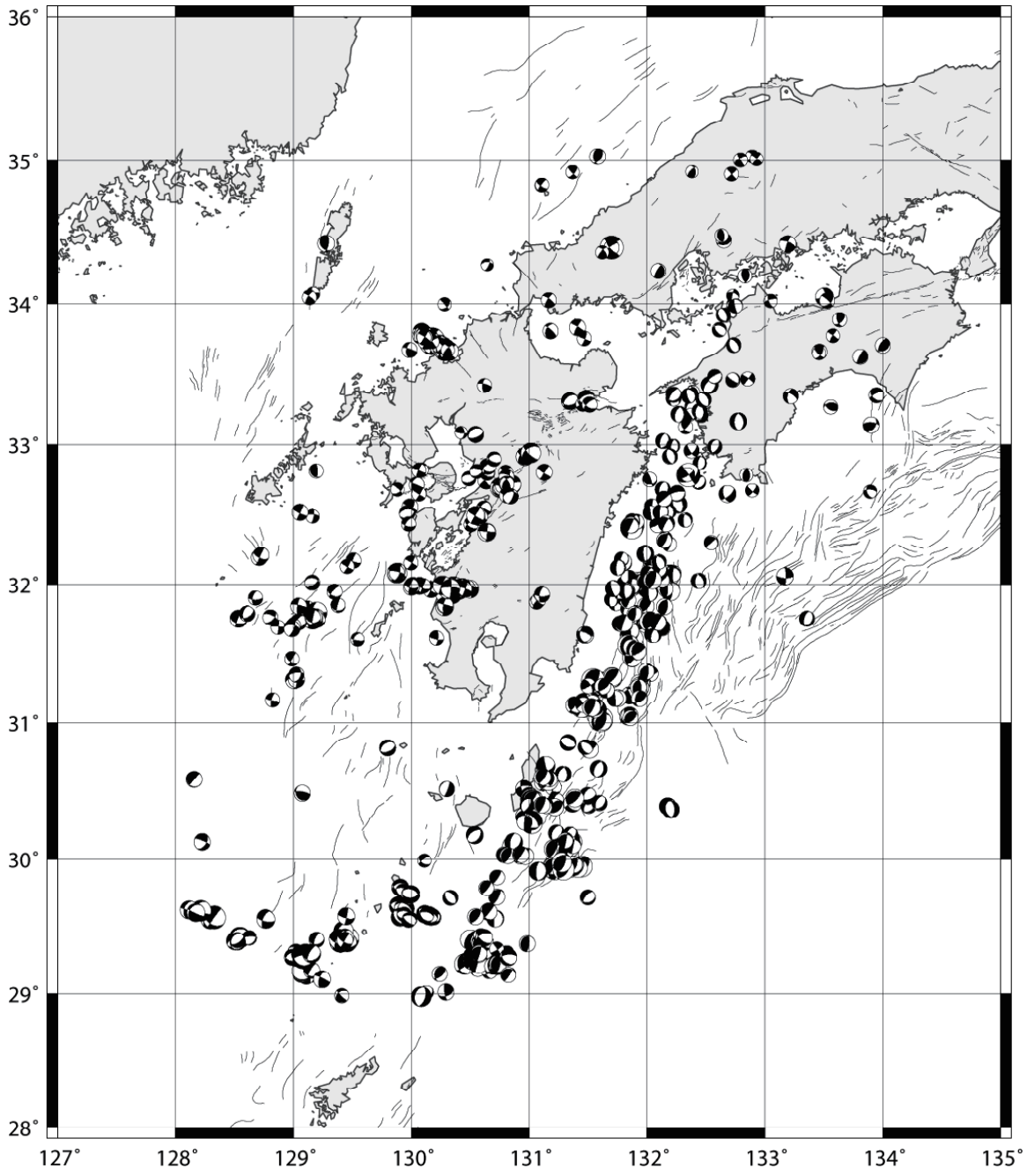

Figure 9.4: Focal mechanism plots for earthquakes in southwest Japan from 1997-2006. Based on CMT solutions from the JMA catalogue (data from http://www.fnet.bosai.go.jp).

The distinction between the models we have conducted here is based upon the division of the forearc and backarc blocks in southwest Japan. For the most complex model, we have

broken the southwest Japan forearc and backarc region into four different blocks (Figure 9.3; Table 9.1), including the Shikoku block, eastern Kyushu block, Ohsumi, and Satsuma blocks, and have divided the backarc into two blocks (the Beppu-Shimabara Block and the Southwest Japan block).

The Shikoku block is bounded to the northwest by the MTL. The Ohsumi block is bounded on the west by the Kagoshima Graben, and on the north by a possibly active left-lateral shear zone that has been highlighted by earthquakes and GPS measurements (e.g., Kodama et al., 1995; Nishimura and Hashimoto, 2006).

We use the Kagoshima graben as a boundary in some of our models based on evidence from GPS (Figures 9.1 and 9.2) and geology (Aramaki, 1984) for active extension in the Kagoshima Graben, and paleomagnetic evidence that southeast Kyushu has rotated independently of the rest of Kyushu for the last 2-6 Ma (Kodama et al., 1995). The Satsuma block is bounded on the east by the Kagoshima graben and on the north by the hypothesised active left-lateral shear zone. The eastern Kyushu block encompasses more than half of the Kyushu forearc, whose western boundary is the southeastern boundary of the Beppu-Shimabara graben.

We have conducted ten different block model scenarios, testing various block combinations (Table 9.1). For example, Model 1 considers the Satsuma, Ohsumi, eastern Kyushu and Shikoku blocks as one composite block. Table 9.1 summarizes the fits to the GPS and earthquake slip vector data in terms of the reduced chi-squared statistic (χ_n^2). In Section 9.4, we discuss the results of the best-fitting block model in further detail.

To define the subduction interface fault (Nankai and Ryukyu Troughs), we approximate the configurations for the Nankai subduction interface in Sagiya and Thatcher (1999) and Shiomi et al. (2004) (Figure 9.3). On the subduction interface, we specify individual nodes defining the interface spaced on average 50 km apart along strike, and at 10 km depth intervals between 0 and 50 km depth (Figure 9.3). We define the MTL as a northward dipping fault, based on geophysical evidence (Ito et al., 1996; Onishi et al., 1999; Tabei et al., 2002).

For the purposes of this initial study, we approximate the boundaries of the Beppu-Shimabara Graben (BSG) block as a single fault on each boundary in the model, although more complex deformation on several faults across a zone is likely to be a more realistic scenario there. We set the southern BSG fault to dip northwest, in part, to deal with possible distributed deformation due to faulting within the BSG block itself.

McCaffrey's (2002) method is used to solve for coupling coefficients at nodes on the Nankai and Ryukyu troughs, the faults representing the BSG boundaries, the extensional zone in the Kagoshima Graben, the MTL, and a possible zone of left-lateral strike-slip cross-cutting southeast Kyushu (Figure 9.3). To represent the change in coupling coefficient (ϕ) values between adjacent nodes, ϕ values on 5 km x 5 km rectangular fault patches between the nodes are estimated by bilinear interpolation.

Additional free parameters in the inversion are the rotation parameters (three for each block) for various combinations of the Amurian Plate, Southwest Japan Block, Shikoku block, Pacific Plate, eastern Kyushu, Beppu-Shimabara Graben, Ohsumi and Satsuma blocks relative to Eurasia, and rotation parameters that rotate each GPS velocity dataset into a Eurasia-fixed reference frame.

Table 9.1: Description and fits to the data of the six different block configurations tested. SATS = Satsuma block; OHSU = Ohsumi block; SHIK = Shikoku block; KYUS = Eastern Kyushu block; SWJP = Southwest Japan block; BSG = Beppu-Shimabara Graben block. The block configurations are explained in terms of whether adjacent blocks are connected as a single, composite block, or whether they represent an independent block. For example, if the line in the table says "SATS+OHSU", it means that the Satsuma and Ohsumi blocks are combined into a single block, while if the line says "SATS" the Satsuma block is independent of the other blocks. χ_n^2 is the reduced-chi squared for each best-fitting model using the prescribed block configuration.

Model Number	Block configuration	χ_n^2	Number of independent blocks in SW Japan
1	SATS+OHSU+KYUS+SHIK BSG+SWJP	5.49	2
2	SATS+OHSU KYUS+SHIK BSG+SWJP	2.07	3
3	SATS+OHSU KYUS+SHIK BSG SWJP	3.13	4
4	KYUS+SHIK SATS OHSU BSG+SWJP	2.17	4
5	KYUS+SHIK SATS OHSU BSG SWJP	2.31	5
6	SATS+OHSU+KYUS BSG+SWJP SHIK	2.4	3
7	SATS+OHSU BSG+SWJP KYUS SHIK	1.9	4
8	SATS+OHSU BSG SWJP KYUS SHIK	2.5	5
9	KYUS SHIK SATS OHSU BSG+SWJP	1.7	5
10	KYUS SHIK SATS OHSU BSG SWJP	1.95	6

9.4 Block Modelling Results for the Best-Fitting Tectonic Model

In general, the models with increasing complexity (i.e., more blocks) appear to produce an improved fit to the data (Table 9.1). This is not unexpected given that there is an increase in the number of free parameters with increasing block model complexity. The best-fitting model (Model 9) is where all four of the forearc blocks (Shikoku, eastern Kyushu, Ohsumi and Satsuma) are independent of one another. The worst-fitting model occurs where all of the forearc blocks constitute a single tectonic block (including Shikoku; Model 1). Models 2 and 7 are similar to the block configuration considered by Nishimura and Hashimoto (2006).

When we break the Kyushu forearc into four separate blocks (Model 9), the fit to the GPS velocities is much better (χ_n^2 = 1.7) than any of the other block model configurations (Table 9.1). In this (the preferred model) 92 free parameters are estimated from 1251 data. The interseismic coupling distribution that we estimate for the Nankai Trough subduction interface (Figure 9.5) is similar to that obtained from previous studies (Nishimura and Hashimoto, 2006).

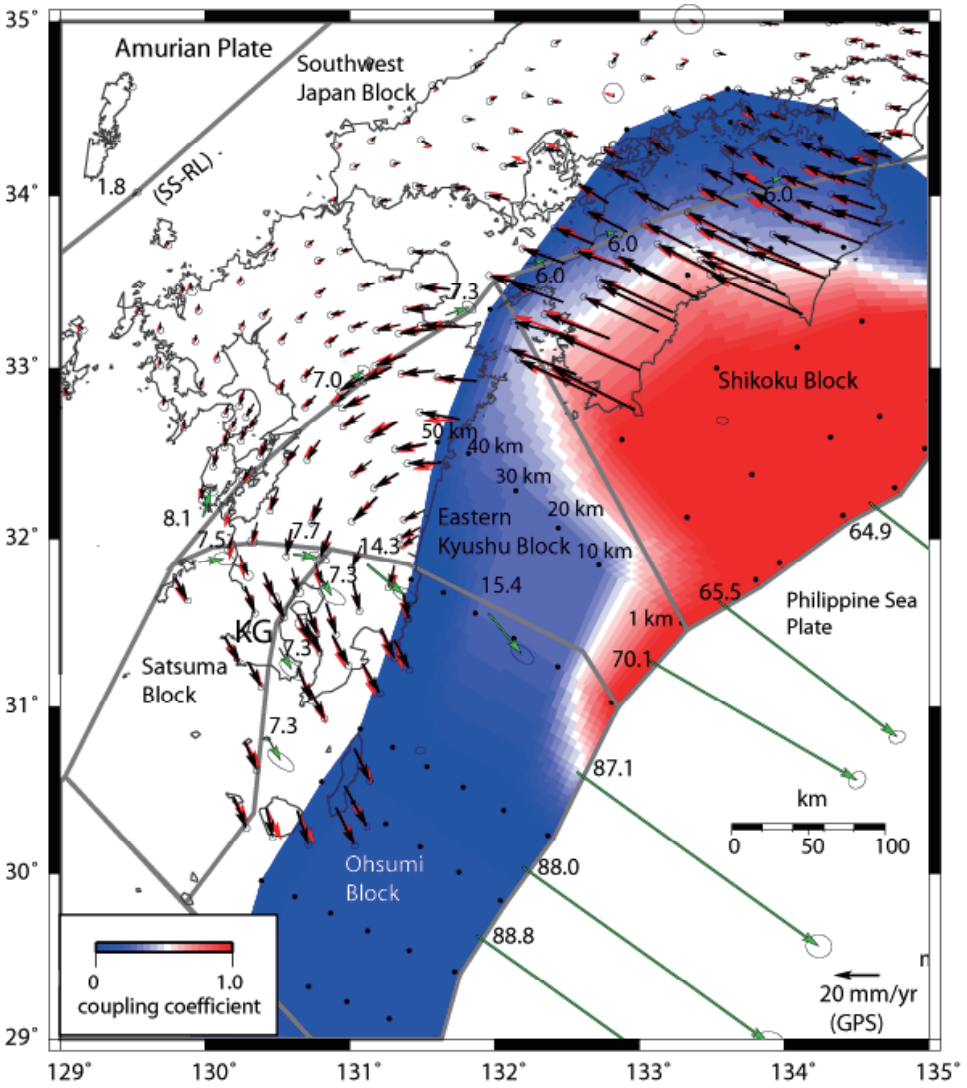

Figure 9.5: Interseismic coupling distribution (in terms of slip rate deficit, mm/a) for the subduction zone from the best-fitting block model (model 9, Table 9.1). Also shown are observed GPS velocities (black), velocities from best-fitting model (red), and relative motion at block boundaries (green, labelled arrows in mm/a). Depth labels for one set of nodes on the subduction zone are shown. Note that the scale for the GPS (observed and modelled) is not the same shown as for the relative block motion vectors. SS-RL = Strike slip-right lateral; KG = Kagoshima Graben.

The interseismic coupling on the subduction interface exerts a great influence on the GPS velocity field (Figure 9.6). The convergence rates we estimate for the Nankai and Ryukyu Troughs are ~70-89 mm/a (Figure 9.5). The rate we estimate for the MTL is ~6 mm/a of pure right-lateral strike-slip, which is in excellent agreement with geological estimates of 5-10 mm/a (Okada, 1970; 1973). This model requires ~7-8 mm/a of right-lateral strike-slip in the eastern BSG, which gradually transitions to more northerly directed extension at up to 8 mm/a. North-south directed extension in the BSG is consistent with focal mechanisms of normal faulting events there (Figure 9.4).

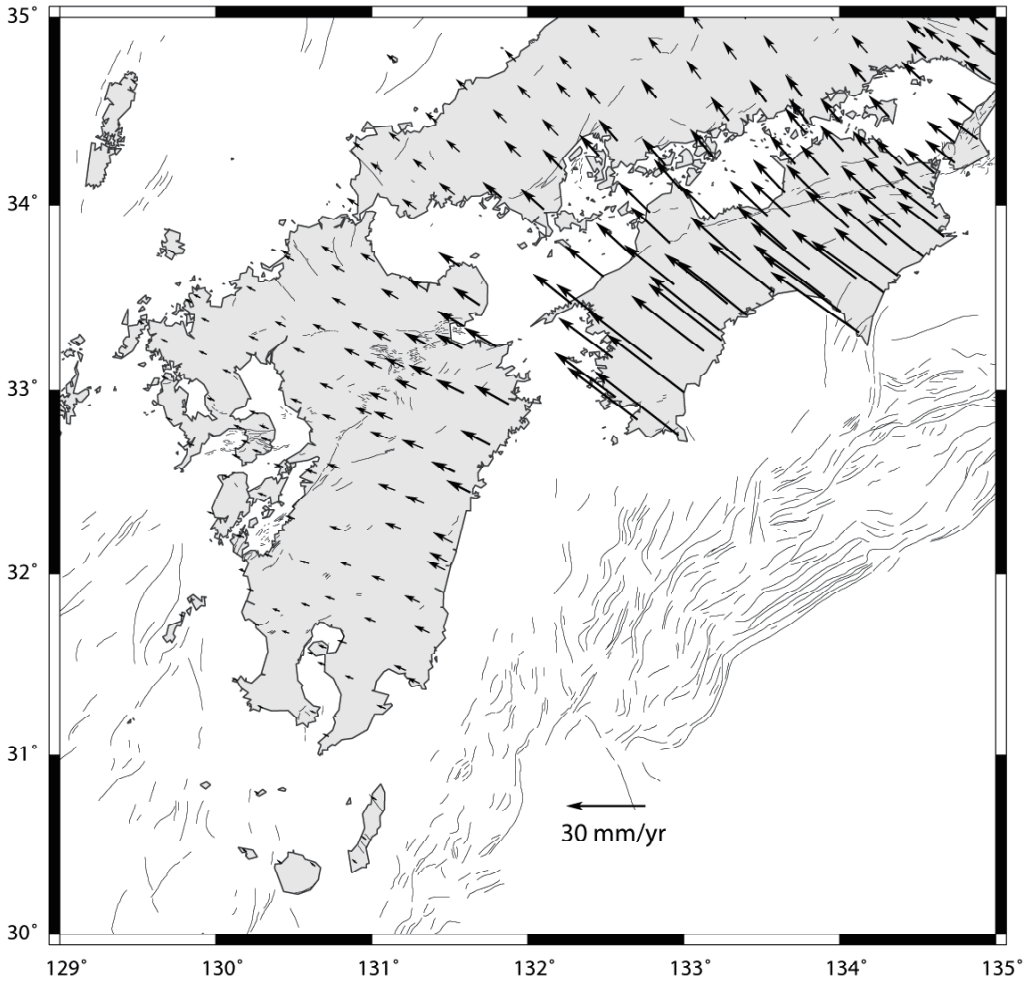

Figure 9.6: Influence on GPS velocities from interseismic coupling distribution in Figure 9.8 shown for the best-fitting model (Model 9, Table 9.1).

The Kagoshima Graben accommodates ~7 mm/a of slightly oblique extension in the best-fitting block model. On the northern boundary of the Ohsumi and Satsuma blocks, ~7-14 mm/a of left-lateral strike-slip is required. The superior fit to the GPS data in Models 2, 4, 5, 7, 9 and 10 compared with Models 1 and 6 (Table 9.1) suggests that left-lateral shear on the northern boundary of the Ohsumi and Satsuma blocks is required by the GPS data (i.e., that the southern Kyushu forearc is a tectonic block independent from the northern Kyushu forearc). The data are well-fitted by ~2 mm/a of right-lateral strike-slip on the offshore Amurian Plate/Southwest Japan block boundary. Due to the small dimensions of the Satsuma and Ohsumi blocks, it is difficult to determine uniquely (with GPS) if the anti-clockwise rotation of southern Kyushu documented in paleomagnetic studies is ongoing today. For example, we are able to fit the GPS data in the Ohsumi block equally well with rapid (~5°/Ma) anti-clockwise vertical axis rotation, and with minimal vertical axis rotation (<0.2°/Ma). However, our best-fitting models do require ~2° per Ma of anticlockwise rotation of the Eastern Kyushu

block about a nearby pole relative to the large, bounding plates (e.g., at 133.86 E, 31.85 S relative to Eurasia).

9.5 Upper Plate Strains in Kyushu

To estimate the strain field due to possible tectonic deformation in Kyushu, we remove the component of the velocity field due to interseismic coupling on the offshore subduction boundary (Figs. 9.5 and 9.6) using Model 9 as an example (Figure 9.7).

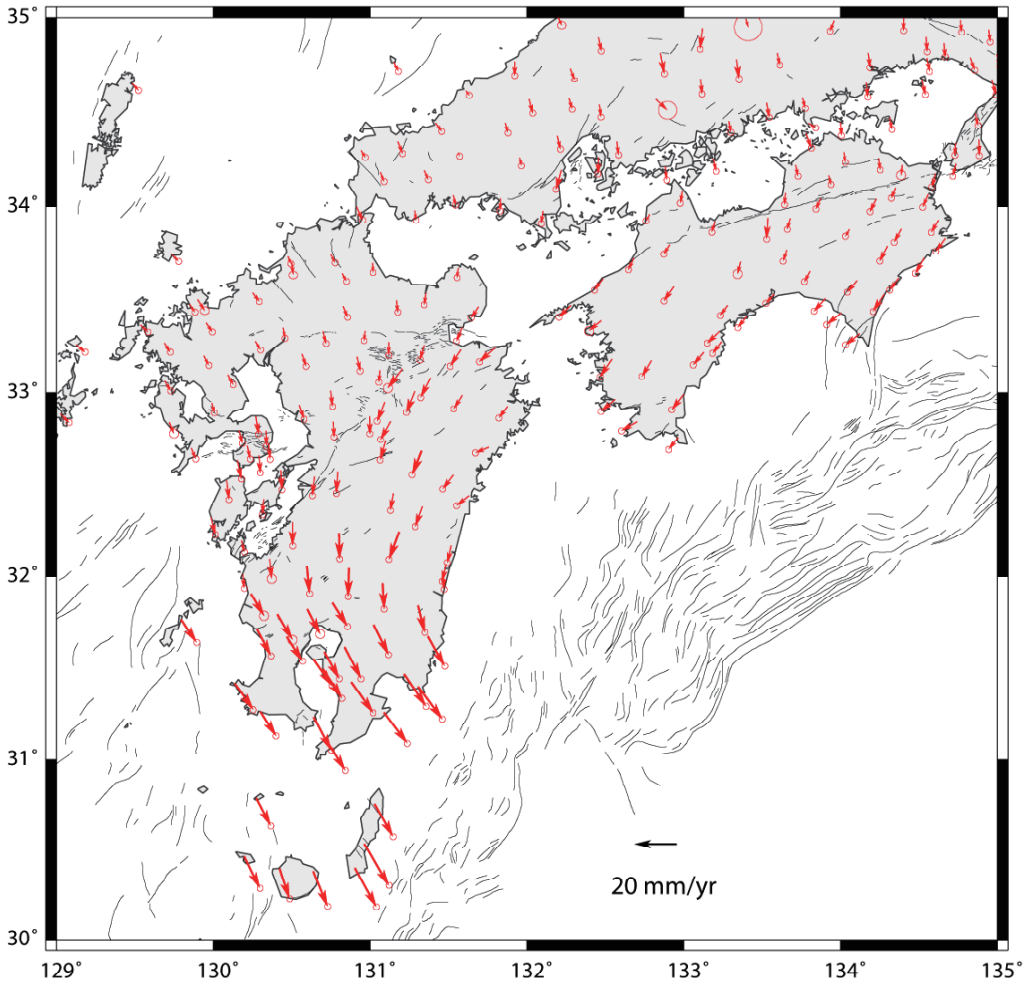

Figure 9.7: GPS velocity field after the component due to interseismic coupling on the subduction zone has been removed (Figure 9.6). This is the velocity field that goes into the Haines/Holt strain modelling (Figures 9.8 and 9.9). Shown for model 9 only.

There are a variety of methods that can be used to convert GPS site velocities to a map of regional strain. Perhaps the most widely used method is one developed by John Haines and Bill Holt (e.g., Haines and Holt, 1993; Beavan and Haines, 2001). To employ their method, a grid (in latitude-longitude) is developed over the area of interest; for the purposes of the Kyushu Case Study, we use a ~5 km x ~5 km grid. Velocities are modelled as bi-cubic splines within each cell, and the inversion attempts both to match the input velocity data and minimize the strain rates within each cell. A strain-rate variance parameter ($1/\nu$ in the terminology of Beavan and Haines, 2001) is defined, with lower values of $1/\nu$ giving smoother solutions. The strain-rate variance parameter is chosen such that the sum of squared residuals between the model and input GPS velocities plus the sum of squares in matching the strain-rate constraints is approximately equal to the number of degrees of freedom in the GPS data set

(i.e., twice the number of velocities). In other words the reduced chi-squared statistic, χ^2_N = (sum of squared residuals)/(degrees of freedom), is approximately equal to 1.

Figure 9.2 shows the shear and areal strain rates for the GPS velocity field without removing the elastic strain due to offshore fault coupling. Clearly, these strain rates are quite high (> 200 nstrain/a), but as discussed previously in this report, much of the strain is related to elastic strains from interseismic coupling on the major offshore subduction faults (Nankai and Ryukyu Troughs) and are unlikely to lead to permanent deformation in the same location where the strain is currently accumulating.

Figures 9.8 and 9.9 show the strain field (areal and maximum shear strain components) after the elastic part of the GPS velocity field due to interseismic coupling (using Model 9) has been removed from the raw velocity field.

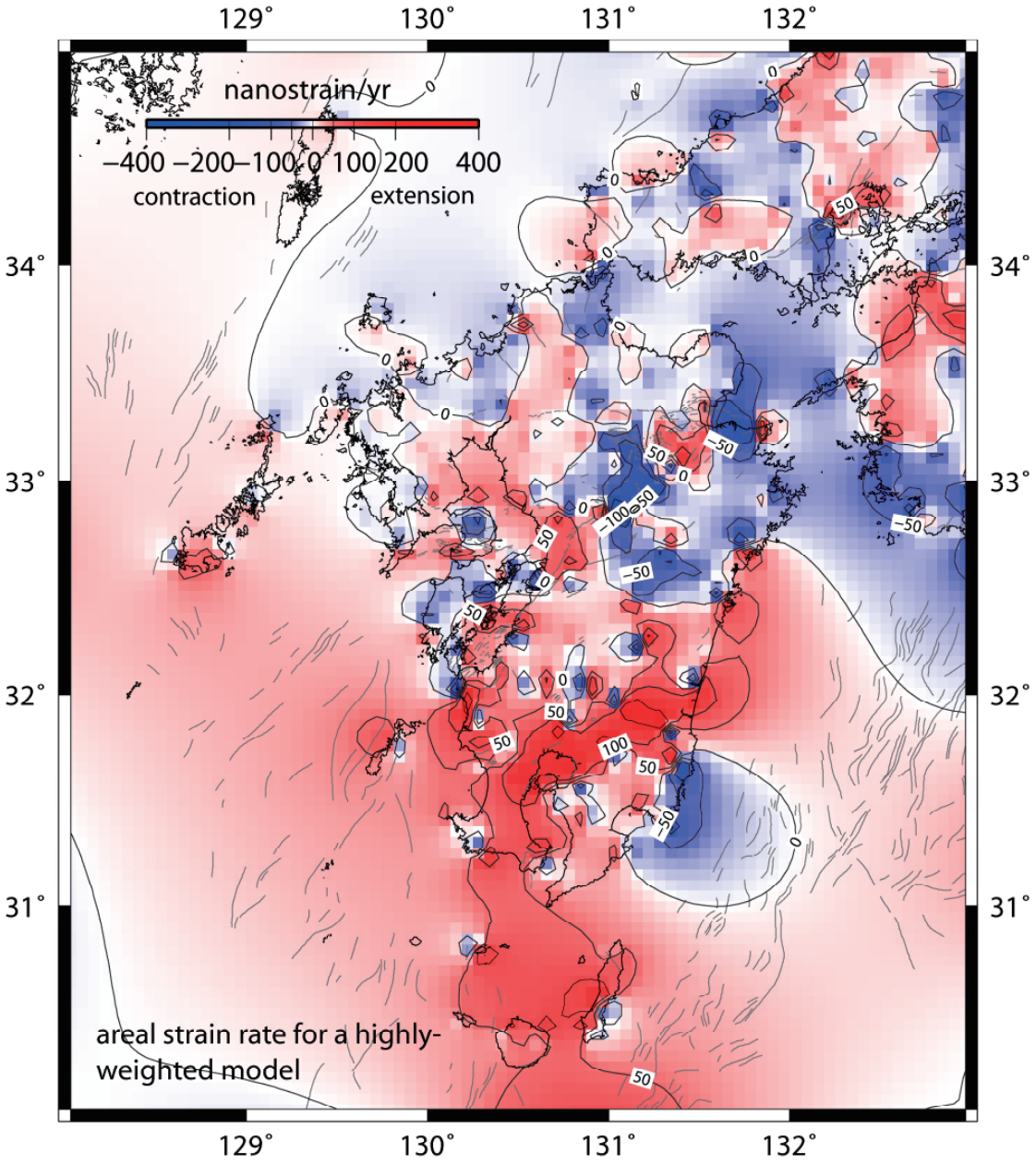

Figure 9.8: Areal strain calculated from the velocity field in Figure 9.7 (with subduction-related elastic strains removed).

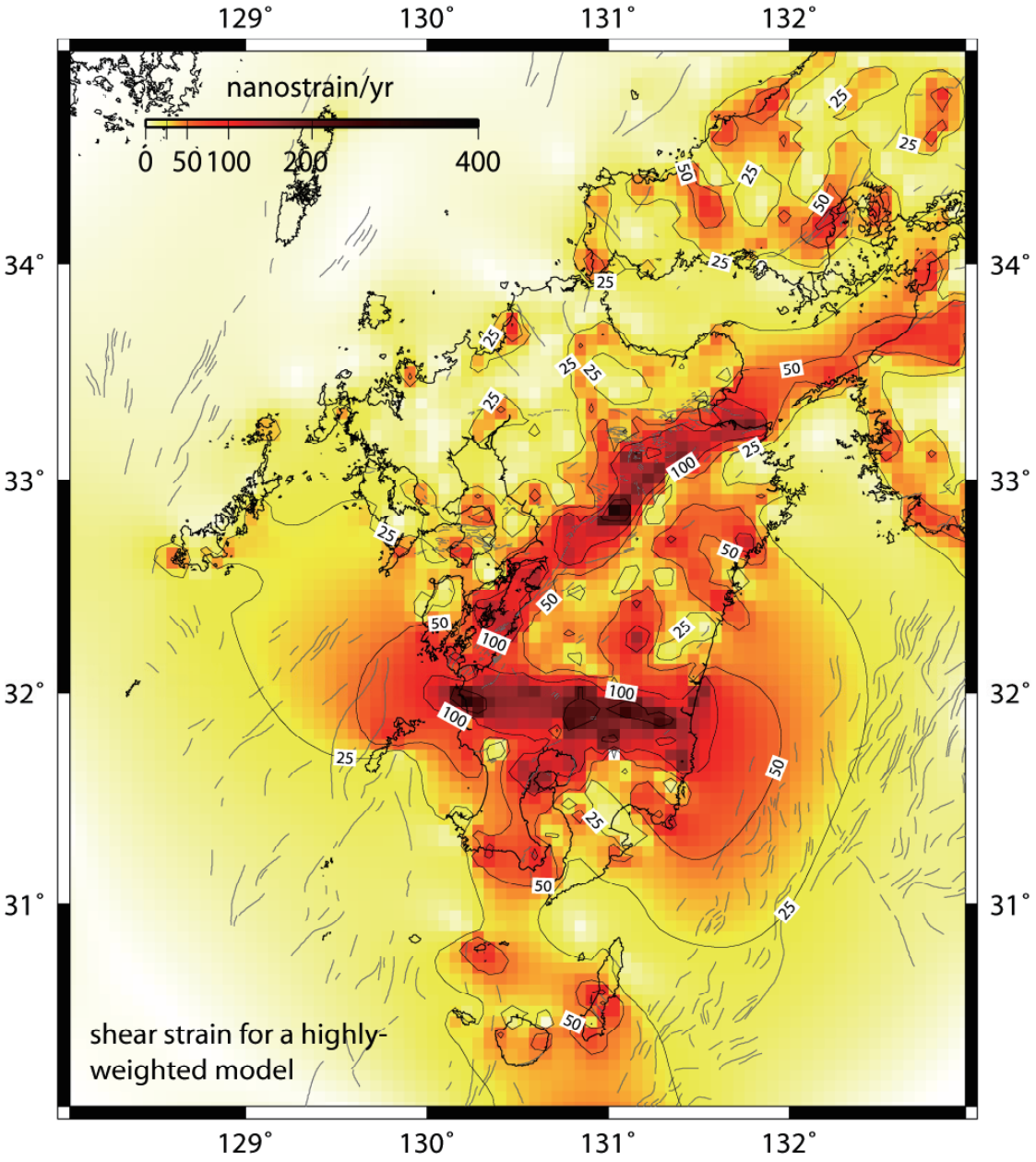

Figure 9.9: Maximum shear strain calculated from the velocity field in Figure 9.7 (with subduction-related elastic strains removed).

The shear strain rate is greatly reduced (Figure 9.9), although the high shear strain zone cutting across southern Kyushu (near the northern boundary of the Ohsumi and Satsuma blocks) is still present, as is a band of elevated shear strain in the region of the MTL and the BSG, consistent with observed strike-slip faulting there. The areal strain maps show high (up to ~50 nanostrains) extensional strain in the Kagoshima Graben region, and a broad zone of residual extensional strain in the western half of the Beppu-Shimabara Graben.

9.6 Tectonic implications

One of the notable results of this study is the discrepancy between the strain rates and fault slip rates estimated from the GPS velocities (Figures 9.5, 9.8 and 9.9) compared with the geological slip rates from the Active Fault Research Centre (AFRC) database (Figure 9.10). Geological studies indicate ~1-3 mm/a of extension and strike-slip in the Beppu-Shimabara Graben region (Figure 9.10), whereas the best-fitting GPS block modelling results indicate up

to 8 mm/a of combined strike-slip and extension (Figure 9.5). Slip rates on normal faults in the Kagoshima Graben are no greater than 1 mm/a in the AFRC database (Figure 9.10), whereas the GPS block modelling results suggests that this graben is the site of up to 7 mm/a of extension (Figure 9.5). Although the zone of large left-lateral shear strain cross-cutting southeast Kyushu is associated with numerous left-lateral strike-slip earthquakes (Figure 9.4), there are no mapped active faults (Figure 9.10) which could be accommodating this strike-slip (~7-14 mm/yr; Figure 9.5). These discrepancies suggest that either there may be some gaps in the geological data (i.e., that some faults accommodating active deformation may be un-discovered or hidden, or that some known faults are not sufficiently characterised), or that extensional strain in the Kagoshima Graben and BSG is partly accommodated by dike intrusion and other volcanic/magmatic processes. In some cases, these discrepancies may also be reconciled by testing alternate block model configurations for interpreting the GPS data (although we suspect this will not be able to reconcile most of the discrepancies we observe).

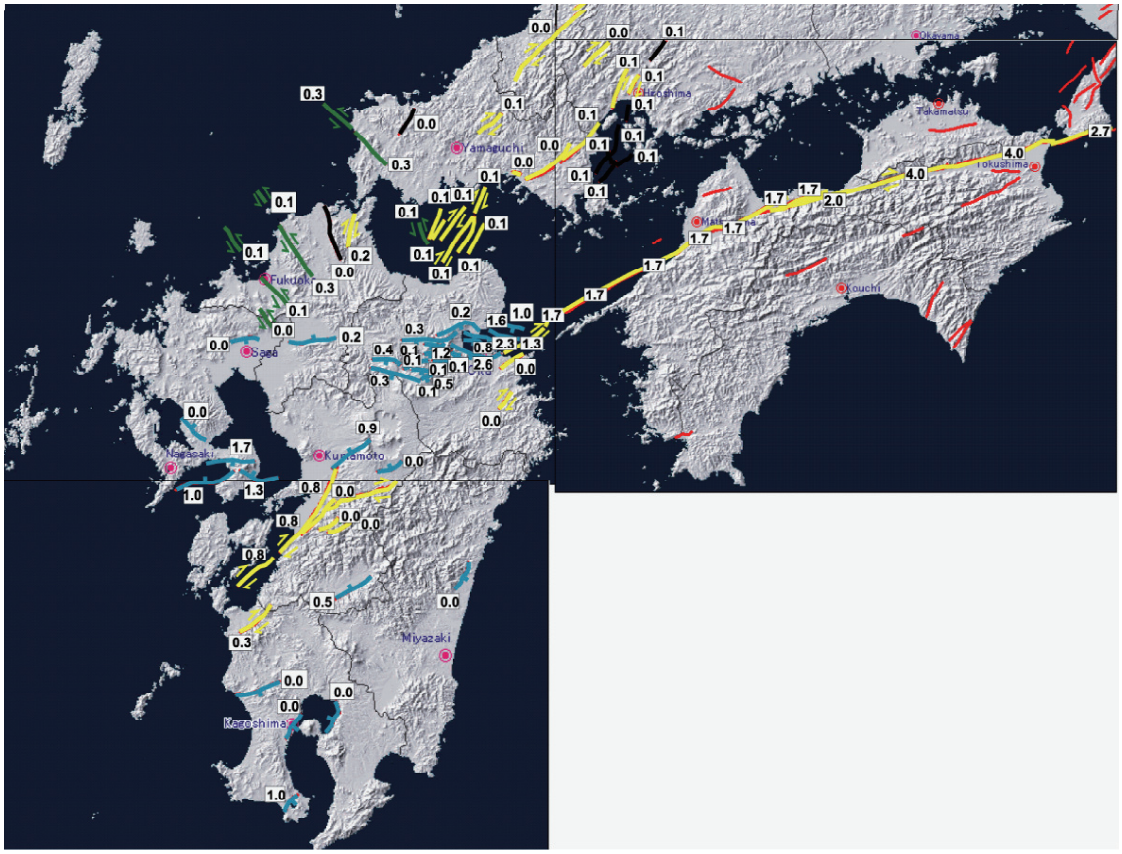

Figure 9.10: Active faults in southwest Japan from the Active Fault Research Centre's active fault database (http://www.aist.go.jp/RIODB/activefault/cgi-bin/index.cgi). The faults are colour-coded by sense of movement (green = dextral, blue = normal, black = reverse, yellow = sinistral. The numbers beside the faults indicate slip rate (mm/a).

9.6.1 Is left-lateral shear in southern Kyushu caused by collision with the Kyushu-Palau Ridge?

Subduction of buoyant features (such as aseismic ridges, oceanic plateaus, and continental fragments) that exist on otherwise normal oceanic plates exert a profound influence on the tectonic and morphological development of subduction margins worldwide (Vogt et al., 1976; McCabe, 1984; Cloos, 1993; Wallace et al., 2005). In some cases, subduction/collision of buoyant features cause curvature (Vogt et al., 1976) and rotation of the subduction margin (McCabe, 1984; Wallace et al., 2005), and deformation of the upper plate (e.g., Marshall et al., 2000; Taylor et al., 1995); in extreme cases, buoyant indentor collision can shut-down subduction, causing it to re-initiate elsewhere (e.g., Cloos, 1993). Margin transverse left-lateral shear in southern Kyushu is localised above the point where there is a change from

subduction of the relatively buoyant Kyushu-Palau Ridge/Shikoku Basin lithosphere (27-15 Ma; Okino et al., 19999) at the Nankai Trough to subduction of more negatively buoyant Cretaceous oceanic lithosphere (Deschamps and Lallemand, 2002) at the Ryukyu Trough (Figure 9.11). We suggest that where buoyant lithosphere is being subducted, the forearc is pushed landward (e.g., northwest) due to the collisional resistance forces transmitted across the plate boundary; conversely, the Cretaceous oceanic slab subducting beneath southwest Kyushu may be rolling back (e.g., Yamaji, 2003), pulling the southern part of the Kyushu forearc seaward relative to the northern half of the forearc. We suggest that these competing effects drive rapid left-lateral shear across southern Kyushu as revealed by GPS and seismicity (Wallace et al., 2009). Similar conceptual models have been proposed to explain deformation of the Costa Rican and New Hebrides forearcs (Marshall et al., 2000; Taylor et al., 1995).

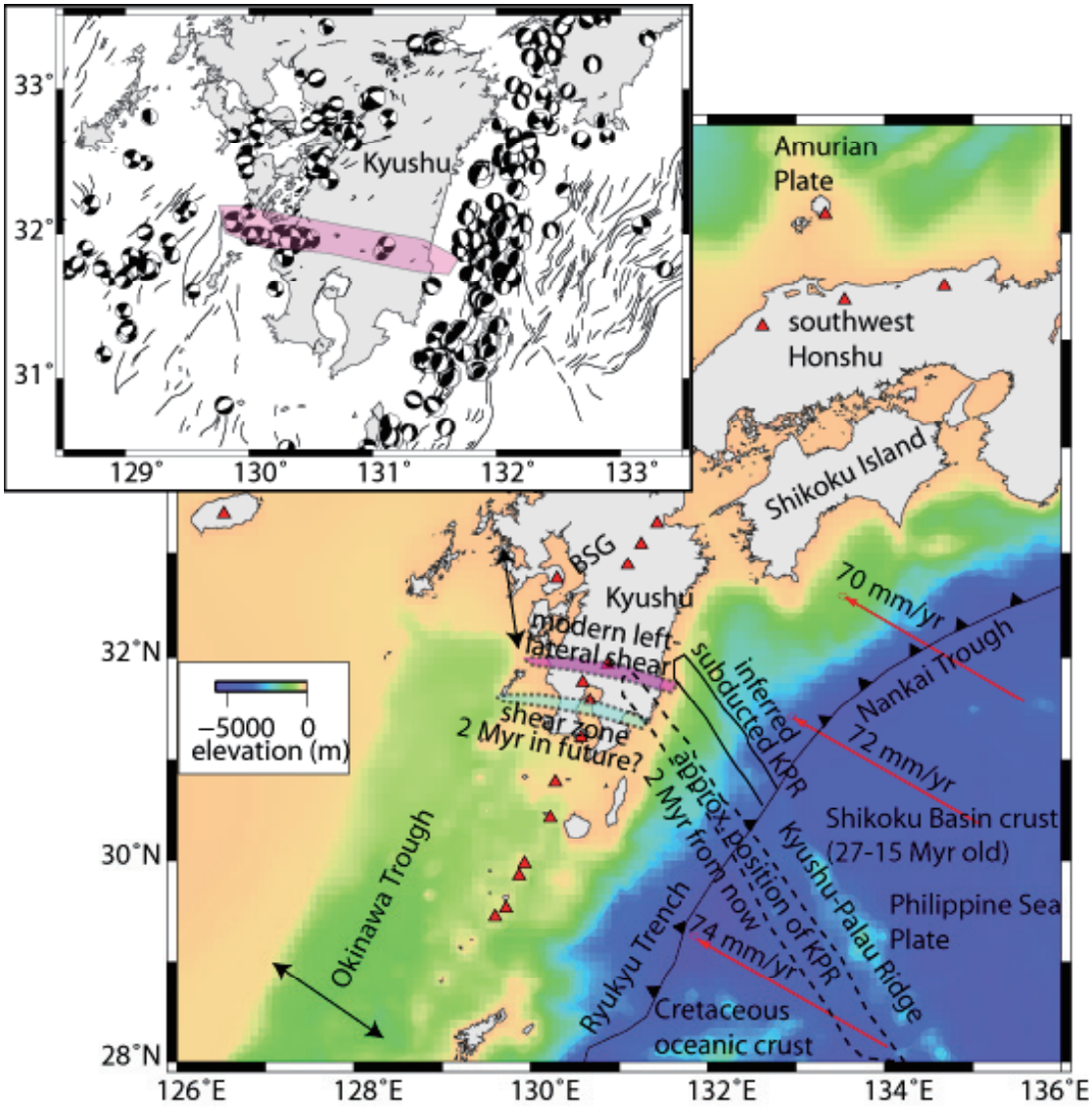

Figure 9.11: Tectonic setting of southwest Japan and schematic illustrating migration of Kyushu/Palau Ridge (KPR) collision point along the Nankai Trough and Ryukyu Trench.

Although GPS and seismological data together argue in favour of active left-lateral strike-slip deformation of southern Kyushu, this interpretation is at odds with the lack of surface faulting evidence for such a shear zone. However, when we consider the Amurian/Philippine Sea Plate relative motion (~70 mm/a pure convergence, with a slight right-lateral sense of ~5 mm/a) and the orientation of the Kyushu-Palau ridge relative to the subduction margin (entering the margin at a 64° angle), we estimate that the Kyushu-Palau ridge subduction

point migrates southwest along the Nankai/Ryukyu trough at ~40 mm/a (or 40 km/Ma) (Figure 9.11). This implies that if the shear zone cross-cutting Kyushu indeed arises from the change in lower plate buoyancy (as we propose here), that the location of this shear zone will follow the Kyushu-Palau ridge subduction point southwest along the margin. Such a continual along-strike migration of the left-lateral shear zone would preclude the accumulation of sufficient surface displacements required to make this a recognizable, through-going fault system at the ground surface.

To test this idea, we have constructed a three-dimensional numerical model of a deforming upper plate (Figure 9.12). The model setup is kept deliberately simple, in order to minimize the number of controlling parameters. Gravity is neglected, the strength of the upper plate is represented by a simple elasto-plastic rheology, and the geometry and strength of a weak visco-elastic region representing the back-arc is imposed (Figure 9.12a).

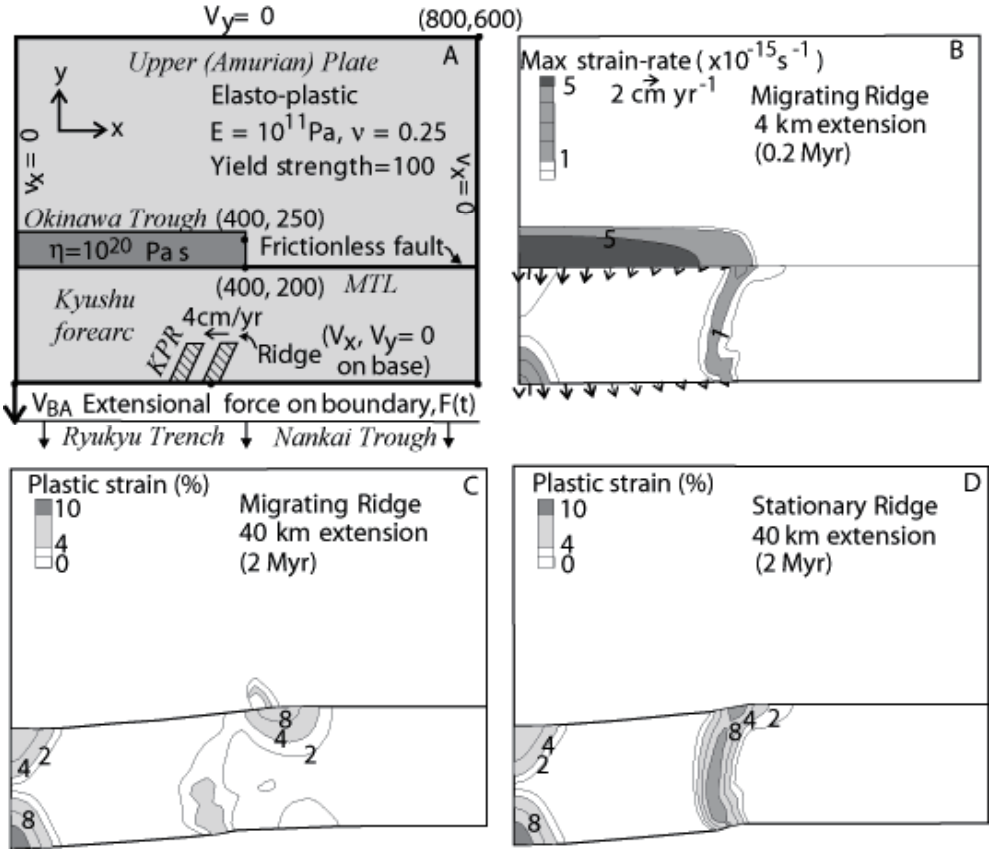

Figure 9.12. (a) Simple three-dimensional model illustrating the effect of a moving ridge on back-arc extension. The model uses the Abaqus/standard finite element code. Model domain is 30 km thick, 800 km long and 600 km wide. The side at y = 0 represents the trench, and an extensional force is applied there with magnitude, *F,* that is adjusted with time to maintain a steady back-arc extension $V_{BA}$of 2 cm/a at the left-hand corner (x = 0, y = 0). The base of the model has zero vertical velocity (out of the page), while horizontal velocity boundary conditions are applied at the other 3 edges of the model as indicated, to prevent material leaving the domain. Rheology is elasto-plastic (light shaded region) and visco-elastic (heavy shaded region, representing a weak back-arc region), where elastic properties of the visco-elastic region are the same as for the rest of the model. A frictionless vertical fault is specified at y = 200 km. Zero horizontal velocities are imposed over a small, basal Section 25 km wide and 60 km long, to simulate the retarding effects of a buoyant ridge on back-arc extension. Tectonic features in southwest Japan corresponding to the numerical model components are labeled in italics. MTL = Median Tectonic Line; KPR = Kyushu-Palau Ridge. (b) Contours of strain rate and velocity vectors early in model evolution (0.2 Ma). Only the left-hand side of the model extends, owing to the presence of a weak viscoelastic region there. (c) Contours of plastic strain after 40 km of extension (2 Ma) for model including ridge migration, illustrating diffuse plastic deformation between the material overlying the ridge, and the corner of the viscoelastic region. (d) Contours of plastic strain after 40 km extension (2 Ma), similar to (c), except that the ridge does not migrate along-strike, producing more focused shear deformation of the forearc.

The subduction interface is simplified to a vertical block boundary at which a spatially uniform extensional force is applied to mimic the effects of rollback, triggering extension in the back-arc region. The magnitude of the force is adjusted automatically during the model run, to reproduce a maximum extensional velocity of 2 cm/a at the left-hand edge, similar to the present rate of extension across the southern back-arc region in Kyushu. The model does not attempt to reproduce compressional effects such as those seen across the Shikoku block in Japan. Model dynamics are therefore simplified and may only be used qualitatively to compare to the tectonics of southwest Japan.

In the model, the effect of a buoyant ridge subduction is simplified to a basal boundary condition, by imposing a region where horizontal velocities are zero (Figure 9.12a). The combined effect of the ridge and the termination along-strike in the visco-elastic region, focus the extensional deformation to the left-hand side, and create a localised, left-lateral shear-zone joining the upper plate immediately above the ridge to the right-hand tip of the visco-elastic back-arc region (Figure 9.12b).

Our ideas regarding the origin of the left-lateral shear zone cutting across southern Kyushu are compatible with results from the simple numerical model, where the ridge is prescribed to move along-strike a rate of 4 cm/a, similar to the along-strike rate of migration of the Kyushu/Palau Ridge. In models where the ridge migrates, plastic strain in the upper plate near to the position of the ridge (Figure 9.12c) remains low and diffuse after 2 Ma of deformation. Conversely, when the ridge is stationary (Figure 9.12d), a zone of localised plastic shear develops above it and cross-cuts the forearc region, with a similar geometry to the contemporary strain-rate pattern (Figure 9.12b). Such a tectonic model will be important to consider in terms of the future rock deformation hazard in Kyushu, because the zone of high shear strain (currently located just north of the Kagoshima Graben) may actually migrate further south (following the Kyushu-Palau Ridge) during the time period of interest.

However, although our explanation of this shear zone as a response to migrating ridge subduction is one viable model for the future tectonic evolution of Kyushu, we must consider other alternative models for the presence of this left-lateral shear zone. For example, it is possible that deformation across this shear zone is currently occurring at a more rapid rate than normal, and that the current rate of strain does not represent the longer-term strain rate across the shear zone. Using the probabilistic methodology we have developed, we can incorporate such alternative models into a tectonic hazard assessment via a logic tree approach. Consultation with Japanese experts on Kyushu tectonics will also facilitate the development of alternate conceptual tectonic models for Kyushu.

9.7 Probabilistic GPS Strain Estimates

9.7.1 Weighted average of GPS strain models from logic tree

To estimate the rock deformation hazard probabilistically using GPS data, we must consider a variety of alternative tectonic models (i.e., using different block and/or fault configurations) to estimate the subduction-related elastic strains, as well as applying a range of smoothing parameters to the strain-rate mapping done with the Haines and Holt method, or use a different strain-rate mapping methodology altogether. An approach that incorporates all viable tectonic models and expert opinions similar to that used in PSHA methodologies is the best way to incorporate all available knowledge about the potential tectonic hazard into a probabilistic rock deformation hazard assessment using GPS. To assess a range of possible strain models from the available GPS data, we construct a logic tree (Figure 9.13) that incorporates the various block model configurations explored in the preceding Sections, as well as implementing different approaches for the strain mapping exercise itself. In terms of the strain mapping approaches, we use the Haines and Holt approach (using a variety of strain variance parameters, see previous discussion), as well as a very simple approach outlined in Miura et al. (2004), where we fit a surface to the GPS velocities, and take spatial derivatives of the surface to estimate strain rates. Our logic tree consists of 120 different branches; we have calculated GPS strain models for each of these branches. We have also weighted each branch of the logic tree (Figure 9.13) based on our own opinion about which models are more or less viable. Ideally, the logic tree would be constructed and weighted via

consultation of an expert panel, similar to what was done for the Tohoku Case Study (Chapman et al., 2009). However, given the limited time frame for the Kyushu Case Study, the expert elicitation exercise was not possible.

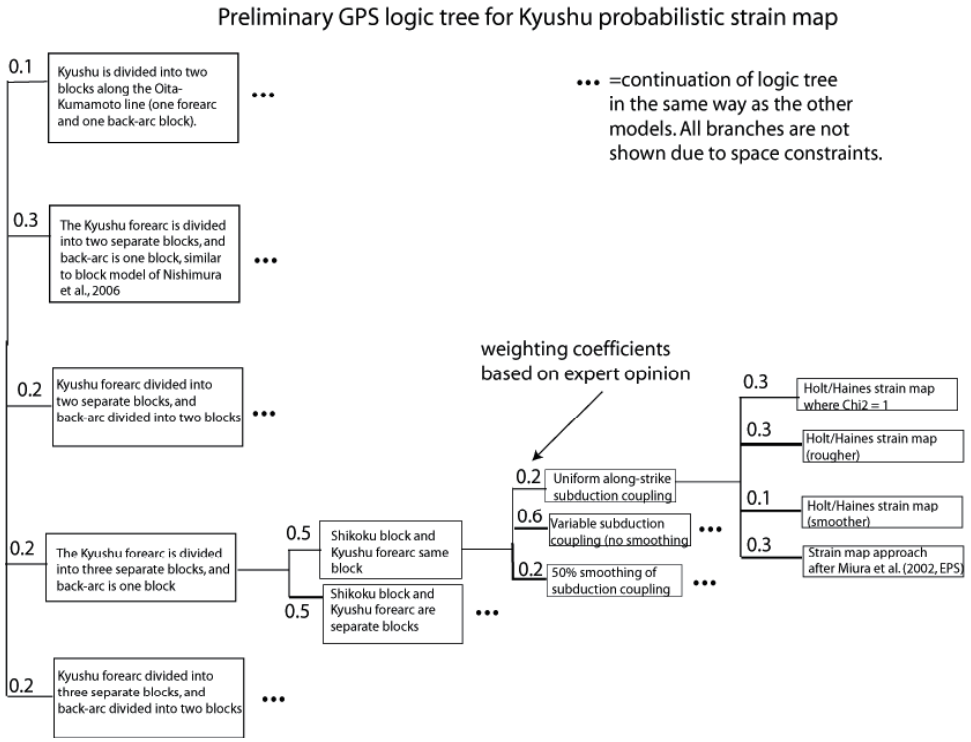

Figure 9.13: Logic tree developed for GPS strain map. Numbers on logic tree branches represent weighting for that logic tree branch.

Figure 9.14 shows a weighted average of all the strain models developed from the logic tree. Given that there is a mix of large shear (Figure 9.14b) and areal strains (Figure 9.14a) within the Kyushu region, we have also chosen to show the strain in terms of the second invariant of the strain tensor (Figure 9.15), which gives us a single measure that incorporates both shear and areal strain. This is largely important to use where we want to use a single strain rate value (rather than both the areal and shear strain values) to determine whether or not there is high or low strain at a given site. The formula for the second invariant of the strain rate tensor (in two dimensions) is: sqrt (Exx^2 + Eyy^2 + 2*Exy^2), where Exx, Eyy, and Exy are the components of the horizontal strain tensor. For reference, the formula for areal strain rate is: Exx +Eyy, and maximum shear strain rate is: sqrt (0.25*(Exx-Eyy)^2 + Exy^2).

Most of the strain patterns obvious in Figures 9.8 and 9.9 are still apparent in the weighted average strain maps (Figure 9.14). For example, the high shear strain cutting across southern Kyushu and along the SE boundary of the Beppu-Shimabara graben are still prominent in the weighted average strain map, suggesting that these features are indeed robust. Similarly high extensional strain persists in the Kagoshima region and southern portion of Kyushu, suggesting that this extensional strain is also real, and not just a model dependent feature.

9.7.2 Histograms of GPS strain values at selected locations in Kyushu

To get an idea of the range of strain rates produced by the different GPS strain models in the logic tree, and to assess the epistemic uncertainties in the GPS strain rate estimates, we can look at histograms (Figure 9.17) of strain rates estimated at several sample locations within Kyushu (Figure 9.16). Similar histograms have also been created for the surface deformation and seismologically-derived strain (see relevant Sections of this report). The strain rates shown are the second invariant of the horizontal strain tensor (to encompass areal and shear strain rates, see discussion in preceding Section).

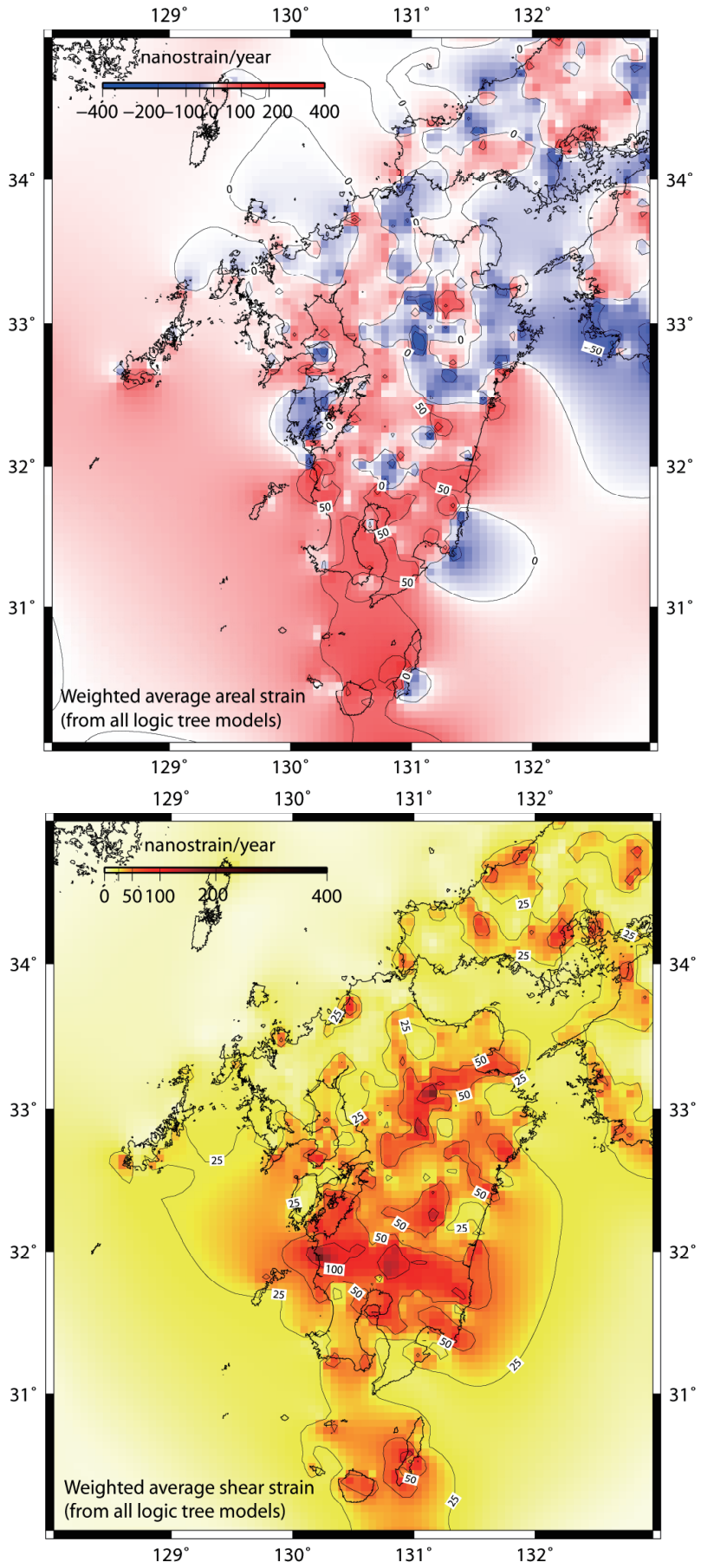

Figure 9.14: Weighted average areal (9.14a) and shear (9.14b) strain (in nanostrains/a) for all 120 strain models from the logic tree (see Figure 9.13).

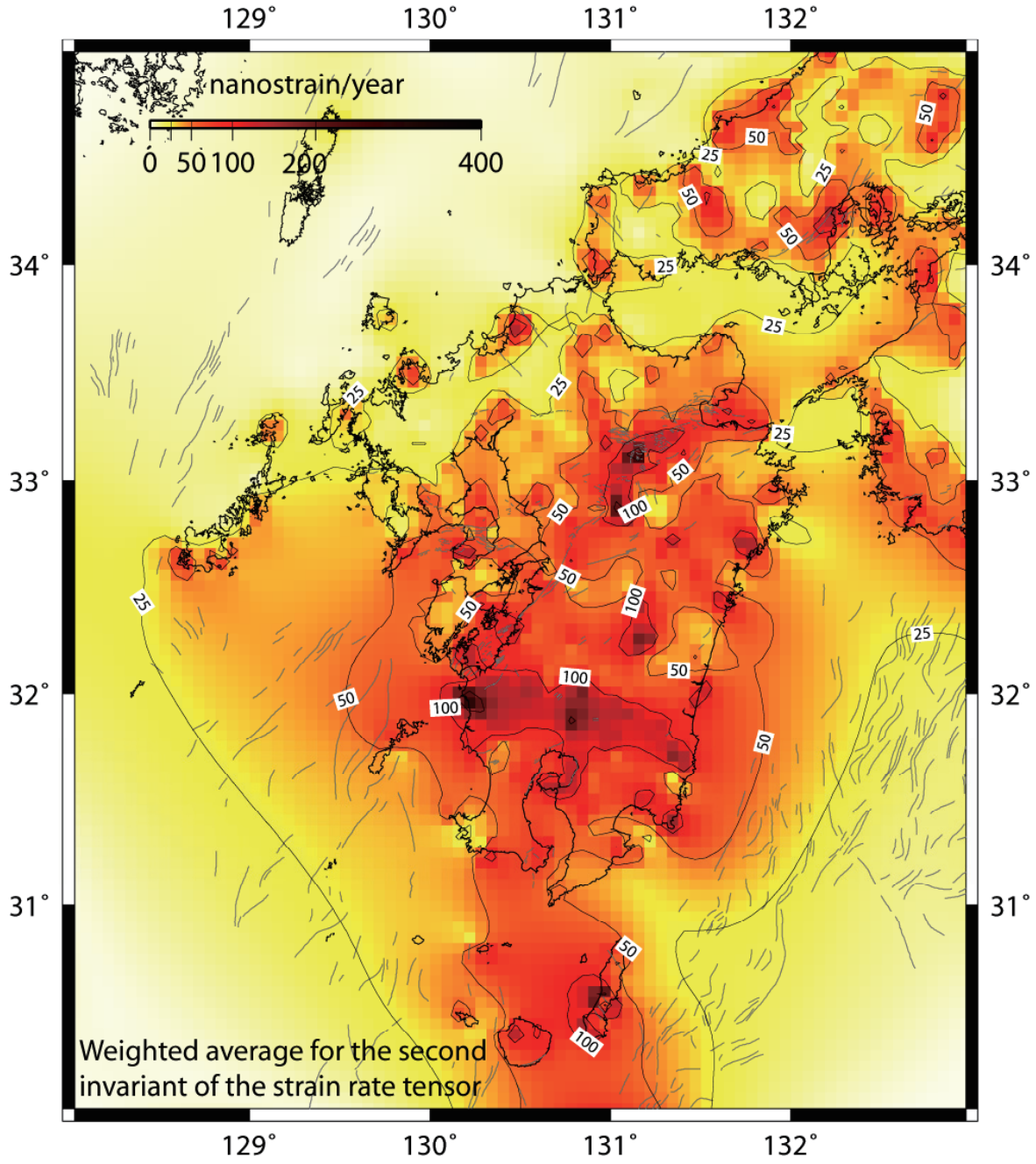

Figure 9.15: Weighted average of the second invariant of the horizontal strain tensor (in nanostrains/a) for all 120 strain models from the logic tree (see Figure 9.13).

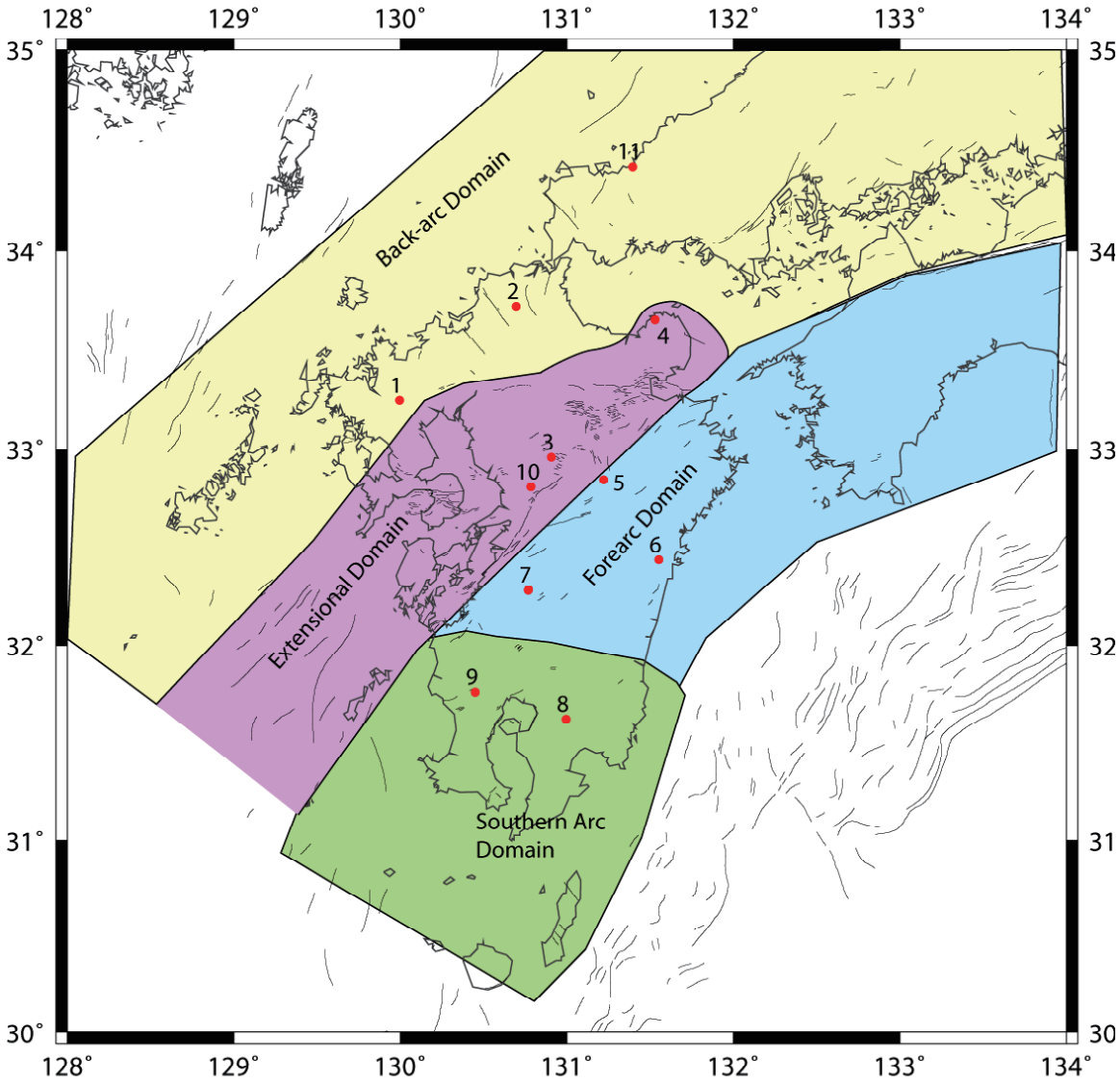

Figure 9.16: Map showing location of sites where we show histograms of GPS-derived strain rates in Figure 9.17. The locations are super-imposed on a map of tectonic domains, discussed in Section 6.

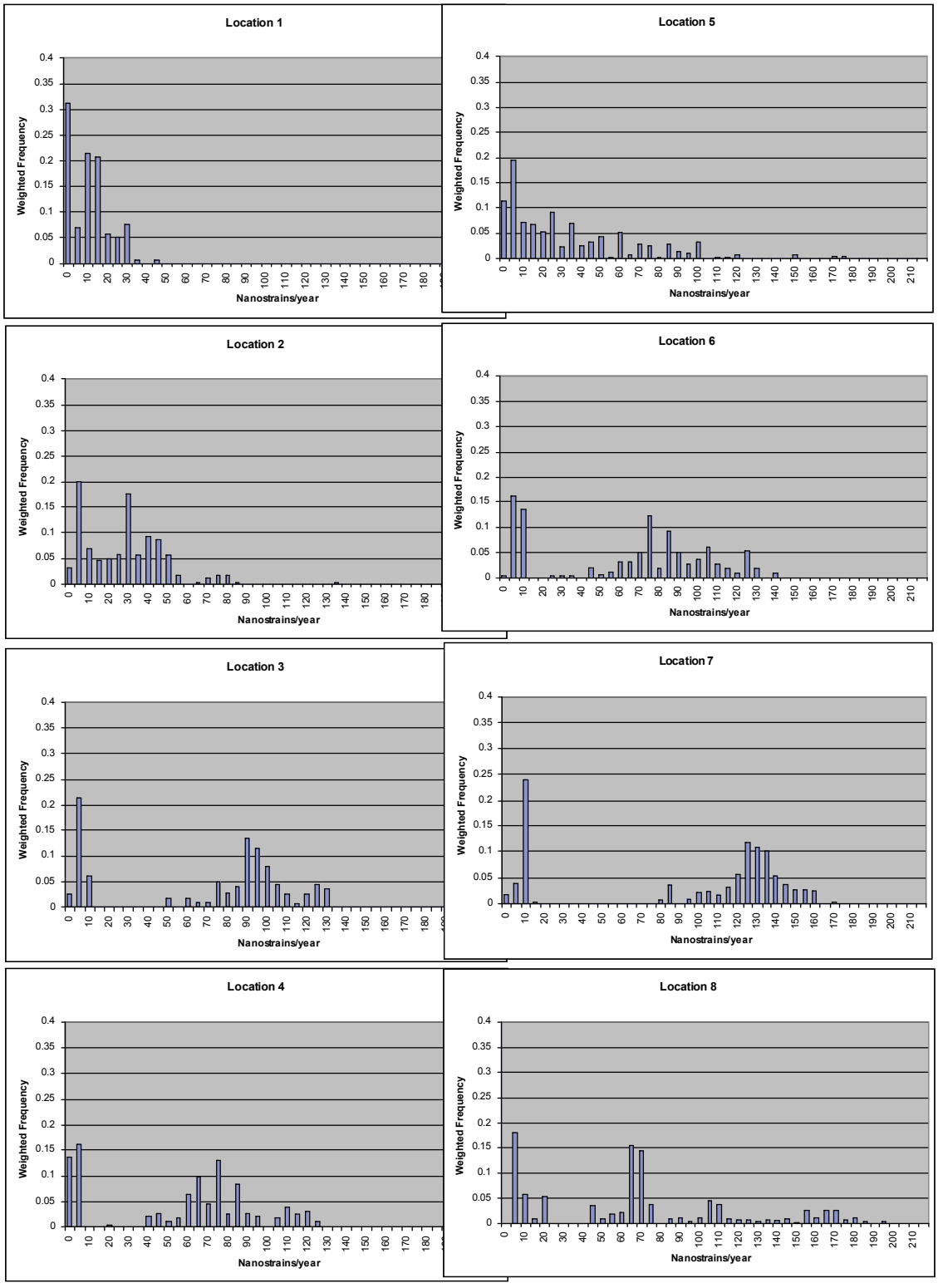

Figure 9.17 (continued on next page): Histogram of GPS strain rates (in terms of weighted frequency) at example locations (see Figure 9.15), after full sampling of the GPS logic tree in Figure 9.13.

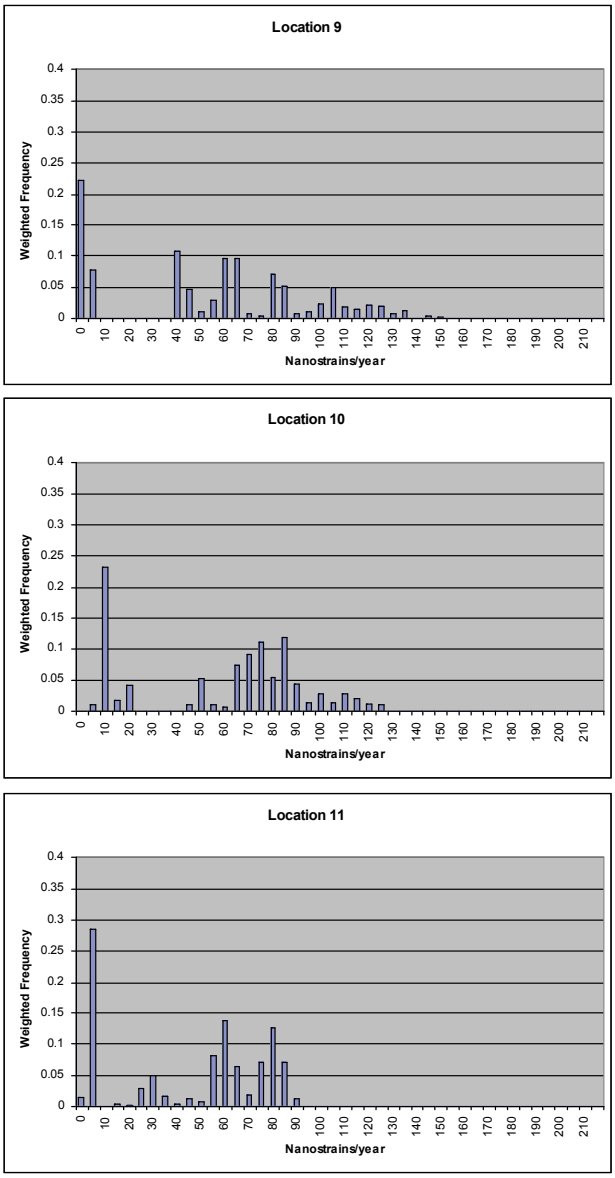

Figure 9.17 (continued from previous page): Histogram of GPS strain rates (in terms of weighted frequency) at example locations (see Figure 9.15), after full sampling of the GPS logic tree in Figure 9.13.

Backarc domain. The histogram for Location 1 shows a relatively narrow distribution of low strain rates from the 120 different strain models, generally less than 20 nanostrains/year. Such low strain rates are consistent with this site being located in the back-arc region, where active fault slip rates are low. Similarly, Location 2 (also in the back-arc region) has strain rates that are generally low (< 40 nanostrains/year), but with a slightly wider distribution of strain rates than Location 1 (indicating slightly higher uncertainties in the strain rates at Location 2 compared to Location 1). Location 11 has higher strain rates than the other back-arc sites, which we think are likely due to effects on the GPS site velocities from the nearby west Tottori earthquake in 2000 (magnitude 7.3), and may not reflect actual background tectonic strain rates.

Extensional Arc domain. Location 3, has a relatively narrow distribution of high strain rates (averaging ~100 nanostrains/year), consistent with its position within a zone of active tectonic extension. The lowest strain rate values in this histogram come from the strain estimates

using the Miura et al. (2004) approach to calculating strain. We suspect that this approach excessively smooths the strain values, hence the very low strain rates we obtain here. In the future, we would recommend strongly down-weighting the strain results using this approach, as these results are probably overly smoothed. The lowest strain rates in the other histograms shown here also contain this problem. Although Location 4 is also in the Extensional Arc domain, and also has reasonably high strain rates, probably due to the close proximity to active faults of the BSG. Location 10 is also within the BSG, and as expected shows a concentration of high strain rates from the GPS strain models, generally around 70-90 nanostrains/year.

Forearc domain. Example locations in this domain exhibit a broad range of strain rates. Location 5, which is close to the southern edge of the BSG shows a broad range of strain rates, but most of them are quite low, < 40 nanostrains/year. These low strain estimates are somewhat surprising given the close proximity of this site to active faulting in the BSG. Location 6 has a surprisingly high strain rate for the forearc domain, ~70-110 nanostrains/year, although it is located close to the continuation of an active fault trend (see Section discussing discrimination of tectonic domains and selection of example locations) and on the edge of an area of moderately high uplift rate (see the strain rates from surface deformation Section). The high strain rates at Location 6 may also be related to imperfect subduction coupling models; perhaps we have not completely removed the elastic strain effect related to interseismic subduction interface coupling, and that has influenced the strain rates there. Location 7 has some of the highest strain rates of any of the locations, generally 120-140 nanostrains/year. This is surprising, given the long distance of this example location from the known, active faults. However, this location is probably also in a region of high shear strain related to the left-lateral shear zone that we have identified cutting across southern Kyushu, as well as any extension along the southeastern margin of the BSG.

Southern Arc domain. Locations 8 and 9 show a large spread of strain rate estimates, indicating a higher uncertainty in the strain rates in those locations. However, most of the strain rates are >50 nanostrains/year, and are up to 140-180 nanostrains/year, so this region does appear to be a generally high strain area. Location number 8 is located on a low slip rate active fault (see Section 8). Strain at both of these example locations is probably influenced by extension in the Kagoshima Graben region, as well as the strong left-lateral shear strain zone cutting across southern Kyushu.

9.8 Notes and Caveats

One of the advantages of the probabilistic approach is that it allows us to assess some of the uncertainties inherent in the strain rate estimates (e.g., epistemic uncertainties due to choice of tectonic models and/or modelling techniques). However, we must also ensure that we have accurately estimated the uncertainties in the GPS velocity data. The large sample interval (3 months) of the GPS timeseries data available to us for this study means that reliable noise models for the GPS data could not be developed. This affects the estimation of uncertainty in the point GPS velocities, which translates into additional uncertainty in the strain-rate estimates. A more complete temporal sampling of the CGPS dataset, and rigorous estimation of changes in CGPS site position due to earthquakes, equipment changes, etc. would improve the velocity estimates substantially, and lower the resulting uncertainties. Additionally, the GPS station spacing is still quite large compared to the 5-km grid over which strain rates are required. In some parts of Japan there are more GPS stations (campaign and continuous, operated by various Japanese universities and other organisations) in addition to the GSI-run Geonet network, and data from these could contribute greatly to an improved strain-rate estimation. Moreover, as longer GPS datasets are collected, the GPS velocity uncertainties will slowly decrease. Also, the velocity uncertainties will become more reliable when proper noise models are adopted. Both these improvements (as well as GPS velocity data from additional sites) would allow us to refine the results of the GPS strain-rate study described here.

9.9 References for Section 9

Altamimi, Z., P. Sillard, and C. Boucher (2002), ITRF2000: A new release of the International Terrestrial Reference Frame for earth science applications, J. Geophys. Res., 107(B10), 2214, doi:10.1029/2001JB000561.

Aramaki, S., 1984, Formation of the Aira Caldera, southern Kyushu, 22,000 years ago, J. Geophys. Res., 89(B10), 8485-8501.

Beavan, J., and, J. Haines (2001), Contemporary horizontal velocity and strain-rate fields of the Pacific-Australian plate boundary zone through New Zealand, *J. Geophys. Res. 106*, 741-770.

Beavan, J., P. Tregoning, M. Bevis, T. Kato, and C. Meertens (2002), The motion and rigidity of the Pacific Plate and implications for plate boundary deformation, *J. Geophys. Res.*, *107,* 2261, doi:10.1029/2001JB000282.

Beutler, G., H. Bock, E. Brockmann, R. Dach, P. Fridez, W. Gurtner, U. Hugentobler, D. Ineichen, J. Johnson, M. Meindl, L. Mervart, M. Rothacher, S. Schaer, T. Springer, R. Weber (2001), Bernese GPS Software Version 4.2, Ed. by U. Hugentobler, S. Schaer, P. Fridez, *Astronomical Institute, University of Berne.*

Bird, P., 2003, An updated digital model of plate boundaries, Geochem. Geophys. Geosyst., 4(3), 1027, doi:10.1029/2001GC000252.

Calais E., M. Vergnolle, V. San'kov, A. Lukhnev, A. Miroshnitchenko, S. Amarjargal, J. Déverchère, 2003, GPS measurements of crustal deformation in the Baikal-Mongolia area (1994–2002): Implications for current kinematics of Asia, *J. Geophys. Res., 108 (B10)*, 2501, doi:10.1029/2002JB002373.

Chapman, N., M. Apted, J. Beavan, K. Berryman, M. Cloos, C. Connor, L. Connor, O. Jaquet, N. Litchfield, S. Mahony, W. Smith, S. Sparks, M. Stirling, P. Villamor and L. Wallace (2009). Development of Methodologies for the Identification of Volcanic and Tectonic Hazards to Potential HLW Repository Sites in Japan: The Tohoku Case Study. Nuclear Waste Management Organisation of Japan, Tokyo. Technical Report: NUMO-TR-08-03. 135 pps.

Cloos, M., 1993, Lithospheric buoyancy and collisional orogenesis; subduction of oceanic plateaus, continental margins, island arcs, spreading ridges, and seamounts, GSA Bulletin, 105: 715-737.

Deschamps, A., and S. Lallemand, The West Philippine Basin: An Eocene to early Oligocene back arc basin opened between two opposed subduction zones, *J. Geophys. Res.*, *107*(B12), 2322, doi:10.1029/2001JB001706, 2002.

Fujiwara, S., H. Yarai, S. Ozawa, M. Tobita, M. Murakami, H. Nakagawa, and K. Nitta, 1998, Surface displacement of the March 26, 1997, Kagoshima-ken-hokuseibu earthquake in Japan from synthetic aperture radar interferometry, *Geophys. Res. Lett., 25(24)*, 4541-4544.

Gutscher, M.-A., and S. Lallemand, 1999, Birth of a major strike-slip fault in SW Japan, Terra Nova, 11(5), 203-209.

Haines, A. J., W. E. Holt, A procedure for obtaining the complete horizontal motions within zone of distributed deformation from the inversion of strain rate data, J. Geophys. Res., 98(B7), 12057-12082, 10.1029/93JB00892, 1993.

Heki, K., S. Miyazaki, H. Takahashi, M. Kasahara, F. Kimata, S. Miura, N. Vasilenco, A. Ivashchenco and K. An, The Amurian plate motion and current plate kinematics in Eastern Asia, J. Geophys. Res., 104, 29147-29155, 1999.

Herring, T. A., 2001, GLOBK global Kalman filter VLBI and GPSanalysis program, version 5.03, Mass. Inst. of Technol., Cambridge.

Hirose, H., K. Hirahara, F. Kimata, N. Fujii, and S. Miyazaki, 1999, A slow thrust slip event following the two 1996 Hyuganada earthquakes beneath the Bungo Channel, southwest Japan, *Geophys. Res. Lett., 26(21)*, 3237-3240.

Ito, T., T. Ikawa, S. Yamakita, and T. Maeda, Gently north-dipping Median Tectonic Line (MTL) revealed by recent seismic reflection studies, southwest Japan, *Tectonophys.*, 264, 51–63, 1996

Kodama, K., H. Tashiro, and T. Takeuchi (1995), Quaternary counterclockwise rotation of south Kyushu, southwest Japan, *Geology, 23,* 823-826, 1995.

Kriswati, E. and Iguchi, M., 2003, Inflation of the Aira Caldera prior to the 1999 eruptive activity at Sakurajima Volcano detected by GPS network in south Kyushu, Disaster Prevention Research Institute Report, 46, 817-825.

Langbein J. (2004), Noise in two-color electronic distance meter measurements revisited, *J. Geophys. Res., 109*, B04406, doi:10.1029/2003JB002819.

Marshall, J. S., D. M. Fisher, T. W. Gardner, Central Costa Rica deformed belt: Kinematics of diffuse faulting across the western Panama block, Tectonics, 19(3), 468-492, 10.1029/1999TC001136, 2000.

McCabe, R., 1984, Implications of palemagnetic data on the collision-related bending of island arcs: Tectonics, 4, 409-428.

McCaffrey, R. (1995), DEF-NODE users guide, Rensselaer Polytechnic Inst., Troy, N.Y.

McCaffrey, R., M.D. Long, C. Goldfinger, P.C. Zwick, J.L. Nabelek, C.K. Johnson, and C. Smith (2000), Rotation and plate locking at the southern Cascadia subduction zone, *Geophysical Research Letters, 27*, 3117-3120.

McCaffrey, R. (2002), Crustal block rotations and plate coupling: *in* Stein, S., and Freymueller, J., eds., Plate Boundary Zones, AGU Geodynamics Series v. 30, p. 100-122.

McCaffrey, R., 2005. Block kinematics of the Pacific-North America plate boundary in the southwestern United States from inversion of GPS, seismological and geologic data, *J. geophys. Res.,* **110**, doi:10.1029/2004JB003307.

McClusky, S. et al., 2001. Present day kinematics of the eastern California Shear zone from a geodetically constrained block model, *Geophys. Res. Lett.,* **28**, 3369-3372.

Meade, B.J., and Hager, B.H., 2005. Block models of crustal motion in southern California constrained by GPS measurements, *J. geophys. Res.,* **110**, B03403, doi:10.1029/2004JB003209.

Miura, S., T. Sato, A. Hasegawa, Y. Suwa, K. Tachibana and S. Yui, 2004, Strain concentration zone along the volcanic front derived by GPS observations in the NE Japan arc, *Earth Planets Space, 56*, 1347-1355.

Nishimura, S. Hashimoto, M., and Ando, M., 2004, A rigid block rotation model for the GPS derived velocity field along the Ryukyu arc, Phys. Earth Planet. Inter. 142, 185-203.

Nishimura, S. and M. Hashimoto, 2006, A model with rigid rotations and slip deficits for the GPS-derived velocity field in Southwest Japan, *Tectonophysics, 421*, 187-207.

Okada, A., 1970, Fault topography and rate of faulting along the Median Tectonic Line in the drainage basin of the River Yoshino, northeastern Shikoku, Japan (in Japanese with English abstract), Geogr. Rev. Jpn., 43, 1-21.

Okada, A., 1973, Quaternary faulting along the Median Tectonic Line in the central part of Shikoku (in Japanese with English abstract), Geogr. Rev. Jpn., 46, 295-322.

Okino, K., Y. Ohara, S. Kasuga, and Y. Kato (1999), The Philippine Sea: New survey results reveal the structure and the history of the marginal basins, *Geophys. Res. Lett.*, *26*, 2287–2290

Onishi, M., T. Ikawa, T. Matsuoka, T. Kawamura, T. Echigo, M. Orito, T. Ito, N. Hirata, T. Iwasaki, E. Kurashimo, and H. Sato, Deep seismic reflection experiment with a highly

dense array of seismograms near the Median Tectonic Line, Shikoku, Japan, *Abstr. 1999 Fall Meeting of the Seismological Society of Japan*, P107, 1999.

Prawirodirdjo, L. and Y. Bock (2004): Instantaneous global plate motion model from 12 years of continuous GPS observations, J. Geophys. Res., 109, B08405, doi:10.1029/2003JB002944.

Rothacher, M., and L. Mervart (eds.), Documentation of the Bernese GPS Software Version 4.0, 418 pp, Astron. Inst., Univ. of Bern, Bern, Switzerland, 1996.

Sagiya, T. and W. Thatcher (1999), Coseismic slip resolution along a plate boundary megathrust: The Nankai Trough, southwest Japan, J. Geophys. Res., 104(B1), 1111-1129.

Sagiya, T., S. Miyazaki, and T. Tada (2000), Continuous GPS array and present-day crustal deformation of Japan, *Pure and Applied Geophysics,* 2303-2322.

Sella, G.F., T.H. Dixon, and A.L. Mao, 2002, REVEL: A model for recent plate velocities from space geodesy: *J. of Geophys. Res., v. 107(B4),* doi:10.1029/2000JB000033.

Shiomi, K., H. Sato, K. Obara, and M. Ohtake, 2004, Configuration of the subducting Philippine Sea plate beneath southwest Japan revealed from receiver function analysis based on multivariate autoregressive model, *J. Geophys. Res., 109(B040308)*, doi:10.1029/2003JB002774.

Tabei, T., and eleven co-authors, 2002, Subsurface structure and faulting of the Median Tectonic Line, southwest Japan inferred from GPS velocity field, *Earth Planets Space, 54*, 1065-1070.

Taylor, F.W., and ten co-authors, 1995, Geodetic measurements of convergence at the New Hebrides island arc indicate arc fragmentation caused by an impinging aseismic ridge, *Geology*, 23(11), 1011-1014.

Vogt, P.R., Lowrie, A., Bracey, D.R., and Hey, R.N., 1976, Subduction of aseismic oceanic ridges: Effects on shape, seismicity, and other characteristics of consuming plate boundaries: Geological Society of America Special Paper 172, 59 p.

Wallace, L.M., J. Beavan, R. McCaffrey and D. Darby, 2004, Subduction zone coupling and tectonic block rotations in the North Island, New Zealand, *J. Geophys. Res.*, 109(B12), doi: 10.1029/2004JB003241.

Wallace, L.M., McCaffrey, R., Beavan, J., and Ellis, S., 2005, Rapid microplate rotations and backarc rifting at the transition between collision and subduction, *Geology, 33***:** 857-860.

Wallace, L.M., J. Beavan, R. McCaffrey, K. Berryman, and P. Denys, 2007, Balancing the plate motion budget in the South Island, New Zealand using GPS, geological and seismological data, *Geophys. J. Int.,* doi: 10.1111/j.1365-246X.2006.03183.x

Wallace, L.M., S. Ellis, K. Miyao, S. Miura, J. Beavan, and J. Goto, 2009, Enigmatic, highly active left-lateral shear zone in southwest Japan explained by aseismic ridge collision, *Geology, 37(2)*, 143-146.

Williams S. D. P., Y. Bock, P. Fang, P. Jamason, R. M. Nikolaidis, L. Prawirodirdjo, M. Miller, D. J. Johnson (2004), Error analysis of continuous GPS position time series, *J. Geophys. Res., 109,* B03412, doi:10.1029/2003JB002741.

Yagi, Y., M. Kikuchi, and T. Sagiya, 2001, co-seismic slip, post-seismic slip, and aftershocks associated with two large earthquakes in 1996 in Hyuga-nada, Japan, *Earth Planets Space, 53,* 793-803.

Zhang, J., Y. Bock, H. Johnson, P. Fang, S. Williams, J. Genrich, S. Wdowinski, and J. Behr (1997), Southern California Permanent GPS Geodetic Array: Error analysis of daily position estimates and site velocities, *J. Geophys. Res.*, *102*(B8), 18,035–18,056.

10 Strain Rates from Seismicity

In this Section we describe the historical seismicity of Kyushu, document the methods used to calculate seismic strain rates for the region, and display and describe the results of the analysis. We also discuss these results in the context of the overall Kyushu Case study.

10.1 Seismicity of Kyushu

The Kyushu region is characterised by generally high rates of crustal seismicity, notably in the form of a southwest trending band roughly bisecting the island (Figures 6.3 and 10.1). The depth to crustal seismicity is around 20 km, the typical depth to the base of crustal seismicity for Japan in general, and there is considerable spatial variability across the island (Figure 6.4). Four seismotectonic zones are defined for Kyushu, and these are shown in Figure 10.1. Zone 1 encompasses the back-arc region of Kyushu, in which sinistral focal mechanisms striking transverse to the coastline are commonly observed in northwestern Kyushu (Figures 4.9 and 6.2). Zone 2 is defined to encompass the Beppu-Shimabara Graben region (generally coincident with the Extensional Arc domain) with associated high rates of seismicity (the southwest trending band of seismicity in the Kyushu region; Figure 10.1), and is bounded to the southeast by the Oita-Kumamoto Tectonic Line (the southwest continuation of the Median Tectonic Line). Zone 3 roughly defines the forearc region, and Zone 4 defines the Kagoshima Graben, which also overlaps with the Southern Arc domain. The north end of Zone 4 is defined by a prominent east-west trending belt of seismicity, which also coincides with a zone of high left-lateral shear strain in the GPS dataset (see Section 9). These zones differ somewhat from the tectonic domains shown the other Sections of the report. This is due to the seismotectonic zones being defined largely on the basis of seismicity at the early stages of the Kyushu Case Study, well before the domains in Section 6 were defined.

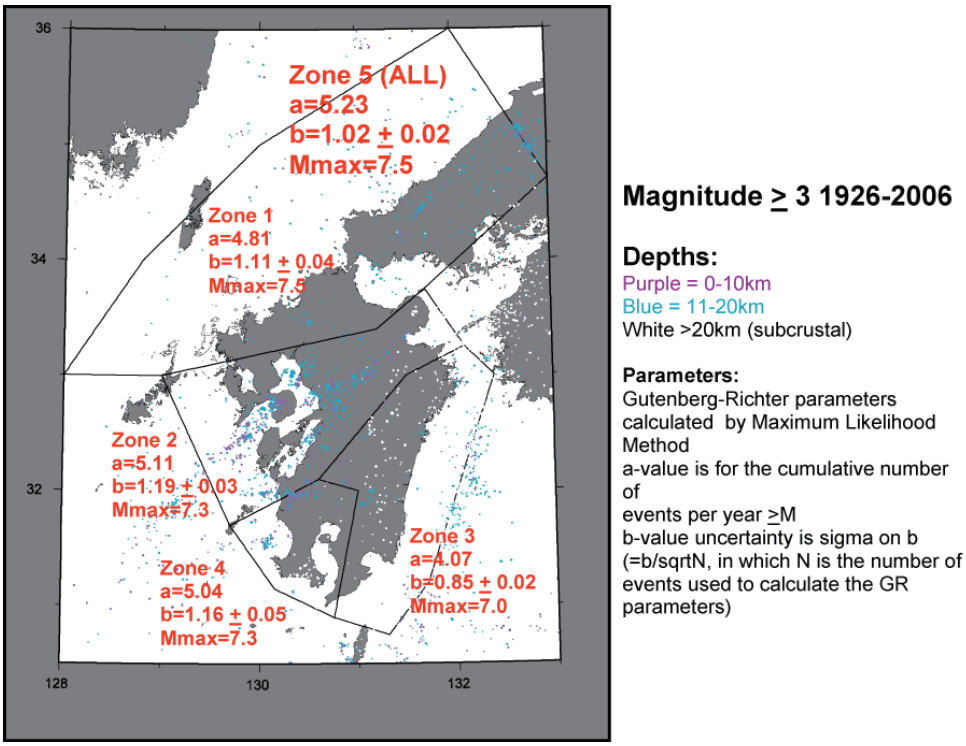

Figure 10.1: Crustal seismicity of the Kyushu region, All earthquakes M≥4 for the period 1926-2006 and down to 20 km depth are shown. The crustal seismicity zones are shown, as well as the seismicity parameters and maximum magnitudes for the Gutenberg-Richter relationship a-value, b-value and Mmax). The a and b-values are calculated from the seismicity catalogue, while the Mmax is based on geologically-derived values from The Research Group for Active Faults of Japan (1992).

Despite the high rates of seismicity in Figure 10.1, there have been relatively few large historical earthquakes in the c. 430 year period of historical records. Only two earthquakes of about magnitude (M) 7 have been recorded in that time, one in the Kagoshima Graben (Zone 4) and the other in Zone 2.

10.2 Methodology

Strain rates are estimated from the spatial and temporal distribution of the c. 430 year record of historical seismicity for the region, using the same methodology as for the Tohoku Case Study (Chapman et al., 2009). The Japanese Meteorological Agency (JMA) seismicity catalogue of M≥4 earthquakes for the period 1926-2006 is combined with the historical catalogue of M≥7 earthquakes for the period 1580-1925 (Wesnousky et al., 1984) to give the c. 430 year record. These earthquakes are then used to define a spatial distribution of Gutenberg-Richter rate parameters (Gutenberg and Richter, 1944), utilising the maximum-likelihood method of Weichert (1980) to derive the rate parameters (a- and b-values) of the Gutenberg-Richter relationship:

$$\log N/yr = a - bM,$$

in which N/yr is the cumulative number of events greater than or equal to magnitude M, and a and b are empirical parameters. Seismicity parameters are shown for each zone in Figure 10.1, along with the parameters for all zones combined. The seismicity parameters are then used to define seismic strain rates via the well-established method of Kostrov (1972).

We calculate the seismic strain rates according to a logic tree developed to quantify the epistemic uncertainty in seismicity parameters (Figure 10.2).

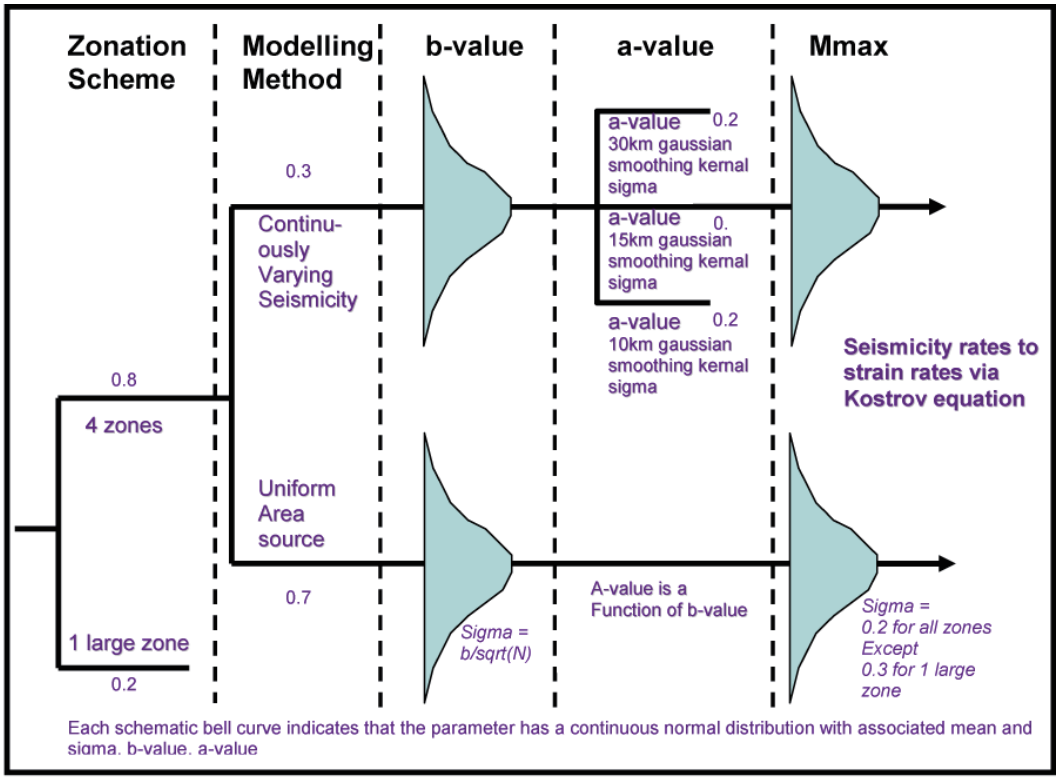

Figure 10.2: Logic tree for the Kyushu seismic strain rate model. Weights for each of the logic tree options are shown as numbers beneath each limb.

The logic tree is similar to the tree established for the Tohoku Case Study, except for the fact that we only use a raw seismicity catalogue as input. Here we found that the available declustering (removal of aftershocks) programmes to be unsuitable for Japan in the Tohoku Case Study (i.e. more than just aftershocks were removed), and now maintain the opinion that aftershocks also contribute to seismic strain rates, we do not include a declustered catalogue as an option in the Kyushu logic tree. As with the Tohoku Case Study, we take account of epistemic uncertainty in: (1) the seismicity modelling method (uniformly distributed seismicity modelling within an area source versus continuously-varying seismicity modelling (e.g. Frankel, 1995); (2) parameters of the Gutenberg-Richter relationship, and; (3) the maximum magnitude cutoff for the various zones. As with the Tohoku Case Study, the continuously-varying seismicity model is a lesser-weighted option than that of using uniformly-distributed parameters for each zone, due to lack of confidence in the c. 430 year record of seismicity being representative of longer time periods. This was an opinion given by the expert elicitation panel of Japanese seismologists at the time of the Tohoku Case Study, and we apply the same opinion to the Kyushu Case Study.

10.3 Results

Seismicity parameters derived for Kyushu are in the realm of parameters expected for areas characterised by extensional tectonic and volcanic processes. B-values of around -0.9 to -1.1 are observed in the various zones, with a b-value of -1 calculated for the entire region. These b-values are generally lower ("steeper") than the b-values obtained for Tohoku (all less than -1), which indicates a higher ratio of smaller to larger earthquakes for Kyushu. Kyushu b-values are also consistent with the global average of -1. The only b-value greater than -1 is calculated for Zone 3, that is, the zone that roughly coincides with the Forearc Domain (about -0.9).

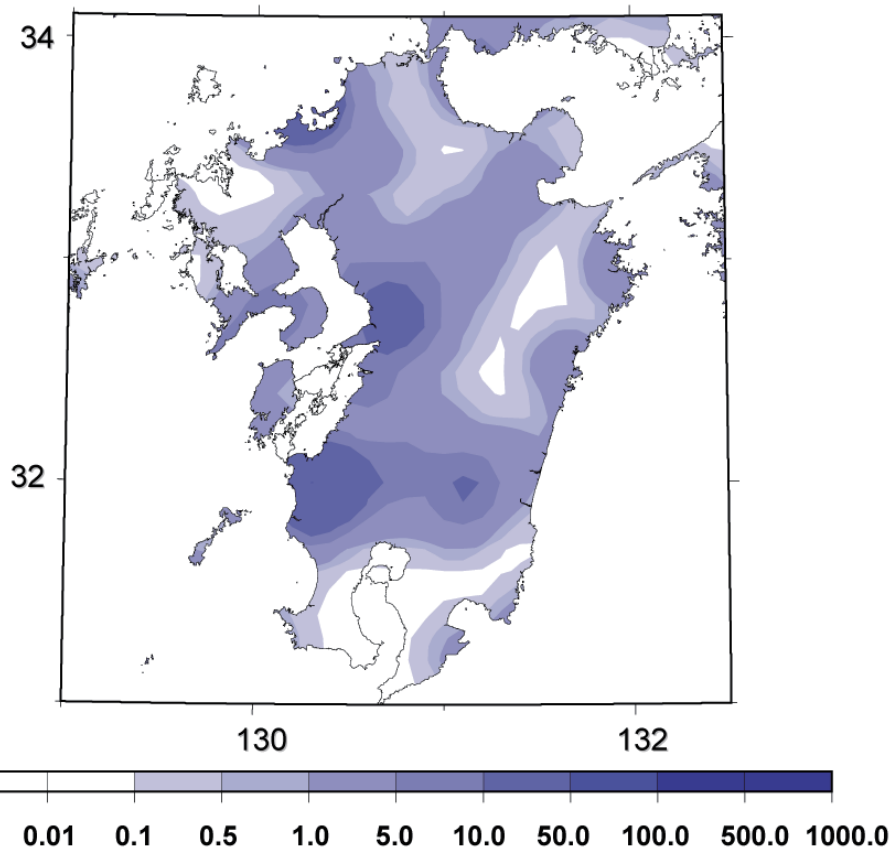

Figure 10.3: Seismic strain rates (nanostrains/a) developed using a smoothing kernel bandwidth of 15 km.

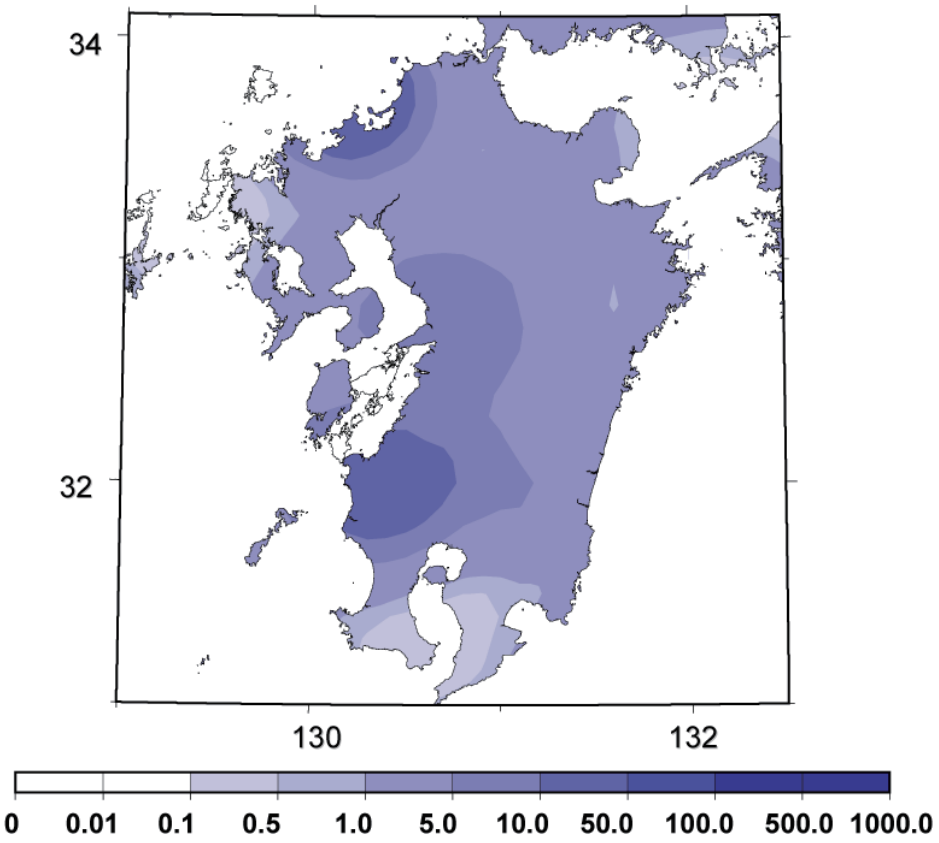

Figure 10.4: Seismic strain rates (nanostrains/a) developed using a smoothing kernel bandwidth of 30 km.

We show some examples of output from our logic tree in map form in Figures 10.3 and 10.4. The two strain rate maps are derived from the continuously varying seismicity parameters (see above) in Figures 10.3 and 10.4. The maps differ in the width of the Gaussian smoothing kernel used to develop the smoothed seismicity rates. The 15 km correlation distance or kernel bandwidth logically gives a much finer spatial distribution of seismicity rates than the 30 km bandwidth, and shows the highest strain rates in areas of highest seismicity (compare Figures 10.1, 10.3 and 10.4). These are primarily within the Beppu-Shimabara Graben (Zone 2 in Figure 10.1), and the east-west-trending zone of seismicity at the northern end of the Kagoshima Graben (north end of Zone 4 in Figure 10.1). Localised strain rates of between 10 and 50 nanostrains/ya are observed in these areas. In contrast, the definition of these features is largely lost when the 30 km bandwidth is applied (Figure 10.4).

Histograms of seismic strain rates for the 11 locations (Figure 10.5) generally show a relatively tight distribution of strain rates between 1 and 10 nanostrains/a. The histograms show the distribution of strain rates that result from sampling of our logic trees. They are developed by taking numerous samples of the logic tree by Monte Carlo methods to develop multiple realisations of strain rates. The simple shape of the majority of histograms shows that there is strong central tendency in the resulting strain rates, in that none of the parameters produces a significant number of outlier strain rates and lead to (for example) a bimodal distribution.

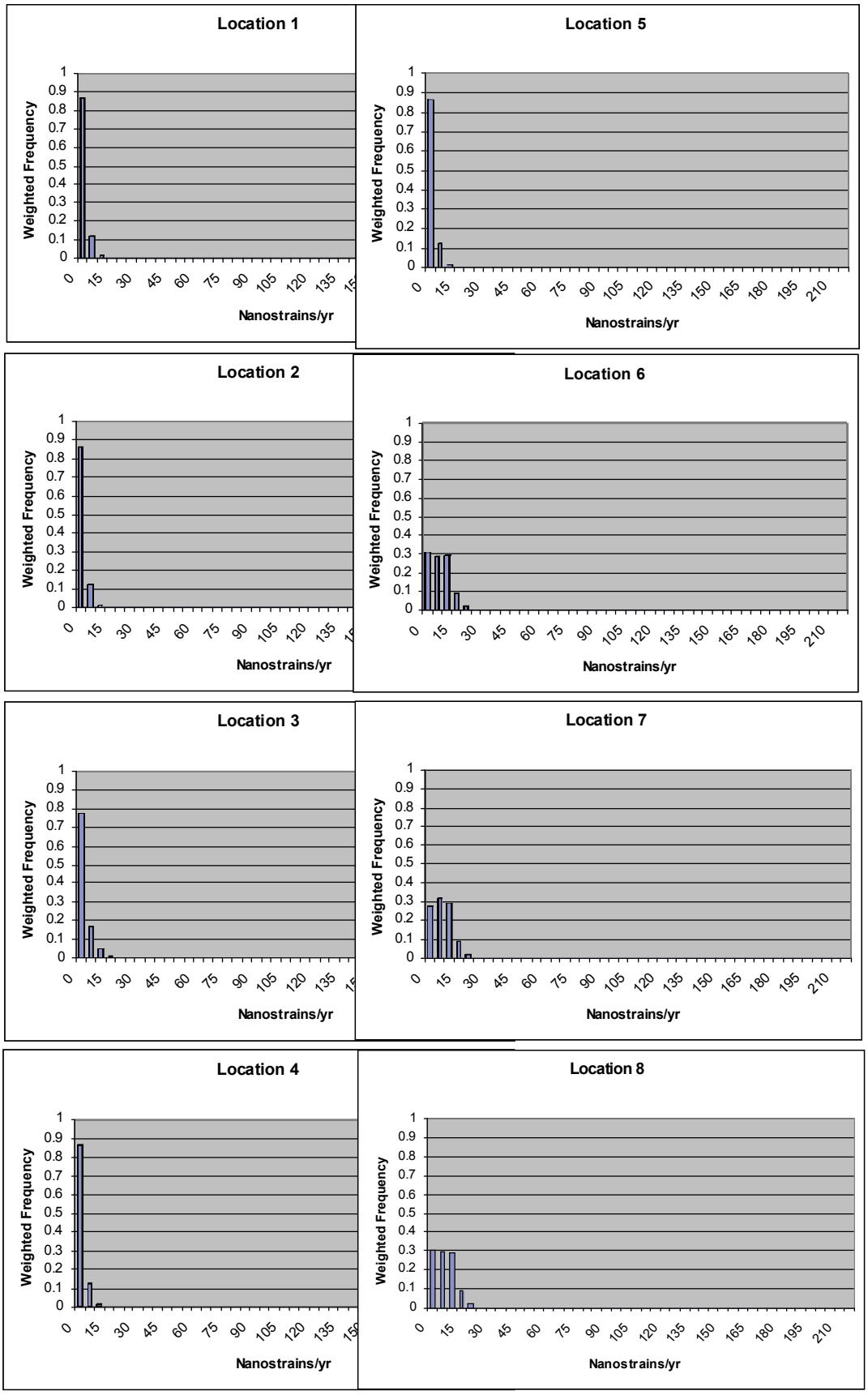

Figure 10.5 (continued on next page). Seismic strain rate histograms for the 11 locations.

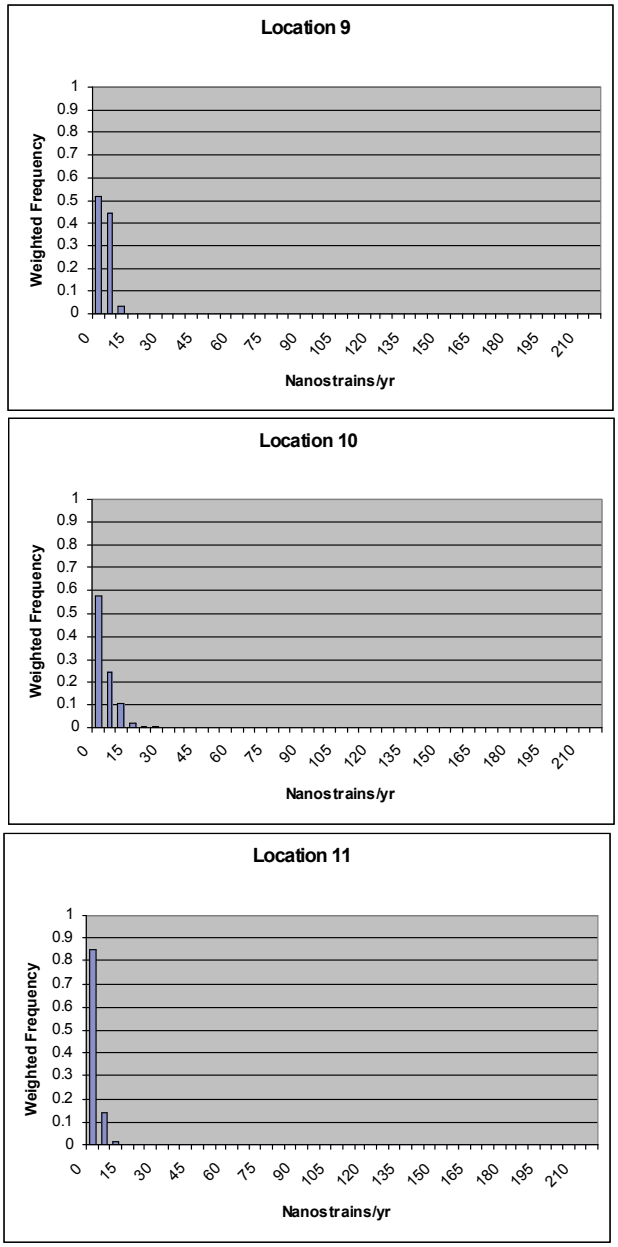

Figure 10.5 (continued). Seismic strain rate histograms for the 11 locations.

10.4 Discussion

The <10 nanostrains/year strain rates calculated for specific example locations within Kyushu (see Section on Discrimination of Tectonic domains and selection of example locations) and shown in Figure 10.5, are surprisingly low relative to strain rate calculations made from the GPS and surface deformation datasets for each of those example locations. The low strain rates are certainly unusual, given the overall high seismicity rates of the island (Figure 10.1). In contrast, our previous Tohoku Case Study analyses revealed much higher strain rates (of the order 10-100 nanostrains/a), despite relatively low observed seismicity rates in Tohoku. The paradox is due to the difference in b-values for the two regions. The generally low b-values of -1 to -1.1 for Kyushu translate to low rates of large earthquakes (the earthquakes that contribute most to the strain rate calculations), whereas the high b-values in Tohoku (greater than -1) produce relatively high rates of moderately sized earthquakes. For example, the seismicity parameters calculated across all four Kyushu zones (labelled Zone 5 in Figure 1; a=5.23, b=-1.02) translate to a recurrence interval of about 80 years for a M7 or greater

earthquake. This compares to about 30 years for the equivalent calculation for Tohoku where the b-value is relatively high (about -0.8). At larger magnitudes the differences between the two regions are even greater.

Given that the low seismic strain rates for Kyushu are conditioned by the low b-values calculated in Figure 10.1, it is important to review the above results critically. The b-values of -1 to -1.1 are typical of regions characterised by a combination of extensional tectonism and volcanism, and therefore appear defensible on that basis. The hydraulic fracturing processes associated with volcanism are consistent with a high ratio of small to large earthquake events, and therefore consistent the low b-values shown in Figure 10.1.

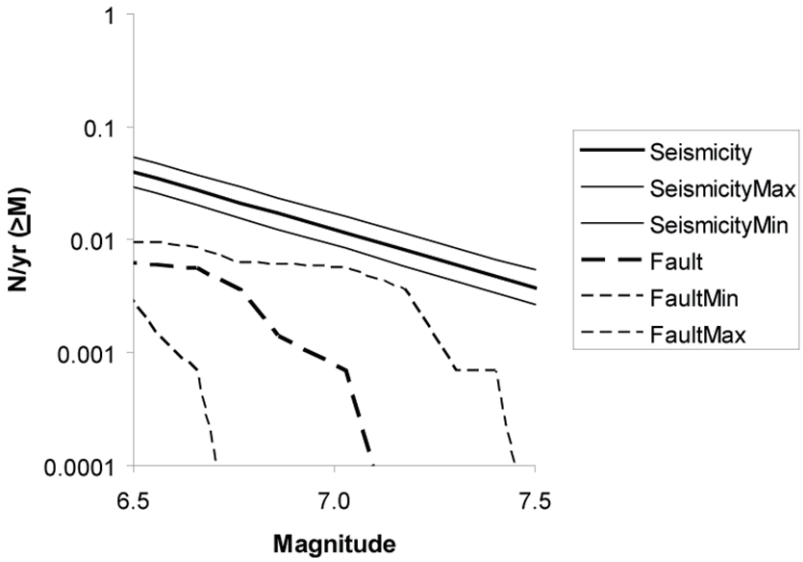

Figure 10.6: Magnitude – frequency distribution showing the cumulative seismicity rates predicted from the parameters calculated for the whole Kyushu region (Zone 5 on Figure 10.1) and the equivalent rates for Kyushu active faults. The latter were derived from the active fault database provided on the website of the Active Fault Research Centre (AIST) (http://riodb02.ibase.aist.go.jp/activefault/index_e.html). The fault magnitudes are estimated from fault length with three equations developed for intraplate Japanese earthquakes given in Stirling et al (1996), and the recurrence intervals are taken directly from the database. The three seismicity curves are calculated with the mean, minimum and maximum b-values for Zone 5.

Our analysis shows that the predicted rate of occurrence of large earthquakes in Kyushu is higher than the historically observed rate. Specifically, the predicted 80 year recurrence interval for a M7 or greater earthquake would produce five events in the c. 430 year historical period, more than double the number of similar-sized events in Kyushu for that same time period (only 2 events of M≥7 observed in c. 430 yrs). Comparison of historically observed and predicted number of M7 or greater events does not, therefore, support the possibility that the seismicity parameters are underestimated. However, it is also possible that the historical record could be a poor sample of the long-term 'parent' distribution of seismicity, in that over periods of thousands of years the actual rates of large earthquakes could be higher than our predicted rates.

In probabilistic seismic hazard analysis the standard approach to countering the possibility of a poorly representative historical record is to combine geologically derived (active fault) and historically derived earthquake datasets to obtain a more complete long-term record of seismicity. Since these datasets have instead been kept independent in the Kyushu Case Study, it is possible that the seismicity dataset may be incomplete with respect to large events, despite the predicted earthquake rates being extrapolated out to the large maximum magnitudes (Mmax) shown in Figure 10.1. However, previous studies have shown that the magnitude-frequency statistics of fault-derived M≥7 earthquakes over Japan are very similar to the historically observed rate of these events, and that b-values of -1.1 or less are

reasonable across the country (Wesnousky et al., 1984). Given that these comparisons are at a regional scale, a useful exercise is to compare the geologically-derived earthquake rates to our predicted rates for Kyushu to see whether or not a similar match is observed at the regional scale.

In Figure 10.6 we compare the rates of moderate-to-large earthquakes from our Zone 5 (i.e., entire Kyushu area in Figure 10.1) seismicity parameters to the rates derived from the major active faults of Kyushu derived from the active fault database provided on the website of the AFRC, AIST (see Figure 10.6 caption for website source). Clearly, the predicted rates of large earthquakes in Kyushu are higher than the active fault-based rates, therefore indicating that the seismicity record does not under-predict the long-term rates derived from the active faults. We do, however, acknowledge that the active fault data are probably incomplete in Kyushu, raising the possibility that a complete fault database might result in a somewhat different comparison to that observed in Figure 10.1.

10.5 Conclusions

A seismic strain rate model has been developed for Kyushu from the c. 430 year record of seismicity. The methodology closely follows that used to develop a model for the Tohoku Case Study (Chapman et al., 2009), including the treatment of epistemic uncertainty by way of logic tree definition and Monte Carlo sampling. The only major difference is that the seismic strain calculations are exclusively from a raw catalogue, whereas the Tohoku study also used a declustered catalogue. The seismicity parameters calculated are comfortably within the range of parameters observed in other regions of the world where seismicity is due to a mix of tectonic and volcanic processes. Surprisingly, strain rates calculated for the 11 locations focussed on in this study are generally low (generally in the range of 1-10 nanostrains/a), an order of magnitude lower than strain rates calculated for the lower seismicity Tohoku Case Study. The paradox is explainable by the marked differences in b-values for the two regions, in that the lower b-values of Kyushu translate to fewer large strain rate-generating earthquakes than in Tohoku. The greater number of small earthquakes in Kyushu is relatively unimportant in terms of calculated strain rates. Further confidence in our results is gained through noting that the low b-value is consistent with the combination of volcanic and extensional tectonic processes in Kyushu. Furthermore, comparison of the predicted rates of large earthquakes from the seismicity model to: (1) the historically observed rates of equivalent events, and; (2) the predicted rates of equivalent events from active fault data do not show an underestimation of these two criteria.

10.6 References for Section 10

Chapman, N., M. Apted, J. Beavan, K. Berryman, M. Cloos, C. Connor, L. Connor, O. Jaquet, N. Litchfield, S. Mahony, W. Smith, S. Sparks, M. Stirling, P. Villamor and L. Wallace (2009). Development of Methodologies for the Identification of Volcanic and Tectonic Hazards to Potential HLW Repository Sites in Japan: The Tohoku Case Study. Nuclear Waste Management Organisation of Japan, Tokyo. Technical Report: NUMO-TR-08-03. 135 pps.

Frankel, A. (1995). Mapping seismic hazard in the central and eastern United States. *Seismological Research Letters* ***66,***8-21.

Gutenberg, B., and Richter, C.F., 1944. Frequency of earthquakes in California. *Bulletin of the Seismological Society of America 34*, 185-188.

Kostrov, B.V. 1974. Seismic moment and energy of earthquakes and seismic flow of rock. *Izv, Acad, Sci. USSR Physics. Solid Earth 1,* 23-40.

Stirling, M.W., Wesnousky, S.G., and Shimazaki, K. 1996. Fault trace complexity, cumulative slip, and the shape of the magnitude-frequency distribution for strike-slip faults: a global survey. *Geophysical Journal International 124*, 833-868.

The Research Group for Active Faults of Japan (1992). *Map of active faults in Japan with an explanatory text.* University of Tokyo Press.

Weichert, D.H., 1980. Estimation of the earthquake recurrence parameters for unequal observation periods for different magnitudes. *Bulletin of the Seismological Society of America 70*, 1337-1346.

Wesnousky, S.G., Scholz, C.H., Shimazaki, K., and Matsuda, T. Integration of geological and seismological data for the analysis of seismic hazard: a Case Study of Japan. *Bulletin of the Seismological Society of America 74*, 687-708.

11 Nature and Spatial Probability of Future Rock Deformation in Each Domain using Example Locations

Two approaches to considering the probability of future rock deformation in Kyushu have been developed. Neither of these approaches is mutually exclusive and, ideally, both should be integrated into a single methodology. The first approach is based on the precept that the past is the key to the future and that we may therefore use current rates of activity to assess the probability of exceedance of various strain rates as a proxy for future rock deformation. Simple calculations relating earthquake energy to scaling of fault slip to earthquake magnitude, and converting that to strain rate, suggests that an annual strain rate of ≥4 nanostrains/a within a unit area of 5 x 5 km is consistent with rock deformation that may occur during the equivalent of 1 m of surface displacement (equivalent to a single magnitude 7 earthquake) in a period of 100,000 years. This calculation of course assumes that *all* strain calculated for a particular 5 x 5 km area from the various rock deformation datasets will be converted to a discrete faulting event across a discrete fault every 100,000 years, which is probably far too simplistic an approach. However, given various assumptions, threshold "hazardous" strain rates can be defined for specific rock deformation scenarios of concern, once those scenarios are decided upon. Plots showing the probability of exceedance of various strain rates for example locations in Kyushu (Figures 11.1 and 11.2) enable comparisons between locations, and give us some idea of how likely a given example location is to exceed a certain level of strain. Whether the various strain rates constitute a risk to a repository depends on the repository design and the manifestation of the rock deformation at those locations. The deformation may range from concentrated displacement on a single fault trace to widely distributed, diffuse, fracturing within a 5 x 5km area enclosing the location.

The second approach is to take note of the rapid geological evolution of the Kyushu region and consider the possibility that future rock deformation may evolve in both space and time, and that while past and current rates of deformation capture this evolution to some extent, we can also qualitatively assess what sort of evolving activity may affect the example locations. Key features or processes we observe to be driving the rapid evolution, and their impacts in Kyushu are:

(i) Roll-back at the Nankai Trough, which may induce migration of arc volcanism southeastward

(ii) Southwestward migration of the Kyushu/Palau Ridge (and its subducted part) beneath Kyushu because of the oblique angle of subduction and the orientation of the volcanic chain comprising the Kyushu/Palau Ridge. We suggest that an active left-lateral shear zone in southern Kyushu (revealed by GPS and seismicity) occurs due to the impingement of the Kyushu-Palau Ridge on the subduction margin (see discussion in Section 9). It has also been suggested by previous studies that uplift in the forearc above the ridge subduction point is related to Kyushu-Palau Ridge subduction. It is also possible and localisation of heat flow and Aso-type volcanism in the arc is related to the position of the Ridge (see Section 7). Thus, we could expect left-lateral shear of southern Kyushu, uplift in the forearc, and localisation of certain types of volcanism to migrate also.

(iii) The northeast limit on extension associated with the Okinawa Trough is adjacent to the western end of the Beppu Shimabara Graben (BSG) in the vicinity of Nagasaki and Kumamoto. It is unclear whether this zone of extension continues to develop, but it could be increasing the likelihood of normal faulting and volcanism in that area.

(iv) Extension in the Kagoshima Graben and volcanism such as at Sakurajima are geologically recent phenomena in southern Kyushu. Future evolution and development of this zone may be expected. Future steepening of subduction at the Ryukyu Trench as a consequence of slab roll-back will encourage migration of the volcanism in the Kagoshima Graben toward the east and southeast.

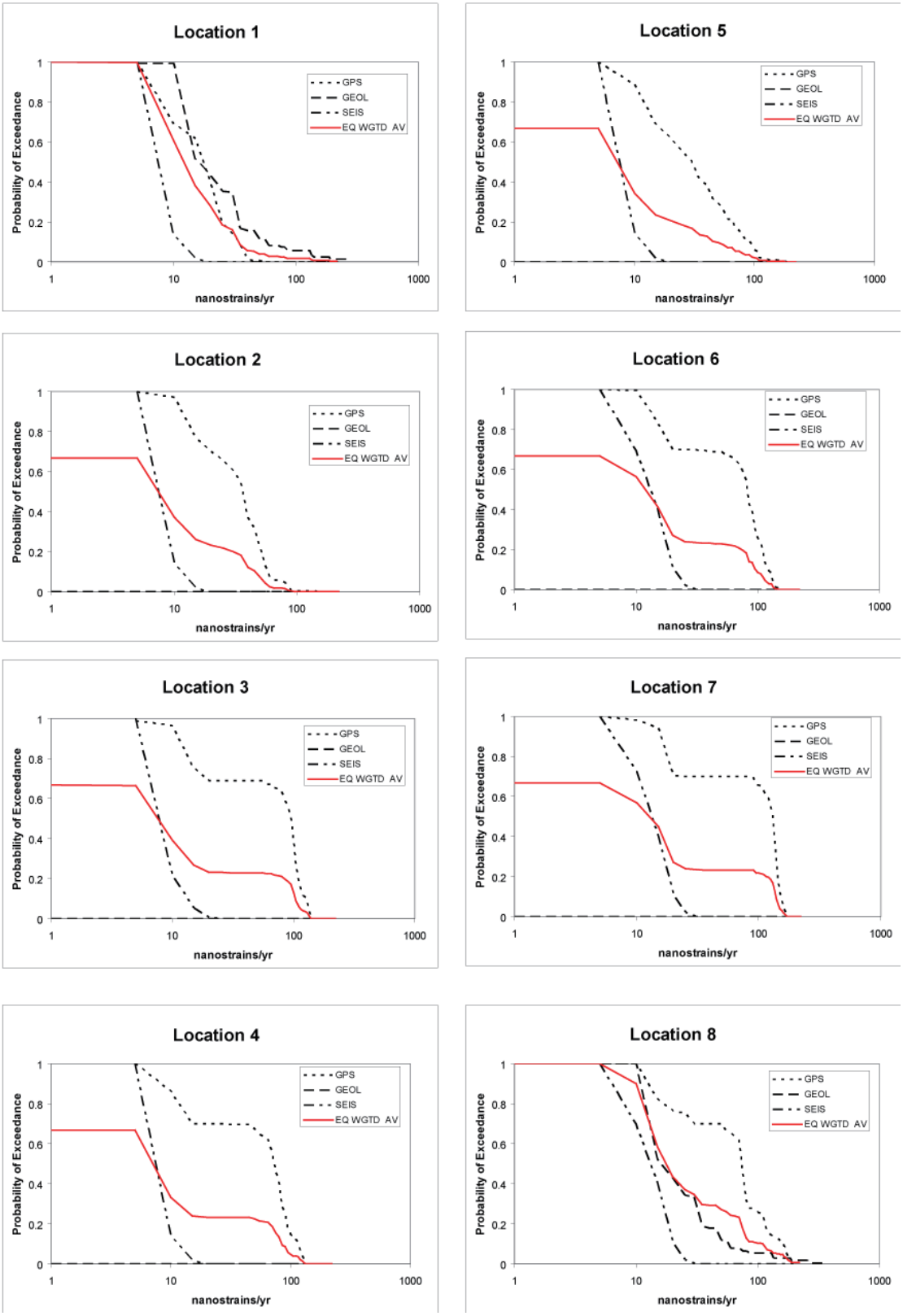

Figure 11.1 (continued on next page): Cumulative strain rate plots for the 11 example locations. EQ WGTD AV is equal weighted average. See Figure 6.4 for location of the 11 example locations.

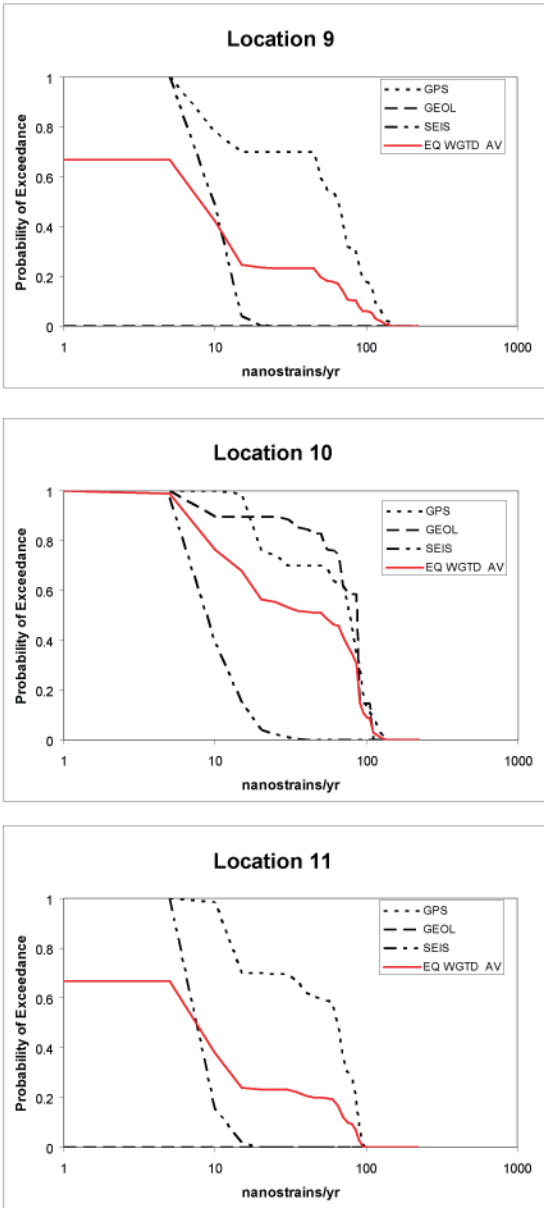

Figure 11.1 (continued): Cumulative strain rate plots for the 11 example locations. EQ WGTD AV is equal weighted average. See Figure 6.4 for location of the 11 example locations.

(v) At present the volcanism and faulting associated with the Kagoshima Graben does not extend further northeastward than Kirishima volcano, with a marked gap in volcanism in central Kyushu between Kirishima and Aso volcanic centres. In normal situations we would expect that the volcanic arc would continue to the north approximately located above the 100 km depth contour on the subducted Philippine Sea Plate. We are not aware of any current data to explain this gap in volcanism and thus should consider the possibility of new volcanoes developing in that area.

(vi) In the Back-arc domain of northern Kyushu and offshore Japan Sea, large earthquakes are occurring on reactivated northwest- and northeast-striking faults. There may also be correlation of these structures to some of the monogenetic volcanism. For example, stress perturbations that arise at fault interSections may be preferred locations for future small volume monogenetic events. The backarc province hosts a wide variety of volcanism that is dominated by processes in the mantle and the mantle wedge rather than subduction. Little is known of the processes leading to irregular volcanic “flare-ups” in the Back-arc domain and there is large uncertainty is forecasting future activity.

Based on the features and processes noted above we discuss current strain rates estimated for these example locations, and offer some suggestions of possible future rock deformation evolution at or adjacent to each of the example locations in the various domains defined in the Kyushu Case Study. To aid with the comparison between locations, Figure 11.2 shows all the probability of exceedance curves on one plot.

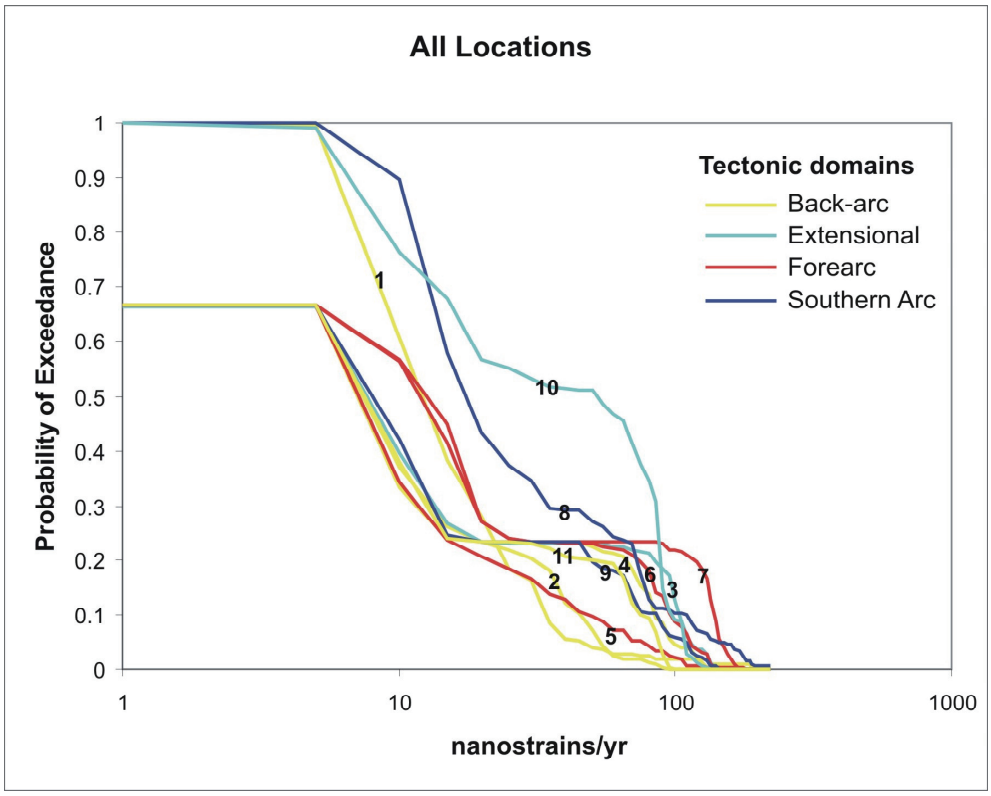

Figure 11.2: Combined equal weighted average cumulative strain rate plot for the 11 example locations, colour-coded by tectonic domain. See Figure 6.4 for location of the 11 example locations.

11.1 Back-arc domain

Example Location 1. Located on an active fault with a low slip rate of 0.1 mm/a. There is a general good agreement on strain rates between all 3 datasets: current GPS strain rates are low-moderate, as are seismicity and active fault strain rates (Figure 11.1). Future deformation can be expected in the form of sinistral strike-slip surface faulting associated with earthquakes up to about M 7.5 (see Section 10). Because the fault is reactivating an earlier structure the fault zone complexity (the process zone) can be expected to be wider than on a long-lived, well-developed, fault.

Example Location 2. Located about 20 km from a low slip rate (0.1 mm/a) active fault. Current GPS strain rates are moderate to low, and seismicity strain rates are very low (Figure 11.1). Future deformation is a possibility but it is unlikely the process zone of future faulting on known active faults in the region (20 km away) will extend to this location. Secondary faulting or fracturing of suitably oriented bedrock faults and fractures is possible in the event of a large nearby earthquake.

Example Location 11. Located in southwestern Honshu in the southern part of the monogenetic Abu volcanic field. In the region there are both northeast- and northwest-striking faults, although the closest known active fault is more than 20 km to the west. The west Tottori earthquake of 2000 occurred approximately 200 km to the northeast in a similar tectonic environment. Current GPS strain rates are moderate, and seismicity strain rates are

very low (Figure 11.1). Reactivation of bedrock structures in this region as strike-slip faults is possible considering other active faults in the region. There is a possible structural control on the location of volcanic edifices of the Abu volcanic field and, at this location, possible future co-location of volcanism and faulting should be assessed.

11.2 Extensional domain

Example Location 3. Located west of Aso Volcano, within the BSG, and about 12km north of a prominent normal fault extending westward from Aso Volcano. Thick, young pyroclastic deposits cover the area, which may have obscured some faulting near to the location. Current GPS strain rates are high, and seismicity strain rates are very low (Figure 11.1). Further development of the normal faults can be expected in the region. Proximity to Aso Volcano suggests that ground deformation associated with future volcanism is also probable.

Example Location 10. Located about 30 km SW of Aso Volcano near the southeast margin of the BSG, and within 5 km of a moderate slip rate normal fault (~0.9 mm/a). Thick, young pyroclastic deposits cover the area, which may have obscured some faulting near to the location. Current GPS and active fault strain rates are high, and seismicity strain rates are very low (Figure 1). Further development of the normal faults can be expected in the region. Proximity to Aso Volcano and associated connected edifices suggests that ground deformation associated with future volcanism is also probable. This location is possibly in the region where future Aso-type volcanism and related tectonism may concentrate with the migration of the Kyushu Palau Ridge subduction point interSection with the BSG. If this process is significant in governing the location and migration of a nexus of volcanism, then Aso-type volcanism could migrate to a location 10 position, 0.5-1.0 million years from now. Current strain rates at Location 10 are among the highest observed in the study.

Example Location 4. Located in northeast Kyushu at the eastern margin of the BSG. The location is on the flanks of a volcano but north of the current extent of normal faulting associated with the BSG. Geodetic strain rates are high and very similar to other locations in the BSG (Figure 11.1). Seismicity strain rates are very low (Figure 11.1). Future hazard may diminish at this location as the shallowly subducting Shikoku Basin crust encroaches on this region and shuts down any remaining extensional deformation, over the next 1-2 Ma.

11.3 Forearc domain

Example Location 5. Located in the Forearc domain immediately east of the boundary with the Extensional domain and about 15 km east of Aso Volcano. The location is between active traces of low slip rate faults (~0.1 mm/a), and bedrock geology in the area has many steep faults oriented parallel to the domain boundary between the Extensional and Forearc domains. Current geodetic strain rates are high and seismicity strain rates are low (Figure 11.1). Future deformation at this location might occur as a result of reactivation of bedrock structures that evolve the current unlinked fault strands into a more continuous feature. If trench roll-back at the Nankai Trough is significant process then it is likely the southeastern margin of the Extensional domain will also migrate into the current Forearc domain. Deformation at the location could therefore be expected to switch to normal faulting and increase in rate. The location is likely to be heavily inundated by ash fall in the event of a major eruption from Aso Volcano.

Example Location 6. Located near the southeast coast of Kyushu approximately 15 km north of the nearest known fault at the margin of the Miyazaki Plain. Current GPS strain rates are high and seismicity strain rates are low (Figure 11.1). However, it is possible that the GPS strain rates are artificially high here due to choice of subduction interface coupling models (see discussion in Section 9). Coastal uplift rates of about 0.2 mm/a have been noted nearby and rates up to 0.7 mm/a further south along the Miyazaki coast. If these rates extend inland to this location this could result in hundreds of metres of uplift over long time periods, and represent a significant rock deformation.

Example Location 7. Located in an area about 30 km distant from the nearest active fault and about 30 km from the BSG. The location is above the 100 km contour on the subducting oceanic plate but in an area of no current or past volcanism. There is strong northeast striking bedrock structure in the area. Current GPS strains are high and seismicity strain rates are low (Figure 11.1). This location is near to the junction of high left-lateral shear strain cross-cutting Kyushu (as seen from the GPS velocities: see Section 9) and the southeast boundary of the BSG. Given that this location is adjacent to the interSection of the left-lateral shear zone with the BSG, we cannot rule out migration of future rock deformation into this region. Obtaining improved mantle structure data may indicate reasons for the gap in arc volcanism. This would be a key future requirement if a location such as this were to be considered as a potential repository site.

11.4 Southern Arc domain

Example Location 8. Located about 15 km to the east of faults marking the eastern boundary of the Kagoshima Graben. The location is on the southern end of one of the northeast striking, low slip rate (~0.1 mm/a), faults of the region, and is just to the south of the left-lateral shear zone cutting across southern Kyushu (from GPS). Current GPS strain rates are high, active fault strain rates are moderate, and seismicity strain rates are low (Figure 11.1). Future rock deformation may be characterised by rare surface rupture of the local active fault, or speculatively by significantly increased rates of deformation if the Kagoshima Graben is migrating with the roll-back of the subducted plate, and by southward migration of the left-lateral shear zone cross-cutting southern Kyushu which may be driven by subduction of the Kyushu-Palau Ridge.

Example Location 9. Located about 15 km west of the western margin of the Kagoshima Graben. The location is within the former volcanic arc (before it migrated eastward to the Kagoshima Graben area) (Yamaji et al., 2003). The location is about 10 km south of northeast striking normal cutting across the old arc volcanoes and is just to the south of the left-lateral shear zone cutting across southern Kyushu (from GPS). Current GPS strain rates are high, but slightly less than location 8, and seismicity strain rates are very low, also less than location 8 (Figure 11.1). Future rock deformation at this location might be less likely than at location 8 because it appears to be in the trailing position of the locus of volcanism in the contemporary Kagoshima Graben. The characteristics and possibility of migration of the faulting located about 10 km to north of the location would be important to understand in further investigations at this locality. In particular, southward migration of the left-lateral shear zone cross-cutting southern Kyushu which may be driven by subduction of the Kyushu-Palau Ridge could be important in future rock deformation at this location.

12 Probability of Future Volcanism

The Kyushu Case Study explored several aspects of volcanism in the greater Kyushu region (including SW Honshu) that were not specifically addressed in the Tohoku Case Study (Chapman et al., 2009). These aspects of volcanism are particularly clear in the Kyushu region, but may be of general concern for proposed geological repository sites in several areas of Japan. These include:

- Development of a methodology for assessing monogenetic volcanism as part of a long-term volcanic hazard assessment
- Testing and refining of proposed models for monogenetic volcanism using data gathered in the region (in this case the Abu volcanic field of SW Honshu)
- Developing general methods for assessing long-term probability of volcanic using a regional Kyushu example
- Assess the influence of tectonic domains in Kyushu on probability models of volcanism
- Development of methodology for local scale volcanic hazard assessment with respect to specific volcanic systems.
- Illustrate methods of estimating the probability of volcanic disruption, including event magnitude.

This Section summarizes the results of our work in all of these areas. Sections 12.1 and 12.2 describe a methodology specifically for evaluating monogenetic volcanism. The subsequent Sections describe the overall analysis and are organised from regional to local scales, reporting the influence of segregating volcanoes in Kyushu by tectonic domain, and summarising results using kernel density methods and Cox Process methods for modelling the potential of volcanism. The probability of volcanic disruption is illustrated using caldera-forming events as an example.

12.1 A Methodology for Assessing Long-term Hazard Due to Monogenetic Volcanism

Monogenetic volcanoes form when igneous dikes ascend through the crust and erupt at the surface. These volcanoes are characterised by a single episode of eruptive activity that may last from weeks to years and, in rare cases, for hundreds of years. During this activity a volcano is formed, such as a cinder cone, maar, tuff ring, dome, or fissure-fed lava flow. In rare cases, shield volcanoes may also be monogenetic. Unlike polygenetic volcanoes, once eruptive activity ceases at monogenetic volcanoes, these volcanoes never erupt again. Rather, renewed magmatic activity involves the propagation of a new dike or dike swarm through the crust and formation of a new monogenetic volcano. Thus, over time, groups of monogenetic volcanoes are created. These monogenetic volcano groups, also referred to as volcanic fields, typically consist of tens or hundreds of volcanoes distributed over thousands to tens of thousands of square kilometres.

In general, average eruptive rates in monogenetic volcano groups are very low compared to single polygenetic volcanoes. Individual eruptions commonly involve <0.1 km^3 magma, and eruption rates are commonly 10^{-4} to 10^{-3} eruptive events per year. From a volcanic hazards perspective, the problem is one of forecasting the potential for new monogenetic volcanoes to form in the site region during a long performance period, accounting for the dispersed nature of monogenetic volcanism and its generally low recurrence rate. This is different from issues associated with polygenetic volcanism, which involves eruptions from existing volcanoes affecting the site, and the extremely rare formation of new polygenetic volcanoes.

Monogenetic volcanism has received a great deal of attention in HLW siting investigations in the US, because Yucca Mountain, the proposed site of a HLW repository, is located at the margins of an active volcanic field. A variety of methods for assessing monogenetic volcanic

hazards at Yucca Mountain have been developed over decades of siting activities. In addition, volcanologists worldwide have considered monogenetic volcanic hazards, particularly to urban areas, such as Mexico City and Auckland, which are built in monogenetic volcanic fields. Some of the methodologies proposed here draw on this experience, but are modified considering the distinctive tectonic settings of potential HLW sites in Japan, compared with the western USA.

12.1.1 Background to an Overall Methodology

The basic problems are to estimate the potential spatial distribution of future monogenetic volcanism, the temporal recurrence rate of volcanism, and the area, particularly in the shallow subsurface, potentially impacted by volcanism. Worldwide, probabilistic methods are used to assess monogenetic volcanism. This is due to the complex distribution of monogenetic volcanism, which requires the application of stochastic models for its characterisation and for evaluating associated uncertainty. Although we develop geologic models for the causes of monogenetic volcanism at a variety of scales, these models cannot be used to forecast precisely the distribution and timing of future events. Nevertheless, probabilistic models may account for our current understanding of the underlying causes of monogenetic volcanism, and even include empirical information derived from the investigation of geological correlations. For example, in the Yucca Mountain region it was eventually determined that monogenetic volcanism tends to concentrate in a tectonic zone known as the Amargosa Trough, and this empirical information was included in probabilistic models (Connor et al., 2000).

In order to estimate volcanic hazards due to monogenetic volcanism, three probabilities must be estimated. These are:

- the probability that monogenetic volcanism will occur within some area about the HLW site; this is determined through estimation of the spatial density of volcanism;
- the probability that monogenetic volcanism will occur within the timeframe of interest, say annually, or within the overall performance period of the site; this is determined through estimation of the temporal recurrence rate of volcanism;
- the probability that, given a volcanic event, the HLW repository will be disrupted in some way; this is determined through study of the magnitude of potential monogenetic events and their interaction with the repository system.

Estimation of these probabilities usually involves using a variety of different models and site-specific information about the volcanic field of interest. For example, geophysical surveys have proven to provide basic and key information about the distribution of monogenetic volcanic events (often some monogenetic events do not crop out at the surface or have been buried by subsequent geological processes), structural and / or tectonic controls on the distribution of monogenetic volcanism, and direct evidence of the potential for future monogenetic volcanism, for example through seismic tomographic studies.

Estimation of these probabilities is also complex. There may be different or competing geological models for volcanism in a region, or different mathematical approaches to estimating probability using these data. In such circumstances, expert assessment is often used to compile and evaluate disparate analyses. This approach has recently been used to assess monogenetic volcanic hazards in the Yucca Mountain region. Here, we consider a similar approach to the assessment of monogenetic volcanic hazards in Japan.

12.1.2 Methods of Estimating Spatial Density

The goal of estimating spatial density in the context of volcanic hazards assessments for a HLW repository site is to determine the likely locations of future igneous events, or the probability of an igneous event at a specific location, given that such events occur within the site region. In this context, spatial intensity refers to the expected mean number of events per unit area defined at a point, **s** (Diggle, 1985; Diggle and Marron, 1988; Gatrell et al., 1996).

Suppose there is a set of events (e.g., monogenetic volcano locations) that occur within a region, *R*. These events can be designated as $\{X_1, X_2, X_3 ... X_N\} \in R$, where *N* is the total number of events and X_n is a matrix whose elements are the *x, y*, location (e.g., given in Easting and Northing coordinates, or, latitude and longitude) of the n^{th} event. These events are realisations of a random variable, **X**, a function that describes the set of all possible realisations. In this case, **X** is the distribution of potential igneous events, from which a set of observed realisations (those volcanoes mapped in the monogenetic volcanic field) are drawn. The spatial intensity is formally written as (Gatrell et al., 1996):

$$\lambda(\mathbf{s}) = \lim_{ds \to 0} \left\{ \frac{E(X(d\mathbf{s}))}{d\mathbf{s}} \right\} \qquad (1)$$

where $E(X(d\mathbf{s}))$ is the expected number of events that fall within a small area *d***s** about the point **s** (hence if the location, **s**, is given in Easting and Nothing (metres), the units of $\lambda(\mathbf{s})$ are m^{-2}). At first glance it appears that the statistical definition of *intensity* is equivalent to the term *density* as commonly used in geosciences. This is not quite true. The stochastic process that leads to the formation of volcanoes is not known, so the true value of the local spatial intensity, $\lambda(\mathbf{s})$, is also unknown. That is, the observed distribution of events is only one realisation of the underlying process that gives rise to these events. Our goal is to find an estimate of the spatial intensity, $\hat{\lambda}(\mathbf{s})$, that approximates the true but unknown value of spatial intensity, $\lambda(\mathbf{s})$.

In hazard assessment, we have a further requirement that we can use this information to forecast the spatial distribution of potential future events. Here we are interested in spatial intensity in terms of the probable location of a future igneous event, given that one occurs within the region of interest. This conditional probability can be estimated by:

$$\hat{f}(s) = \frac{\widetilde{\lambda}(s)d(s)}{\int_R \widetilde{\lambda}(s)d(s)} \qquad (2)$$

Integrating $\hat{f}(\mathbf{s})$ across the region of interest, *R*, gives unity, if *R* is sufficiently large. Furthermore, all values of $\hat{f}(\mathbf{s})$ within this region are greater than or equal to zero, so $\hat{f}(\mathbf{s})$ is a probability density function and may be used in probabilistic hazard models, and we can refer to $\hat{f}(\mathbf{s})$ as an estimate of the spatial density.

Assumptions behind Spatial Density Estimates

How do we develop a best estimate of spatial density? The problem is that we have only one realisation of the underlying statistical process, the distribution of past volcanic events, and geology is not conducive to repeating the experiment in a natural system. In a region of monogenetic volcanism in Japan, for instance, there is only one geologic map of volcano distribution. Perhaps ideally we would have a complete geophysical model for events. Presumably, the distribution of melt in the asthenosphere and lithosphere were known, and if the state of the lithosphere through which the magma rises were known, we might have a better sense of where volcanoes are most likely to form next. Currently, we lack such a complete geophysical perspective. Some data sets, for example seismic tomographic models of "slowness" in the lithosphere and asthenosphere, give an idea of where partial melting of the mantle might occur (e.g., Zhao, 2001, Humphries, personal communication). Other data, such as gravity and magnetic anomalies in the region (Connor et al, 2000; Parsons et al., 2006), may show some correlation with the existing distribution of volcanoes in some circumstances, but the mechanisms relating gravity anomalies to the origin of magmas are incompletely understood and the correlation is likely imperfect. As a result, these types of

data have been used to support estimates of spatial density of monogenetic volcanism (e.g., Connor et al., 2000; Martin et al., 2004), but no model has yet been proposed that does not rely principally on the spatial distribution of past events. Similarly, in seismology there have been attempts to create blended hazard maps based on a variety of geophysical criteria, but these methods generally rely on the earthquake catalogue (e.g., Ward, 1994).

The reliance on the distribution of past events implies that these realisations are representations of the underlying random variable, **X,** that will govern the distribution of potential events in the future. This assumption immediately raises a fundamental question. Which are the past events that should be used to develop the spatial intensity estimate, $\hat{\lambda}(\mathbf{s})$, and density, $\hat{f}(\mathbf{s})$? Event datasets used to estimate the spatial density of future events need to be consistent with several features of geological processes that give rise to monogenetic volcanism.

First, any spatial intensity function for a geologic process must change with time. On time scales of tens of millions of years, plate boundaries change, volcanic systems wax, wane, and mantle is depleted. In very long term probabilistic hazard assessments for high-level waste repositories, which may have 10^6 year performance periods, these factors have to be considered in weighing the validity of using specific data in developing spatial intensity models. For processes like monogenetic volcanism, where a geologic record of past events usually persists of tens of millions of years, consideration needs to be given to which events best represent the distribution of future volcanism. For example, the distribution of Miocene monogenetic volcanoes might be much less relevant than the distribution of Pliocene and Quaternary volcanoes. Thus, in order to develop an estimate of the spatial intensity, a model of the geologic evolution of the system is required. This geological model is used to justify the inclusion of some geological features in the event dataset, and the exclusion of others.

Second, it is necessary to assess the completeness of the geologic record. The record of igneous events in monogenetic volcanic fields might give an incomplete picture of the unknown distribution of potential igneous events, $\lambda(\mathbf{s})$. Igneous events might be missed by geological investigations, as volcanic vents might be buried in sediment or otherwise obscured (e.g., Connor et al., 1997). Furthermore, it is well-known that igneous events that did not produce volcanic features but which intruded to the stratigraphic level of the proposed repository are unlikely to be detected, except through drilling and /or extremely detailed geophysical investigations.

Therefore, a major assumption of the spatial density estimate is that the distribution of intrusive igneous features is described by the distribution of known volcanic features. This is an important assumption because, as described further in the following, the limited number of volcanic events creates uncertainty in the spatial density estimate. Therefore, it generally is assumed that the distributions of igneous events in these areas are captured by the distributions of surface features.

Third, igneous events, even when they are all identified, may be so rare that they give an incomplete picture of the underlying geophysical process that gives rise to monogenetic igneous events. Consider an igneous event as a single event, X_n, a realisation of a random variable, **X**. If, for example, **X** has a uniform random distribution, then it is likely that the observed set of realisations will have a completely spatially random distribution in the region *R*. The underlying density often has additional statistical structure, causing independent realisations to cluster. Volcano clustering in monogenetic volcanic fields is well-documented in virtually every tectonic setting on Earth (e.g. Connor, 1990; Connor and Conway, 2000; Weller et al., 2006, Jaquet and Carniel, 2006), presumably because such clusters form above zones of partial melting in the mantle. For random variables with a great deal of statistical structure, such as many modes in spatial intensity, a great number of events might be required to identify the statistical structure of the random variable.

Obviously monogenetic volcanism in many parts of Japan, such as NW Kyushu, is comparatively rare, even in comparison with other active monogenetic volcanic fields in the

western US (Connor and Conway, 2000), or the site would not be considered for a potential HLW repository at all. Because relatively few igneous events are known to have occurred, statistical structure in the spatial intensity of volcanism may be missed. This uncertainty can be assessed, as is done in the following, but cannot be eliminated from the analysis. In a practical sense, because few events are used to construct the spatial density estimate, the spatial density is a smoothed representation of reality. Some areas might have higher spatial intensity, and others lower spatial intensity, than estimated.

Fourth, it is critical to ascertain which geologic features are actually independent events. The statistical structure of the random variable, **X**, might be obscured if some events included in the event dataset are not independent. For example, great earthquakes are followed by aftershocks. An earthquake aftershock, however, is not a random sample of the random variable "*spatial distribution of great earthquakes"*, because these aftershocks are not realisations of this particular random variable. Rather, they are independent realisations of another random variable, say *"spatial distribution of aftershocks about a great earthquake"*. So, the distribution of aftershocks does not necessarily give the best sense of the spatial intensity of great earthquakes, although these two random variables are correlated.

Similarly, volcanoes are complex geologic structures. In monogenetic volcanic fields alignments of volcanic cones develop in response to single igneous events, episodes of magma rise through the shallow crust. This is because single igneous dikes ascending through the crust might form segments and rotate within the shallow crust, each segment feeding a separate vent and each building a volcanic cone. If the goal of analysis is to forecast the distribution of future igneous events, each of which might produce more than one monogenetic volcano, geological data must be gathered and volcanoes formed by the same magmatic event must be somehow grouped as single events.

12.2 Testing Models with Data from the Abu volcanic field, SW Honshu

The ITM Group investigated rates and patterns of activity in the Abu Monogenetic Volcano Group, located in Southwest Honshu, as a Case Study to illustrate methodologies for volcanic hazard assessment in monogenetic volcanic fields. The goal of this effort was to refine a methodology for volcanic hazard assessment for monogenetic volcanism, paying particular attention to how various models of volcanism (e.g., constant magma supply rates) and data (e.g., seismic tomographic data), might influence such hazards assessments.

This monogenetic volcano group is ideal for such analysis because many K-Ar dates have already been reported (Uto and Koyaguchi, 1987; Kakubuchi et al., 2000 and Kimura et al., 2003) and because the field has been mapped in detail. We analyzed the temporal-spatial distribution of volcanism in the Abu area using 56 individual monogenetic volcanoes mapped in the field. Spatial density was assessed using a nonparametric kernel method. Overall volcanoes in the Abu Monogenetic Volcanic Group are located in a broadly E-W elongated area. NW-SE extended parallel volcano bands within the field, perhaps reflecting structural control on volcanism, are also seen in some spatial density analysis. Furthermore, orientations of individual dikes are deduced from volcano alignments. These more local scale volcano alignments lie in various directions. Different scales of geological mechanisms should govern these different characteristics of the monogenetic volcano distribution. Based on volume of each volcano and reported K-Ar dates, we infer that the size and the activity of basaltic magma source in upper mantle had been constant yet, the volcanic activity on the surface increased due to partial melting of lower crust caused by the induced heating from basaltic dike intrusions. This idea is supported by seismic tomographic results, which indicate a broad one of low velocity anomalies beneath the volcano field. Furthermore, the volcano eruption pattern is possibly affected by regional stress conditions.

12.2.1 The Abu Monogenetic Volcano Group

In the Southwest Japan Arc, late Cenozoic monogenetic volcano groups are thought to originate from the upwelling of small mantle diapirs (Iwamori, 1991; Uto, 1995; Kimura et al., 2003). The Abu Monogenetic Volcano Group is one such monogenetic volcano group consisting of alkaline basalt and calc-alkaline andesite-dacite lavas and pyroclastics

distributed in an area of 400 km^2 (Figure 12.1; Oji, 1961; Koyaguchi, 1986). Some volcanoes of this Group are located under the Sea of Japan (The Maritime Safety Agency of Japan, 1996a, b). Basement rocks of these volcanoes are Cretaceous and Palaeogene in age (Koyaguchi, 1986).

Koyaguchi (1986) concluded that geochemical trends observed in Abu lavas over time were produced by the magma mixing of primitive alkali basalt magma and dacite magma, which was provided by the partial melting of the lower crust, caused by induced heating from repeated intrusion of basalt. Reported K-Ar dates range for the entire field range from 10 ka to 3.3 Ma (Uto and Koyaguchi, 1987; Kakubuchi et al., 2000 and Kimura et al., 2003). There is a quiescent period from ca. 0.8 to 1.6Ma in the field, during which no volcanic activity appears to have occurred. Kakubuchi et al. (2000) classified the volcanic activity into alkaline basalt dominated early period (ca.1.6 - 2 Ma) and calc-alkaline andesite-dacite dominated late period (ca. <0.8 Ma), concluding that these distinct episodes originated from different mantle diapirs.

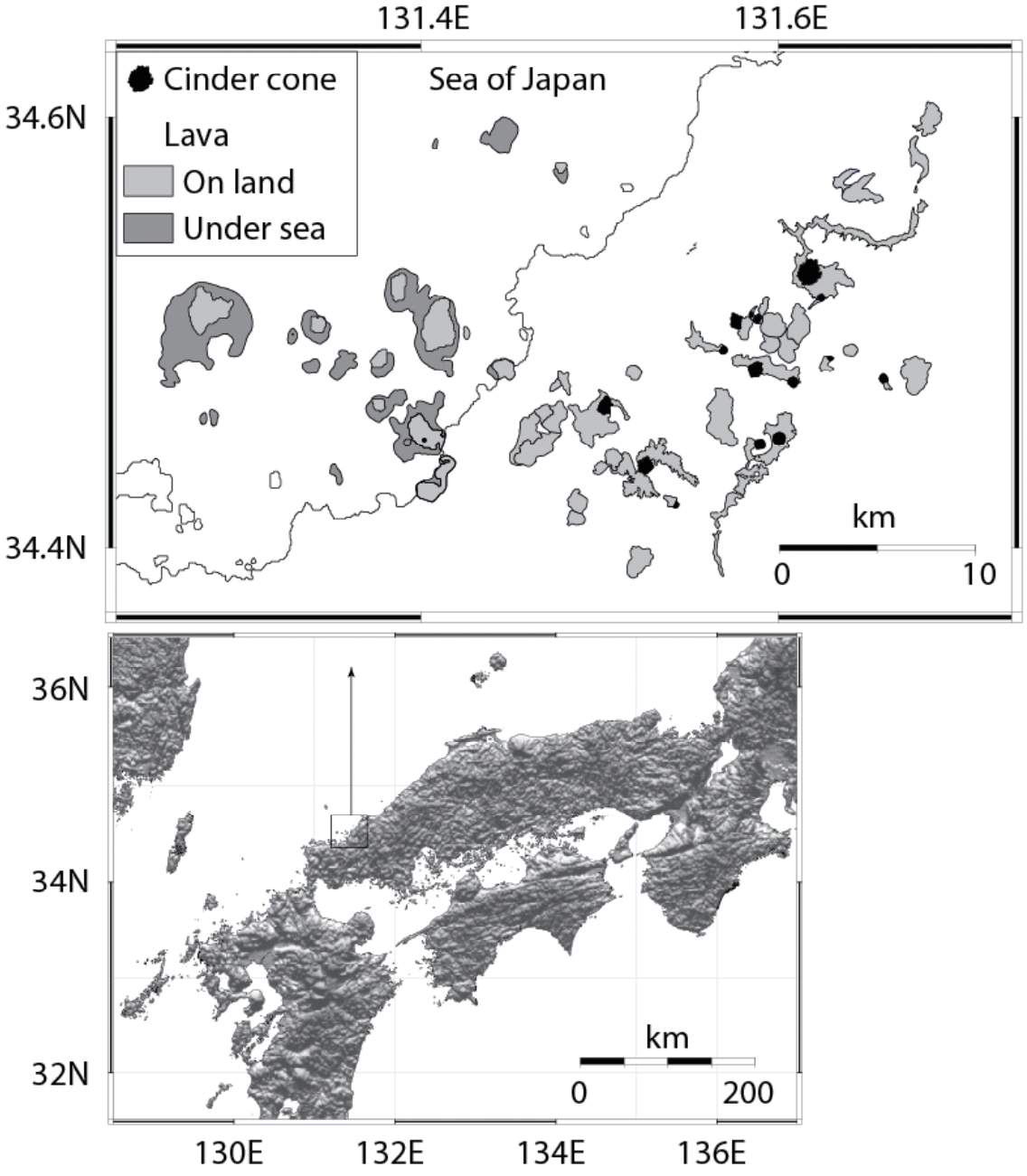

Figure 12.1. Location map for the Abu Monogenetic Volcano Group.

Although seismic activity is not high in the area of the Abu Monogenetic Volcano Group, E-W compressive stress is suggested by the focal mechanisms of earthquakes in this area (Figure 12.2a). Ito and Arato concluded this stress condition (σ_1 = N70-90W) has continued since 4 Ma based on an analysis of active structures in the Sea of Japan. Kanaori (1997) divided this region into three sub-areas by two NE-SW oriented fault systems (Figure 12.2b); the Abu Monogenetic Volcano Group is located in the area where both NW-SE and NE-SW oriented lineaments and faults are found. The initiation of the lineaments, faults and related cataclasite zones probably date back to late Cretaceous-early Palaeogene, and reactivation partly occurred along the old cataclasite zones during the Quaternary (Kanaori, 1997). Various planer structures within the cataclasite zones indicate lateral shear sense. Also, many minor earthquakes occur along the zones, whose depth of the epicentre is less than 30 km (Figure 12.2a). These active fault systems may cut entirely through the earth's brittle crust (Kanaori, 1997).

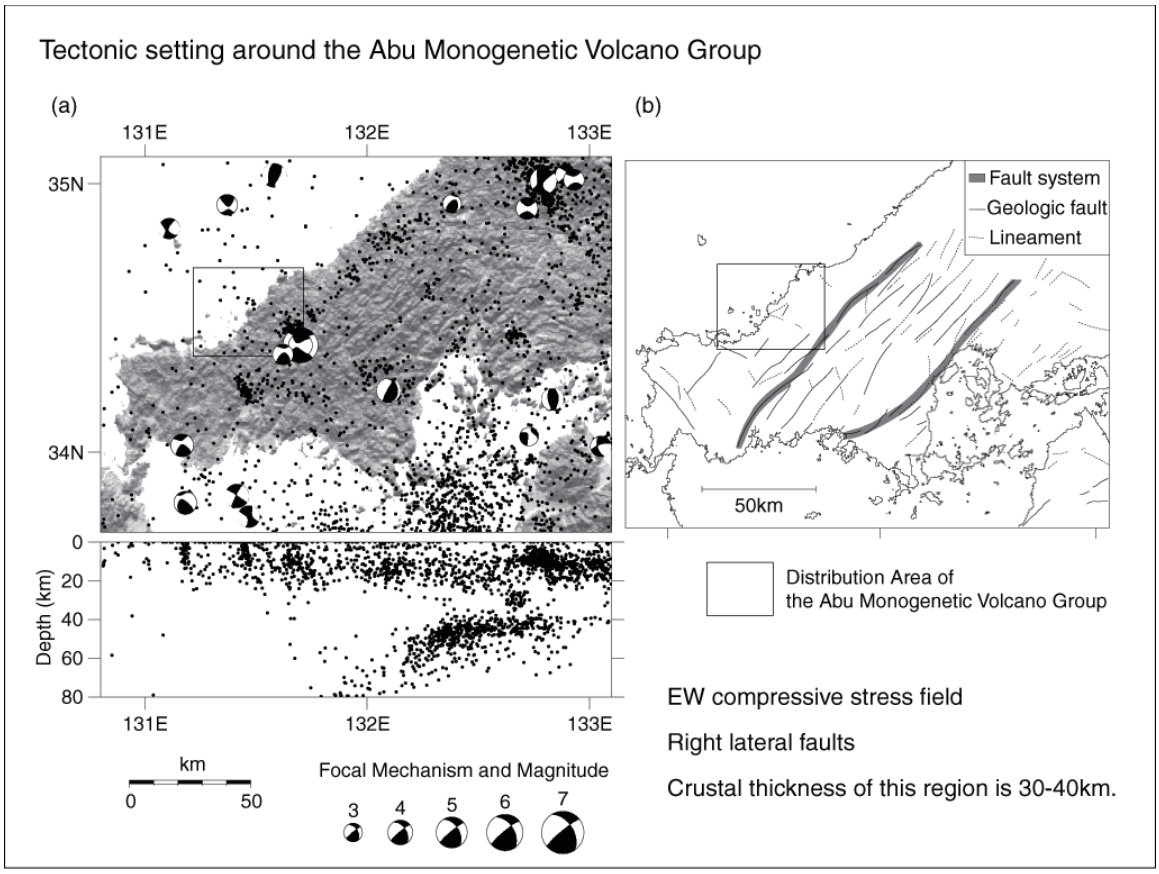

Figure 12.2. Tectonic setting around the Abu Monogenetic Volcano Group. (a) Distribution and E-W plot of earthquakes and focal mechanisms (Depth <30 km). Dots show hypocentres of earthquakes (M >2) occurred from 1988 to 1998 based on the Japan University Network Earthquake Catalogue (JUNEC). The focal mechanisms are based on a broadband data recorded in the F-net network of the National Research Institute for Earth Science and Disaster Prevention (NIED) in Japan between January in 1997 and October in 2007. Shuttle Radar Topography Mission (SRTM) used for the digital elevation model. Swarms of earthquakes occur at more than 40km in depth delineating the subducting Philippine Sea plate. Although an ENE-WSW-trending earthquake zone lies to the east, seismic activity is not high in the area of the Abu Monogenetic Volcano Group. (b) Distribution of faults and lineaments around this region modified after Kanaori (1997).

12.2.2 Determination of volcanic centres in the Abu Monogenetic Volcano Group

To analyze the temporal-spatial distribution of the Abu Monogenetic Volcano Group, we identified volcanic centres of the individual volcanic events based on topographic features and geological studies. According to the criteria of Condit and Connor (1996), individual lava flows were distinguished geologically and morphologically, and traced to their sources such as cinder cones, lava domes and topographic highs on lava flows. If a lava flow can be associated with a cinder cone or lava dome, the cinder cone or lava dome can be regarded as its source. The tops of these cones, and one dome, were recognised as volcanic centres. Some lava flows cannot be associated with cones or domes by geologic mapping. In these cases, the topographically highest point of the lava flow was considered to be the volcanic centre. Characteristic arc-shaped landforms, which were probably formed by collapse of cinder cones or lava domes, are seen on higher areas of some lava flows. The volcanic centres of these lava flows are determined at the centres of these landforms. We also identified one volcanic centre based on the presence of a depression 630 m long, 350 m wide and more than 20 m deep, because it is located on the highest part of a lava flow. Based on these criteria, 56 volcanic centres were identified in the Abu Monogenetic Volcano Group.

Eruption dates of volcanic centres were determined by relating these centres to lava flows that have previously been radiometrically dated by K-Ar methods. If several similar dates were obtained from one unit, the mean of these radiometric age determinations was used. When a variety of dates were obtained in one unit, a geologically acceptable value was deduced from stratigraphic relationships. Volumes of individual units were calculated from the distribution and thickness of lava flows, cinder cones, and similar features. For individual volcanoes and their lava flows, each considered to be an igneous event, volume ranges from 10^{-4} to 10^{-1} km^3, and the total volume of the Abu Monogenetic Volcano Group is about 4 km^3.

12.2.3 Spatial density and temporal recurrence rate

Once this dataset is compiled, the next step in the hazard assessment is to estimate spatial density and temporal recurrence rate. A two-dimensional elliptical kernel bandwidth that depends on direction is used to estimate spatial density, given by (Connor and Connor, 2008):

$$\hat{\lambda}(\mathbf{S}) = \frac{1}{2\pi N\sqrt{|\mathbf{H}|}}\sum_{i=1}^{N}\exp\left[-\frac{1}{2}\mathbf{b}^{T}\mathbf{b}\right]$$

where $\mathbf{b}=\mathbf{H}^{-1/2}\mathbf{x}$ and $\mathbf{H}$ is a 2×2 element bandwidth matrix that is positive and definite, $|\mathbf{H}|$ is the determinant of this bandwidth matrix, $\mathbf{H}^{-1/2}$ is read as the inverse of the square root of the matrix $\mathbf{H}$, $\mathbf{b}^{T}$ is the transform of the matrix $\mathbf{b}$, and $\mathbf{x}$ is a distance matrix composed of distances between the set of points $\{\mathbf{s}\}$, usually distributed on a grid to make a map in the region R, and volcanic centre locations, $\{X_1,X_2,X_3\ldots X_N\}\in R$.

A difficulty with using elliptical kernel functions is that all elements of the bandwidth matrix must be estimated. We use an optimal bandwidth selector algorithm minimising the sum of the asymptotic mean square error (SAMSE) of spatial density (Wand and Jones, 1995).

We also show a result of the least square cross validation (LSCV) of spatial density (Wand and Jones., 1995) because this kernel estimation method may indicate a relationship between crustal structure and volcanism for the Abu Monogenetic Volcano Group. For the dataset of 56 volcanic centres, the SAMSE and LSCV bandwidth selector algorithm yields:

$$\sqrt{\mathbf{H}} = \begin{bmatrix} 3.81 & 0.23 \\ 0.23 & 2.05 \end{bmatrix}$$

and

$$\sqrt{\mathbf{H}} = \begin{bmatrix} 3.89 & -1.39 \\ -1.39 & 1.19 \end{bmatrix}$$

respectively. The square roots of the matrixes are calculated to show units of bandwidth in kilometres. The diagonal elements are unequal in magnitude, indicating that the kernels are elongate and the off-diagonal elements indicate that the kernels are rotated to NNE and NW. Overall, they create NNE-trending and NW-trending bands of comparatively high estimated spatial density of volcanic centres through the map region.

Some features of volcano distribution are revealed by this method (Figure 12.3). The result based on SAMSE shows a E-W elongated broad high-density area (Figure 12.3a). This method yields a relatively smooth estimate of spatial density. In this case, spatial density is basically characterised by several modes in vent distribution. On the other hand, high-density areas based on LSCV appear as NW-SE extended narrow bands (Figure 12.3b). These bands are relatively evenly spaced, and each band contains both basaltic and andesite-dacitic volcanoes erupted at various times.

Next, we considered the temporal pattern of volcanism in the Abu Monogenetic Volcano Group. Figure 12.4a shows the cumulative number of volcanic centres and their volume. Ages of all the volcanic units have not been determined and the volume estimates of the volcanoes have some error. Nevertheless, it is possible to discuss the trend of volcanic activity assuming that samples for K-Ar dating were collected without spatial bias, and the estimated volumes reflect real changes in eruption volume.

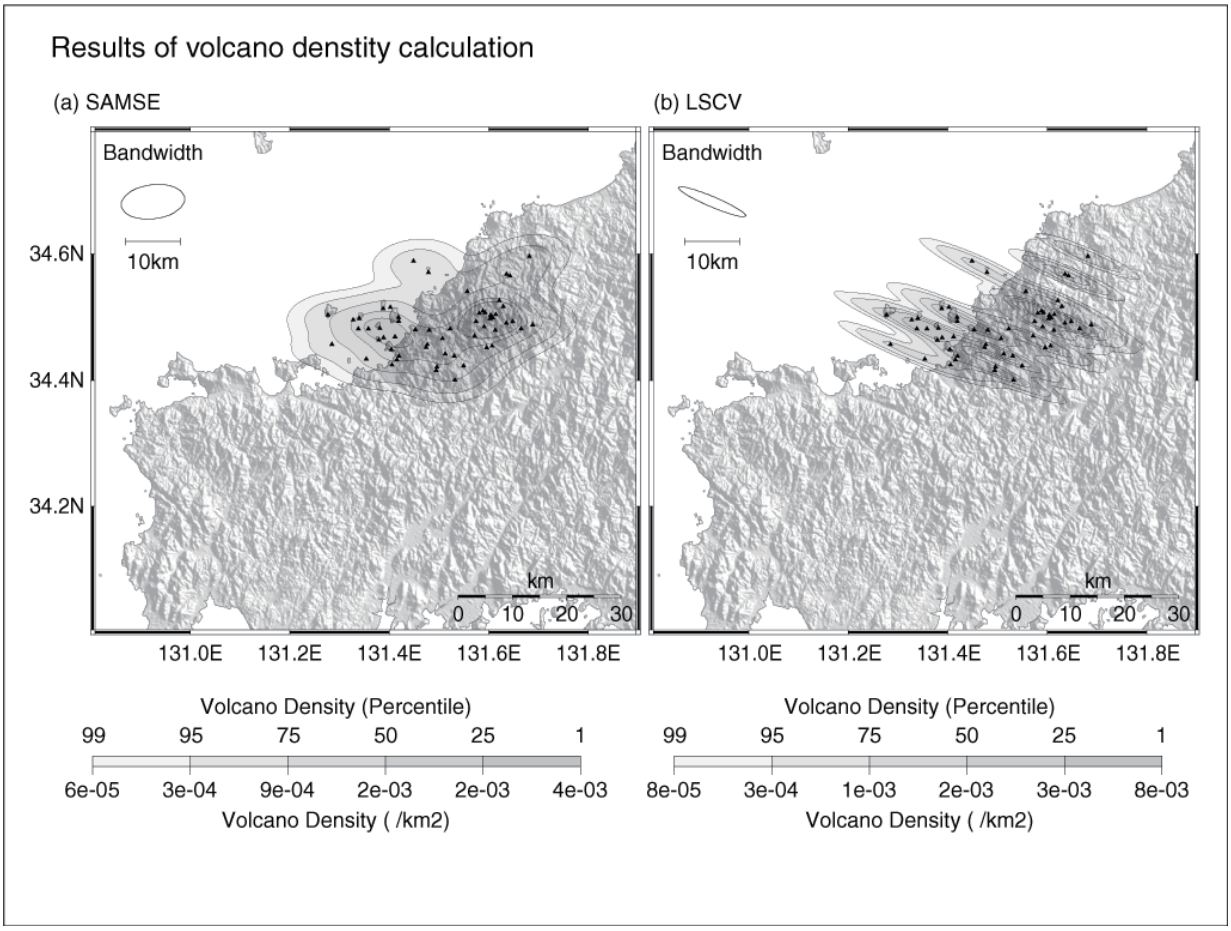

Figure 12.3. Spatial density maps of the Abu Monogenetic Volcano Group. (a) The map based on the SAMSE algorithm. The maximum density is 4.0×10^{-3}event/km^2. (b) The map based on LSCV. The maximum density is 7.9×10^{-3} event/km^2. The contour lines are 25, 50, 75, 95 and 99% percentile. The elevation data of Shuttle Radar Topography Mission (SRTM) used to draw the map.

The early activity of the Abu Monogenetic Volcano Group occurred 1.9 - 1.6 Ma, and the late activity is < 0.46 Ma. During this second episode of activity, the rate of volcanism increased, at approximately 0.2 Ma. This change corresponded to the onset of andesitic volcanism (Figure 12.4a and 12.4b). On the other hand, Figure 12.4b also shows the eruption rate of basalt decreased somewhat at this time. Although formation of both basaltic and andesitic volcanoes increased since about 0.2 Ma, the volume of individual basaltic eruptions decreased.

The early activity of the Abu Monogenetic Volcano Group was low volume and occurred in limited areas. By contrast, the later volcanism impacted a much larger area larger, including the early active parts of the volcanic field. Although the eruption rate increased about 0.2 Ma, obvious change of area of volcanic activity did occur at the time. In addition, there is no obvious difference between distributions of basaltic and andesitic volcanoes.

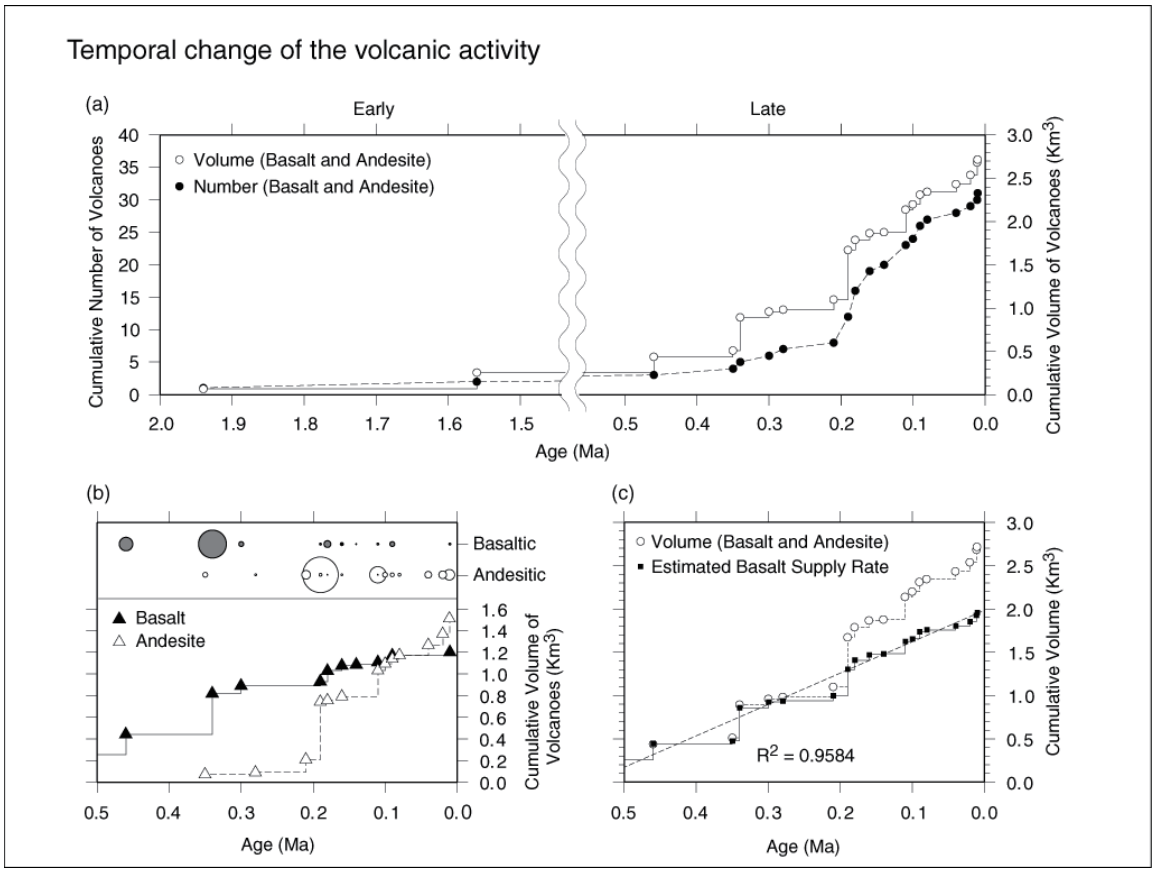

Figure 12.4. Timing of volcanism in the Abu Monogenetic Volcano Group (a) Cumulative number and cumulative volume of 31 dated volcanoes. (b) Relative and cumulative volume of basalt and andesite volcanoes during the most recent stage of activity. (c) Cumulative volume of volcanoes and estimated basalt supply rate.

12.2.4 Seismic tomography

Correlation between spatial density data and other geologic information, such as seismic tomography anomalies, can help reinforce geological modes of monogenetic volcanism, and reduce uncertainty in the application of spatial density and temporal recurrence rate models. Figure 12.5 shows P-wave tomographic images under the Abu volcanic area from the surface down to 40 km depth, which are determined by applying the tomographic methods of Zhao et al. (2002, 2007) to a large number of high-quality arrival time data of local earthquakes

recorded by the dense seismic networks operated by the Hi-net, Japanese national universities and Japan Meteorological Agency.

The image shows the perturbations (in percent) from the average velocity at each depth under Southwest Japan. The resolution scale of the tomography is 20-25 km in the horizontal direction and 5-10 km in depth. It is clear that significant low-velocity zones exist in the lower crust and uppermost mantle under the Abu volcanic area. These seismic velocity anomalies may reflect high-temperature anomalies associated with zones of dike intrusion, sill formation, and partial melting under the volcanic field. The upper crust exhibits average to slightly higher velocities with some crustal earthquakes, suggesting that shallow magma chambers do not exist under the Abu volcano field, at least in the brittle upper crust. This is entirely consistent with geological models of volcanic fields, which are thought to form due to low rates of magmatism and low rates of heat transfer in the brittle crust.

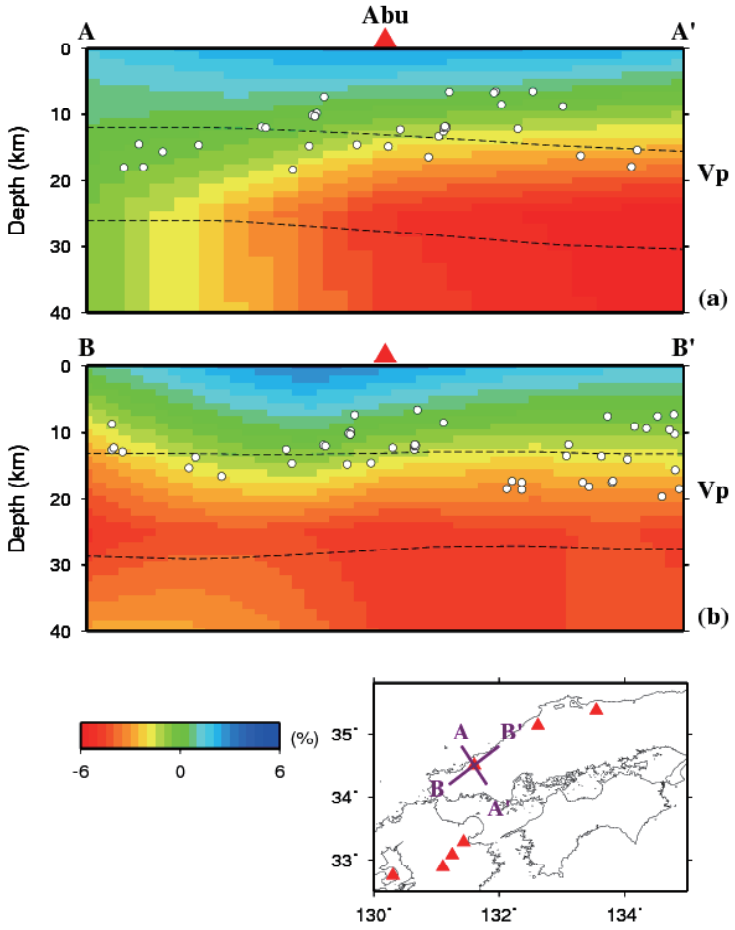

Figure 12.5. Vertical cross Sections of P-wave tomography under the Abu volcanic area (red triangle) along the profiles shown on the insert map. Red and blue colours denote low and high velocities, respectively. The velocity perturbation (in %) scale is shown at the bottom. The two dashed lines denote the Conrad and Moho discontinuities. White dots show the local crustal earthquakes (M > 1.5) occurred within 10 km of each profile.

There is a tendency that earthquake hypocentres become shallower toward the volcanic field, which also reflects the higher temperature in the lower crust right beneath the volcanic field. Such a feature of seismicity was also revealed in other active polygenetic volcanoes such as Unzen in Kyushu (Zhao et al., 2002), but has not been previously observed for monogenetic volcanic fields.

12.2.5 Discussion

The two different kernel bandwidth optimisation algorithms (SAMSE and LSCV) yield very different spatial density maps. The result based on the SAMSE algorithm provides a smoothed distribution of volcanoes in the Abu Volcano Group. The geometry of the E-W elongated high volcano density area (Figure 12.3a) suggests the shape of a magma source region. The scale of this region is consistent with the seismic tomography results, which indicate roughly the same scale of low velocity zones in the mantle and lower crust. This suggests that the SAMSE method provides a reasonable estimate of the spatial density of volcanism for the Abu Volcanic Group.

On the other hand, the LSCV algorithm identifies NNW-trending bands in the volcano distribution (Figure 12.3b). A legitimate question is whether these bands represent an important feature of volcano distribution in the Abu Monogenetic Volcano Group, for example reflecting regional structural control. If so, the likelihood of future volcanism is significantly higher in some parts of the field than in others, compared to the spatial density estimated with the SAMSE method. One geological explanation for the parallel high-density bands and their almost constant separation is that feeder dikes occur in the field in this orientation. This direction is not concordant with the azimuth of horizontal maximum compressive stress in this region (E-W). Furthermore, the compositions and K-Ar dates of volcanoes in each band are not same strongly suggesting they were fed by different dikes.

Alternatively, fractures in the crust may also affect volcano distribution. Perhaps the bands in volcano distribution reflect NNW-trending structures in the crust. However, no NW-SE lineaments and faults have been mapped in the region, and the bands do not appear to be parallel to closely spaced vent alignments, presumably related to very shallow igneous intrusions. Furthermore, the separation of bands (<5 km) are much narrower than the crustal thickness (30-40 km) of Southwest Japan, so it is difficult to relate these bands to pre-existing crustal structure.

Of these possibilities, it may be that the best explanation for the LSCV spatial density is that its complexity is an artefact of the sparse volcano density in the area, and does not reflect deep-seated geologic processes. If so, this points out that spatial density estimates require interpretation and expert judgment, in this case facilitated by comparison with seismic, seismic tomographic, and structural data.

The change in the geochemistry of magmas, and change in the eruption rates of magmas with time are important features of the Abu Monogenetic Volcano Group. In most recent volcanic activity, the andesitic magma eruption rate increased, and volumetric output of andesite was greater than basalt since 0.2 Ma (Figure 12.4b). During this change in the geochemistry of the system, the spatial distribution of volcanism did not obviously change. This is in contrast to volcanic fields in the western US, where geochemical changes in volcanic fields have correlated with changes in spatial distribution of volcanoes (e.g. Condit and Connor, 1996).

These observations support the conclusion of Kakubuchi et al. (2000) that heating from repeated intrusion of basalt caused partial melting of the lower crust and higher magma productivity in the most recent history of the volcanic field. Partial melting of the lower crust in response to continued influx of basaltic magmas is supported by the seismic tomographic Section (Figure 3.5), which clearly indicates the occurrence of low velocity anomalies in the lower crust (> 20 km depth) beneath the volcanic field.

Assuming that andesite magmas in this volcanic field result from mixing of silicic and basaltic magmas, a model can de developed for volumetric output of magma (Kakubuchi et al., 2000). Koyaguchi (1986) suggested that a silicic end member for this mixing model must have less than 70% SiO_2. Following from Kakubuchi et al. (2000), therefore, we consider the change of original basalt production by adding half the erupted volume of andesite to the erupted volume of basalt (a 1:1 mixing ratio). A cumulative plot of the result (Figure 12.4c) shows the basalt supply rate to the lower crust is almost constant since the initiation of volcanism 0.46 Ma, assuming this mixing ratio is correct.

Thus, there is a geological argument that the timing of volcanism in the Abu Monogenetic Volcanic Field is relatively steady-state. The estimated basalt productivity (Figure 12.4c) behaves as a volume-predictable model rather than a time-predictable model, with a constant supply of magma to the lower crust. On the other hand, the volume decrease of individual basaltic eruptions since about 0.2 Ma may reflect a change of regional stress field. The change of crustal conditions from cold to hot might ease the crustal differential stress. In this situation, coalesce of dikes is more difficult (Takada, 1994) and volume of individual eruptions would be smaller.

Unlike volcanic fields in the western US, for example near Yucca Mountain (Valentine and Perry, 2006), the Abu Monogenetic Volcanic Field is in a compressive tectonic setting. In such a setting, one might imagine that eruptions stop when magma pressure in feeder dike is reduced to some threshold value. In this case, little volume of magma remains in each feeder dike after eruptions under compressive stress conditions, assuming that dike walls relax sufficiently following eruptions.

In contrast, in the Coso volcanic field, California, basaltic eruptions show time-predictable relations under extensional stress condition (Bacon, 1982). It is expected that dike intrusions relieve extensional strain in roof rocks accumulated at a constant rate. In these circumstances, there would be variations in the volume of magma left in feeder dikes after eruptions depending on the extensional stress conditions. Thus, under constant magma supply, volcanic fields in compressional setting may be volume-predictable, and in extensional settings time-predictable, but not volume-predictable.

As in the case of spatial density estimation, models and data for the temporal recurrence rate of volcanism in the Abu Monogenetic Volcanic Field help constrain the expected rates of future volcanic activity. In the case of the Abu Volcanic field, a volume-predictable model appears to work best, and we have developed a model to suggest that in compressional tectonic settings with constant magma supply, monogenetic volcanism should be generally volume-predictable. In other words, the exact timing of future eruptions is uncertain, but in a given time interval a given volume of magma should erupt. Once again, it is clear that these various models of the recurrence rate of monogenetic volcanism are amenable to assessment using expert elicitation.

Having looked specifically at monogenetic volcanism, Section 12 now goes on to look at the overall, comprehensive assessment of volcanism in the Kyushu region.

12.3 Introduction to the Comprehensive Evaluation of Kyushu

We advocate the use of probability models to forecast potential future volcanic events for HLW repository sites. The primary reason for using probability models is that these models can account for the inherent uncertainties in geologic processes that give rise to complex variability in the spatial distribution and timing of volcanic events. In addition, geological models of volcanism are evolving rapidly, as new data become available and new understanding of volcanic processes is achieved.

At some point in time, the volcanic hazard assessment will be finalised for a specific site using the current state of knowledge. Application of these volcanic hazard models will be uncertain in part because they are based on the current state of knowledge. Probability models, especially when coupled to expert assessment, can transparently account for data uncertainty and model uncertainty.

As in our assessment of the Tohoku region, it is clear that there is uncertainty in the use of data to assess volcanic hazards in the Kyushu region. Figure 12.6 shows the distribution of Quaternary volcanic vents in Kyushu. Our compilation of vents is based on the analysis of map and literature data by Dr. Masaya Miyoshi of Kumamoto University and Koji Kiyosugi of the University of South Florida. A total of 240 vents were identified from the literature in the study region. These vents are further organised into 31 volcanic systems. Spatial density maps were created using these two alternative datasets (volcanic vents and volcanic systems). The organization into volcanic systems reflects the fact that individual volcanic

vents may not represent independent events. That is, some vents (e.g., cinder cones and domes) are formed at a specific location due to their association with a larger volcanic system. Thus, using all vents in the spatial analysis may bias the spatial density estimate. The 31 volcanic systems are thought to represent independent magmatic systems. That is, their distribution reflects regions of partial melting and ascent through the crust, rather than interaction at shallow crustal levels. Analysis of their distribution, therefore, indicated that areas more prone to formation of similar volcanic systems in the future. Of course, this independence is difficult to verify and a range of data sets would be considered in a site-specific hazard assessment.

Furthermore, it is noted that only Quaternary events are included in this analysis. This constraint is simply made because the Quaternary record is far more comprehensive for Kyushu than the record of pre-Quaternary volcanism. Nevertheless, it is clear that older volcanism on Kyushu may offer insight into the distribution of future volcanism, and reduce uncertainty associated with using the Quaternary record alone. In a site-specific hazard assessment, it is recommended that a longer record of volcanism be used and that the effect of using data sets encompassing different time scales of volcanism be assessed.

We developed a set of methods for estimation of spatial density of volcanism as part of the Tohoku Case Study and these were applied in the Kyushu Case study on different scales. These methods are summarised in detail in Connor and Connor (2009), Kiyosugi et al. (2009), Jaquet et al. (2008), Jaquet et al. (2009), and Mahony et al. (2009). Briefly, non-parametric kernel density functions with anisotropic bandwidths estimated by optimisation algorithms (Smoothed Asymptotic Maximum Squared Error, SAMSE) were applied in the Kyushu Case Study. Application of these methods suggests that different sites, in different tectonic settings, are best assessed using different bandwidth estimates. Consequently the analysis was repeated by subdividing volcanism into three tectonic domains, the northern Extension arc, the Southern arc, and the Back-arc, as described in the rock deformation Section of this report. Cox Process models were also applied in the Kyushu Case Study. Cox process models were refined for this study to include the use of multivariate potential, which integrates geophysical data and rock deformation data directly into the analysis.

NUMO will eventually identify a specific site for a HLW repository. In addition to development of an understanding of volcanism on a regional scale, and hence regional variations in volcanic hazard, it is important to assess how models of volcanic hazard operate on a site scale. Consequently volcanic hazard was assessed in the region about Kirishima volcano, located in the northern part of the Southern arc, to illustrate the application of these models on a local scale. These spatial density maps do not directly account for event magnitude. For example, caldera-forming volcanic events affect a much larger area of the subsurface than a one square kilometre area. The methodology of including event magnitude and its impact on probability is explored in the final Section.

12.4 Assessing volcanism on a regional scale

Figure 12.7 shows the spatial density map of volcanism calculated for all of Kyushu and adjacent areas using a single optimal kernel bandwidth. The map is dominated by zones of high spatial density in the Southern arc and Extensional arc. Volcanic events in southern Honshu (e.g., in the Abu volcanic field) also contribute significantly to spatial density.

While the kernel bandwidth creates a smooth elongate region of high volcano spatial density in the Extensional arc and in the Southern arc, the map pattern is more complicated in the Back-arc. Volcanoes cluster on Goto Island, but isolated volcanoes also occur in the Back-arc. For example, one small volume basaltic volcano on Iki island forms an isolated high in volcano density in the back-arc. This suggests that the same kernel bandwidth might not be appropriate across the entire map region and some model refinement is useful.

12.5 Assessing volcanism within tectonic domains

Several tectonic domains were identified during modeling of GPS-derived strain on Kyushu, as described in previous Sections. Volcanism lies entirely within three of these domains, the Southern arc domain in southern Kyushu, the Extensional arc domain in northeast Kyushu, and the Back-arc domain including northwest Kyushu and the Goto Island region.

These tectonic domains subdivide Kyushu in ways relevant to volcanic processes. Subduction processes dominate in the Southern arc and Extensional arc domains, and both domains are dominated by formation of large volume volcanic systems, but the geometry of the subduction zone is different in these two zones. Magmatism in the Back-arc domain is dominated by small-volume basaltic volcanism, monogenetic volcanism, and short-lived isolated centres.

It makes sense that the spatial density of volcanism would differ between these zones, given the variation in tectonic setting and the processes giving rise to magmatism. Consequently we recomputed the optimal kernel bandwidths for volcanoes within each tectonic domain and formed a composite map of the vents (Figure 12.8) and the volcanic systems (Figure 12.9) within each domain. It is clear from comparison of Figures 12.7 and 12.8 that the kernel bandwidths on these maps are not vastly different. For example, in Figure 12.8 the Back-arc domain is still dominated by isolated systems.

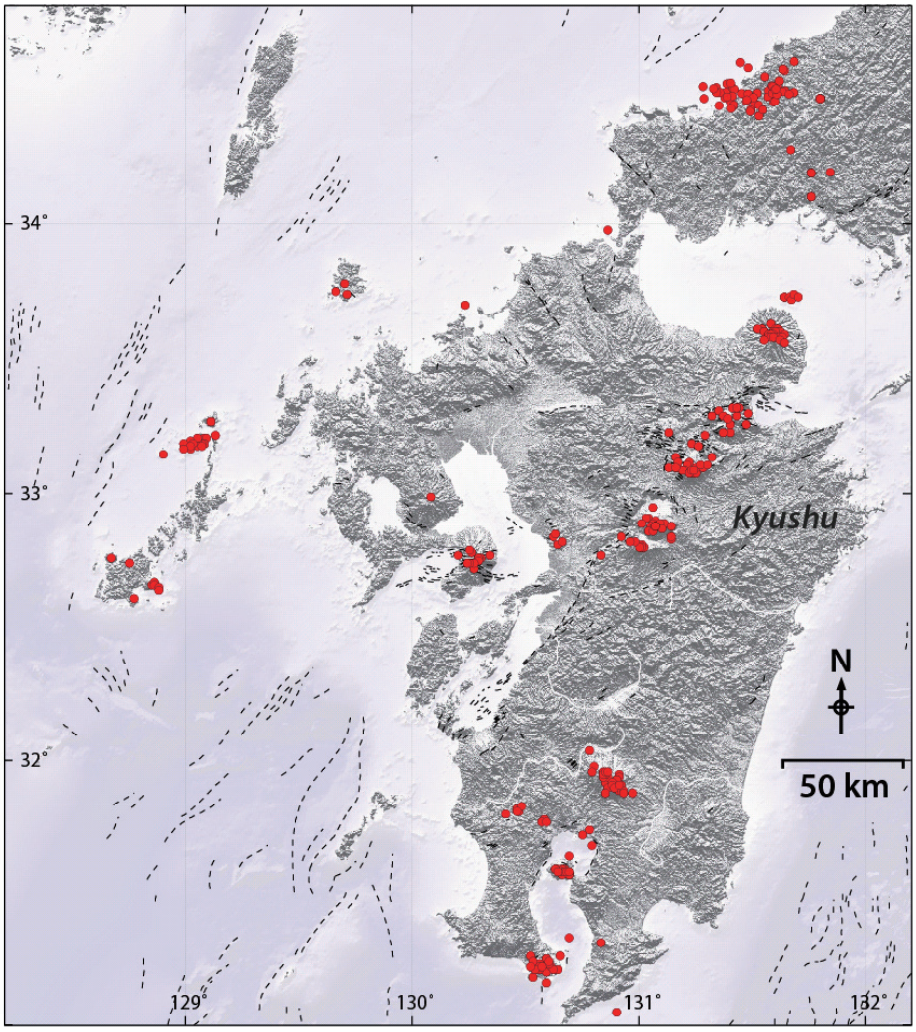

Figure 12.6: Locations of 240 volcanic vents in Kyushu and adjacent regions. Quaternary volcanic vents are shown as red circles. Faults are shown as dashed lines. Data compiled by M. Miyoshi and K. Kiyosugi.

In contrast, the map of the spatial distribution of volcanic systems by tectonic domain has a smoother structure with more pronounced differences among the kernel bandwidth estimates between tectonic domains (Figure 12.9). In the Southern arc domain, the kernel bandwidth is elongate N-S, parallel to the arc and major fault systems in this region. Similarly, in the Extensional arc domain (including Unzen volcano) the kernel bandwidth is elongate NE, also parallel to the arc and to major fault systems in this region. The most obvious change on the map involves the Back-arc domain, for which the kernel bandwidth is larger, and hence volcanic systems less isolated, that shown on previous maps of volcanic vent spatial density (Figures 12.7 and 12.8). In addition, the kernel bandwidth is trending east-northeast at a clearly oblique angle to the trend in spatial density in the Extensional arc tectonic domain.

Overall, we prefer the spatial density estimate using the tectonic domains and volcanic systems (Figure 12.9), rather than volcanic vents either on a regional scale or separated into tectonic domains (Figures 12.7 and 12.8). This preference arises because (i) there are substantial differences between optimal kernel bandwidth estimates in the different tectonic domains, and (ii) the map using volcano systems creates a smoother model in the Back-arc tectonic domain, resulting in fewer isolated centres.

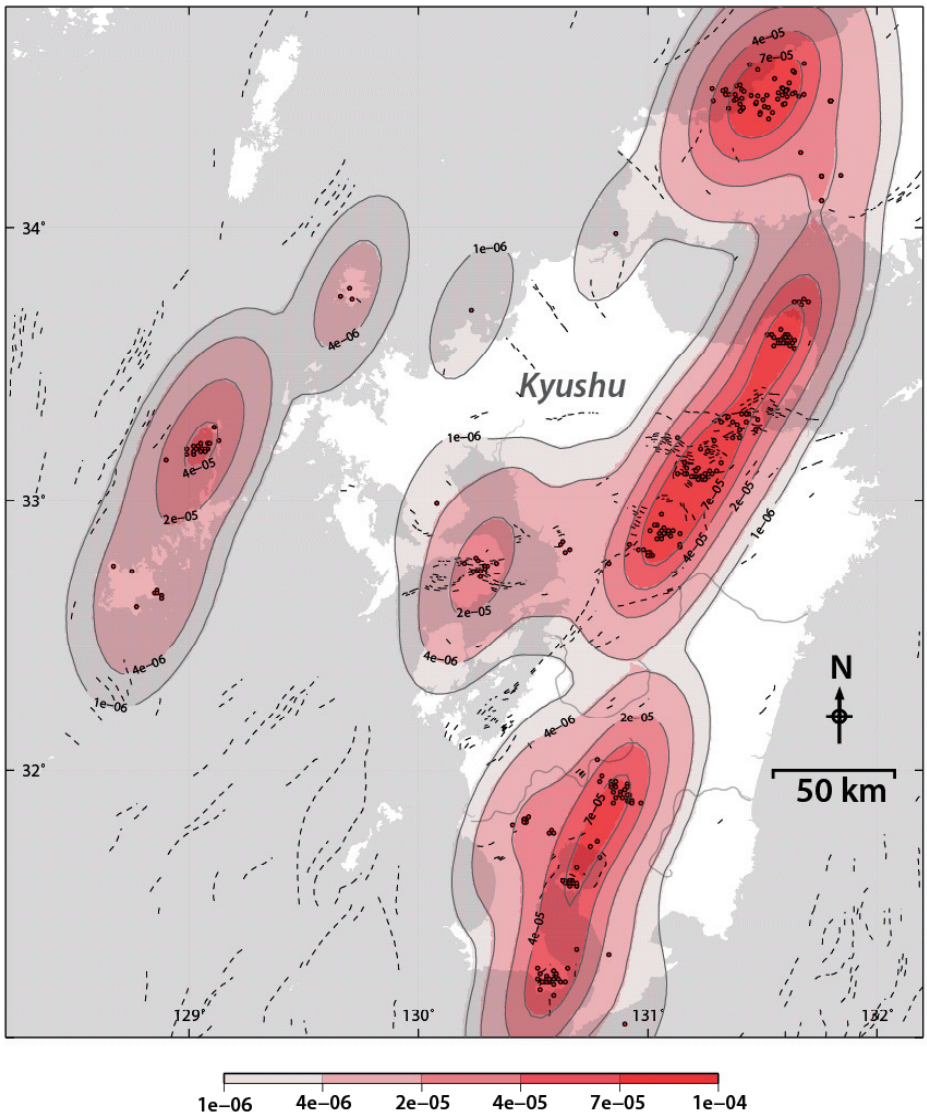

Figure 12.7: Spatial density of volcanism in Kyushu and adjacent regions calculated using SAMSE bandwidth optimisation. A single kernel is fit to the entire dataset. Thus, this regional map is not sensitive to more local changes in the pattern of Quaternary volcanic activity. The spatial density of volcanism (volcanoes per square kilometre) is contoured.

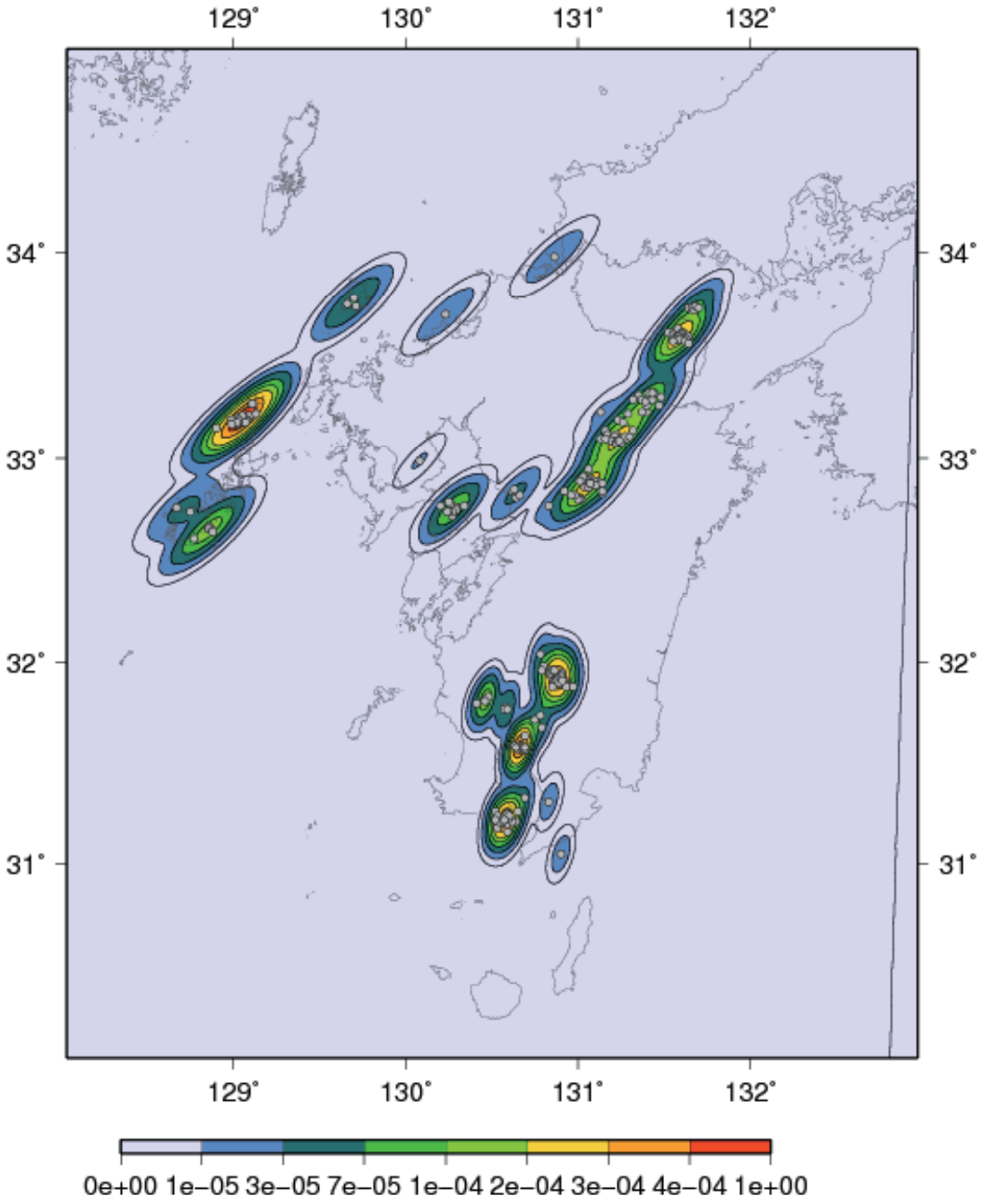

Figure 12.8. Spatial density map of volcanism in Kyushu created using different optimisation bandwidths for the Extensional arc, Southern arc, and Back-arc tectonic domains.

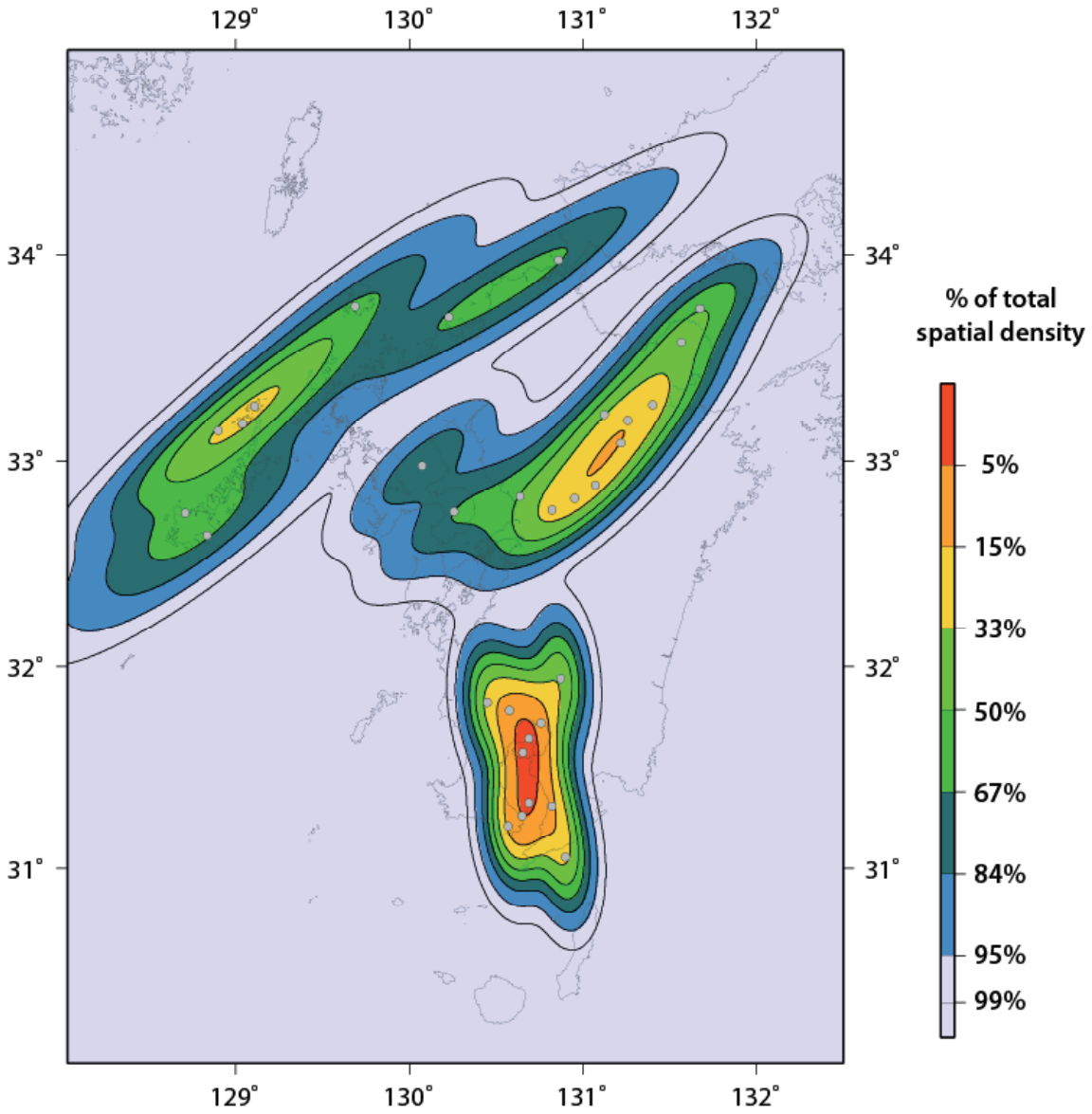

Figure 12.9: Spatial density of volcanic systems in Kyushu

12.6 Assessing volcanic hazard on the scale of individual volcanic systems

Eventually, NUMO will apply these models of a site-specific scale in order to compare and contrast a range of potential hazards in the context of performance assessment. As illustrated by Section 12.8, the scale of the investigation does influence the hazard estimate. Spatial density of volcanoes changes, depending on the event definition and the events included in the estimate (Figures 12.7 – 12.9). In this Section we explore spatial density on the scale of an individual volcanic system – the Kirishima volcano complex, located in the Southern arc tectonic domain near it northern border.

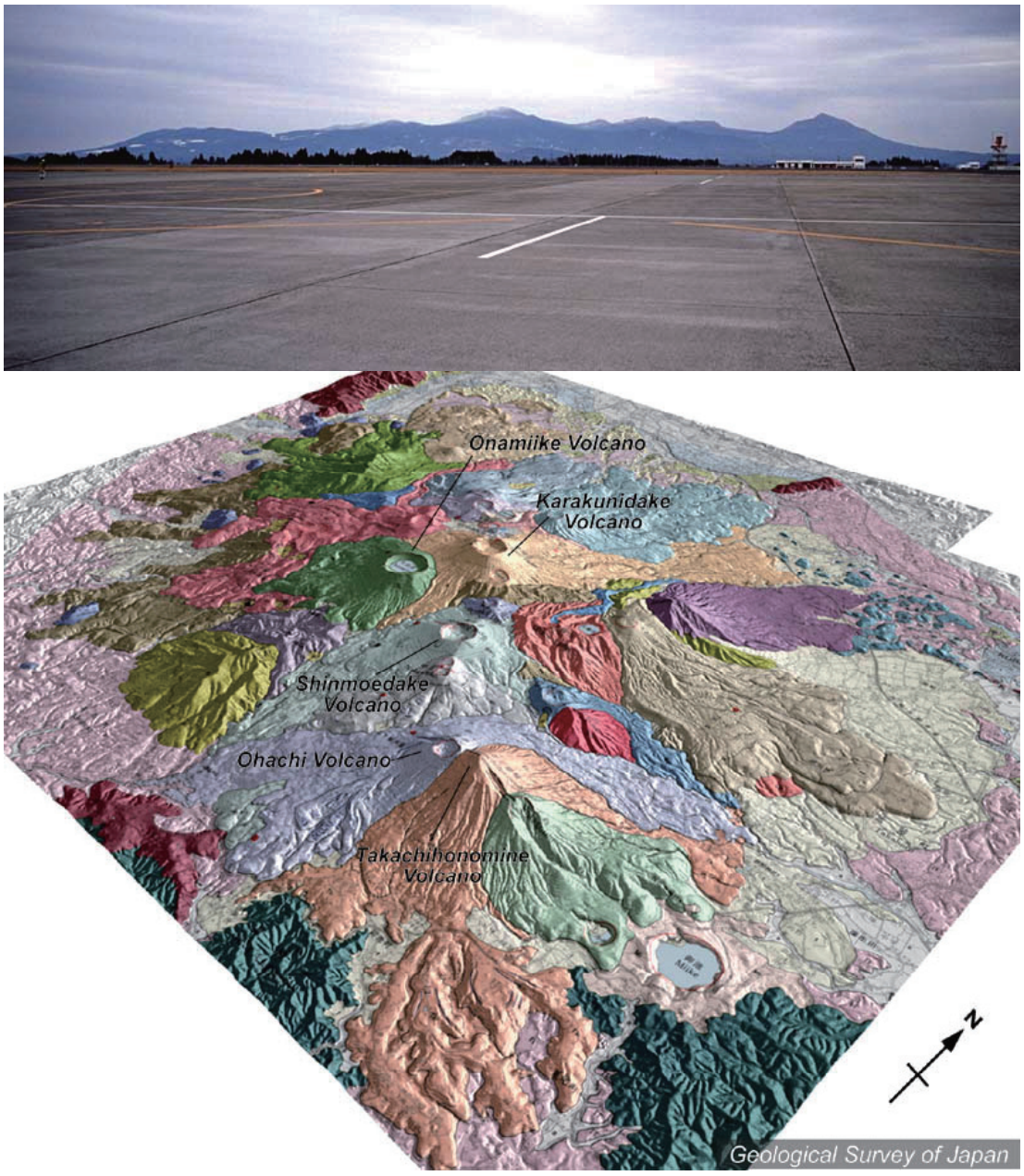

Figure 12.10: The Kirishima volcano complex consists of a number of vents. These form a NW-trending group and young to the SE (photograph: Photo Gallery of Kirishima-yama, AIST database "Quaternary Volcanoes in Japan", and perspective geological map: 11 Geologic Map of Kirishima Volcano, AIST database "Database of Japanese Active Volcanoes" , AIST permission No. 63500-A-20090824-001).

Kirishima volcano is an active volcanic system with historical volcanic eruptions and last reported eruptive activity in 2008. Kirishima comprises a group of at least 26 Quaternary volcanoes located north of Kagoshima Bay (Figure 12.10). Late-Pleistocene to Holocene volcanic activity has been dominantly andesitic and includes eruptions from composite volcanoes, pyroclastic cones, maars, and underlying shield volcanoes located over an area of approximately 20 x 30 km. The larger composite volcanoes include the 1700-m-high Karakuni-dake. Two large maars in the system are Onami-ike and Mi-ike, located SW of Karakuni-dake and at its far eastern end, respectively. Holocene eruptions have been concentrated along an E-W line of vents from Mi-ike to Ohachi, and at Shinmoe-dake to the NE (Figure 12.10). Kakuto caldera lies adjacent to this volcano complex. Overall there appears to be a trend in the spatial distribution of vents with time, with younger vents tending to be located to the southeast.

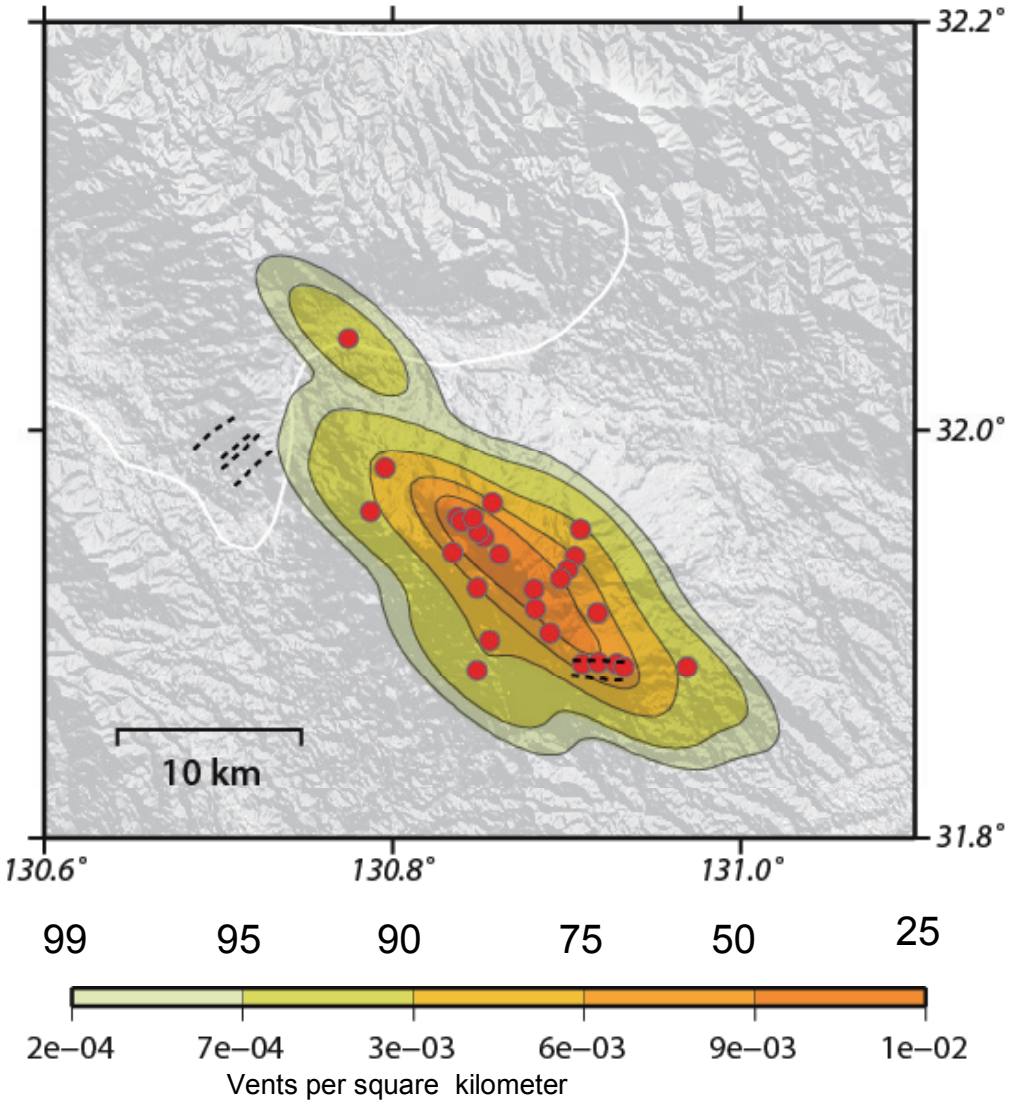

Figure 12.11: Spatial density of vents in the area of Kirishima volcano complex

Fitting an optimum kernel bandwidth to these 26 Quaternary vents emphasizes a NW-trend in the vent distribution (Figure 12.11), in contrast to the volcano systems map (Figure 12.9), which shows and overall N-S trend in spatial density of volcanic systems in the region. The estimated spatial density of volcanic vents is also much higher on the local map of Kirishima volcano (Figure 12.11) than the regional map of volcanic events (Figures 12.7 and 12.8) because of the close spacing of volcanoes in the complex, and hence the smaller bandwidth of the optimal kernel.

This scale dependence reemphasizes a basic point from the ITM Tohoku Case Study (Chapman et al., 2009), that different models are likely most appropriate for hazard evaluation at different sites. In Tohoku, we discovered that strongly clustered models were appropriate for modelling the spatial density of volcanism, and hence volcanic hazard, within the volcanic arc. These models emphasised the clustering of volcanoes along the axis of the arc. At Kirishima volcano, the volcanic vents also have a different trend than the overall trend of the arc, possibly a reflection of slab roll-back or perhaps some crustal control on dyke orientation and magma ascent. In contrast, smoother models were more appropriate for investigating volcanism in the back-arc of Tohoku, as in the Back-arc tectonic domain of Kyushu. Similarly, the model of volcano systems of the Southern arc tectonic domain emphasizes the overall N-S trend of the cluster (Figure 12.9), while the map based on vent distribution is more strongly clustered and similar to the results based on Kirishima vent distribution alone.

What scale of investigation is most appropriate for a specific site? Obviously this depends on the site and a sensible approach is to formulate a range of models using regional to local data sets and explore the differences in the resulting hazard estimates. The Kirishima example brings out an additional factor that warrants consideration, particularly on a local scale. Volcano distribution is stationary on a regional scale. That is, the geophysical processes that give rise to volcanism within the arc do not result in changes in the rate of new volcano system formation along the arc. On local scales this assumption may not be appropriate. At Kirishima volcano, vent distribution appears to change with time, with the youngest volcano vents in the southeast. This non-stationarity can be modelled, for example by weighting events based on their age or by using Markov-process models. Again, it is most appropriate at a specific site to use stationary and non-stationary models to explore the differences in hazard estimates made with these different models.

Finally, the events themselves vary widely at Kirishima volcano. The 26 Quaternary vents consist of composite volcanoes, where eruptive activity persists over time scales of 10,000 years or more, and maars characterised by single explosive events. These different events have different consequences for repository performance. For example, the formation of a new composite volcano near a repository would result in prolonged exposure to dyke injection and long-lived hydrothermal systems. In contrast, maars are short-lived, although intense, disruptive events. Incorporation of magnitude into probability estimates is discussed in the following Section.

A fundamental result of this spatial analysis is that the spatial density of volcanism varies throughout Kyushu, and this variation in spatial density appears to be related to tectonic setting. In the context of volcanic hazard assessment, it is generally much more appropriate to attempt to screen hazards based on spatial distribution of events rather than their temporal recurrence rate, which is always less well-constrained. The regional analysis of Kyushu volcanism confirms this. Whereas spatial models may be developed for the region and evaluated, temporal data, such as the time of initial formation of many of the volcanoes, is less well known. Screening of sites based on recurrence rate and temporal patterns of activity requires site specific data that are simply not available on a regional scale at this time. That said, large events, such as the frequency of caldera formation (see following sections) and detailed analyses of specific site areas, will yield sufficient temporal models, where it is necessary to do so.

12.7 Event Magnitude and Probability Estimates

What is the probability of disruption of the repository directly by magma? Several factors must be considered to address this question including:

- Definition of the disruptive volcanic event
- Estimation of the recurrence rate of these events
- Estimation of the spatial density of these events
- Definition of the repository area and performance period

- Method of calculating probability

In the following Sections, the probability of a caldera-forming event is considered for a repository footprint of 25 km^2 and performance period of 100,000 years.

12.7.1 Event definition

For caldera-forming eruptions, the event is the formation of a new caldera system. Nine caldera systems have formed in Kyushu (including islands just south of Kyushu) during the last approximately one million years. Although some of these calderas have experienced multiple large eruptions (e.g., Aso caldera) we are primarily concerned with the formation of new caldera systems that may disrupt the site of a geological repository in the future. The effects of caldera eruption at the surface are widespread, and in fact the effects of such eruptions can be global in scale. However, from the point of view of geological repositories, we are concerned with the potential of disruption of the repository in the subsurface and consequent transport of radionuclides into the biosphere. Thus, to a first order the effects of the caldera-forming eruption in the subsurface are confined to the lateral extent of the caldera itself.

Caldera eruptions potentially disrupt large volumes of rock in the shallow subsurface – at repository depths. At the surface, calderas in Kyushu range in diameter from about 4 km (e.g., Ikedo-ko caldera) to roughly elliptical structures of diameter 25 x 18 km (e.g., Aso caldera). The average radius of Quaternary calderas in Kyushu is 7 km. For the purposes of this example analysis, the disruptive event is defined as a circular caldera that is 7 km in radius. It is assumed that rock within a 7 km radius of the centre of a caldera is completely disrupted. A repository in such a zone would experience disruption by magma injection, rock deformation, and the development of hydrothermal systems. Caldera-forming eruptions are of sufficient volume and intensity that they may potentially transport HLW directly to the surface.

For assessment of a specific site, this event definition can become more complicated to reflect a range of possible processes. For example, a probability distribution of caldera shape and radius might be developed. Hydrothermal systems can develop beyond the geographic boundaries of calderas and such secondary effects might be considered. Similarly, other types of volcanic phenomena (e.g., dyke injection associated with monogenetic volcanism) may be considered using appropriate geometries for such events. In volcanic hazard assessment studies for the proposed Yucca Mountain repository, a library of events was constructed and this library of events was used in the probabilistic assessment of disruption of the planned repository by volcanic events.

Event: *The formation of a new caldera system, 7 km in diameter. The analysis, therefore, considers the probability of a given geographic location falling within 7 km of the centre of one or more new calderas of this radius, formed during the performance period of the HLW repository. It is assumed that the repository itself does not influence the probable future distribution of such events.*

12.7.2 Recurrence Rate of Caldera Events

Numerous models are extant in the volcanological literature to estimate the recurrence rate of volcanic events. For rare geological events, such as the formation of new calderas, Ho (1991) has shown that a maximum likelihood estimate of the recurrence rate of volcanic events is:

$$\lambda_t = \frac{N-1}{t_o - t_y}$$

where N is the number of events having occurred within the time interval defined by the oldest event (t_o) and the youngest event (t_y).

In Kyushu, nine calderas have formed since 1 Ma. The oldest of these calderas, Shishimuta caldera, is thought to have formed 0.99 Ma and the youngest of these calderas, is thought to have formed 0.01 Ma. Therefore a maximum likelihood estimate of the rate of caldera formation in the Quaternary is 8 events per one million years.

Recurrence rate: *The maximum likelihood estimate of caldera-forming events in Kyushu is λ_t = 8 events per million years, based on the geologic record of known caldera formation in the Quaternary.*

12.7.3 Spatial Density of Caldera Events

As illustrated in this report, the spatial density of volcanic events may be estimated using a variety of techniques, such as the Cox Process and the nonparametric kernel density models. In analysis of volcanic hazards at a specific site, it is recommended that a variety of models be used, as the results give a sense of epistemic uncertainty in the probability estimate.

Here we use the nonparametric kernel density model to estimate spatial density of caldera-forming events in Kyushu. We base the spatial density on the distribution of calderas and other volcanic systems formed in the Quaternary in the Extensional- and Southern arc tectonic domains, including composite volcanoes such as Kuju in the spatial density estimate. The reason for including composite volcanoes is the assumption that the distribution of these volcanoes provides additional information about the possible location of calderas that may form during the next 100,000 years. Volcanoes in the Back-arc tectonic domain are not included in this spatial density estimate because there is no evidence of caldera formation in the back-arc during the Quaternary. The distribution of these monogenetic volcanoes is not thought to be an indication of the location of possible caldera formation.

Spatial density: *The spatial density λ_s is estimated from the distribution of volcanic systems in the Extensional and Southern arc domains of Kyushu. These values are convolved with the event magnitude (7 km radius caldera) to estimate the magnitude-weighted spatial density, $\lambda_{s,M}$. The magnitude-weighted spatial density is the probability that a given small region (the repository area: 25 km^2) will be disrupted by a caldera-forming eruption, given that such an eruption occurs within the region.*

12.7.4 Calculation of probability

The probability of one or more caldera-forming disruptive events can then be estimated using Poisson's equation. The probability that an event will occur during the performance period of the repository, here taken to be 100,000 yr is:

$$P_1[N \geq 1] = 1 - \exp\left[-\lambda_t \Delta t\right]$$

where:

$$\lambda_t = 8 \times 10^{-6}\, events \cdot yr^{-1}$$

$$\Delta t = 100000\, yr.$$

The probability that a repository site will be disrupted, given an event in the region, is:

$$P_2[N \geq 1] = 1 - \exp\left[-\lambda_{s,m}\right]$$

where $\lambda_{s,M}$ is the magnitude-weighted spatial density. Then the probability of disruption of any portion of the repository directly by caldera formation is:

$$P[N \geq 1] = P_1 \times P_2$$

Figure 12.12 illustrates the probability estimates for such an event across the entire map region. Probabilities range from >0.1% in some locations within the active volcanic arc <1 x 10^{-5}% across wide regions of the back-arc and forearc.

These calculations and map (Figure 12.12) are provided simply to demonstrate a methodology for estimating probability of volcanic disruption of a potential repository site. It is emphasised that for a specific site, a range of models and model assumptions would be used to estimate probability and to estimate uncertainty in these estimates. Such an investigation is facilitated through the use of expert judgment.

It is useful to compare the probabilities of disruption of a 25km^2 location by a caldera-forming eruption. Eleven locations are shown in Figure 12.12. These example locations illustrate the range in probabilities across the region and are the same as those illustrated in the previous, rock deformation Sections of this report.

Probabilities at these sites (see Table 12.1) range from 6.9 x 10^{-12} at location 11 in SW Honshu to 1 x 10^{-2} at location 3 in the northern extensional arc. In general, sites located in and near the southern arc and northern extensional arc have the highest probabilities. These probabilities decrease quickly away from the arc, but particularly in the forearc (e.g., locations 8 and 6. Note that locations 1 and 11 in the backarc have low probabilities of being disrupted by caldera-forming eruptions. Location 11, however, is near the Abu monogenetic volcanic group. Although the probability of caldera-forming eruptions is low at this location, other types of volcanism, such as dyke intrusion during monogenetic volcanism would need to be analyzed as part of a comprehensive volcanic hazard assessment.

Table 12.1: Probability of a caldera-forming eruption disrupting a 25 km^2 area during a 100,000 year performance period, calculated at each example site location.

Example Location	Probability of Eruption
1	2.6 x 10^{-4}
2	5.3 x 10^{-6}
3	1.0 x 10^{-2}
4	5.7 x 10^{-3}
5	3.6 x 10^{-3}
6	1.3 x 10^{-8}
7	1.3 x 10^{-3}
8	1.4 x 10^{-3}
9	5.3 x 10^{-3}
10	9.2 x 10^{-3}
11	6.9 x 10^{-12}

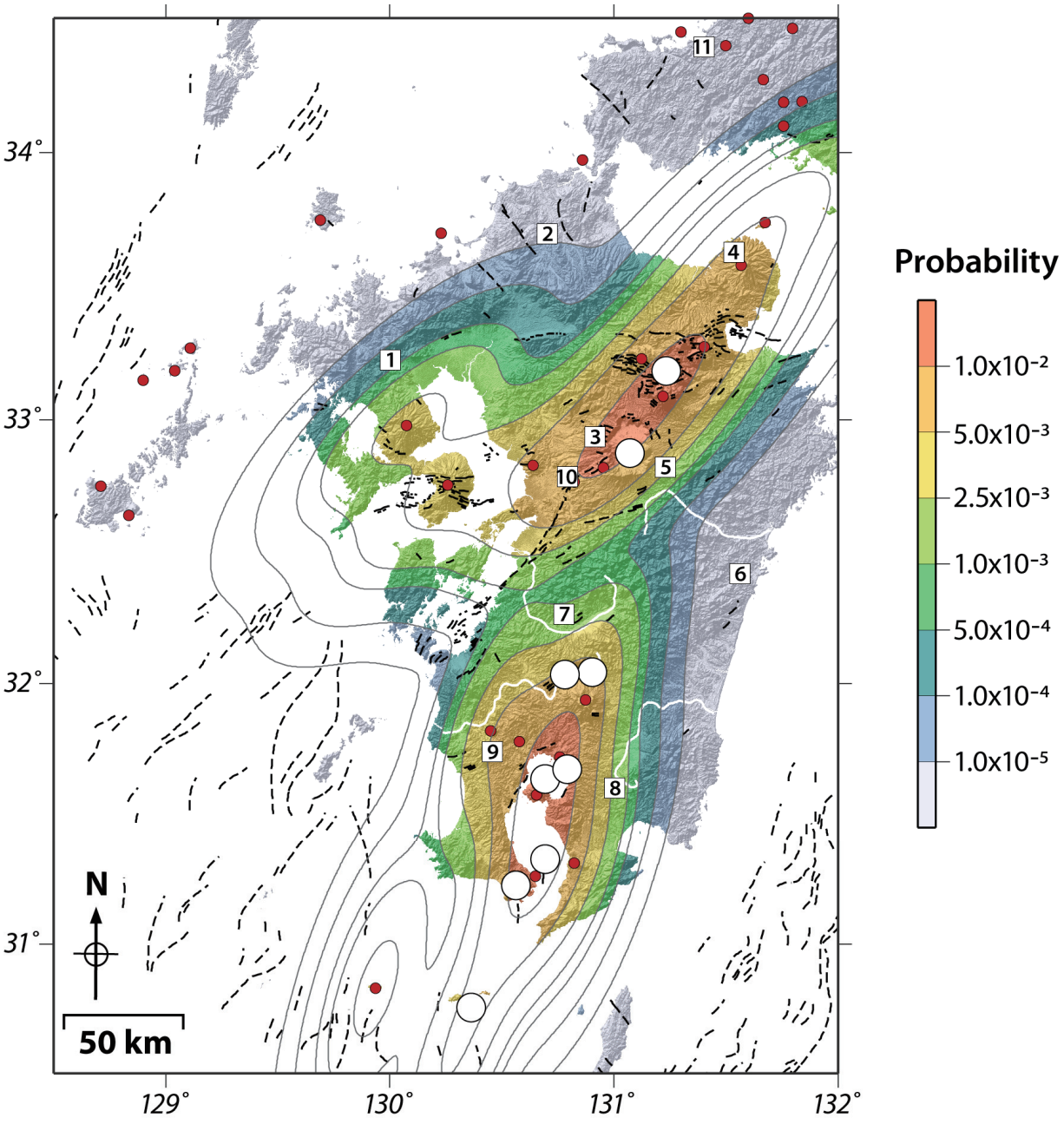

Figure 12.12: Map showing the probability of a caldera-forming event in the next 100,000 years. The red circles represent the volcanic events used to calculate volcano spatial density. The white circles represent known calderas. The numbered white squares are example site locations where probability values are known and can be compared (see Table 12.1). Volcano spatial density is based only on those volcanic events located within the northern extensional arc and the southern arc. Zones of increasing probability are coloured from blue to orange. The colour coding is clipped at the sea-land border although the contour lines extend into both regions.

12.8 Estimation of volcanic hazard using a Cox process with a multivariate potential

The Cox process constitutes the second stochastic model that was applied for the estimation of volcanic hazard in Kyushu. Besides describing the distribution of volcanic events, the Cox process enables the uncertainty characterisation related to its intensity function, considered as random. Therefore, this stochastic process becomes doubly stochastic and corresponds to a generalisation of the non-homogeneous Poisson process applied when using kernel density methods.

For the Kyushu Case Study, developments were undertaken in order to extend the assimilation capabilities of the Cox process with respect to additional data types, such as rock deformation and age data.

First, the conceptual elements are given that constitute the basis for the model development, and then the stochastic model is presented followed by its application to the Kyushu Case Study. The volcanic hazard estimation was performed at the scale of the whole island as well as in relation to specific tectonic domains determined by rock deformation analysis.

12.8.1 Conceptualisation

The stochastic model is based on the following conceptual elements and hypotheses related to the current geoscientific knowledge:

- The distribution of Quaternary volcanic events presents spatial patterns described using a random potential of volcanism.
- The spatial distribution of events is statistically correlated to the geophysical signature of crustal and mantel structures.
- The spatial distribution of events is statistically correlated to the location of active faults.
- The spatial distribution of events is statistically correlated to strain rates obtained from rock deformation modelling.
- Future events are likely located in zones of past activity and their location presents some degree of statistical correlation with geophysics and rock deformation data.

12.8.2 Model development

The notion of potential of volcanism (Jaquet et al., 2009) is applied for the characterisation of volcanic events; it is defined as the propensity of a given region to be affected in the future by volcanic events. The potential of volcanism, being unknown, is considered as randomly structured within the context of the stochastic model. Such randomly structured behavior can be detected and parametrised using the variogram. While the structured part represents the current geoscientific knowledge, the random part corresponds to the uncertainty associated with this information. Using the potential of volcanism allows for the description of volcanic events in terms of statistical distribution and scale of spatial patterns as well as for the integration of additional relevant information such as geophysics and rock deformation data.

The probability of new volcanic events occurring within a small domain of the region of interest is estimated using the Cox process (Lantuéjoul, 2002):

$$P\{N_i = n\} = E\left(e^{-Z_i}\,\frac{Z_i^n}{n!}\right)$$

The volcanic region of interest is partitioned into small domains, where the random potential of domain A_i is denoted by Z_i and $E(\ )$ is the mean. The potential corresponds to the mean number of volcanic events in domain A_i and is interpreted as a realization of a random intensity function. In addition, the numbers of volcanic events within disjoint domains are no longer independent, due to the structured behaviour of the random potential modelling the observed patterns. In comparison, the potential of the non-homogeneous Poisson process (cf. kernel density methods) is described using a smooth deterministic intensity function, and the numbers of volcanic events remains independent within disjoint domains.

The multivariate character of the random potential is modelled by introducing the following dependence relation between the Gaussian potential Y_i^Z and additional data Y_i^S and Y_i^T, expressed in Gaussian space:

$$Y_i^Z = \left(\frac{\rho_{ZS} - \rho_{ZT}\rho_{ST}}{1-\rho_{ST}^2} \right) Y_i^S + \left(\frac{\rho_{ZT} - \rho_{ZS}\rho_{ST}}{1-\rho_{ST}^2} \right) Y_i^T + f(\rho_{ZS}, \rho_{ZT}, \rho_{ST})\, Y_i^R$$

Where ρ_{ZS} represents the correlation between potential and geophysical data; ρ_{ZT} corresponds to the correlation between potential and tectonic data; and ρ_{ST} is the correlation between geophysical and tectonic data. Under the assumption that the correlations for the potential prevail, it follows:

$$Y_i^Z = \rho_{ZS}\ Y_i^S + \rho_{ZT}\ Y_i^T + \sqrt{1-\rho_{ZS}^2-\rho_{ZT}^2}\ Y_i^R$$

In the developed model, the potential of volcanism assimilate multiple statistical correlations, since it presents dependencies with past volcanic activity as well as with geophysical and tectonic data.

The estimation of volcanic hazard is performed by simulating the distribution of volcanic events likely to occur during a certain period of time in the future within the region of interest. In addition, the simulation has to deliver volcanic events that are more likely to be located in zones of past activity. Therefore, the simulation requires to be conditioned to the number of past volcanic events known in each domain A_i. The idea is to simulate the potential of volcanism conditioned on the number of volcanic events and on the geophysical and tectonic data known for the analyzed region. Based on the iterative algorithm, given in Jaquet et al. (2008), the following extended algorithm is proposed for the multivariate conditional simulation of the potential:

(i) generate $Y_i^R \sim Gaussian(0, 1)$ *for each* A_i *;*

(ii) select an index i *at random;*

(iii) generate $y_0 \sim D\left(Y_i^R \mid Y_j^R = y_j^R,\ j \neq i\right)$;

(iv) compute $y_i^S = \phi_S^{-1}(s_i),\ y_i^T = \phi_T^{-1}(T_i)$ and

$$z_0 = \phi_Z\left(\rho_{ZS}\ y_i^S + \rho_{ZT}\ y_i^T + \sqrt{1-\rho_{ZS}^2-\rho_{ZT}^2}\ y_0\right);$$

(v) generate $n_0 \sim Poisson(z_0)$;

(vi) if $n_0 = n_i$ *; then put* $y_i^R = y_0$ and $z_i = z_0$;

(vii) go to (ii).

In its design, the algorithm runs forever. In practice, it is stopped when each potential z_i has been effectively updated more than several hundred times.

The simulated potential z_i is representative only of the period of time t_p at which all data originate. For the simulation of volcanic events, occurring in a future period of time t_f, the future potential z_i^f is required. Its estimation requires the simulation of the distribution of volcanic events likely to occur during a certain interval of time in the future. Such simulation is performed using the Cox process with a random potential in time:

$$P\{N_k = n\} = E\left(e^{-Z_k}\ \frac{Z_k^n}{n!}\right)$$

where N_k is the number of volcanic events in a time interval τ_k, partitioning the time series of interest, and Z_k its corresponding potential. The time series of interest describes the occurrence of past volcanic events during a given period, e.g. the Quaternary. Therefore, along the time axis, each volcanic event is therefore characterised by its age; generally taken as the age of the onset of volcanic activity. The period under study is partitioned into small time intervals; the analysed variable is then the number of events that have occurred in these time intervals. The characterisation of the past behaviour of volcanic events enables to simulate the distribution of the number of events likely to occur in a future time interval with a given duration, for example, of 100,000 years. In general, future volcanic activity is not independent of the volcanic patterns that have occurred in the past. Therefore, this additional complexity requires the application of Monte Carlo Cox simulations for the estimation of the future potential in time, z_k^f. This leads to the following algorithm to simulate the future volcanic events n_i^f:

(i) compute $z_i^f = z_i \cdot \left(t_f / t_p\right) \cdot \left(z_k^f / z_{Poisson}\right)$ *for each* A_i *;*

(ii) generate $n_i^f \sim Poisson\left(z_i^f\right)$ *for each* A_i *.*

The conditional simulation algorithm allows the estimation of volcanic hazard for each domain of the region of interest during the period of time considered. A Monte Carlo approach (cf. Figure 12.10) is performed using several thousand simulations in order to derive stable probability estimates for the future volcanic events:

$$P\left\{N_i^f \geq 1\right\} \approx \frac{1}{K_{sim}} \sum_{k=1}^{K_{sim}} 1_k\left(n_i^f \geq 1\right)$$

where K_{sim} is the total number of simulations and $1_k\left(n_i^f \geq 1\right)$ equals 1 when the k^{th} simulation assigns the domain A_i one or more volcanic events, and 0 otherwise.

The estimation of volcanic hazard was carried out at the scale of Kyushu and for two tectonic domains: the Extensional arc domain and the Southern arc domain.

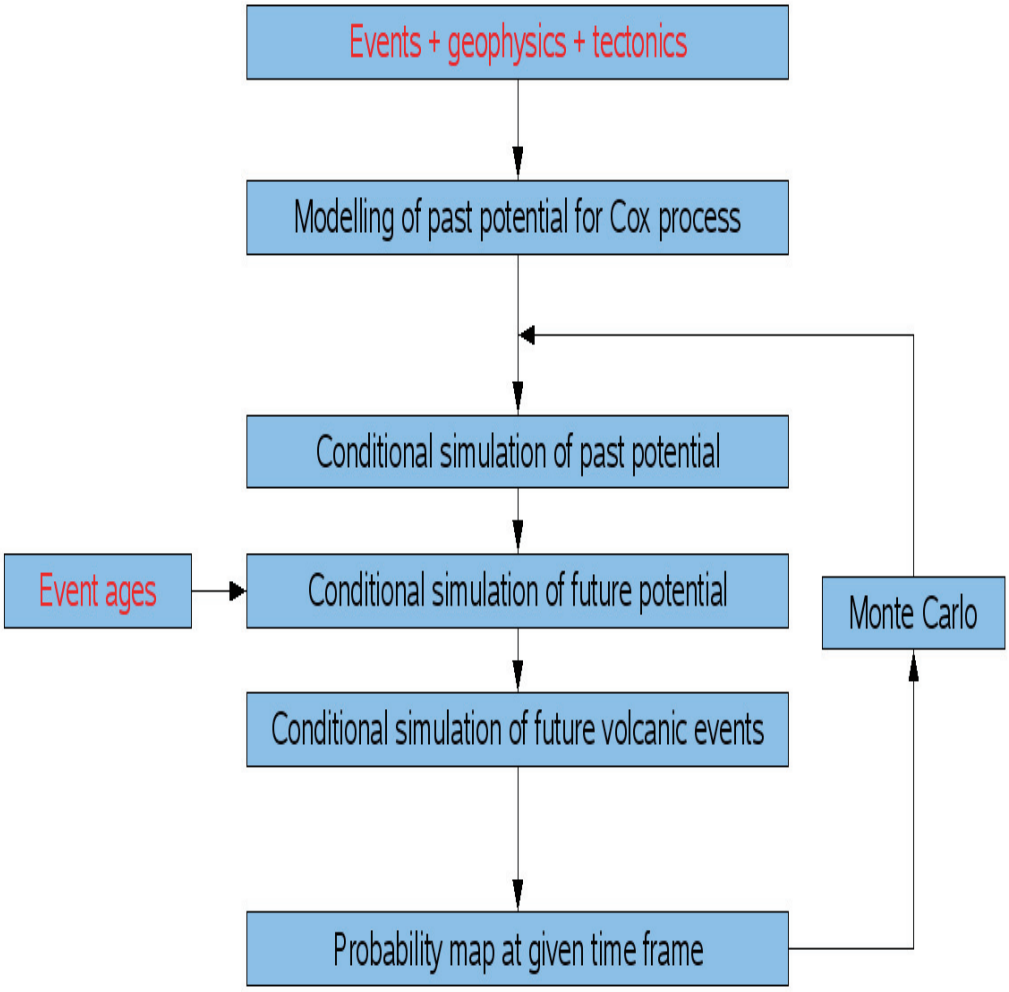

Figure 12.10: Cox stochastic modelling with assimilation of multivariate datasets for the estimation of volcanic hazard.

12.8.3 Application at regional scale to Kyushu

The datasets used for the hazard assessment comprises (Figure 12.11):

- 240 Quaternary volcanic events compiled by Masaya Miyoshi (Kumamoto University) and Koji Kiyosugi (South Florida University) from a literature search.

- 76 active faults from the dataset of the Active Fault Research Centre (AFRC) of the National Institute of Advanced Industrial Science and Technology (AIST) (http://www.aist.go.jp/RIODB/activefault/index_eng.html) and from the analysis of the additional digital datasets described in Section 8.1.

- Regional digital map of gravimetric anomalies (Geological Survey of Japan, AIST, 2002b).

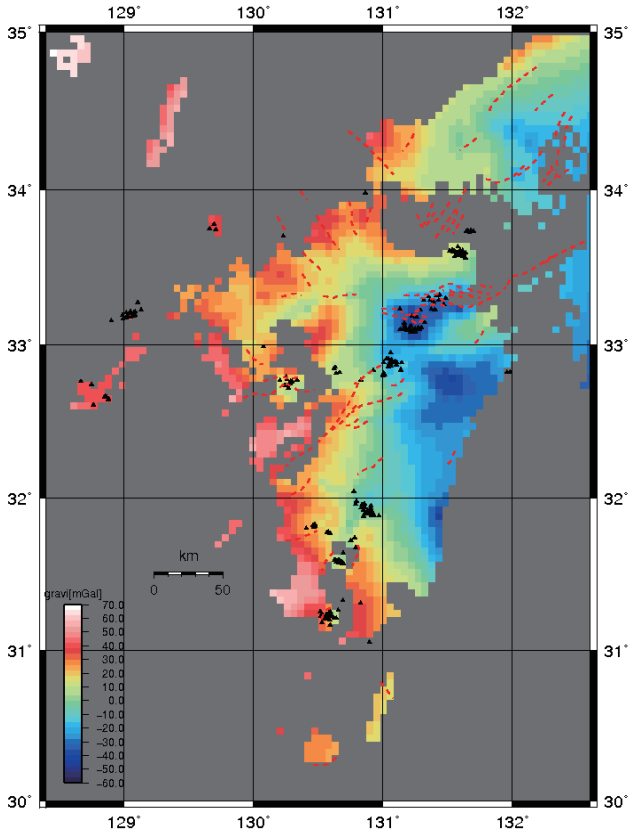

Figure 12.11: Datasets for Kyushu, with Quaternary volcanic events (black triangle), active faults (red dashed line) and gravimetric anomalies (colours).

The spatial variability of fault data was characterised using the density of faulting expressed in terms of cumulative fault length, L_c, in domain A_i (Figure 12.12):

$$L_c(A_i) = \sum_j l_j$$

Where l_j is the length of fault j within the domain A_i.

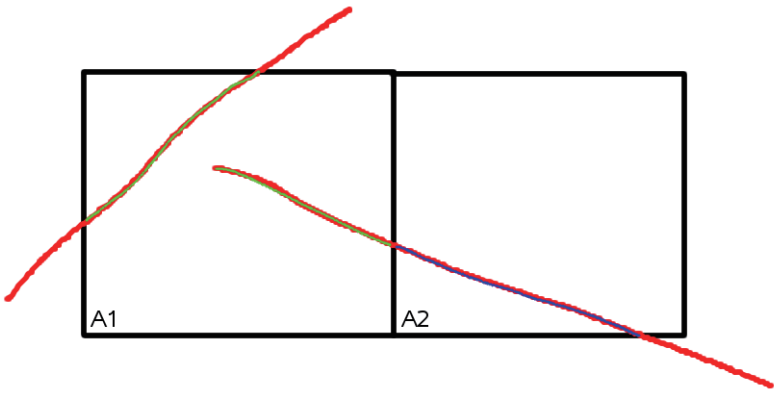

Figure 12.12: Cumulative fault length for domains A1 (in green) and A2 (in blue).

The size of domain A_i is 5 km x 5 km, which corresponds to the representative area selected by the ITM methodology to include a geological repository. The cumulative fault length was estimated at the regional scale of Kyushu (Figure 12.13).

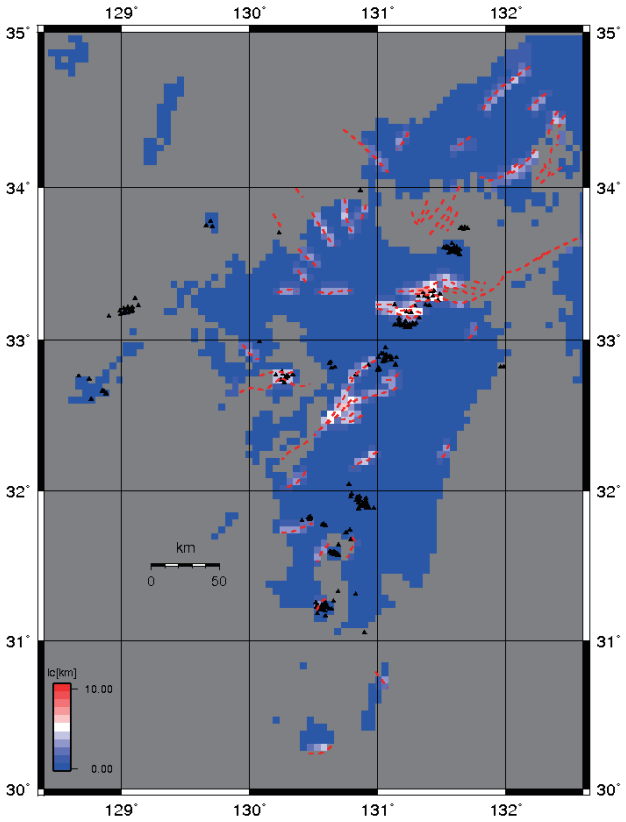

Figure 12.13: Cumulative fault length for Kyushu for 5 km x 5 km domain.

For the estimation of volcanic hazard for Kyushu, the potential of volcanism assimilates the following spatial distributions: (a) Quaternary volcanic events, (b) gravimetric anomalies and (c) cumulative lengths of active faults. All of these datasets were sampled at a 5 km x 5 km for the whole of Kyushu island. The parameters required for the simulation of the potential were estimated using the methodology described in Jaquet et al. (2009); their values are given in Table 12.2. Past and future potential in time were assumed proportional; i.e. $z_i^f = z_i \cdot \left(t_f / t_p \right)$. Using the Cox model, simulations of future volcanic events were performed over a period of 0.1 Ma for Kyushu. 10,000 Monte Carlo simulations were carried out to obtain stable probability estimates. These results were displayed in form of a volcanic hazard map for Kyushu (Figure 12.14).

Table 12.2: Parameters for Kyushu island.

Case	ρ_{ZS} *	ρ_{ZT} **	Variogram correlation scale	Time component
I	-0.18	0.40	50 km	proportional

* S: gravimetric data; ** T: cumulative fault length.

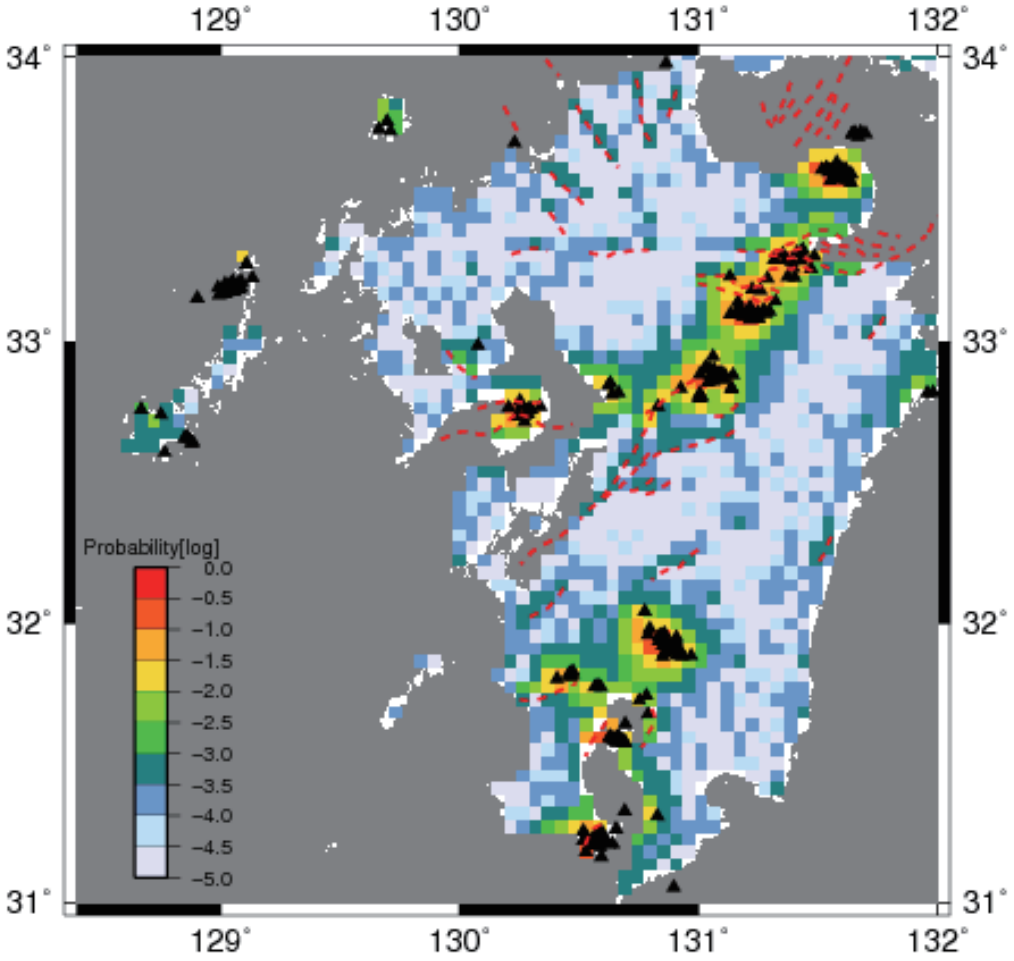

Figure 12.14: Volcanic hazard map for Kyushu displaying the probability of one or more volcanic event for the next 100,000 years and 5 km x 5 km domain (case I).

12.8.4 **Application to Kyushu Tectonic Domains**

The datasets used for the hazard assessment of the two tectonic domains comprises the following data types (Figure 12.15):

- **Extensional arc domain**: 87 Quaternary volcanic events, 31 active faults and strain rates from GPS data.

- **Southern arc domain**: 86 Quaternary volcanic events, 28 active faults and strain rates from GPS data.

The GPS data is from the Geographical Survey Institute's CGPS network called Geonet (http://mekira.gsi.go.jp). The strain was calculated after removing a subduction coupling component that was estimated; more details can be found in Section 9.2.

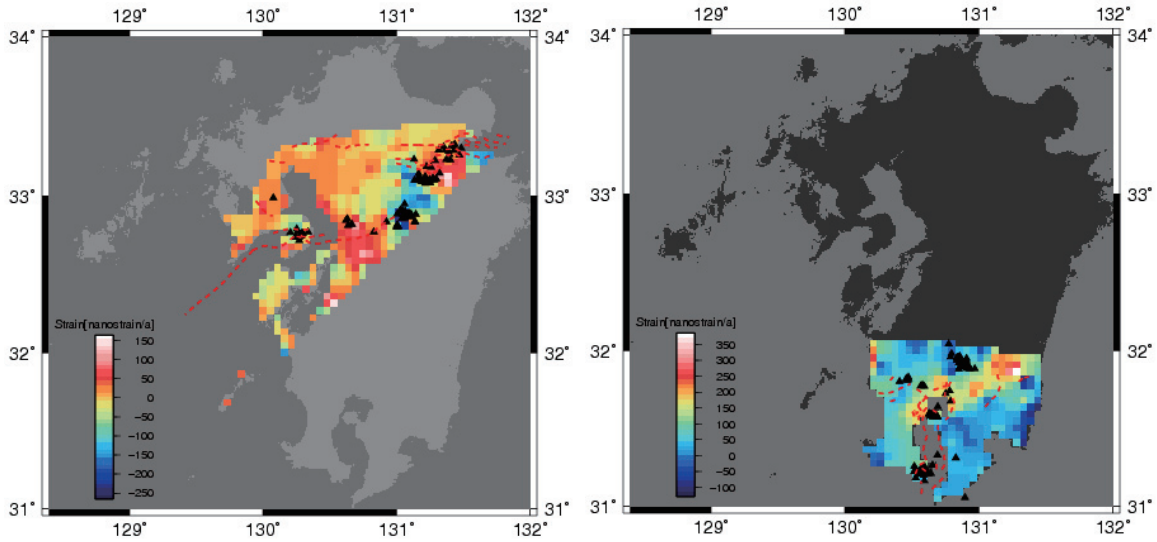

Figure 12.15: Datasets for the Extensional (left) and Southern arc (right) domains with Quaternary volcanic events (black triangle), active faults (red dashed line) and strain rates (colours).

For the estimation of volcanic hazard for the arc domains of Kyushu, the following spatial distributions are assimilated by the potential of volcanism: (a) Quaternary volcanic events, (b) strain rates and (c) cumulative lengths of active faults. All these datasets were sampled at a 5 km x 5 km for the different tectonic domains. As before, the simulation parameters for the potential simulation were estimated as described in Jaquet et al. (2009); their values are given in Table 12.3.

Table 12.3: Parameters for the Extensional and Southern arc domains of Kyushu.

Case	Domain	ρ_{ZS} *	ρ_{ZT} **	Variogram correlation scale	Time component
IIa	Extensional	**-0.20**	0.27	45 km	proportional
IIb	Southern	**0.26**	0.31	30 km	proportional
IIIa	Extensional	-0.20	0.27	45 km	simulated
IIIb	Southern	0.26	0.31	30 km	simulated

* S: strain rate; ** T: cumulative fault length.

The correlation between potential and strain rate differs remarkably when comparing Extensional and Southern arc domains. For the former domain, the correlation value is negative and for the latter domain, it is positive. Such correlation means that for the Extensional arc domain, volcanic events would tend to be more located in zones where contraction occurs. This result would deserve additional analysis as most of the strain rates present quite low values. However, such difference in correlation values justifies the estimation of volcanic hazard for each tectonic domain. Regarding the correlation between potential and cumulative lengths of active faults, the Extensional and Southern tectonic domains present similar values.

Sensitivity cases were carried for the time component of the Extensional and Southern arc domains. For cases IIa and IIb, past and future potential in time were assumed proportional, and for cases IIIa and IIIb, the future potential was estimated by Cox simulations using a Monte Carlo approach (Figure 12.16). Compared to the proportional case, this leads to increase of the future potential to about a factor 6 for the simulated case.

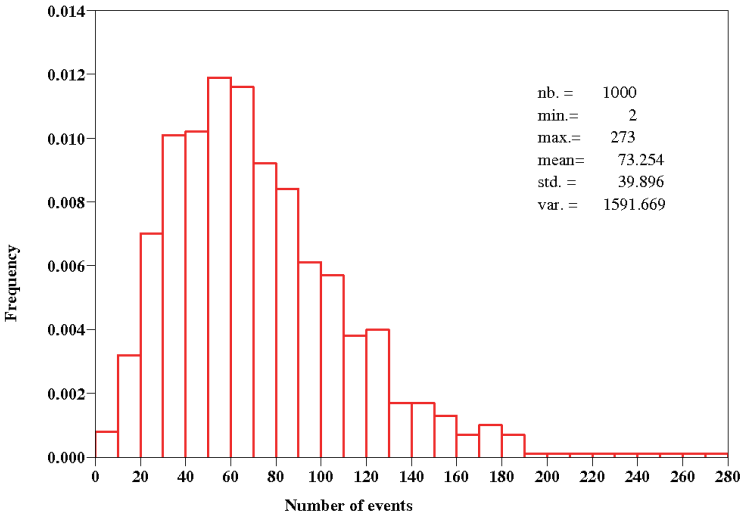

Figure 12.16: Histogram of simulated number of events for a future period of 100,000 years. The future potential in time is estimated at 73.3 events.

Using the Cox model, simulations of future volcanic events were performed over a period of 0.1 Ma for each tectonic domain and for the two sensitivity cases. As before, 10,000 Monte Carlo simulations were required to obtain stable probability estimates. The hazard estimates are mapped for the regional scale of Kyushu in order to correspond to the Extensional and Southern arc domains (Figures 12.17 and 12.18).

Table 12.4: Percentiles and surfaces with low probability values at 100,000 year scale.

Case	P_5	P_{15}	P_{33}	P_{50}	P_{67}	P_{84}	P_{95}	Surface [km^2] with probability value below 10^{-3}
I	NA	NA	NA	10^{-4}	$3 \cdot 10^{-4}$	**10^{-3}**	$2 \cdot 10^{-2}$	**33’432**
IIab*	10^{-4}	$2 \cdot 10^{-4}$	$4 \cdot 10^{-4}$	$6 \cdot 10^{-4}$	**10^{-3}**	$5 \cdot 10^{-3}$	$4 \cdot 10^{-2}$	**14’020**
IIIab*	$8 \cdot 10^{-4}$	**10^{-3}**	$2 \cdot 10^{-3}$	$3 \cdot 10^{-3}$	$7 \cdot 10^{-3}$	$3 \cdot 10^{-2}$	$2 \cdot 10^{-1}$	**3’139**

* Extensional and Southern arc domains cover about 53 % of Kyushu island (≈ 39,800 km^2).

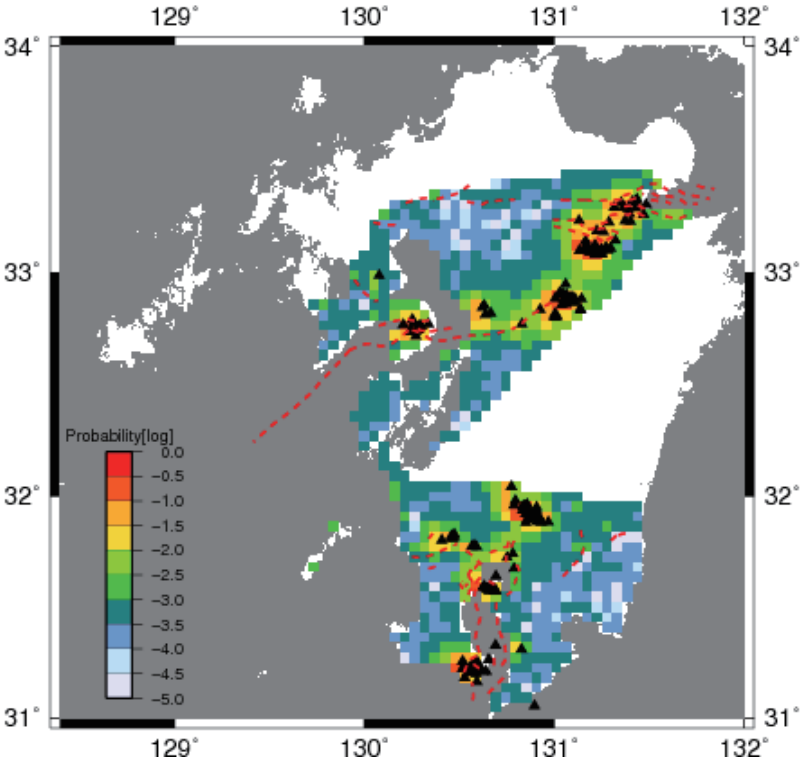

Figure 12.17: Volcanic hazard map for Extensional and Southern arc domains displaying the probability of one or more volcanic event for the next 100,000 years and 5 km x 5 km domain (case IIab).

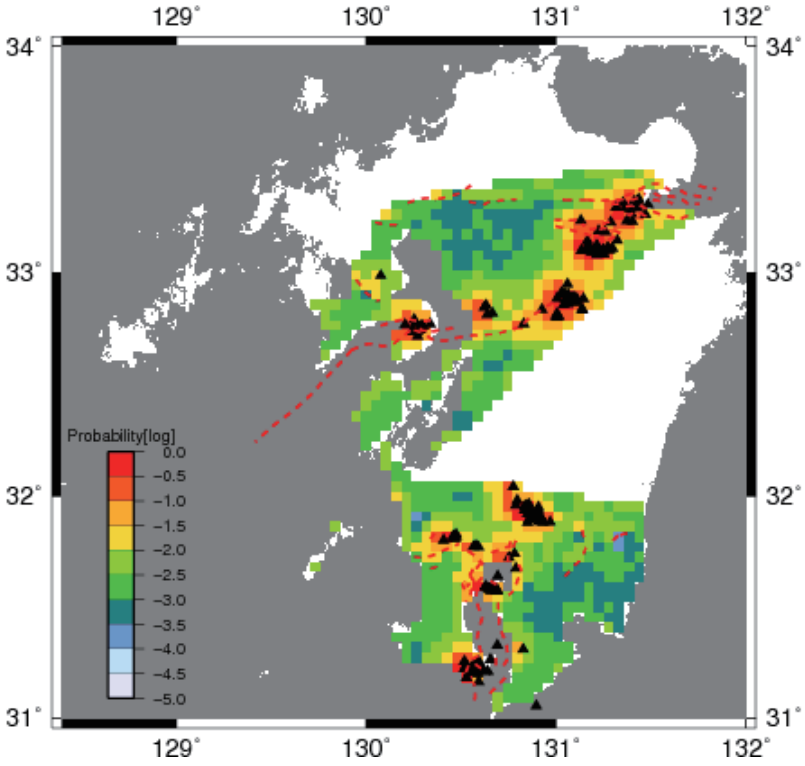

Figure 12.18: Volcanic hazard map for Extensional and Southern arc domains displaying the probability of one or more volcanic event for the next 100,000 years and 5 km x 5 km domain (case IIIab).

The results of sensitivity calculations can be measured in terms of surfaces presenting low probability values (Table 12.4); i.e. these surfaces include only 5 km x 5 km domains presenting probability values below 10^{-3}. When comparing case I (whole Kyushu) and case II (with tectonic domains), the surface with low probability values decreases from 84 % (of the whole Kyushu region) to 67 % (of Extensional + Southern arc domains). Regarding case III, the higher values taken for the future potential, compared to case II, leads to a major reduction (down to 15 %) of the surface with low probability values. This result highlights the importance of gathering good and sufficient radiometric data as input for hazard assessments.

Therefore, such domain delineation is of importance, as it allows fitting a model that better account for local characteristics of tectonic domains and potentially avoids overestimating the surface of Kyushu island presenting low probability values of volcanic hazard.

12.8.5 Conclusions and perspectives

By considering a Cox process with a multivariate potential of volcanism, the assimilation of Quaternary geological information (events and ages), strain rates and geophysical data becomes operational for hazard calculations. This modelling approach constitutes a step forwards with respect to the integration of rock deformation and volcanism results for probabilistic hazard assessments; i.e. it improves the characterisation of uncertainty when forecasting volcanic activity on the long term. In particular, the use of multivariate datasets will enhance hazard estimation for regions located between clusters of past volcanic events.

The comparison of hazard results relying on different concepts such as the non-homogeneous Poisson process using kernel density methods (with a smooth deterministic potential) and the Cox model (using a random potential) shows that the integration of the uncertainty for the potential of volcanism causes the resulting probability estimates to have an increased spatial variability (Jaquet et al. 2009). Such results reveal the importance of accounting for the potential of volcanism uncertainty (aleatory) when assessing long-term volcanic hazard. In addition, the application of several probabilistic models is of paramount importance for hazard estimation, as they provide contribution to the perception of epistemic uncertainty; i.e. evidence in terms of its variability and possible reduction.

Further developments are needed for the assessment of volcanic hazard at site scale. This downscaling methodology (see Section 14.5) will integrate hazard estimates from regional simulations and consider various volcanic scenarios (with uncertainty) likely to occur, as well as assimilate data from site investigations (Figure 12.19).

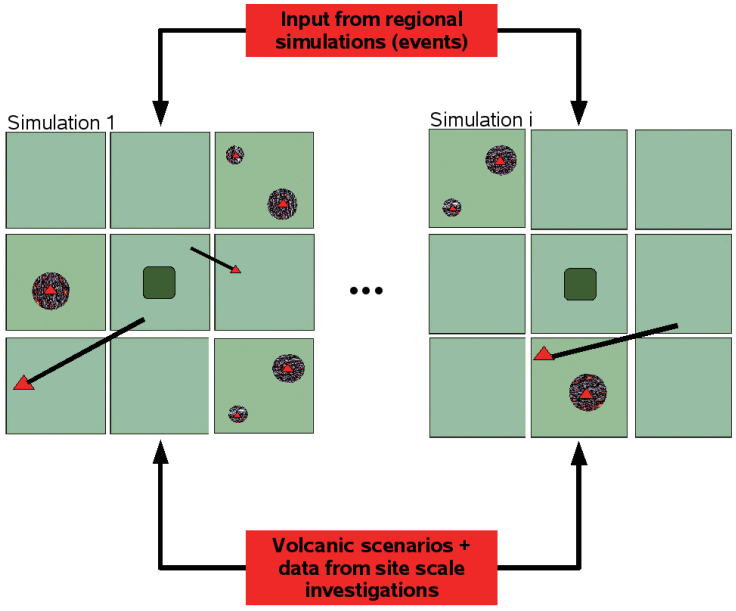

Figure 12.19: Principles for a probabilistic downscaling methodology at site scale with various volcanic scenarios likely to occur.

12.9 References for Section 12

Chapman, N., M. Apted, J. Beavan, K. Berryman, M. Cloos, C. Connor, L. Connor, O. Jaquet, N. Litchfield, S. Mahony, W. Smith, S. Sparks, M. Stirling, P. Villamor and L. Wallace (2009). Development of Methodologies for the Identification of Volcanic and Tectonic Hazards to Potential HLW Repository Sites in Japan: The Tohoku Case Study. Nuclear Waste Management Organisation of Japan, Tokyo. Technical Report: NUMO-TR-08-03. 135 pps.

Geological Survey of Japan, AIST (2002b). Geoscientific maps of Southern part of Korea, western part of Japan and their adjoining areas. Digital Geoscience Map P-4.

Jaquet O., Lantuéjoul C. and Goto J. (2008). Estimation of long-term volcanic hazard using a Cox process with a multivariate potential. VIII International Geostatistics Congress, GEOSTATS 2008, Santiago Chile, pp.167-176.

Jaquet O., Lantuéjoul C. and Goto J. (2009). Cox process models for the estimation of long-term volcanic hazard. In Volcanism, Tectonism, and the Siting of Nuclear Facilities, edited by C.B. Connor, N.A. Chapman and L.J. Connor, Cambridge University Press, pp.369-384.

Lantuéjoul C. 2002. Geostatistical simulation: models and algorithms. Springer, 256 pps.

13 Comparison of Rock Deformation Strain and Volcanic Hazard Results for Kyushu

As we have discussed throughout the Kyushu Case Study report, there appear to be spatial and temporal relationships between volcanism and rock deformation processes (see, also, Section 7). In that sense, it is useful to compare spatial variations in rock deformation and volcanic hazard directly. Moreover, combining the rock deformation strain and volcanic hazard estimates can give us some idea of areas within Kyushu that are "high hazard" or "low hazard" from *both* rock deformation and volcanological perspectives.

The outputs of the rock deformation and volcanic hazard studies are quite different. Volcanic hazard is assessed in terms of spatial density of volcanic systems and reflects the probability that a volcano will form in a specific area, given the development of a new volcano in the region. Rock deformation results are presented in terms of a common measure of strain rate. In previous work, we have converted the rock deformation strain rates to a hazard value using the ITM methodology (see Tohoku Case Study: Chapman et al., 2009) by defining some arbitrary "hazardous" strain threshold. However, converting the rock deformation strain rates to a hazard value that has some meaning requires a clear definition of the event that is considered "hazardous", which requires input from performance assessment teams modelling repository performance.

In order to facilitate comparison between the volcanic hazard estimates and rock deformation strain rates, we have normalised[7] the volcanic hazard estimates and the rock deformation strain estimates (separately, for GPS, surface deformation and seismicity). We plot them in the figures in this Section in terms of percentiles; for example, the highest 5% of strain values in a given dataset is shown in dark orange. Although these are not probabilistic hazard estimates, normalising these values allows us to look at the datasets in terms of a "relative" hazard for the Kyushu region and to identify regions of relatively high and low overall tectonic hazard with the aid of these normalised maps.

13.1 Normalised rock deformation strain rates

Some interesting patterns arise from normalisation of the surface deformation, seismological, and GPS-derived strain rate estimates from the Kyushu Case Study. For the surface deformation derived from fault strain (Figure 13.1) and seismologically-derived strain rate estimates (Figure 13.2 and Figure 13.3), we use the median strain value from the suite of strain models defined in the active fault deformation and seismicity logic trees (see Section 8 and Section10).

The GPS strain estimates used in the normalised GPS map (Figure 13.4) are a weighted average of all logic tree branches (using the second invariant of the strain tensor), with weightings based on logic tree branch weightings (see Section 9). Given that the uniform source area model is weighted very highly in the seismic strain rate model (due to the recommendation of the expert panel in the Tohoku Case Study; see discussion in Section 10), we also show our preferred model, which is a continuously varying model that is more representative of the spatial patterns of historical seismicity.

Uniform source area models assume that future earthquakes will be "gap-filling" events and distributed uniformly over the region, rather than being concentrated along particular zones of concentrated deformation.

[7] Normalisation means that the sum of the probabilities in the area of the normalised map integrates to 1.

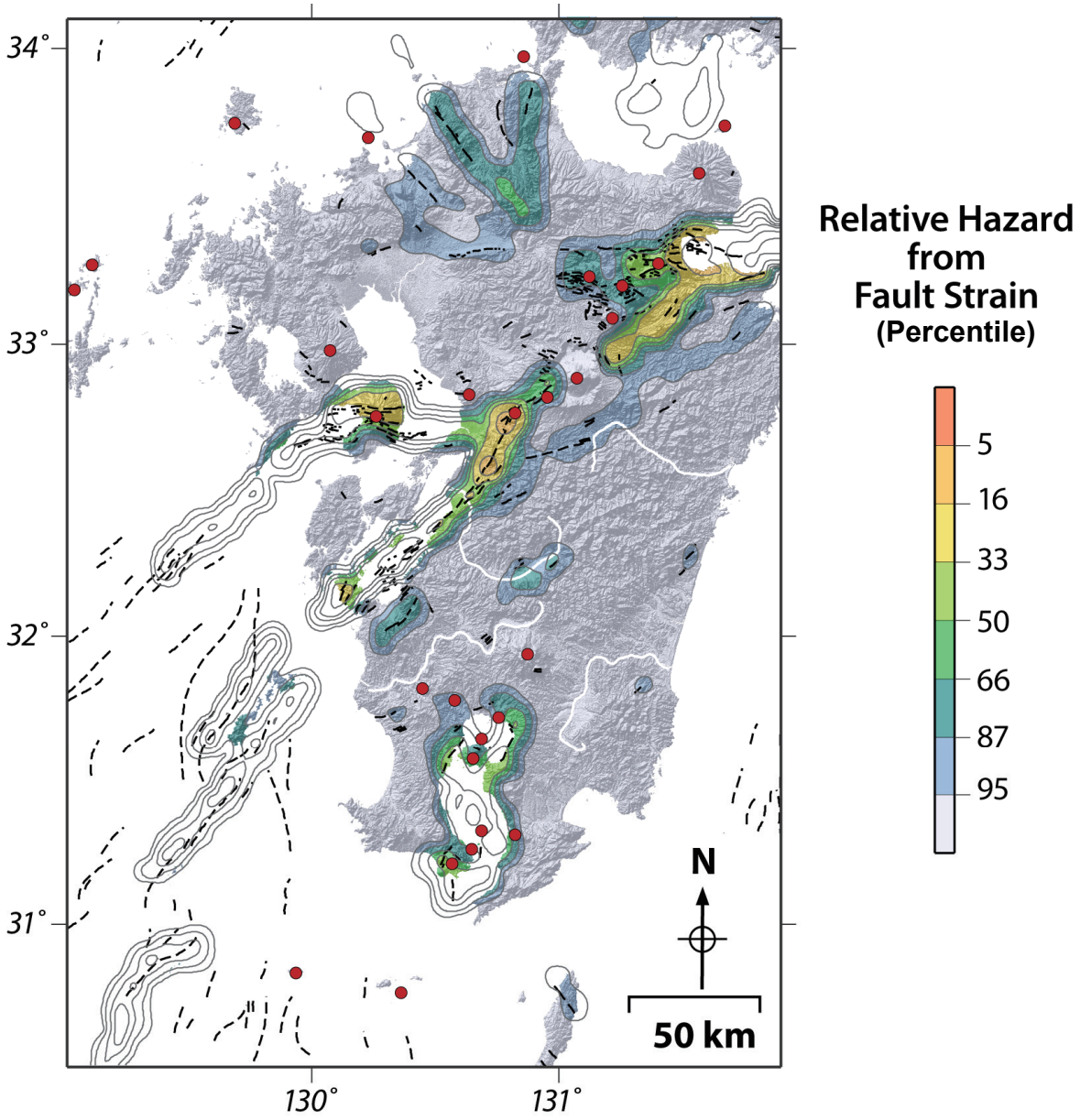

Figure 13.1: Relative rock deformation hazard in Kyushu as described by strain rate derived from known surface deformation (active fault) features. On this and following figures, volcanic systems are plotted as red circles. Rather than contouring probability, the map contours represent relative hazard. Each successive contour encloses an increasing percentage of the relative hazard. So for example, given an event, there is a 95% chance of it falling within the 95th percentile contour, and a five percent chance of it falling within the fifth percentile contour, based on this relative hazard model. On land the percentages are color-coded based on the shown color scale. The contours extend off land but the color codes are clipped at the sea-land border.

In the surface deformation (active fault) normalised strain map (Figure 13.1) the highest strains are concentrated within the Beppu Graben of northeast Kyushu, and along the Oita-Kumamoto line. Elevated strains are also apparent in the Kagoshima Graben and along left-lateral faults in the back-arc region. The normalised median seismic strain map (Figure 13.2) is quite different from the other normalised strain maps due to the dominance of the uniform source area assumption in the seismicity strain logic tree (see Section 10). The strain rates in the median seismic strain model largely reflect the defined boundaries chosen for the seismic source areas. However, our preferred seismic strain model (assuming a continuously varying model) highlights some interesting patterns. The highest strains in this model are in the region of large, historical earthquakes (e.g., the 2005 M_w 7.0 offshore Fukuoka, and the 1997 Kagoshima-ken-hokuseibu earthquake). However, the normalised seismic strains are also

elevated in the Shimabara Graben region, and along the zone of left-lateral shear deformation cutting across southern Kyushu identified by GPS (see Section 9). The highest GPS-related strains occur along the zone of left-lateral shear cutting across southern Kyushu, in the Beppu Graben (northeast Kyushu), and in the Kagoshima Graben. The lowest GPS strain rates are in the back-arc region.

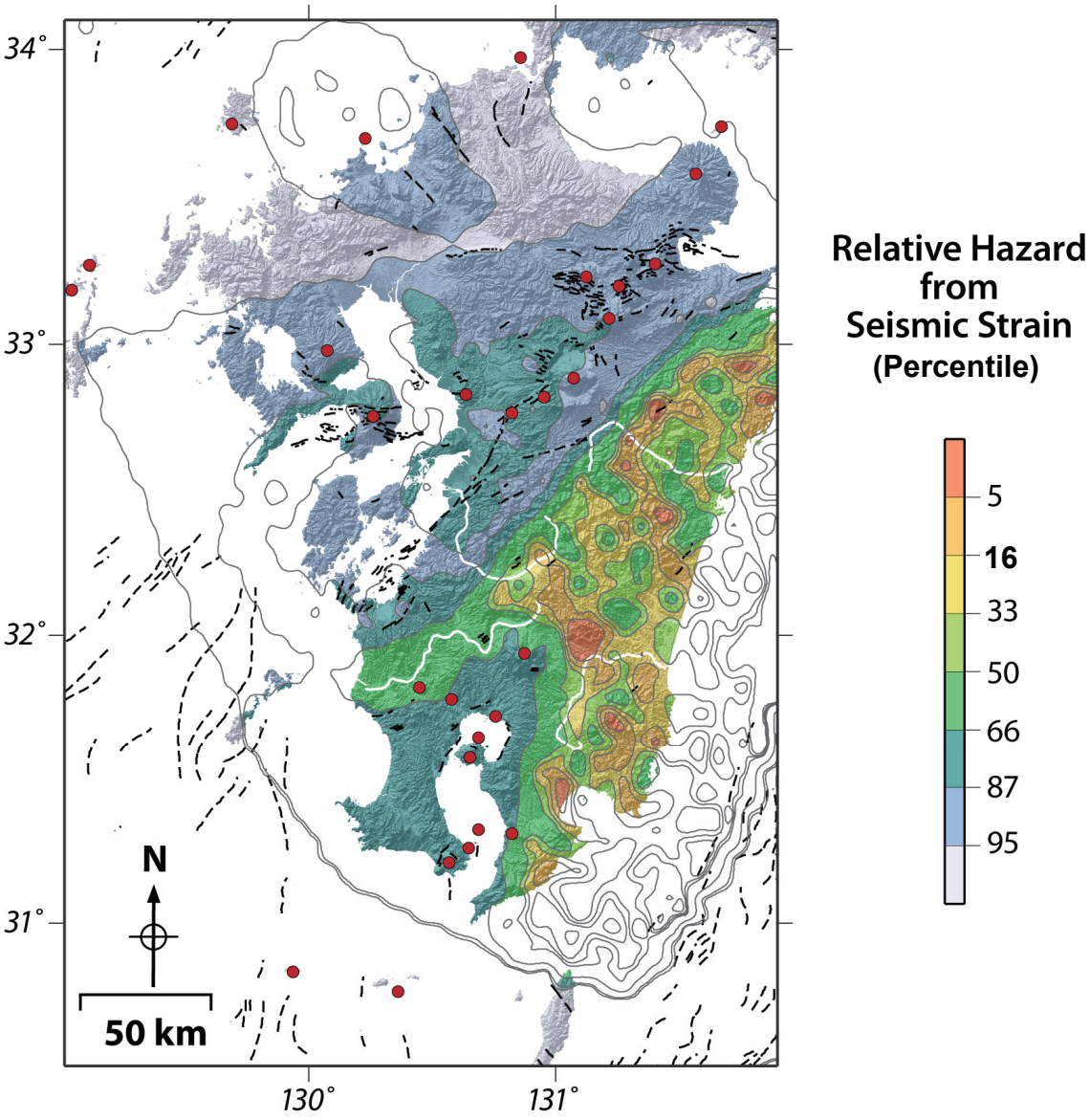

Figure 13.2: Relative rock deformation hazard in Kyushu as described by strain rate derived from seismic normalised strain (median value—dominated by uniform source).

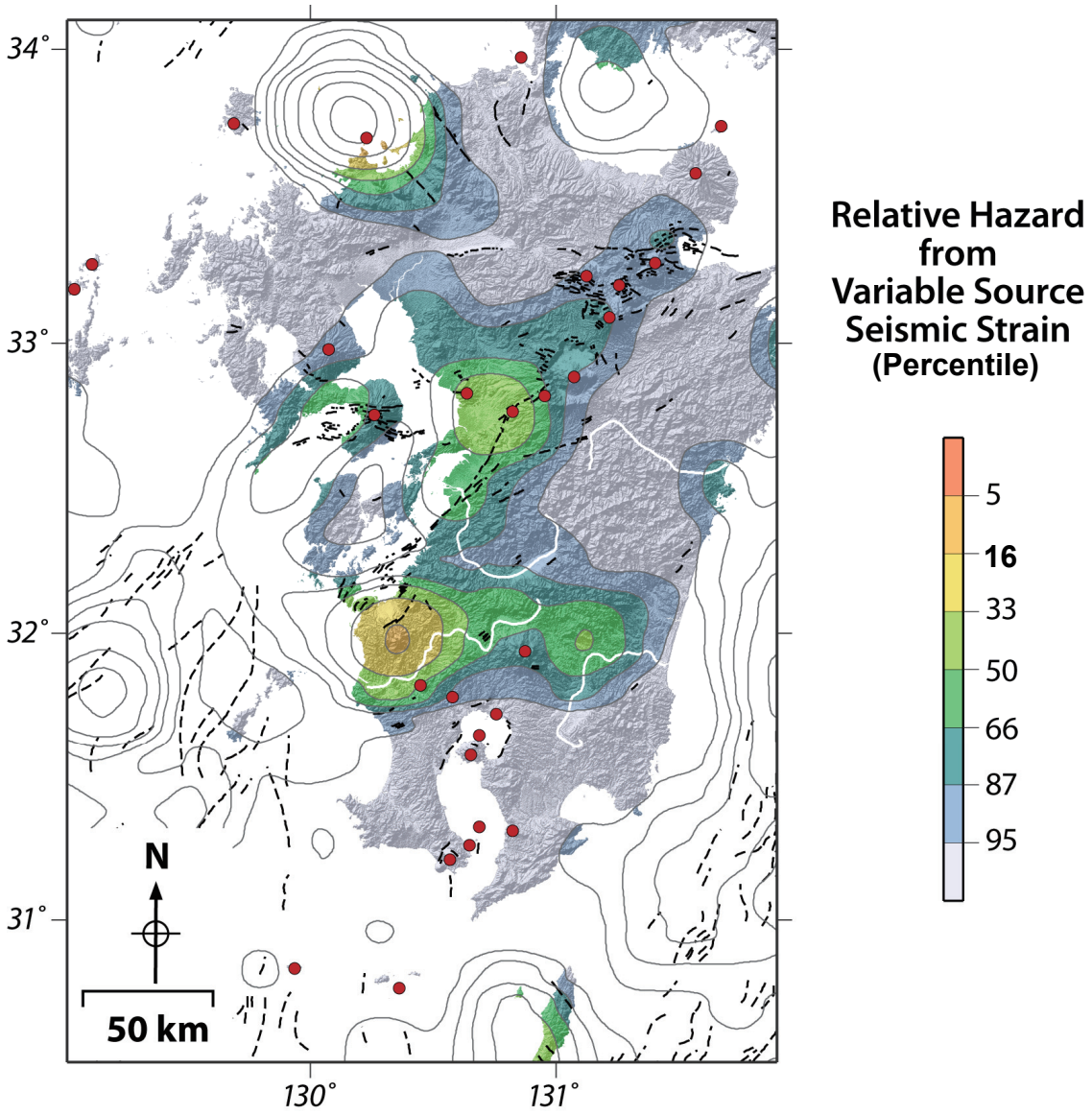

Figure 13.3: Preferred model of rock deformation hazard derived from seismic strain (continuously varying model).

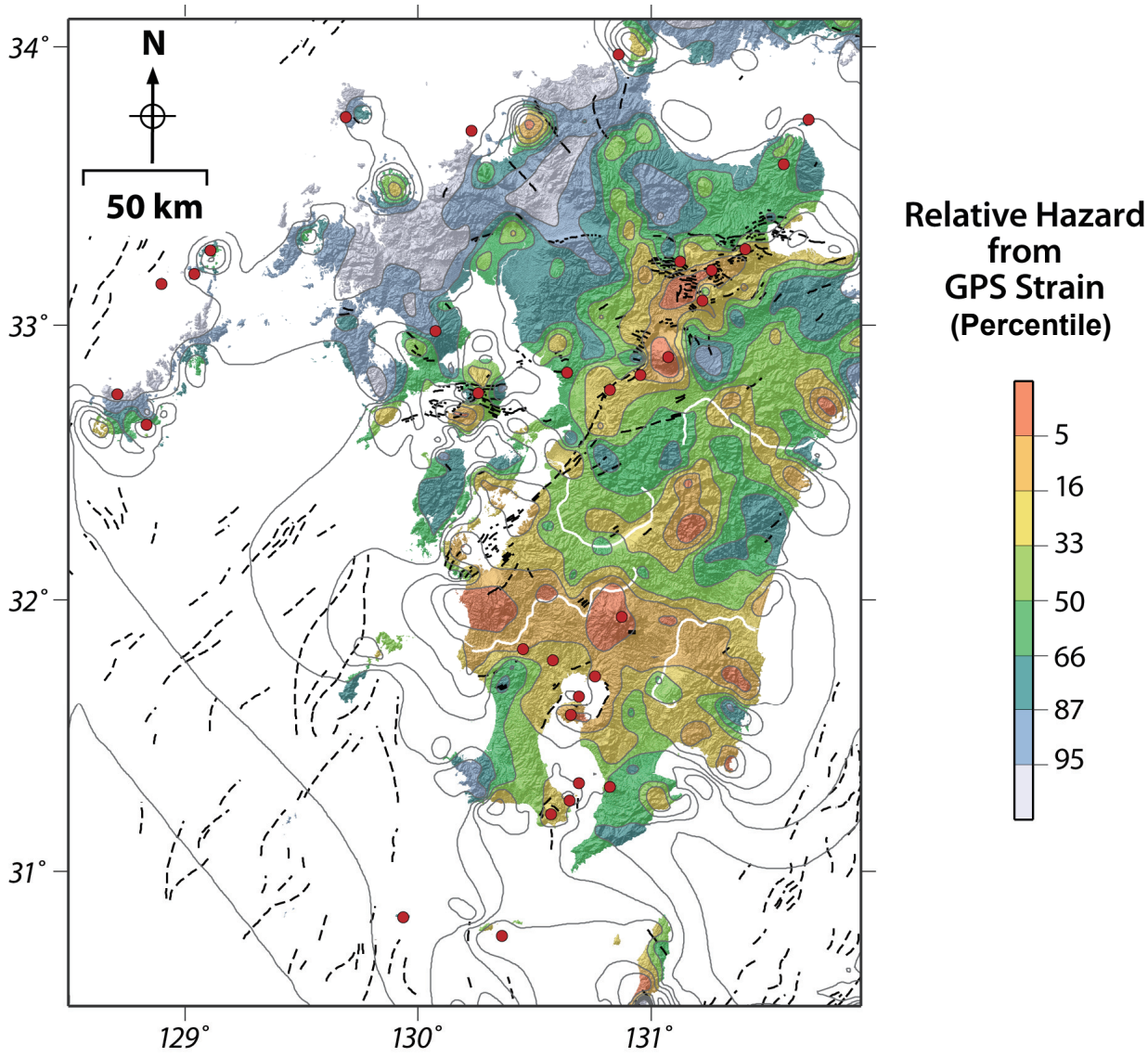

Figure 13.4: Relative rock deformation hazard in Kyushu as described by strain rate derived from GPS weighted average strain (normalised).

13.2 Normalised volcanic hazard

As described in previous Sections, volcanic hazards for proposed geological repositories largely involve the potential for magma disruption of a geological repository and eruption of magma and radioactive waste materials into the biosphere.

Volcanism in Kyushu may be broadly divided into zones that are consistent with the tectonic domains developed for rock deformation hazard assessment in the Kyushu Case study. These zones are the extensional arc, southern arc, and back-arc. Volcanoes cluster in these three tectonic domains on several scales. For example individual volcanic systems, such as Kuju volcano, consist of many vents formed over hundreds of thousands of years. This clustering means that given future volcanic activity volcanism is most likely to occur within or near currently active volcanic systems.

On larger spatial scales and longer temporal scales, magmatism results in new volcanic systems and currently active systems may become extinct. The probability of new volcanic

systems forming is of particular interest for assessment of volcanic hazard for geological disposal facilities.

Given the clustered nature of volcanism, nonparametric kernel density models are used to characterize the spatial density of volcanic events, with the understanding that future volcanism, say during the next 100,000 years, is mostly likely to follow the pattern of volcanic activity developed during the Quaternary (e.g., the last 2 million years) (Connor and Connor, 2009; Mahony et al., 2009). Other spatial density estimates, made for example using the Cox Process model, may also be used to estimate spatial density (Jaquet et al., 2008; Jaquet et al., 2009).

The spatial density map of volcanic hazard shown in Figure 13.5 was constructed using the SAMSE bandwidth optimisation algorithm to objectively estimate spatial density of volcanic systems within each of the three tectonic domains. The map shows the spatial density of volcanic systems. For example, Kuju volcano is shown as a single volcanic system, rather than as a set of volcanic vents. From a hazard perspective, spatial density maps like Figure 13.5 represent a conditional probability.

Given the formation of a new volcanic system in Kyushu, what is the likelihood that this system will form in a specific area? This probability is represented by the spatial density, assuming that the formation of new volcanic systems is a stationary process within each of the three tectonic domains. That is, spatial shifts in the formation of new volcanic systems have not occurred in the Quaternary and are unlikely to occur during the performance period of the geological repository. This assumption is reasonable, given the distribution and timing of volcanism in these volcanic systems and the nature of geophysical processes involved in magma generation, ascent, and eruption in arc and back-arc settings.

As is the case for the rock deformation maps (Figure 13.1 – Figure 13.4), the volcanic hazard map is normalised (integrates to one), and is contoured by percentile. Thus areas outlined by the 5% contour represent the highest volcanic hazard (dark orange) as this contour outlines the highest 5% of spatial density estimates. Conversely the 95% contour outlines all but the areas of relatively lowest volcanic hazard in Kyushu.

13.3 Comparison and combination of rock deformation strain and volcanic hazards

Given that the rock deformation and volcanic hazard maps are normalised it is possible to mathematically blend these maps (e.g., Connor et al., 2000; Martin et al., 2003). For each grid point, *i*, representing a small area *a* within the map region, *R*

$$T_i = \frac{V_i + D_i}{\sum_R V_i D_i}$$

where V_i is the relative volcanic hazard and D_i. is the relative rock deformation hazard, as defined previously and given the assumptions discussed previously. Then T_i is the relative "tectonic hazard", here defined as the relative likelihood of a volcanic or rock deformation events within the area *a*. This definition assumes that there is no causal relationship between V_i and D_i. That is, volcanic events are not caused by rock deformation events and vice versa. Given the methods of constructing these maps (e.g., the use of regional fault and volcano databases, GPS and seismicity) this assumption is reasonable, as discussed in the following. It is emphasised that for a specific site for a proposed repository, independent analyses of volcanic hazards and deformation hazards should be made. These tectonic hazard maps (Figure 13.6 – Figure 13.9) are prepared only to facilitate comparison of the spatial distribution of volcanic and rock deformation hazards in Kyushu.

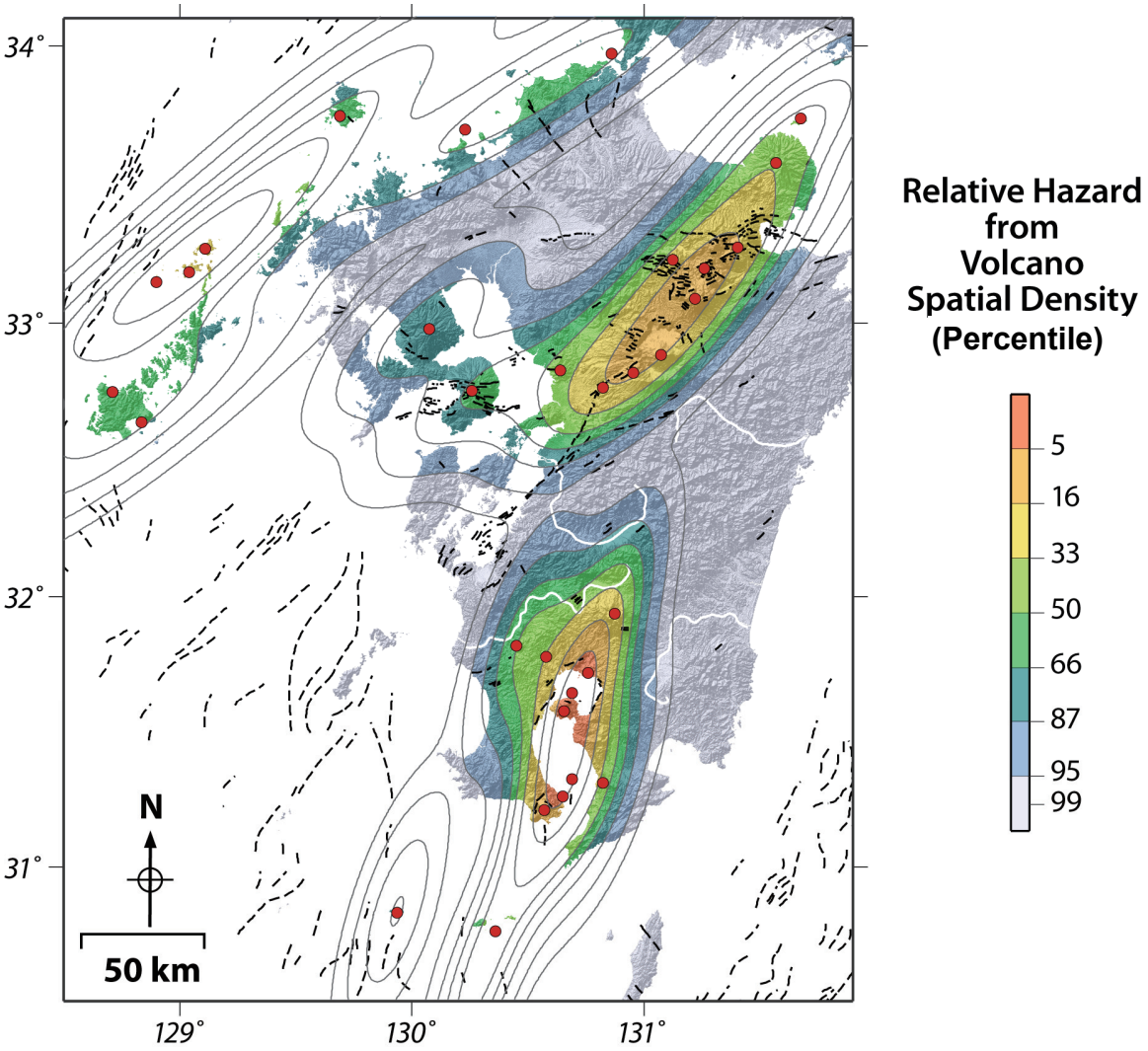

Figure 13.5: Relative volcanic hazard in Kyushu as described by the spatial density of volcanic systems.

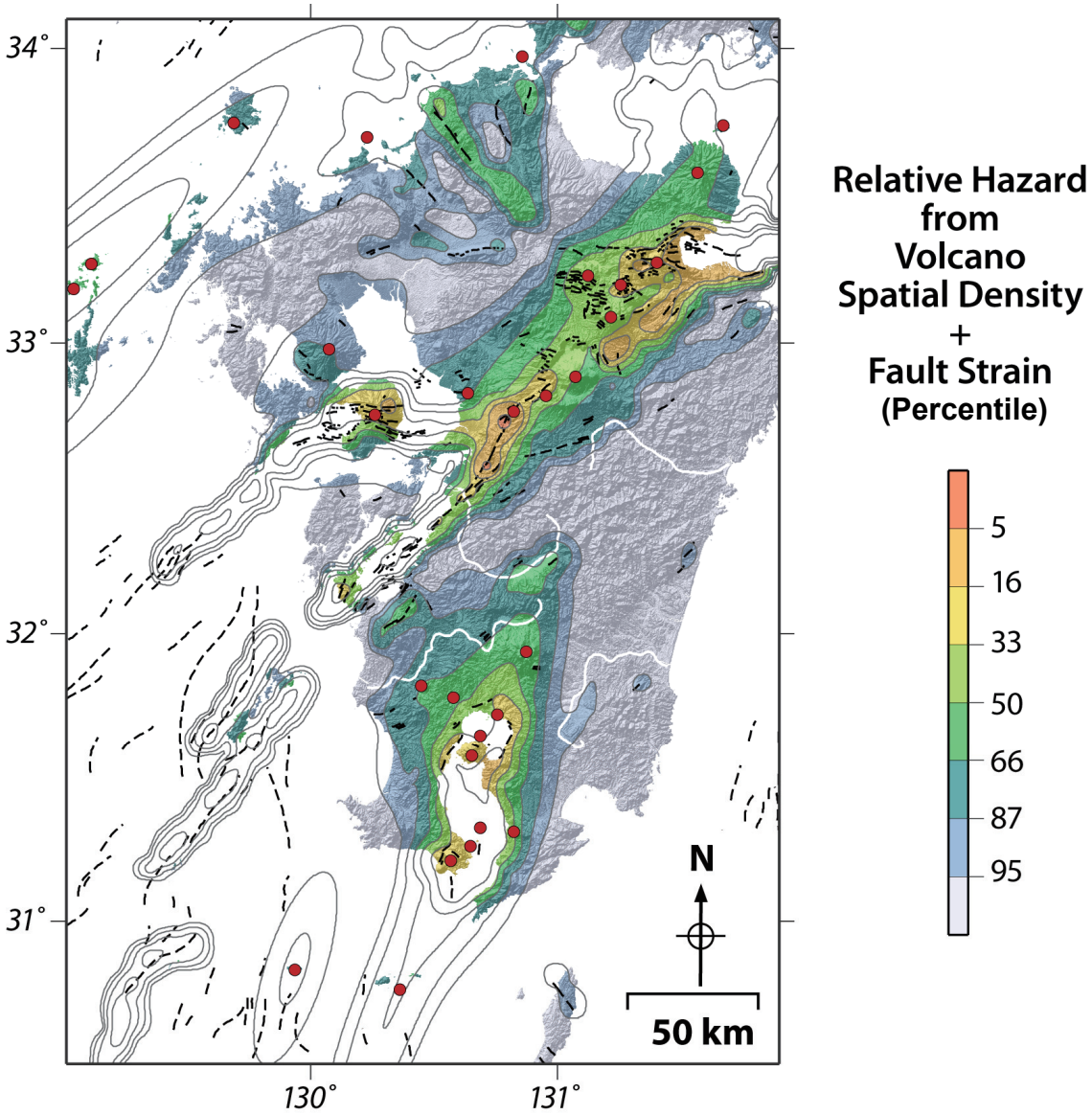

Figure 13.6: Relative tectonic hazard in Kyushu derived by equally weighting the surface deformation (active fault) map (Figure 13.1) and the volcano spatial density map (Figure 13.5).

13.4 Volcanic hazard and surface deformation

Some interesting patterns emerge from combination of the normalised volcanic hazard and surface deformation (active fault) strain datasets. Due to the co-location of zones of active normal faulting and active volcanism, the highest values (>15%) occur in the Kagoshima Graben and Beppu-Shimabara Graben region (Figure 13.6). The combined tectonic hazard is generally the lowest in the Forearc, due to the lack of volcanism or significant active faulting in this region. In contrast, the Extensional Arc and Southern Arc domains have the highest combined tectonic hazard values. Parts (but not all — see the region of active monogenetic volcanism) of the Back-arc domain also have low combined values.

13.5 Volcanic hazard and GPS-derived strain

The highest relative tectonic hazard, based on the highest 5% of the combined GPS strain and volcanic hazard values, occur in the Kagoshima Graben region (Figure 13.7). The Beppu-Shimabara Graben has similarly elevated values (15% and higher) due to the complementary high strain and high volcanic hazard estimates there. Some of the GPS strain patterns appear to be quite noisy (possibly due to problems with velocity estimates at specific GPS sites and/or the variety of subduction coupling models considered in the logic tree; see further discussion in the Strain from GPS Section). The affect of this "noise" is minimised when the GPS normalised strain values are combined with the normalised volcanic hazard estimates (which are more smoothed, due to kernel density estimation methods used to calculate the volcanic hazard). Combined values of hazard and GPS strain in the Forearc and Backarc domains are generally the lowest (with the exception of the area of monogenetic volcanism in the back-arc), while the Extensional Arc and Southern Arc domains have the highest combined values.

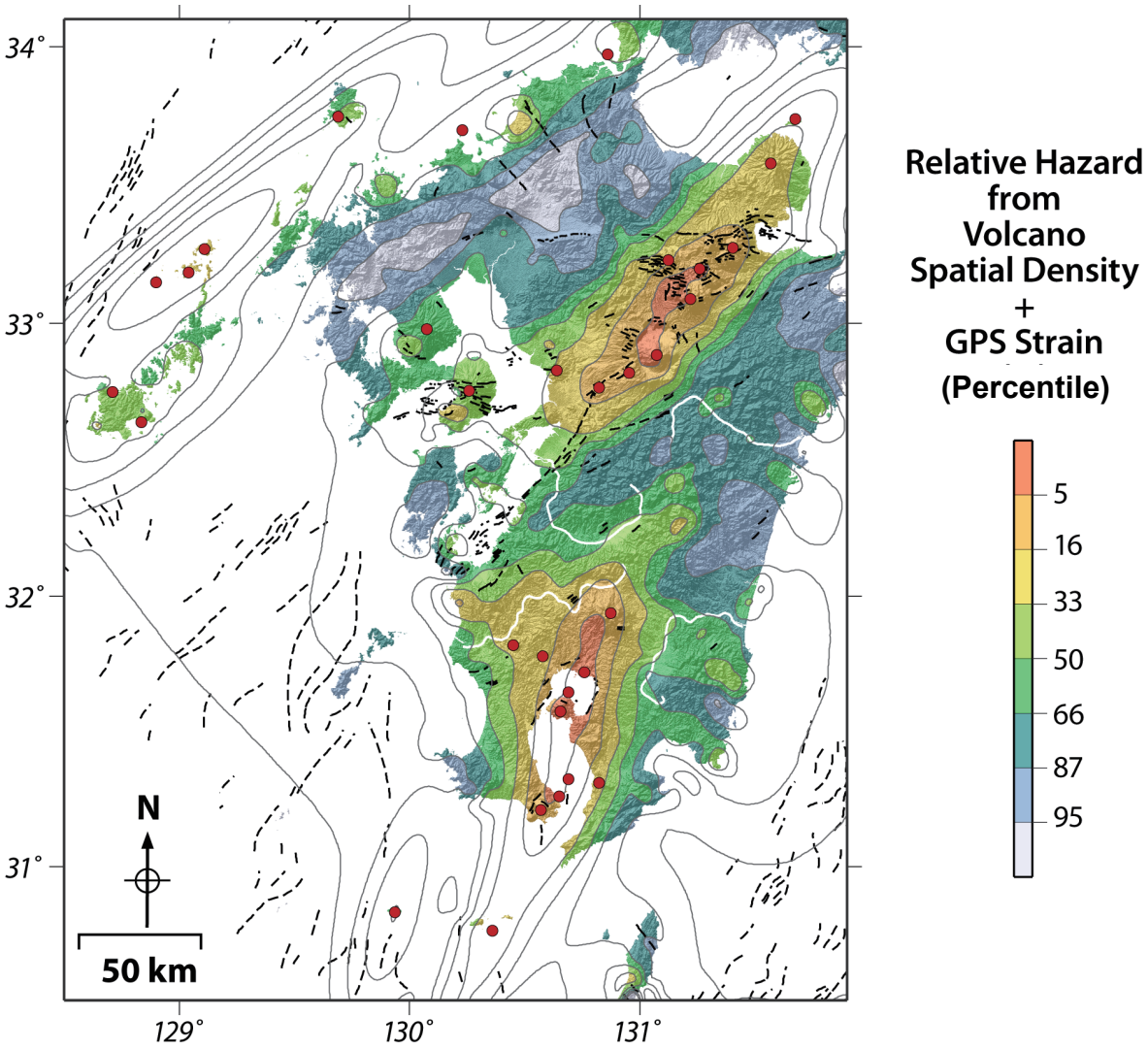

Figure 13.7: Relative hazard in Kyushu derived by equally weighting the GPS-derived normalised strain map (Figure 13.4) and the volcano spatial density map (Figure 13.5).

13.6 Volcanic hazard and seismic strain

The seismic-derived strain map blended with the volcanic hazard map (Figure 13.8) yields a relatively smooth surface. Comparison with the GPS-derived strain and volcanism map (Figure 13.7), relative values are lower within the Extensional arc and Southern arc domains and higher in isolated areas of the Back-arc and forearc region due to the distribution of high estimated seismic strain. Overall, this map correlates less well with tectonic features and produces isolated areas of relative high hazard away from the volcanic arcs.

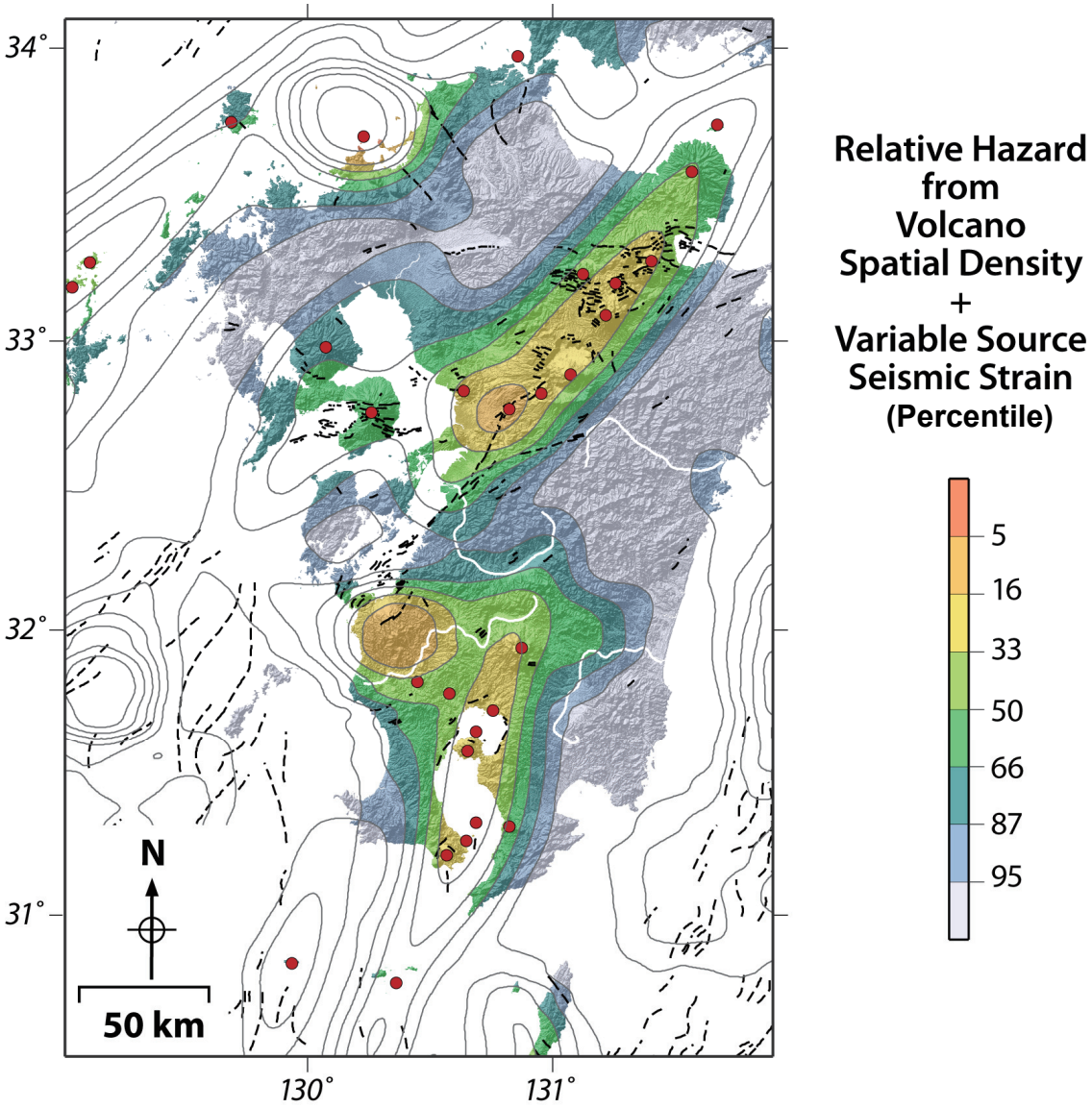

Figure 13.8: Relative hazard in Kyushu derived by equally weighting the seismic strain map (continuously varying source) (Figure 13.3) and the volcano spatial density map (Figure 13.5).

13.7 Combination of volcanic hazard and all rock deformation strain estimates

As different aspects of strain are reflected in the active fault deformation-, GPS-, and seismic-derived strain maps, it is possible to combine these three maps, weighting each map equally, and combine the resulting comprehensive strain map with the volcanic hazard map (Figure 13.9). The resulting, blended map is quite consistent with tectonic and volcanological models

of Kyushu, with highest relative values in the Extensional arc and Southern arc, and a broad zone of relatively high values in the Back-arc region.

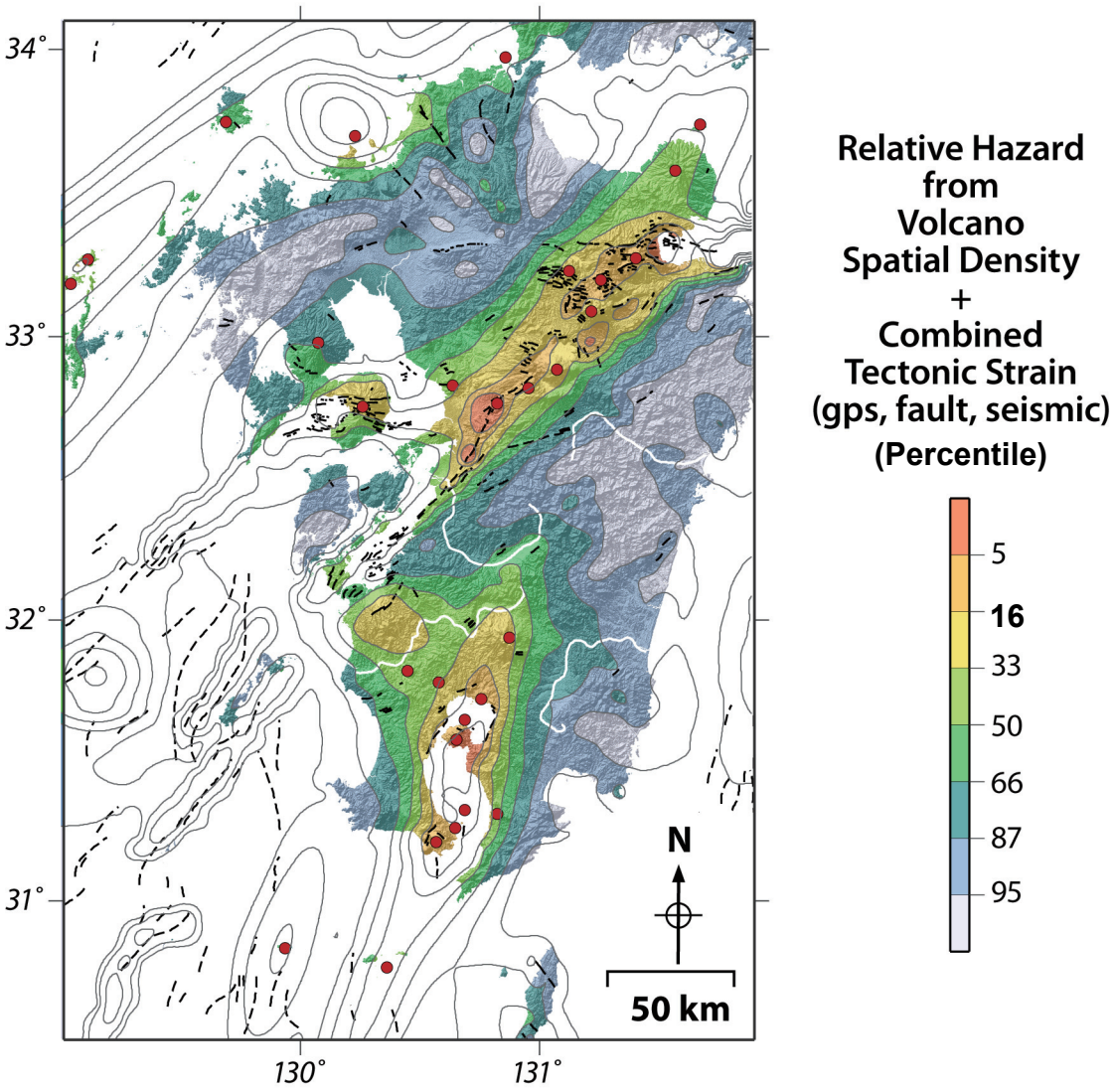

Figure 13.9: One method of assessing rock deformation hazards is to combine the results of the strain maps derived from surface deformation, GPS, and seismicity. This map shows the results of combining such an averaged strain map with the volcano spatial density map.

13.8 Discussion

It is emphasised that, while the combination of strain data and spatial density of volcanism may reflect overall tectonic hazard, these maps are not hazard maps in the sense of providing a probabilistic estimate of hazard. This is because the event definition varies among these maps. Nevertheless, the maps are useful for comparing areas where rock deformation and volcanism are relatively high or low in the study region. The maps also provide a basis for considering the possible mechanisms that give rise to common distribution of strain estimates and volcano distribution.

Comparison of the relative tectonic hazard maps (Figure 13.6 – Figure 13.9) suggests that regions characterised by relatively high volcanic hazard also are regions of high rock deformation hazard. Conversely, there are broad areas on Kyushu that are characterised by relatively low volcanic and low rock deformation hazards. This correlation is strongest within the Extensional and Southern Arc domains, the most tectonically active portions of Kyushu. Volcanic hazard is lower in the Back-arc domain and less closely correlated with relative rock deformation hazard (Figure 13.9).

The differences between relative tectonic hazard maps based on different strain models (surface deformation, GPS strain, and seismicity) are also interesting to assess. Volcano distribution and faults may be more likely to be correlated in the sense that these are both long-term data sets. The volcano spatial density is based on the distribution of Quaternary volcanic systems. The fault dataset is Holocene, but certainly reflects the distribution of long active structures. The spatial correlation in the combined maps (Figure 13.9) suggests that a common geological process leads to the development of these features on a regional scale. This is reinforced by the fact that the best-fit kernel in the extensional-arc domain is elongate parallel to the Shimabara-Beppu graben, and some volcanoes in this domain (e.g., Akai and Omine) lie along faults and fault planes appear to have influenced dyke ascent at these volcanoes. Similarly, the best-fit kernel in the Southern arc is N-S trending, parallel to faults in this region. Such a correlation may arise from many possible geological processes. For example, crustal extension associated with crustal thickening (underplating due to magmatism), localisation of strain accommodation due to rheologic changes in the lower crust near volcanic systems, and focusing of magmatism in regions of preferential strain accommodation all might account for this correlation on a regional scale. Of course we cannot identify the mechanism by identifying the correlation, but the correlation does reinforce the notion that relative tectonic hazards are high (and concentrated) in parts of Kyushu. Such strong clustering also implies that other areas are comparatively lower in tectonic hazard rates in the long term.

The rock deformation hazard based on GPS strain rate is a much shorter-term indicator of strain than faulting. Because the volcanic hazard map is based on a 2 million year record and the GPS-derived strain map is based on a decadal record, it is not surprising that the correlation with volcanism is more complex than the correlation between volcanism and faulting. The timescales represented by the maps are vastly different. Nonetheless, the patterns seen on the "long term volcano-surface deformation" map (Figure 13.6) are reinforced by the “volcano-GPS strain map” (Figure 13.7), which is sensitive to the current tectonism. This suggests that there is no reason to discount previously active regions as less active now. Furthermore, Figure 13.7 seems to suggest that the volcano gap between the Extensional arc and the Southern arc is more prone to tectonic hazard than it appears to be based on the volcano hazard map alone. It does not necessarily follow that because the rock deformation hazard is high in this volcano gap region, volcano hazards might be higher than forecast by the volcano hazard map alone, but hazard models would need to explore this possibility for a potential site in this gap region. Features of the tectonic hazard map based on GPS strain (Figure 13.7) offer additional insights into the correlation between GPS strain and volcanism. The correlation between volcano density and GPS strain is best where the GPS strain is extensional. The worst correlation occurs in high GPS shear strain zones (e.g., the major left-lateral shear zone cutting across southern Kyushu), suggesting that the main link between volcanism and rock deformation is in the extensional environments on Kyushu.

13.9 References for Section 13

Chapman, N., M. Apted, J. Beavan, K. Berryman, M. Cloos, C. Connor, L. Connor, O. Jaquet, N. Litchfield, S. Mahony, W. Smith, S. Sparks, M. Stirling, P. Villamor and L. Wallace (2009). Development of Methodologies for the Identification of Volcanic and Tectonic Hazards to Potential HLW Repository Sites in Japan: The Tohoku Case Study. Nuclear Waste Management Organisation of Japan, Tokyo. Technical Report: NUMO-TR-08-03. 135 pps.

Connor, C.B., and L. J. Connor, Estimating spatial density with kernel methods. In: C. B. Connor, N. A. Chapman, and L. J. Connor (eds.), Volcanic and Tectonic Hazard Assessment for Nuclear Facilities, Cambridge University Press, in press.

Connor, C.B., J. Stamatakos, D. Ferrill, B.E. Hill, G. Ofoegbu, and F.M. Conway, 2000, Volcanic hazards at the proposed Yucca Mountain, Nevada, high-level radioactive waste repository Journal of Geophysical Research, 105: 417-432.

Jaquet, O., C. Lantuéjoul and J. Goto. Cox process models for the estimation of long-term volcanic hazard. In: C. B. Connor, N. A. Chapman, and L. J. Connor (eds.), Volcanic and Tectonic Hazard Assessment for Nuclear Facilities, Cambridge University Press, in press.

Jaquet, O., C. Connor, L. Connor, 2008. Probabilistic modeling for long-term assessment of volcanic hazards, Nuclear Technology, 163(1), 180-189.

Mahony, S. H. , R. S. J. Sparks, L. J. Connor and C. B. Connor, Exploring long-term hazards using a Quaternary volcano database. In: C. B. Connor, N. A. Chapman, and L. J. Connor (eds.), Volcanic and Tectonic Hazard Assessment for Nuclear Facilities, Cambridge University Press, in press.

Martin, A.J., K. Umeda, C.B. Connor, J.N. Weller, D. Zhao, M. Takahashi, 2004, Modeling long-term volcanic hazards through Bayesian inference: example from the Tohoku volcanic arc, Japan, Journal of Geophysical Research, 109, B10208, doi:10.1029/2004JB003201.

14 Conclusions

The Kyushu Case Study has helped to extend and test the ITM Methodology further, from the basis developed in the Tohoku Case Study. However, it is emphasised at the start of these conclusions that both Case Studies were intended to be development tools, rather than demonstrations of a completed, mature and systematic technical methodology that was already available and widely tested. However, despite this caveat, we believe that the two Case Studies together have produced all the main elements of such a methodology and illustrated comprehensively how it can be used to provide probabilistic assessments of tectonic hazard. The methodology is now ready, at a 'beta-test' level, for deployment in any areas that may arise in NUMO's repository siting programme.

The methodology will need to be refined, adjusted to the scale of the area under consideration and adapted to the geological and tectonic complexity of the region. In particular, those early Steps of the methodology that use expert elicitation to develop and weight appropriate models will need to be managed rigorously – and with the input of considerably more resources and local expert knowledge than was possible in our methodology development project.

In these conclusions, we look first at how the methodology performed when extended from the relatively simple Tohoku application and applied to the considerably more tectonically varied terrain of Kyushu. We make observations about the limitations that are inevitably evident at this 'working prototype' level of development. These observations lead on to suggestions for how the methodology would need to be upgraded for actual application in making siting decisions at 'real sites' and in feeding quantitative information to safety assessment work. Finally we look at two aspects of extension of the methodology for such use: how it might be downscaled to a single site level and how it might address time periods that are longer than those of principal concern in siting (i.e. beyond 100,000 years).

14.1 Performance of the ITM Methodology in Kyushu

The Kyushu and Tohoku Case Studies differ in a number of respects. Tohoku is a region that has a relatively stable plate tectonic setting, while the Kyushu region is one of the most dynamic and rapidly changing plate boundaries in the world. The situation in Kyushu is intrinsically more complex. The datasets are also less complete or confident in Kyushu compared to Tohoku. GPS rates appear to be higher in Kyushu, while paradoxically the active faults and seismicity are much lower in Kyushu. The apparent discrepancy in Kyushu between GPS data and uptake of deformation on active faults may reflect some combination of the historical seismicity sampling too short a time period, the presence of active faults that have not yet been identified, deformation by aseismic creep, and that some of the deformation is taken up by magmatic intrusions in regions of extensional tectonics. The various modes of strain accommodation in the Kyushu are not yet fully understood, as reflected in these multiple explanations. The style of volcanism and geochemistry of the magmas varies considerably across Kyushu, but is reasonably simple arc volcanism in Tohoku. Predictability of future volcanism and faulting in Kyushu is less certain because geological setting is evolving very rapidly, while the fundamental assumption in Tohoku that the plate motions driving intraplate deformation are stable over periods up to a hundred thousand years are not appropriate in Kyushu.

Overall, the Methodology has performed very well in Kyushu, with good agreement between the essentially seismotectonic domains and the volcano chemistry dataset, good general agreement between probability surfaces and volcanism (although the volcanism is too young and the tectonics too dynamic to establish steady state patterns), and good integration between volcanism and tectonism, owing to the use of coherent geological models on which the probabilistic procedures are based.

We note that the differences observed between the different rock deformation datasets are mark of the success of the methodology, in the sense that it highlights specific issues that

would need to be resolved before one could be sure of the level of confidence in the geological model of the region.

14.2 Limitations of the Current Version of the Methodology

The Kyushu Case Study has revealed a number of limitations to the methodology, which should be addressed when it is being deployed in an actual siting programme.

Depending on the area being evaluated and the stage of the site evaluation programme, there may be a requirement to look at the likelihood of lower impact volcanic events (than vent formation at the repository site), such as dike or sill intrusion, the development of large-scale hydrothermal activity or, possibly, events that could affect surface facilities over the multi-decade operating life of a repository (e.g. tephra deposition).

Some of the rock deformation datasets used in this study are inherently regional to sub-regional in their utility – GPS for example. Here, a denser network of observations and data-points can refine uncertainties, but it cannot yield variations in strain rates at <10 km spatial dimension, unless the deformation is very shallow in the crust.

Faults and seismicity are currently assessed as independent datasets but it may be more appropriate in future to merge them, as is done in PSHA for nuclear facilities. This would provide areal continuity, although it mixes temporal scales. The seismicity dataset requires further assessment – it shows uniformly low strains and it is unclear whether this is a data limitation or a methodological problem.

At a site scale, the methodologies cannot be a substitute for site-specific deterministic studies of the nature, history and impacts of tectonic processes as evidenced by field investigation data. However, these site data should be consistent with, and further inform, the range of alternative geological models that underpin the ITM Methodology. At the PIA and DIA stages of the project the ITM probabilistic methods will support the site investigations and the results of site investigation can be used to modify the weightings of various parameters in the probabilistic model – perhaps providing more confidence (and weight) to one or other geological model.

14.3 Limitations of the Kyushu Dataset

Significant data limitations have been identified in the study. These include active fault parameters, inland uplift data, the very limited range of recorded historical seismicity (which is generally of low magnitude events that nowhere approach a M_{max} event) and uncertainty in historical earthquake catalogues. Inverting the seismicity rates suggests the return time for an M_{max} event somewhere in Kyushu is about 80 years. No M 7.5 events are known and only two events in the 400-year period of the record are near M7 (1912 in the Kagoshima Graben and 2006, near Fukuoka).

There are many opportunities for further datasets, especially geophysical, to be used to inform alternate viable geological models of both rock deformation and volcanism For example, it is not clear at present whether the gap in the volcanic arc is related to the subducting slab or whether there are upper plate or mantle processes that control the extent of the active arc. An obvious question is whether the gap will continue to be an anomaly out to, say, 1 Ma. A related question is whether volcanism in the Beppu-Shimabara graben and in the Kagoshima trough is localised owing to tectonic extension, or whether slab geometry or mantle constraints are the fundamental driver. Also, we have not yet explored how much of the geodetic strain observed in Kyushu may be related to volcanism in various parts of the region.

14.4 Opportunities for Further Methodology Development

Prior to, or in the course of, applying the Methodology in an actual site evaluation programme, whether in Kyushu or elsewhere in Japan, it would be reasonable to carry out some further developments. Itemised below is an initial checklist of topics that could be considered, although it is suggested that this is revisited at the time of deployment.

There are opportunities for considerably more analysis of how various logic tree options and branches should be weighted and further analysis of what elements of the probabilistic formulation constitute aleatory uncertainties (natural, earth system variability) and epistemic uncertainties (knowledge uncertainties that can be reduced with further investigation). It is probable that different weighting profiles could be used in different time periods, reflecting confidence in the applicability of data over different periods of interest.

Further opportunity exists to assess whether strain has the same annual probability for all return periods and the form that the strain will manifest itself in. At some stage of site evaluation, it will be essential to explore the range of forms that strain release may take in a volume of rock, which will depend on the geological context. Only by considering the manifestation of the strain can the estimated strain rates and likelihoods be factored properly into safety assessment models for a repository. One aspect that needs to be considered when looking at strain manifestation is how much strain is taken up by volcanic intrusion across a region. When repository design becomes more specific, then a useful strain parameter may be displacement. This measure can be developed from the probabilistic procedures already in place.

Further development of analysis methods pertaining to the seismicity catalogue may be warranted. The uniformly low seismicity strain rates in Kyushu may be related to the use of the maximum likelihood method of developing seismicity parameters “a” and “b”. This, coupled with the strong effect in the model of smoothing by placing highest weights on a uniform source characterisation, strongly implies that earthquakes of similar magnitude and rate can occur anywhere in Kyushu. This represents a strong preference for “gap-filling”. The alternative is that earthquake occurrence is localised to crustal processes and structure and that future earthquakes are more likely to occur in places where they have occurred in the past.

There are many opportunities for further analysis of uncertainties and sensitivities in the probabilistic methodologies. The figures produced to demonstrate the application of the ITM probabilistic methodologies for future volcanism and rock deformation in Kyushu often represent preferred or mean estimate models, but the sensitivity and uncertainties of these mean estimates is only rather poorly assessed at present.

The potential for uplift of the repository into the oxidising zone could be a significant issue in some locations if the safety case extends to time periods of 1 Ma. Uplift rates as low as 0.2 mm/a may represent significant risk if the requirement for geological stability extends to 1 Ma. Very detailed work is required to assess uplift and uncertainty confidently, at this level of precision.

14.5 Refining the Methodology for Downscaling to Sub-regional or Site Scale

The ITM Methodology has been developed principally to consider hazard from future volcanism and tectonic activity on a regional scale. In the context of Japan this means regions of the order 10^5 to > 10^6 km^2. The methodology has been developed for a variety of purposes, including comparison of the relative hazard at competing sites, testing the adequacy of exclusion criteria, investigating the uncertainty in the assessment of hazard at specific places, and mapping out hazard across the region to identify places of low hazard and therefore with promise as site location. The hazard is expressed in terms of strain rates, locations of major tectonic structures, and for volcanism the probability of a new volcano forming in a specified time period. Such hazard assessments will inform the PIA stage. Once a potential site or

volunteer community has been identified then the detail with which the hazards are assessed needs to be commensurately improved. While the same essential questions are being asked, in essence *what is the probability of a site being disrupted or compromised by volcanic or tectonic activity*, the change in scale will require some refinement of the methodology.

Perhaps the most important aspect of down-scaling is that there needs to be an increase in the volume and completeness of data. Existing data can be gathered during the PIA stage and gathering of new data with associated interpretive analysis may be essential as the programme moves towards specific site investigation. The more detailed data and analysis of all the tectonic and volcanic datasets will be needed principally to reduce or constrain the uncertainties.

For volcanic hazards the questions to be addressed are likely to change with reduced scale. At large-scale whole regions of order 10^5 to > 10^6 km^2 have been considered using the ITM methodology. The hazards have been expressed as probability of a volcanic event defined as a volcano at a specific site over a specified period of time. The ITM Methodology thus far has considered specific sites to mean areas of 5 x 5 km and time-scales of 10^4 to 10^6 years. The modification of the methodology at intermediate and site specific scales is now discussed.

At sub-regional scale (~10^4 to 10^3 km^2) the probability of new volcanoes forming needs to investigated not just at the site itself but in areas that are close enough to the site that they might pose direct or indirect effects. The “15 km” exclusion criterion provides a yardstick but indirect effects (such as hydrothermal systems) might indicate larger distances should be considered. The method could, for example, be modified to look at the probability of a new volcano forming in an area being affected by a volcano sited at a distance of 15 km from the site. At this intermediate scale, the different kinds of hazards may need to be considered individually. The most important hazard is intrusive disruption of the site. Thus, models may need to be developed which look in more detail at the probability of intrusive disruption across the region, taking into account local tectonic, geophysical and geological data in more detail. It is likely that much more detailed geochronological, paleovolcanological and palaeosiemological studies will be needed within the sub-region to characterise recurrence rates of volcanism, styles of volcanism and past history of faulting. Deterministic assessments are likely to also be important. For example, probability of rock deformation or volcanism might change discontinuously across a major fault between two different tectonic domains, and using smoother probability algorithms may give misleading results. As another example, probability of intrusion might be represented as some functional form of the distance from the centre and the hazard of intrusion might be some combination of intrusive hazard related to multiple volcanic events.

At a scale close to the repository footprint itself (~ 10^2 to 10^1 km^2) the very local factors will start to affect probabilities and a more deterministic approach may be essential. Site evaluation should be based upon standard geological principles, but guided by “potential issues” identified via coherent geological models at regional and sub-regional scale. An example from the rock deformation perspective would be found when the fault process zone width is highly dependent on factors such as the sense of fault movement and lithology of the surrounding rock. For instance, the zone may be wider for a reverse fault in weak rock versus a strike-slip fault in hard rock. Alternatively, the fault zone complexity may reflect fault maturity. Therefore the distance from a known fault will have to be carefully defined (in the current Kyushu Case Study we have taken a rough centreline for the fault position) and the likelihood of future changes to the fault zone width should be assessed. Another example is that a site located along strike of a region of young volcanic vents and related tectonic features might be expected to have higher hazard than the other sites located in the same distance from volcanoes but in a direction normal to the volcanic lineament. Local geological or tectonic fabrics are likely to have a major influence on the nature of future volcanism and its interaction with the repository. At the scale of the repository the hazards analysis is likely to be strongly linked to consequence analysis.

In regions like Kyushu, the arc volcanism and active fault systems are exceptionally young and unsteady and therefore harder to predict. Down-scaling will require incorporation of

understanding of how the large scale changes in plate configuration and tectonics relate to the smaller scale relationships at the sub-region scale and specific sites.

A key aspect of sub-regional and site scale characterisation will be to understand stress distributions and strain rates. Monitoring of strain rates down bore-holes is an example of the kind of technique that could be applied.

14.6 Refining the Methodology for the 100 k years to 1 million years period

If the requirement for forecasting geological stability were to be extended to 1 million years it would present formidable challenges. Plate motions and configurations may not remain constant in space and time. For example, the volcanic front can be expected to migrate and subducted features that may affect the intensity, style, and location of volcanism and faulting, such as sea floor island chains or ridges, may change their position beneath Kyushu. The forcing factors in back-arc volcanism are poorly understood with apparent volcanic “flare-ups” such that the hazard is not constant in time. Other datasets would be needed to inform coherent geological models to overcome the requirement to drop the constraint of plate tectonic stability over the time period of interest. Potential unsteadiness in tectonics and volcanism will lead to greater uncertainty in the probabilistic models. A wider range of viable geologic models could accommodate increased uncertainty of the temporal and spatial evolution of faulting and volcanism.

For volcanism, this time period presents formidable problems in that very large volcanic systems, such as calderas, can develop on time scales that are well within this time period, Aso being a very good example. Any location that is within the footprint of the volcanic arc or back arc region could be affected by future volcanism. Back arc regions are less prone to major changes, but over a million years the possibility of any given location within the back arc region with no previous record of volcanism developing monogenetic volcanism cannot be ruled out. Slab roll back provides issues for assessing fore-arc regions, especially close to the contemporary volcanic front. It is clear that significant adjustments in plate configurations and regional tectonics are possible in a period of 1 million years, so assessment over such a long period would necessarily have large uncertainties.